www.cardiol.br

www.dicsbc.org

ABC Imagem Cardiovascular

Sociedade Brasileira de Cardiologia • ISSN 2675-312X • Volume 35, Nº 2, April/May/June 2022

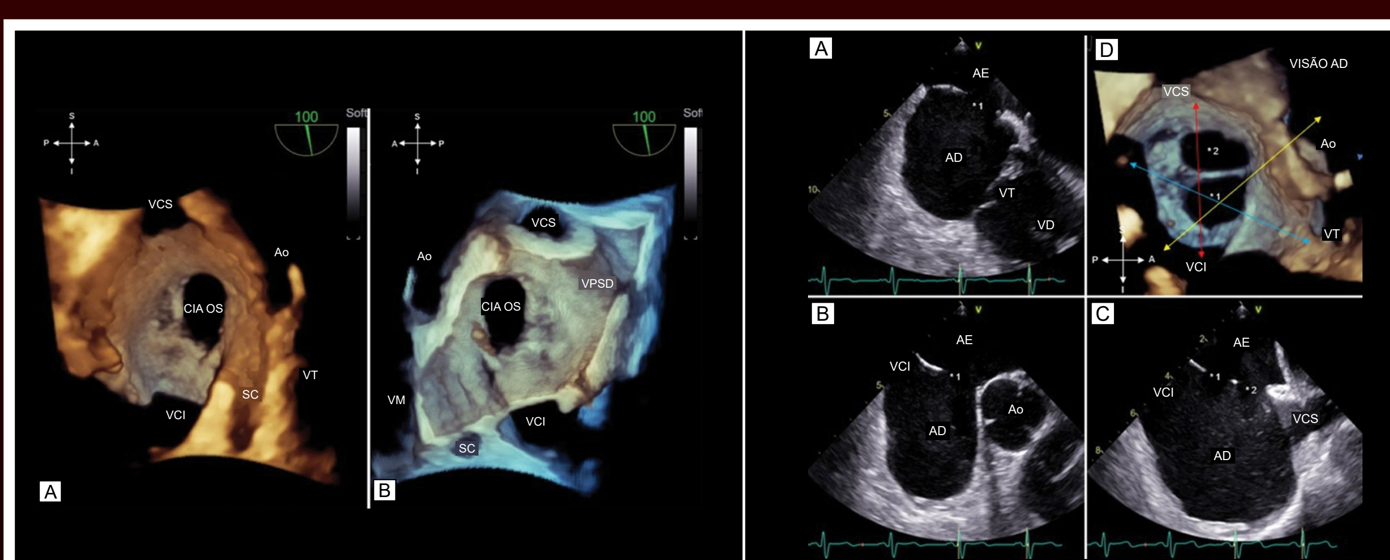

Arquivos Brasileiros de Cardiologia - Imagem Cardiovascular

Volume 35, Nº 2, April/May/June 2022

Indexing source: LILACS - Literatura Latino-Americana e do Caribe em Ciências da Saúde - www.bireme.br, LATINDEX - Sistema Regional de Información en Línea para Revistas Científicas de América Latina, El Caribe, España y Portugal - www.latindex.unam.mx

Department of Cardiovascular Imaging/ Brazilian Society of Cardiology
Rua Barata Ribeiro nº 380 cj.54
01308-000 - São Paulo - SP - Brasil
Fone/Fax: +55 (11) 3259-2988
Fones: +55 (11) 3120-3363
+55 (11) 3259-2988 / +55 (11) 2589-4168

Editorial Coordination
Atha Comunicação e Editora
Rua Machado Bittencourt, 190 - conj. 409
São Paulo, SP, Brasil
Tel.: (11) 50879502

Editorial Support
revista@dicsbc.com

The journal Arquivos Brasileiros de Cardiologia — Imagem Cardiovascular is the official body of the Department of Cardiovascular Imaging of the Brazilian Society of Cardiology.

www.cardiol.br
www.dicsbc.org
ABC Imagem Cardiovascular

Contents - *Sumário*

Click on the title to read the article

www.cardiol.br
www.dicsbc.org
ABC Imagem Cardiovascular

Review article - Artigo de Revisão

Systematic Review Article - Artigo de Revisão Sistemática

Case Reports - Relatos de Caso

www.cardiol.br

www.dicsbc.org

ABC Imagem Cardiovascular

Brivaldo Markman Filho - Hospital das Clínicas da Universidade Federal de Pernambuco – PE

Bruna Morhy Borges Leal Assunção - Hospital Sírio Libanês e Instituto do Câncer do Estado de São Paulo (ICESP), São Paulo - SP

Caio Cesar Jorge Medeiros - Hospital São Luiz, São Paulo - SP

Carlos Eduardo Rochitte - Instituto do Coração do Hospital das Clínicas da Faculdade de Medicina da Universidade de São Paulo (INCOR/FMUSP), São Paulo - SP

Carlos Eduardo Suaide Silva - DASA (Diagnósticos da América) São Paulo - SP

Carlos Eduardo Tizziani Oliveira Lima - Hospital Casa de Saúde de Campinas, Campinas – SP

Cecília Beatriz Bittenciurt Viana Cruz - Instituto do Coração Hospital das Clínicas da Faculdade de Medicina da Universidade de São Paulo (INCOR/FMUSP), Hospital Sírio Libanês e Instituto do Câncer do Estado de São Paulo (ICESP), São Paulo - SP

Cintia Galhardo Tressino - Instituto Dante Pazzanese e Grupo DASA, São Paulo - SP

Claudia Cosentino Gallafrio - Hospital do GRAACC - Universidade Federal de São Paulo/Hospital Israelita Albert Einstein/Grupo DASA São Paulo - Alta diagnósticos, São Paulo – SP

Claudia Pinheiro de Castro Grau - Instituto do Coração Hospital das Clínicas da FMUSP e Hospital e Maternidade São Luiz, São Paulo - SP

Claudia Gianini Monaco - Hospital Israelita Albert Einstein, São Paulo - SP

Cláudio Henrique Fischer – Universidade Federal de São Paulo (UNIFESP) e Hospital Israelita Albert Einstein, São Paulo - SP

Cláudio Leinig Pereira da Cunha - Universidade Federal do Paraná, Curitiba - PR

Claudio Tinoco Mesquita - Universidade Federal Fluminense (UFF), Rio de Janeiro - RJ

Clerio Francisco de Azevedo Filho - Universidade do Estado do Rio de Janeiro (UERJ), Rio de Janeiro – RJ

David Costa de Souza Le Bihan - Instituto Dante Pazzanese da Cardiologia, São Paulo - SP

Djair Brindeiro Filho - Serviço de Ecocardiografia do Recife Ltda. e Real Hospital Português de Beneficência em Pernambuco - PE

Edgar Bezerra Lira Filho - Hospital das Clínicas, FMUSP; Hospital Israelita Albert Einstein, São Paulo – SP

Edgar Daminello - Hospital Israelita Albert Einstein, São Paulo – SP

Eliza de Almeida Gripp - Hospital Pró Cardíaco e do Hospital Universitário Antônio Pedro (UFF), Rio de Janeiro - RJ

Eliza Kaori Uenishi - Instituto do Coração do Hospital das Clínicas da Faculdade de Medicina da Universidade de São Paulo (INCOR/FMUSP), São Paulo - SP

Estela Suzana Kleiman Horowitz - Fundação Universitária de Cardiologia, Porto Alegre – RS

Fabio de Cerqueira Lario - Hospital Alemão Oswaldo Cruz, São Paulo – SP

Fabio Villaça Guimarães Filho - Faculdade de Medicina de Marília/Instituto do Coração de Marília, Marília – SP

Fernando Antônio de Portugal Morcerf - Ecor Ecocardiografia Ltda, Rio de Janeiro – RJ

Frederico José Neves Mancuso - Escola Paulista de Medicina - Universidade Federal de São Paulo (UNIFESP/EPM), São Paulo - SP

Gabriel Leo Blacher Grossman - Hospital Moinhos de Vento e Clínica Cardionuclear, Rio Grande do Sul – RS

Gabriela Liberato - Instituto do Coração do Hospital das Clínicas da Faculdade de Medicina da Universidade de São Paulo (INCOR/FMUSP), São Paulo - SP

Gabriela Nunes Leal - Hospital das Clínicas da Faculdade de Medicina da Universidade de São Paulo (HC-FMUSP), São Paulo - SP

Giordano Bruno de Oliveira Parente - Hospital Agamenon Magalhães, Recife - PE

Gláucia Maria Penha Tavares - Instituto do Coração do Hospital das Clínicas da Faculdade de Medicina da Universidade de São Paulo (INCOR/FMUSP) e Hospital Israelita Albert Einstein, São Paulo - SP

Henry Abensur - Departamento de Ecocardiografia, A Beneficência Portuguesa de São Paulo, São Paulo - SP

Ibraim Masciarelli Francisco Pinto - Instituto Dante Pazzanese de Cardiologia, São Paulo - SP

Ilan Gottlieb - Casa de Saúde São José e Clínica São Vicente, Rio de Janeiro - SP

Iran de Castro - Instituto de Cardiologia do Rio Grande do Sul (IC/FUC), Porto Alegre - RS

Isabel Cristina Britto Guimaraes - Hospital Ana Neri, Universidade Federal da Bahia, Bahia - BA

Ivan Romero Rivera - Universidade Federal de Alagoas, Maceió - AL

Jaime Santos Portugal - Proecho - Cardiologia Serviços Médicos Ltda, Rio de Janeiro - RJ

Jeane Mike Tsutsui - Instituto do Coração do Hospital das Clínicas da Faculdade de Medicina da Universidade de São Paulo (INCOR/FMUSP), Fleury Medicina e Saúde, São Paulo – SP

João Marcos Bemfica Barbosa Ferreira - Universidade do Estado do Amazonas, Amazonas - AM

José de Arimatéia Batista Araujo-Filho - Hospital Sírio-Libanês, São Paulo, Brasil. Memorial Sloan-Kettering Cancer Center, Nova Iorque – Estados Unidos.

José Lázaro de Andrade - Hospital Sírio Libanês, São Paulo – SP

José Luis de Castro e Silva Pretto - Hospital São Vicente de Paulo/Hospital de Clínicas de Passo Fundo, Rio Grade do Sul - RS

José Luiz Barros Pena - Hospital Felício Rocho, Belo Horizonte - MG

José Maria Del Castillo - Pronto Socorro Cardiológico de Pernambuco (PROCAPE - UPE), Recife – PE

José Olimpio Dias Júnior - Hospital Mater Dei, Belo Horizonte - MG

José Sebastião de Abreu - Clinicárdio de Fortaleza e Cardioexata, Fortaleza – PE

José Roberto Matos-Souza - Faculdade de Medicina da UNICAMP, São Paulo - SP

Joselina Luzia Menezes Oliveira - Fundação São Lucas, Aracaju – SE

Jorge Andion Torreão - Hospital Cárdio Pulmonar, Bahia – BA

Juliana Fernandes Kelendjian - CDI Centro de Diagnóstico por Imagem, Goiânia - GC

Laise Antonia Bonfim Guimarães - Sociedade Beneficente Israelita Brasileira de Ensino e Pesquisa Albert Einstein, são Paulo – SP

Lara Cristiane Terra Ferreira Carreira - Cardiologia Nuclear de Curitiba e Hospital Nossa Senhora do Pilar, Curitiba, Paraná – PR

Leina Zorzanelli - Instituto do Coração do Hospital das Clínicas da Faculdade de Medicina da Universidade de São Paulo (INCOR/FMUSP), São Paulo - SP

Lilian Maria Lopes - ECOKIDGRAFIA - Serviços Médicos Ecodoppler, São Paulo – SP

Liz Andréa Baroncini - Hospital da Cruz Vermelha e Instituto Saber e Aprender, Paraná - PR

Luciano Aguiar Filho - Hospital Salvaluz, DIAGMED (Tomografia e Ressonância Cardíaca), Hospital Municipal de Barueri e Instituto Dante Pazzanese de Cardiologia, São Paulo -SP

Luciano Herman Juaçaba Belém - Instituto Nacional de Cardiologia, Rio de Janeiro - RJ

Luiz Darcy Cortez Ferreira - OMNI - CCNI - Medicina Diagnóstica, São Paulo - SP

Luiz Felipe P. Moreira - Instituto do Coração do Hospital das Clínicas da Faculdade de Medicina da Universidade de São Paulo (INCOR/FMUSP), São Paulo - SP

Manuel Adán Gil – Universidade Federal de São Paulo – Escola Paulista de Medicina, São Paulo – SP

Marcela Momesso Peçanha - Instituto Dante Pazzanese de Cardiologia, São Paulo – SP

Marcelo Dantas Tavares - Universidade Federal da Paraíba, Paraíba - PB

Marcelo Haertel Miglioranza - Instituto de Cardiologia do Rio Grande do Sul, Rio Grande do Sul - RS

Marcelo Luiz Campos Vieira - Instituto do Coração do Hospital das Clínicas da Faculdade de Medicina da Universidade de São Paulo (InCor-HCFMUSP) e Hospital Israelita Albert Einstein, São Paulo - SP

Marcelo Souza Hadlich - Instituto Nacional de Cardiologia, INC., Hospital da Unimed-Rio, ACSC - Casa de Saúde São José, RioImagem CDI, Rede D´Or de Hospitais, Rede Labs D'Or, Rio de Janeiro – RJ

Marcia Azevedo Caldas - Faculdade de Medicina de Campos, Rio de Janeiro - RJ

Marcia de Melo Barbosa – ECOCENTER, Belo Horizonte – MG

Marcia Ferreira Alves Barberato - CardioEco – Centro de Diagnóstico Cardiovascular, Curitiba - PR

Márcio Silva Miguel Lima - Instituto do Coração do Hospital das Clínicas da Faculdade de Medicina da Universidade de São Paulo (InCor-HCFMUSP), São Paulo – SP

Marcio Sommer Bittencourt - Hospital Universitário de São Paulo/Hospital Israelita Albert Einstein, São Paulo - SP

Márcio Vinícius Lins de Barros - Faculdade de Saúde e Ecologia Humana FASEH, Vespasiano - MG

Marcos Valério Coimbra de Resende - Hospital Samaritano Paulista, São Paulo – SP

Maria Clementina Di Giorgi - Instituto do Coração do Hospital das Clínicas da Faculdade de Medicina da Universidade de São Paulo (InCor-HCFMUSP), São Paulo – SP

International Editorial Board

Editorial

Left Atrial Appendage: Anatomy, Function, and Importance in Thrombus Formation

Apêndice Atrial Esquerdo: Anatomia, Função e Importância na Formação de Trombos

Taylla Mendes Silva[1], Gustavo Brandão de Oliveira[1,2], Thais Lins de Souza Barros[1], André Barbosa de Andrade[3], Bruno Bom Furlan[3], Maria do Carmo de Pereira Nunes[1,2]

[1]Hospital das Clínicas, School of Medicine, Federal University of Minas Gerais, Belo Horizonte, MG, Brazil. [2]Graduate Program in Sciences Applied to Adult Health, School of Medicine, Federal University of Minas Gerais, Belo Horizonte, MG, Brazil. [3]Medical Student, School of Medicine, Federal University of Minas Gerais, Belo Horizonte, MG, Brazil.

Introduction

The left atrial appendage (LAA) is an extension of the left atrium (LA) and has complex anatomical structure and unique pathophysiological properties. The LAA functions as a decompression chamber during left ventricular (LV) systole and under increased left atrial pressure conditions. Despite previously being considered a relatively insignificant portion of the cardiac anatomy, the LAA has been highlighted as an important structure involved in the genesis of thrombus formation and thromboembolic events. With the recent development of percutaneous closure devices, LAA morphology assessments have become increasingly important. This article aims to describe LAA anatomy and morphology, function assessment parameters, thrombus diagnostic challenges, and the main imaging modalities, particularly transesophageal echocardiography.

LAA anatomy

The LAA is a long, thin tubular structure with a narrow base that originates from the LA body (Figure 1).[1] Macroscopically, the LAA is visualized at the left border of the heart between the LV and the pulmonary veins.[2,3] It commonly extends between the anterior and lateral LA walls. Its tip can be variously positioned, most commonly being in the anterosuperior direction and overlapping the left border of the right ventricular outflow tract or the pulmonary trunk and the main branch of the left coronary artery and the circumflex artery, but it can also be in the lateral or posterior direction, reaching the transverse sinus of the pericardium in some patients.[2] Anatomically, the superior portion of the LAA is closely related to the pulmonary artery, while its inferior portion is close to the free LV wall.[4]

The LAA ostium (LAAO) is separated from the left pulmonary vein orifices by the left lateral crest.[5] On the other side, the smooth LA wall separates the LAAO from the mitral annulus.[2] A narrowing that marks the orifice of the appendix is visualized in the transition between the smooth LA endocardium and the wrinkled LAA surface. Morphologically, the LAAO can be elliptical (68.9%), while its long axis is usually oriented obliquely to the mitral annulus in a foot-like (10%), triangular (7.7%), or round (5.7%) shape.[6–8]

The LAA passes through a narrowed region before its body opens up.[2] In this region, one to four lobes can be observed, and a multilobulated LAA (with two or more lobes) was seen in 80% of patients in a relevant study by Veinot JP et al. of 500 postmortem hearts.[9] That study reported the frequency of one, two, three, and four lobes as 20%, 54%, 23%, and 3%, respectively, not corroborating a more recent postmortem study in which two lobes were observed in 64.3% and three lobes in 35.7% of specimens.[8] The quantification of the number of lobes is important because a greater number of lobes is associated with the presence of thrombus regardless of clinical risk and blood stasis.[10,11]

The LAA presents great anatomical diversity. Wang et al.[7] established the classification used to categorize four morphological types, with the "chicken-wing" shape being the most common (48%), followed by the "cactus" (30%), "windsock" (19%), and "cauliflower" (3%) shapes.[12] These categories are related to the risk of clot formation, with the cauliflower shape being apparently more associated with embolic events.[12] This morphology is also associated with lower blood flow velocity,[1] a greater predisposition to blood stasis, while the chicken-wing shape is associated with a lower risk.[13] A Czech study by Stefan et al. related the cauliflower and chicken-wing shapes with a higher risk of silent cerebral ischemia.[14] However, this classification is limited by its subjective and observer-dependent nature as well as the possibility of overlapping morphologies according to viewing angle.[2,15] Other factors also influence the risk of thromboembolic events,[16,17] including a smaller orifice diameter, higher number of trabeculations,[18] and higher number of lobes.[10] Another study[11] highlighted that number and size of lobes and their orifices may be more important factors in risk of thromboembolic events than LAA shape.

Unlike the LA, whose wall is smooth, the internal LAA surface is trabecular, presenting muscle bundles[9] called pectineal muscles that form complex indentations (Figure 1). These muscle bundles resemble feather- or fan-shaped palm leaves.[19] Larger muscle groups can be confused with thrombi or intra-atrial masses.[9] The LAA also presents great size variability by sex (greater in men), age (growing about 0.20 cm^3 per decade),[20] and the presence of atrial fibrillation.

Mailing Address: Maria do Carmo do Pereira Nunes •
Avenida Professor Alfredo Balena, 190, Santa Efigênia. CEP: 0130 100 – Belo Horizonte, MG, Brasil.
E-mail: mcarmo@waymail.com.br
Manuscript received 3/10/2022; revised 4/20/2022; accepted 5/4/2022

DOI: 10.47593/2675-312X/20223502eabc301

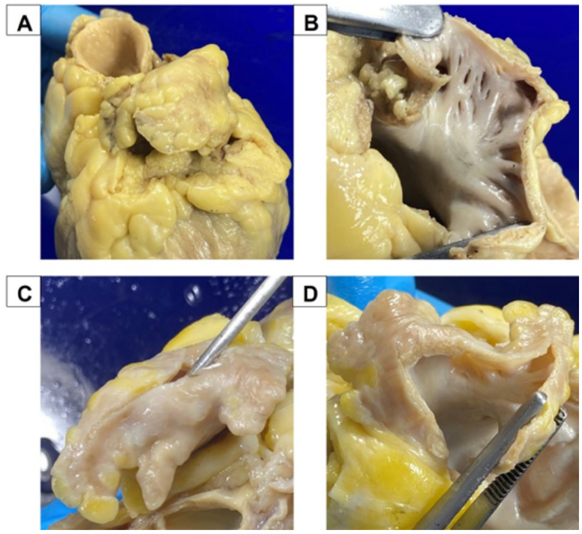

Images acquired in collaboration with anatomopathologist Geraldo Brasileiro Filho.

Figure 1 – *Macroscopical view of the LAA. Images made from explanted hearts showing the external and internal aspect of the LAA. (A) External view of a one-lobe appendage. (B) Internal view of a one-lobe appendage. (C) External view of a multilobed appendage. (A) Internal view of a multilobed appendage.*

LAA dimensions are significantly more voluminous and have larger orifices in patients with atrial fibrillation than in those with sinus rhythm.

LAA function

The LAA has both mechanical and endocrine functions.[21] Its compliance is greater than that of the rest of the atrium; therefore, it can modulate the pressure in the chamber and compensate for volume overloads and pressure increases. In addition, the appendix has the highest concentration of atrial natriuretic peptide (ANP) granules in the LA (about 30%).[4,22,23] Cardiomyocyte distention stimulates ANP secretion; therefore, as it is more compliant and concentrates the largest amount of ANP, the LAA is more sensitive to volume and pressure changes and has greater control of decreased blood pressures and increased heart rate, diuresis, and natriuresis.[4,23,24]

The LAA performs active contraction,[4] and its flow velocity can be quantified by pulsed Doppler. In most patients undergoing transesophageal echocardiography (TEE), this is a four-phase flow (Figure 2).[4,25,26] The first wave corresponds to the outflow caused by appendage contraction at the end of ventricular diastole. The second wave represents the antegrade LAA filling flow during atrial diastole. The third wave has positive and negative components that reflect the mechanical waves at ventricular end systole (in this phase, numerous patterns of low-amplitude positive and negative waves are described).[26] And finally, outflow from the LAA occurs during the rapid ventricular filling phase. The decreased flow velocity in the LAA relates to the presence of spontaneous contrast (SC), sludge, and thrombus.[21,25,27]

LAA function can be assessed by several parameters. LAA filling and emptying velocities by pulsed Doppler express the LAA contractile function. In addition, LAA area, volume, and ejection fraction measurements by different methods reflect LAA function.

Blood stasis and thrombus formation

LAA contractility changes can lead to thrombus formation and subsequent thromboembolic events[27] regardless of the presence of atrial fibrillation (AF). AF generally presents with decreased LAA contractility, decreased blood flow velocities, and LAA dilation.[28,29] The AF-related remodeling process makes the LAA function a static pocket, resulting in stagnation and thrombosis.

Approximately 75% of patients with cardioembolic episodes are estimated to have emboli arising from the LAA. LAA thrombi are present in up to 14% of patients with acute AF (<3 days).[30] Thrombus formation can develop even in AF patients receiving therapeutic anticoagulation therapy. A previous study showed that 1.6% of patients treated with anticoagulants for 1 month had echocardiographic evidence of a thrombus in the LAA.[31]

Limited data suggest that LV failure and increased LV end-diastolic pressure may also be risk factors for LAA thrombus in the absence of AF. Vigna et al.[36] identified LAA thrombi in eight of 58 patients with dilated cardiomyopathy and sinus rhythm. Consequently, the risk of thrombus formation in the LAA appears to be related to LAA dysfunction resulting from increased filling pressures regardless of cause.

The complex interaction of atrial endothelium, blood constituents, and blood stasis (i.e., the components of Virchow's triad) results in the formation of activated platelet aggregates and leukocytes[32] or fibrinogen-mediated erythrocyte aggregates[33,34] that present as spontaneous dense echocardiographic contrast or "smoke." These aggregates can progress to sludge and, eventually, thrombus.[2,35]

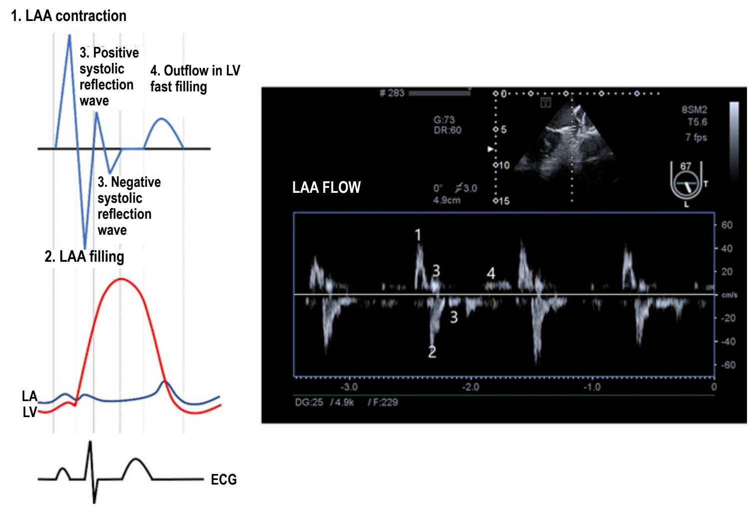

Adapted from Delgado et al.[26] LA: left atrium; LV: left ventricle.

Figure 2 – *Comparison between the flow pattern in the LAA in sinus rhythm, the cardiac cycle, and the electrocardiogram (ECG).*

Imaging methods for assessing the LAA

Transesophageal echocardiography

TEE is the method of choice for studying LAA anatomy and function. Its sensitivity and specificity for detecting LAA thrombi compared to those observed intraoperatively are 92% and 98%, respectively,[2,37,38] with negative and positive predictive values of 100% and 86%, respectively[38]. The absence of a thrombus confirms that it is safe to proceed with cardioversion, with a low rate of thromboembolic events (0–0.8%) in adequately anticoagulated patients.[39,40]

A complete LAA assessment should include LA, LV, and mitral valve imaging associated with a detailed assessment of LAA morphology, contraction, and flow velocities using two- and three-dimensional (3D) echocardiography.[2] LAA assessments can be started using a four-chamber section; however, as it is a lateral structure, the probe must be rotated counterclockwise and flexed to bring it to the center of the screen. Also, using a two-chamber section, the LAA can be zoomed or screen depth can be reduced to increase assessment accuracy.[41] Two-dimensional TEE provides excellent LA and LAA characterization due to the anatomical proximity of these structures to the esophagus. Despite the LAA being a narrow tubular structure with a complex anatomy, thrombi within it can be identified with satisfactory accuracy by TEE. However, assessment sensitivity decreases in cases of small thrombi or those located within a lateral lobe.

Functional Doppler assessment is routinely used to improve LAA analyses (Figure 3). The pulsed Doppler should be placed at 1–2 cm from the LAAO. LAA flow velocity measured by pulsed Doppler is an indicator of risk of thrombus formation (risk increases as velocity decreases).[2] Velocities < 40 cm/s are associated with an increased risk of stroke and the presence of SC,[42] with decreasing velocities of <20 cm/s being associated with thrombi in the LAA and a higher incidence of thromboembolic events.[43–47] Velocities < 40 cm/s require meticulous LAA assessments before cardioversion or interventions involving the LA and LAA.

LA thrombus is defined as an echogenic mass in the LAA or LA distinct from the LA endocardium or pectineal muscles (Figure 4).[38] Several differential diagnoses and thrombi misinterpretations should be considered, including acoustic shadowing of the ligament of Marshall, pectineal muscles, or non-differentiation of sludge and dense spontaneous echogenic contrast.[2,48]

In cases in which the LAA images are suboptimal, ultrasound contrast agents help improve LAA visualization. The use of contrast eliminates many artifacts and usually demonstrates complete LAA opacification or filling defects.[49,50]

LAA echocardiographic imaging is operator-dependent and, therefore, has a learning curve. Interobserver variability is an important limitation of this investigation since interobserver disagreement rates can reach 22% in the diagnosis of thrombus.

Challenges in diagnosing LAA thrombus

Echocardiographic evaluation of the LAA requires careful analysis by the echocardiographer. In some situations, LAA imaging misinterpretations can lead to hasty decisions. Exuberant pectineal musculature or appendage lobes can be interpreted as thrombi, thereby resulting in the use of unnecessary anticoagulant therapy (Figure 5). Thrombus misdiagnosis also leads to suspended percutaneous procedures, such as LAA, patent foramen ovale, and atrial septal defect occlusion, MitraClip implantation, AF ablation, and mitral valvuloplasty with a balloon catheter. Such procedures involve manipulation of catheters inside the atria and, consequently, increase the risk of embolization.

Ruling out LAA thrombi using TEE may enable early and safe cardioversion without the need for prolonged

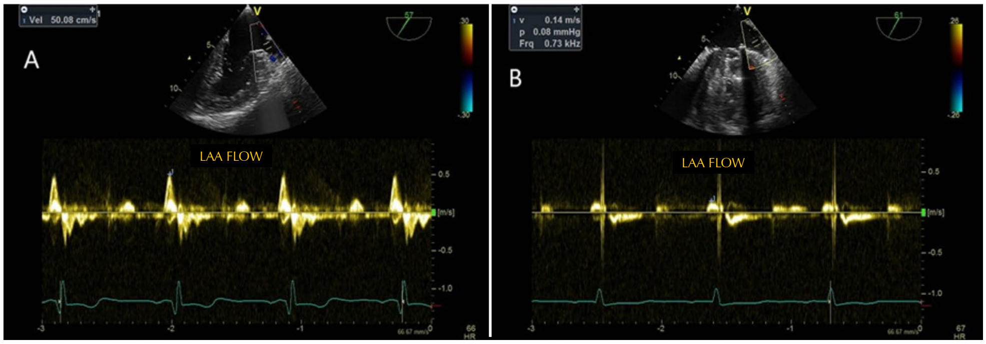

AAE: apêndice atrial esquerdo.

Figure 3 – *TEE demonstrating in (A) the normal velocity (50 cm/s) flow in the LAA of a patient in sinus rhythm, with an LA of normal dimensions and without the presence of SC. In (B), the reduced velocity (14 cm/s) flow in the LAA of a patient in the postoperative period of mitral valve replacement (mechanical prosthesis), in sinus rhythm, with dilated LA and presence of SC in the LAA.*

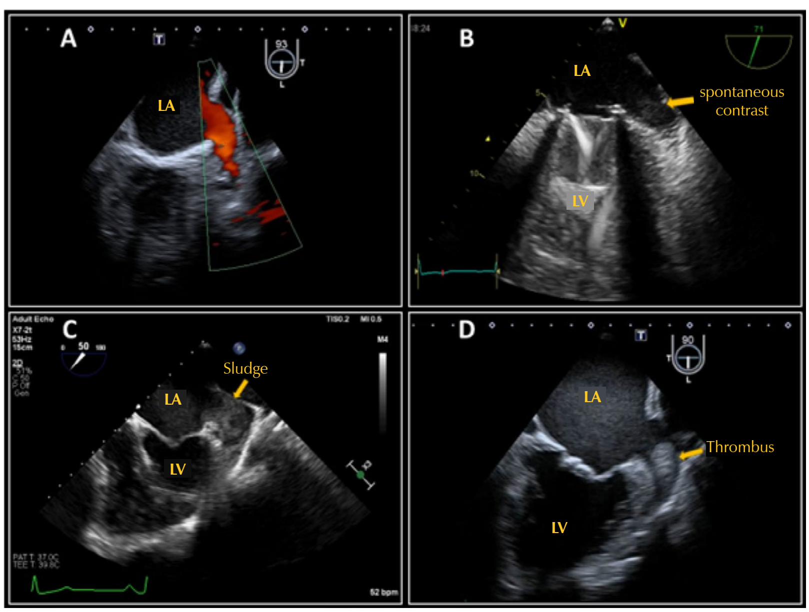

LV: left ventricle. LA: left atrium.

Figure 4 – *TEE showing the LAA filled in by color Doppler in image A. Images B and C show the presence of SC (B) and sludge (C) inside the LAA, respectively. In image D, the arrow indicates a thrombus in the LAA and the presence of SC in the LA.*

previous anticoagulation.[38,51] Thrombi within the LAA must be differentiated from the pectineal muscles, reverberation artifact originating from the coumadin ridge, septa between multiple lobes,[52] SC, and sludge.

Thrombi are often located at the distal end of the LAA, almost always confined to its lumen and adherent to its walls. They have independent movement and echogenicity patterns as well as uniform consistency and textures that differ from those of the LAA wall. Their morphology varies, but they are generally rounded (Figure 4). They are often associated with the presence of SC within the LA.

Reverberation artifacts are also found within the LAA, being located at a position twice the distance from the transducer to the coumadin ridge. Its mobility totally depends on the coumadin crest movement. Its morphology is compatible with that of the object or structure that causes the artifact and is not related to the presence of SC in the LA. Reducing gain and using other imaging planes are strategies that the echocardiographer can use to avoid artifact formation. On the other hand, the stepped appearance and the position at a doubled distance reinforce the presence of a reverberation artifact inside the LAA. The echocardiographer should be

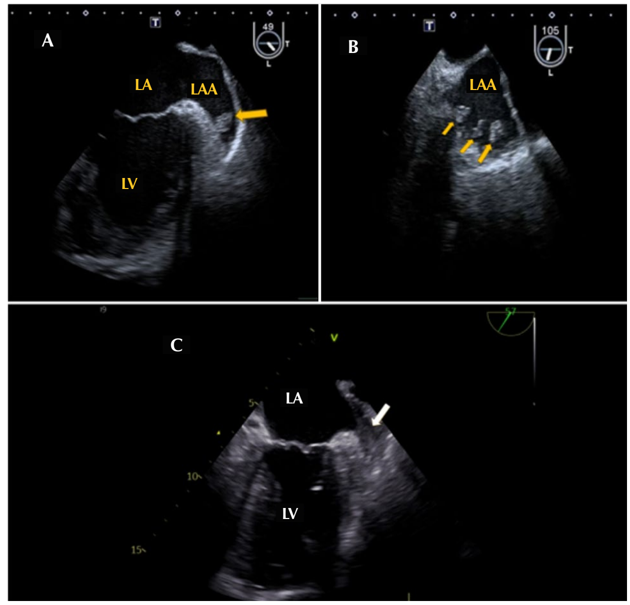

LV: left ventricle; LA: left atrium; LAA: left atrial appendage.

Figure 5 – *Mid-esophageal slice TEE at 50º showing a mass within the LAA that can be easily interpreted as a thrombus (arrow) (A). Image of the same patient at 105º, clarifying that the mass is probably the three LAA lobes (B). Image C shows a reverberation artifact (arrow) produced by the coumadin ridge and visualized inside the LAA.*

aware of the presence of a prominent coumadin ridge, which can also be misdiagnosed as a thrombus.

The pectineal muscles, in turn, are confined to the body of the LAA. Their mobility follows LAA movement, and they have identical echogenicity to that of the LAA wall. They are not related to the presence of SC.

SC, also known as smoke, is a swirling mist of varying density that reflects the low blood flow velocity (Figure 4).[53] It can be classified into four groups (1 to 4) by intensity, location, and presence of a vortex (movement) as proposed by Fatkin et al.[42] (Table 1). However, SC quantification in clinical practice is difficult and depends on image quality, gain settings, and operator experience.

SC is reportedly noted in up to 60% of patients with AF.[54] Aspirin and warfarin therapy does not appear to affect the presence of SC in the LA.[55] Although patients with dense SC visualized in the LAA have a stroke rate of 18.2% per year if not treated with warfarin and a risk of stroke of 4.5% per year despite dose-adjusted warfarin, the presence of an LAA thrombus triples the overall rate of stroke.[40]

Sludge, a dynamic fluid of gelatinous echogenicity with no well-defined mass, is present throughout the cardiac cycle.[48] It is often difficult to differentiate between sludge and thrombus. Sludge represents a stage after SC prior to thrombus formation that may have prognostic significance.[56]

Other imaging methods for assessing LAA

Transthoracic echocardiography

Transthoracic echocardiography (TTE) has a limited capacity to identify or exclude thrombi in the LA and LAA, with a reported sensitivity of 40–60%, mainly due to poor visualization of the LAA, where most atrial thrombi are located (Figure 6). In this sense, the use of harmonic images and the administration of ultrasound contrast agents can increase its ability to detect intracavitary thrombi.[37,38,48]

Contrast echocardiography

Since the late 1990s, ultrasound contrast agents have been administered to improve the visualization of endocardial borders, including an improved LAA assessment. Recent studies of LA and LAA enhanced interrogation techniques reported statistically significant improvements in dimensional measurements and emptying characteristics. In cases of suboptimal LAA images, contrast agents help improve LAA visualization, eliminate artifacts, and reveal body filling defects.[2,57]

Contrast agents improve the delineation of cardiac chamber endocardial borders, but their use has not been implemented in clinical routine to detect or exclude thrombi. Several reasons explain this circumstance, such as the use of predictive markers of thrombus formation such as pulsed Doppler of LAA blood flow and SC assessments; the low prevalence of thrombus in the LAA (5–13% in patients with AF but without therapeutic anticoagulation); and the even lower risk of an embolic event. In addition, the use of ultrasound contrast increases the time required to perform the test as well as its cost.[48,58]

The ability of the contrast agent to completely opacify the LAA even in the presence of artifacts during native imaging minimizes the false identification of thrombi and allows the delineation of atrial thrombi, reducing the amount of inconclusive TEE and improving the echocardiographer's degree of interpretive

Table 1 - Classification of spontaneous contrast as proposed by Fatkin et al.

Grade	SEC	Description
0	None	Absence of echogenicity
1+	Mild	Minimal echogenicity located in the LAA or sparsely distributed in the LA main cavity that may be only transiently detectable during the cardiac cycle
2+	Mild to moderate	Swirling pattern denser than 1+ but similarly distributed, detectable without increased gain settings
3+	Moderate	Moderate and dense swirl in the LAA usually associated with lower intensity in the main cavity; may fluctuate in intensity but is constantly detectable throughout the cardiac cycle
4+	Intense	Intense echogenicity and very slow swirl patterns in the LAA, often with similar density in the main cavity
Sludge	Intense	Prethrombotic state can be defined as gelatinous echogenicity without a well-defined mass; present throughout the cardiac cycle

SEC, spontaneous echogenic contrast.

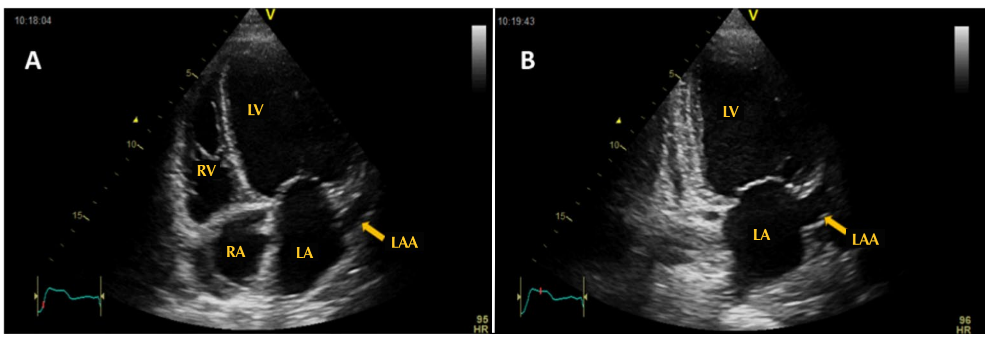

LV: left ventricle; RV: right ventricle; LA: left atrium; RA: right atrium; LAA: left atrial appendage.

Figure 6 – *TTE showing the LAA in apical four-chamber (A) and two-chamber view (B).*

confidence. However, in cases in which non-contrast images are diagnostic and in the absence of SC evidence, the use of contrast fails to improve diagnostic confidence.[50,57]

Three-dimensional echocardiography

The development of 3D TEE improves the ability to assess the LAA, allowing a selective perspective of its anatomy and better discrimination between artifacts, masses, and thrombi (Figure 7). The 3D method allows a more comprehensive assessment of multiple LAA lobes, which can be located in different planes, as well as a more accurate estimate of its geometry, size, and function with better distinction between pectineal muscles and thrombi.[26]

Data remain limited regarding the sensitivity and specificity of 3D TEE for thrombus detection in the LAA. However, with recent advances in percutaneous device therapy for LAA closure, 3D TEE has become important for planning and guiding interventions.[2]

Intracardiac echocardiography

Intracardiac echocardiography (ICE) is an alternative imaging method when TEE is unavailable or inconclusive. ICE can provide multiple views and detailed LAA images to enable the reliable diagnosis of the presence of thrombus.[3]

Although it is less sensitive than TEE for thrombus detection, it can be a complementary method, especially when TEE findings require further assessment. However, as an invasive procedure, its use in daily practice is limited, being primarily reserved for the cardiac catheterization laboratory during planned interventional procedures.[2]

Computed tomography

Computed tomography (CT) can identify LAA thrombi with good sensitivity and moderate specificity. Recent studies have concluded that LA and LAA thrombus analysis with isolated multislice CT is probably sufficient and non-inferior to TEE in patients with paroxysmal AF and normal systolic function.[7] However, CT is not currently recommended for identifying thrombi in the LA and LAA (Figure 8).[11–13,43]

CT generates 3D volumetric data of the heart, which can be reconstructed across different cardiac planes and phases to provide an accurate assessment of LAA anatomy with high spatial and temporal resolution and quantitative assessment.[2,3] However, CT is not highly specific for the presence of a thrombus and, therefore, the high rate of false-positive results, together with the use of radiation and iodine-based contrast media, are the main limitations for its widespread use.

Cardiac magnetic resonance imaging

Cardiac magnetic resonance imaging (CMRI) is the main imaging method for evaluating cardiac masses.[2] Several imaging techniques provide relevant information about the histological components and vascularization of the masses that, together with clinical data, can help distinguish between benign and malignant neoplastic masses, non-neoplastic masses (thrombi and cysts), or other structures.[26]

Intracavitary thrombus is the most common non-neoplastic mass, and its appearance on CMRI depends on the time of their formation. In more acute cases, in which the thrombus has a large amount of oxyhemoglobin, the thrombi tend to appear with increased signaling on T1- and T2-weighted sequences. Subacute cases present hypersignaling on T1 and low signal intensity on T2 due to the paramagnetic effects of methemoglobin. In chronic cases, the thrombus is water-depleted and cellular debris is replaced by fibrous tissue, thus leading to low signaling on T1 and T2.

The paramagnetic contrast agent has an important role in aiding tissue differentiation between thrombi and tumors. First-pass perfusion imaging allows a clear distinction between the thrombus and the adjacent myocardium since the thrombus is an avascular structure and classically does not absorb the contrast medium. In addition, late gadolinium enhancement can quantify atrial fibrosis, which is independently associated with the presence of thrombus in the LAA and SC and may be an additional risk stratification method.

However, CMRI has been evaluated in a limited number of studies, and its sensitivity and specificity for identifying LAA thrombus are similar to those of CT with high agreement with those of TEE. Thus, despite the evident advantages of CMRI, limitations remain to its widespread use in clinical practice, and it is not the recommended imaging modality for assessing thrombi in the LA or LAA.

Conclusions

The LAA, a complex structure with variable anatomy, constitutes the most common site of thrombus formation in the context of non-valvular AF. LAA function plays an important role in blood flow stasis and the risk of thrombus formation with subsequent thromboembolic events. TEE is the imaging modality of choice in LAA assessments, with high accuracy for detecting thrombi. Current and emerging transcatheter therapies, especially the implantation of LAA occlusion and exclusion devices, have further highlighted the importance of understanding LAA anatomy and function in clinical practice.

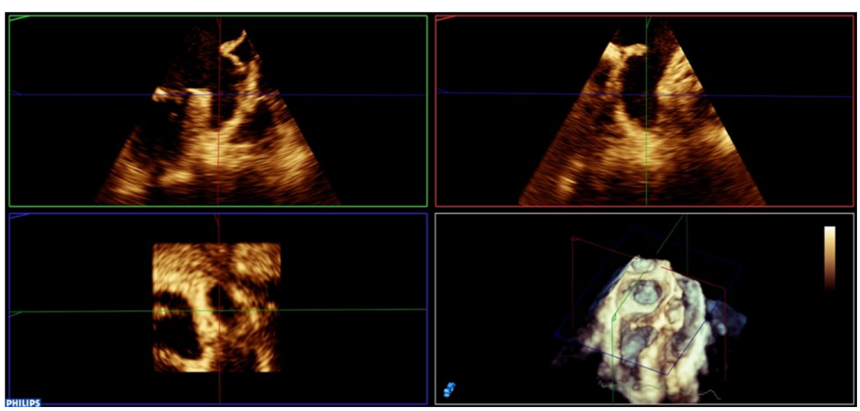

Figure 7 – *Three-dimensional TEE showing the LAA in several projections and allowing contractile function assessment.*

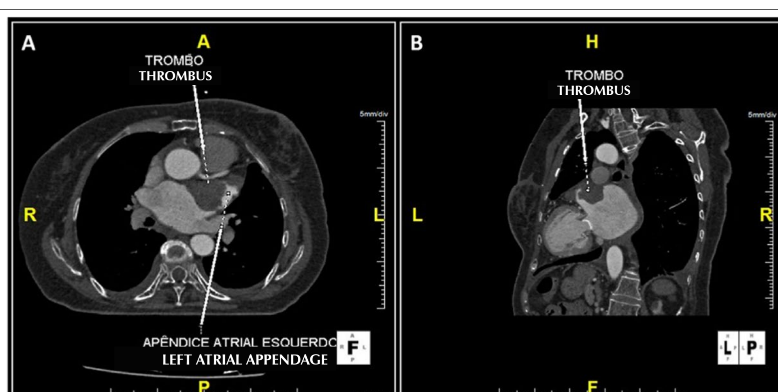

Images provided by cardiologist Victor Pimentel de Matos.

Figure 8 – *CT angiography image showing a thrombus in the LAA and LA.*

Authors' contributions

Research conception and design: Silva TM e Oliveira GB; data collection: Silva TM, Andrade BA; Furlan BB e Barros TLS; data analysis and interpretation: Oliveira GB e Nunes MCP; manuscript writing: Silva TM, Andrade BA; Furlan BB e Barros TLS; critical review of the manuscript for important content: Nunes MCP.

Conflict of interest

The authors have declared that they have no conflict of interest.

References

1. Bosi GM, Cook A, Rai R, Menezes LJ, Schievano S, Torii R, et al. Computational Fluid Dynamic Analysis of the Left Atrial Appendage to Predict Thrombosis Risk. Front Cardiovasc Med. 2018;5:34. doi: https://doi.org/10.3389/fcvm.2018.00034

2. Beigel R, Wunderlich NC, Ho SY, Arsanjani R, Siegel RJ. The left atrial appendage: anatomy, function, and noninvasive evaluation. JACC Cardiovasc Imaging. 2014;7(12):1251-65. doi: https://doi.org/10.1016/j.jcmg.2014.08.009

3. Cabrera JA, Saremi F, Sánchez-Quintana D. Left atrial appendage: anatomy and imaging landmarks pertinent to percutaneous transcatheter occlusion. Heart. 2014;100(20):1636-50. doi: https://doi.org/10.1136/heartjnl-2013-304464

4. Al-Saady NM, Obel OA, Camm AJ. Left atrial appendage: structure, function, and role in thromboembolism. Heart. 1999;82(5):547-54. doi: https://doi.org/10.1136/hrt.82.5.547

5. Wongcharoen W, Tsao HM, Wu MH, Tai CT, Chang SL, Lin YJ, et al. Morphologic characteristics of the left atrial appendage, roof, and septum: implications for the ablation of atrial fibrillation. J Cardiovasc Electrophysiol. 2006;17(9):951-6. doi: https://doi.org/10.1111/j.1540-8167.2006.00549.x

6. Su P, McCarthy KP, Ho SY. Occluding the left atrial appendage: anatomical considerations. Heart. 2008;94(9):1166-70. doi: https://doi.org/10.1136/hrt.2006.111989

7. Wang Y, Di Biase L, Horton RP, Nguyen T, Morhanty P, Natale A. Left atrial appendage studied by computed tomography to help planning for appendage closure device placement. J Cardiovasc Electrophysiol. 2010;21(9):973-82. doi: https://doi.org/10.1111/j.1540-8167.2010.01814.x

8. Üçerler H, İkiz ZA, Özgür T. Human left atrial appendage anatomy and overview of its clinical significance. Anadolu Kardiyol Derg. 2013;13(6):566-72. doi: https://doi.org/10.5152/akd.2013.181

9. Veinot JP, Harrity PJ, Gentile F, Khandheria BK, Bailey KR, Eickholt JT, et al. Anatomy of the normal left atrial appendage: a quantitative study of age-related changes in 500 autopsy hearts: implications for echocardiographic examination. Circulation. 1997;96(9):3112-5. doi: https://doi.org/10.1161/01.cir.96.9.3112

10. Yamamoto M, Seo Y, Kawamatsu N, Sato K, Sugano A, Machino-Ohtsuka T, et al. Complex left atrial appendage morphology and left atrial appendage thrombus formation in patients with atrial fibrillation. Circ Cardiovasc Imaging. 2014;7(2):337-43. doi: https://doi.org/10.1161/CIRCIMAGING.113.001317

11. Korhonen M, Muuronen A, Arponen O, Mustonen P, Hedman M, Jäkälä P, et al. Left atrial appendage morphology in patients with suspected cardiogenic stroke without known atrial fibrillation. PLoS One. 2015;10(3):e0118822. doi: https://doi.org/10.1371/journal.pone.0118822

12. Di Biase L, Santangeli P, Anselmino M, Mohanty P, Salvetti I, Gili S, Horton R, et al. Does the left atrial appendage morphology correlate with the risk of stroke in patients with atrial fibrillation? Results from a multicenter study. J Am Coll Cardiol. 2012;60(6):531-8. doi: https://doi.org/10.1016/j.jacc.2012.04.032

13. Lupercio F, Carlos Ruiz J, Briceno DF, Romero J, Villablanca PA, Berardi C, et al. Left atrial appendage morphology assessment for risk stratification of embolic stroke in patients with atrial fibrillation: A meta-analysis. Heart Rhythm. 2016;13(7).

14. Anselmino M, Scaglione M, Di Biase L, Gili S, Santangeli P, Corsinovi L, et al. Left atrial appendage morphology and silent cerebral ischemia in patients with atrial fibrillation. Heart Rhythm. 2014;11(1):2-7. doi: https://doi.org/10.1016/j.hrthm.2013.10.020

15. Anselmino M, Frea S, Gili S, Rovera C, Morello M, Jorfida M, et al. Left atrial appendage morphology at transesophageal echocardiography: how to improve reproducibility? Minerva Cardiol Angiol. 2021;69(2):178-84. doi: https://doi.org/10.23736/S2724-5683.20.05215-9

16. Reiffel JA. Optimum Risk Assessment for Stroke in Atrial Fibrillation: Should We Hold the Status Quo or Consider Magnitude Synergism and Left Atrial Appendage Anatomy? Arrhythm Electrophysiol Rev. 2017;6(4):161-6. doi: https://doi.org/10.15420/aer.2017.33.1

17. Kreidieh B, Valderrábano M. Malignant Left Atrial Appendage Morphology and Embolization Risk in Atrial Fibrillation. HeartRhythm Case Rep. 2015;1(6):406-10. doi: https://doi.org/10.1016/j.hrcr.2015.02.016

18. Khurram IM, Dewire J, Mager M, Maqbool F, Zimmerman SL, Zipunnikov V, Beinart R, et al Relationship between left atrial appendage morphology and stroke in patients with atrial fibrillation. Heart Rhythm. 2013;10(12):1843-9. doi: https://doi.org/10.1016/j.hrthm.2013.09.065

19. Victor S, Nayak VM. Aneurysm of the left atrial appendage. Tex Heart Inst J. 2001;28(2):111-8. PMID: 11453121; PMCID: PMC101149.

20. Boucebci S, Pambrun T, Velasco S, Duboe PO, Ingrand P, Tasu JP. Assessment of normal left atrial appendage anatomy and function over gender and ages by dynamic cardiac CT. Eur Radiol. 2016;26(5):1512-20. doi: https://doi.org/10.1007/s00330-015-3962-2

21. Delgado V, Di Biase L, Leung M, Romero J, Tops LF, Casadei B, et al. Structure and Function of the Left Atrium and Left Atrial Appendage: AF and Stroke Implications. J Am Coll Cardiol. 2017;70(25):3157-72. doi: https://doi.org/10.1016/j.jacc.2017.10.063

22. Chapeau C, Gutkowska J, Schiller PW, Milne RW, Thibault G, Garcia R, Genest J, et al. Localization of immunoreactive synthetic atrial natriuretic factor (ANF) in the heart of various animal species. J Histochem Cytochem. 1985;33(6):541-50. doi: https://doi.org/10.1177/33.6.3158698

23. Evora PRB, Menardi AC, Celotto AC, Albuquerque AAS, Chagas HMA, Rodrigues AJ. The Left Atrial Appendage Revised. Braz J Cardiovasc Surg. 2017;32(6):517-22. doi: https://doi.org/10.21470/1678-9741-2017-0085

24. Davis CA 3rd, Rembert JC, Greenfield JC Jr. Compliance of left atrium with and without left atrium appendage. Am J Physiol. 1990;259(4 Pt 2):H1006-8. doi: https://doi.org/10.1152/ajpheart.1990.259.4.H1006

25. Yaghi S, Song C, Gray WA, Furie KL, Elkind MS, Kamel H. Left Atrial Appendage Function and Stroke Risk. Stroke. 2015;46(12):3554-9. doi: https://doi.org/10.1161/STROKEAHA.115.011273

26. Qamruddin S, Shinbane J, Shriki J, Naqvi TZ. Left atrial appendage: structure, function, imaging modalities and therapeutic options. Expert

Rev Cardiovasc Ther. 2010;8(1):65-75. doi: https://doi.org/10.1586/erc.09.161

27. Kurzawski J, Janion-Sadowska A, Sadowski M. Left atrial appendage function assessment and thrombus identification. Int J Cardiol Heart Vasc. 2016;14:33-40. doi: https://doi.org/10.1016/j.ijcha.2016.11.003

28. Pollick C, Taylor D. Assessment of left atrial appendage function by transesophageal echocardiography. Implications for the development of thrombus. Circulation. 1991;84(1):223-31. doi: https://doi.org/10.1161/01.cir.84.1.223

29. Nucifora G, Faletra FF, Regoli F, Pasotti E, Pedrazzini G, Moccetti T, et al. Evaluation of the left atrial appendage with real-time 3-dimensional transesophageal echocardiography: implications for catheter-based left atrial appendage closure. Circ Cardiovasc Imaging. 2011;4(5):514-23. doi: https://doi.org/10.1161/CIRCIMAGING.111.963892

30. Stoddard MF, Dawkins PR, Prince CR, Ammash NM. Left atrial appendage thrombus is not uncommon in patients with acute atrial fibrillation and a recent embolic event: a transesophageal echocardiographic study. J Am Coll Cardiol. 1995 Feb;25(2):452-9. doi: https://doi.org/10.1016/0735-1097(94)00396-8

31. Ho SY, Cabrera JA, Sanchez-Quintana D. Left atrial anatomy revisited. Circ Arrhythm Electrophysiol. 2012;5(1):220-8. doi: https://doi.org/10.1161/CIRCEP.111.962720

32. Zotz RJ, Müller M, Genth-Zotz S, Darius H. Spontaneous echo contrast caused by platelet and leukocyte aggregates? Stroke. 2001;32(5):1127-33. doi: https://doi.org/10.1161/01.str.32.5.1127

33. Mahony C, Ferguson J, Fischer PL. Red cell aggregation and the echogenicity of whole blood. Ultrasound Med Biol. 1992;18(6-7):579-86. doi: https://doi.org/10.1016/0301-5629(92)90072-i

34. Merino A, Hauptman P, Badimon L, Badimon JJ, Cohen M, Fuster V, et al. Echocardiographic "smoke" is produced by an interaction of erythrocytes and plasma proteins modulated by shear forces. J Am Coll Cardiol. 1992;20(7):1661-8. doi: https://doi.org/10.1016/0735-1097(92)90463-w

35. Saric M, Armour AC, Arnaout MS, Chaudhry FA, Grimm RA, Kronzon I, et al. Guidelines for the Use of Echocardiography in the Evaluation of a Cardiac Source of Embolism. J Am Soc Echocardiogr. 2016;29(1):1-42. doi: https://doi.org/10.1016/j.echo.2015.09.011

36. Vigna C, Russo A, De Rito V, Perna G, Villella A, Testa M, et al. Frequency of left atrial thrombi by transesophageal echocardiography in idiopathic and in ischemic dilated cardiomyopathy. Am J Cardiol. 1992;70(18):1500-1. doi: https://doi.org/10.1016/0002-9149(92)90310-u

37. Acar J, Cormier B, Grimberg D, Kawthekar G, Iung B, Scheuer B, Farah E. Diagnosis of left atrial thrombi in mitral stenosis--usefulness of ultrasound techniques compared with other methods. Eur Heart J. 1991;12 Suppl B:70-6. doi: https://doi.org/10.1093/eurheartj/12.suppl_b.70

38. Manning WJ, Weintraub RM, Waksmonski CA, Haering JM, Rooney PS, Maslow AD, et al. Accuracy of transesophageal echocardiography for identifying left atrial thrombi. A prospective, intraoperative study. Ann Intern Med. 1995;123(11):817-22. doi: https://doi.org/10.7326/0003-4819-123-11-199512010-00001

39. Roijer A, Eskilsson J, Olsson B. Transoesophageal echocardiography-guided cardioversion of atrial fibrillation or flutter. Selection of a low-risk group for immediate cardioversion. Eur Heart J. 2000;21(10):837-47. doi: https://doi.org/10.1053/euhj.1999.1869

40. Klein AL, Grimm RA, Murray RD, Apperson-Hansen C, Asinger RW, Black IW, et al.; Assessment of Cardioversion Using Transesophageal Echocardiography Investigators. Use of transesophageal echocardiography to guide cardioversion in patients with atrial fibrillation. N Engl J Med. 2001;344(19):1411-20. doi: https://doi.org/10.1056/NEJM200105103441901

41. Hahn RT, Abraham T, Adams MS, Bruce CJ, Glas KE, Lang RM, et al. Guidelines for performing a comprehensive transesophageal echocardiographic examination: recommendations from the American Society of Echocardiography and the Society of Cardiovascular Anesthesiologists. J Am Soc Echocardiogr. 2013;26(9):921-64. doi: https://doi.org/10.1016/j.echo.2013.07.009

42. Fatkin D, Kelly RP, Feneley MP. Relations between left atrial appendage blood flow velocity, spontaneous echocardiographic contrast and thromboembolic risk in vivo. J Am Coll Cardiol. 1994;23(4):961-9. doi: https://doi.org/10.1016/0735-1097(94)90644-0

43. Transesophageal echocardiographic correlates of thromboembolism in high-risk patients with nonvalvular atrial fibrillation. The Stroke Prevention in Atrial Fibrillation Investigators Committee on Echocardiography. Ann Intern Med. 1998;128(8):639-47. doi: https://doi.org/10.7326/0003-4819-128-8-199804150-00005

44. García-Fernández MA, Torrecilla EG, San Román D, Azevedo J, Bueno H, Moreno MM, et al. Left atrial appendage Doppler flow patterns: implications on thrombus formation. Am Heart J. 1992;124(4):955-61. doi: https://doi.org/10.1016/0002-8703(92)90978-5

45. Mügge A, Kühn H, Nikutta P, Grote J, Lopez JA, Daniel WG. Assessment of left atrial appendage function by biplane transesophageal echocardiography in patients with nonrheumatic atrial fibrillation: identification of a subgroup of patients at increased embolic risk. J Am Coll Cardiol. 1994;23(3):599-607. doi: https://doi.org/10.1016/0735-1097(94)90743-9

46. Santiago D, Warshofsky M, Li Mandri G, Di Tullio M, Coromilas J, Reiffel J, et al. Left atrial appendage function and thrombus formation in atrial fibrillation-flutter: a transesophageal echocardiographic study. J Am Coll Cardiol. 1994;24(1):159-64. doi: https://doi.org/10.1016/0735-1097(94)90557-6

47. Li YH, Lai LP, Shyu KG, Hwang JJ, Kuan P, Lien WP. Clinical implications of left atrial appendage flow patterns in nonrheumatic atrial fibrillation. Chest. 1994;105(3):748-52. doi: https://doi.org/10.1378/chest.105.3.748

48. Maltagliati A, Galli CA, Tamborini G, Celeste F, Muratori M, Pepi M. Incidence of spontaneous echocontrast, 'sludge' and thrombi before cardioversion in patients with atrial fibrillation: new insights into the role of transesophageal echocardiography. J Cardiovasc Med (Hagerstown). 2009;10(7):523-8. doi: https://doi.org/10.2459/JCM.0b013e32832b355a

49. Yao SS, Ilercil A, Meisner JS, Strom JA, Shirani J. Improved Doppler echocardiographic assessment of the left atrial appendage by peripheral vein injection of sonicated albumin microbubbles. Am Heart J. 1997;133(4):400-5. doi: https://doi.org/10.1016/s0002-8703(97)70180-7

50. von der Recke G, Schmidt H, Illien S, Lüderitz B, Omran H. Use of transesophageal contrast echocardiography for excluding left atrial appendage thrombi in patients with atrial fibrillation before cardioversion. J Am Soc Echocardiogr. 2002;15(10 Pt 2):1256-61. doi: https://doi.org/10.1067/mje.2002.123961

51. Mizuguchi KA, Burch TM, Bulwer BE, Fox AA, Rizzo RJ, Shernan SK. Thrombus or bilobar left atrial appendage? Diagnosis by real-time three-dimensional transesophageal echocardiography. Anesth Analg. 2009;108(1):70-2. doi: https://doi.org/10.1213/ane.0b013e3181857e53

52. Manning WJ, Silverman DI, Gordon SP, Krumholz HM, Douglas PS. Cardioversion from atrial fibrillation without prolonged anticoagulation with use of transesophageal echocardiography to exclude the presence of atrial thrombi. N Engl J Med. 1993;328(11):750-5. doi: https://doi.org/10.1056/NEJM199303183281102

53. Black IW. Spontaneous echo contrast: where there's smoke there's fire. Echocardiography. 2000;17(4):373-82. doi: https://doi.org/10.1111/j.1540-8175.2000.tb01153.x

54. Goldman ME, Pearce LA, Hart RG, Zabalgoitia M, Asinger RW, Safford R, Halperin JL. Pathophysiologic correlates of thromboembolism in nonvalvular atrial fibrillation: I. Reduced flow velocity in the left atrial appendage (The Stroke Prevention in Atrial Fibrillation [SPAF-III] study).

J Am Soc Echocardiogr. 1999;12(12):1080-7. doi: 10.1016/s0894-7317(99)70105-7.

55. Black IW, Hopkins AP, Lee LC, Walsh WF. Left atrial spontaneous echo contrast: a clinical and echocardiographic analysis. J Am Coll Cardiol. 1991;18(2):398-404. doi: https://doi.org/10.1016/0735-1097(91)90592-w

56. Troughton RW, Asher CR, Klein AL. The role of echocardiography in atrial fibrillation and cardioversion. Heart. 2003;89(12):1447-54. doi: https://doi.org/10.1136/heart.89.12.1447

57. Bernier M, Abdelmoneim SS, Stuart Moir W, Eifert Rain SS, Chandrasekaran K, Ammash NM, et al. CUTE-CV: a prospective study of enhanced left atrial appendage visualization with microbubble contrast agent use during transesophageal echocardiography guided cardioversion. Echocardiography. 2013;30(9):1091-7. doi: https://doi.org/10.1111/echo.12240

58. Posada-Martinez EL, Trejo-Paredes C, Ortiz-Leon XA, Ivey-Miranda JB, Lin BA, McNamara RL, et al. Differentiating spontaneous echo contrast, sludge, and thrombus in the left atrial appendage: Can ultrasound enhancing agents help? Echocardiography. 2019;36(7):1413-7. doi: https://doi.org/10.1111/echo.14405

Editorial

Infective Endocarditis In India: A Broad Picture Of A Very Large Country

Endocardite Infecciosa na Índia: Um Panorama de um País Enorme

Ashish Agrawal[1], Shantanu P Sengupta[2]
Korba Diabetic & Cardio Center Korba,[1] Sengupta Hospital & Research Institute,[2] Nagpur, Índia.

Everything is recycled in India,
Even dreams
Shashi Tharoor

Infective endocarditis (IE) has always been challenging for the medical field, which has responded with newer innovations and persistent efforts. Habib et al. stated "Infective endocarditis is still a life-threatening disease with the frequent lethal outcome despite profound changes in its clinical, microbiological, imaging, and therapeutic profiles"[1].

Various factors affect the different aspects of IE diagnosis and management. As a developing country, India has a very polar healthcare delivery system. Primary health centers range from basic facilities that provide very primary level healthcare in rural areas to center of excellence hospitals that offer the latest medical innovations in metropolitan areas. The crucial point is the time it takes for a patient to reach to suitable center to receive the appropriate interventions. In particular, the diagnosis of IE by primary healthcare physicians must be obtained as soon as possible. Socio-economic factors play a pivotal role in patient outcomes. All three of these issues pose great challenges, especially in very large countries like India. Sengupta et al. concluded that socio-economic factors influence the clinical profile of patients presenting with IE worldwide[2], leading to delayed diagnosis and lower use of surgery[2]. Gupta et al. reported observations about IE such as increasing patient age and increased proportions of patients without a history of cardiac ailments, better cultural positivity rates, an increasing incidence of staphylococcal infections, increased usage of transesophageal echocardiography (TEE), and increasing elective surgery rates[3].

Gupta et al. summarized the risk factors for IE as a longer lifespan contributing to degenerative heart disease and the risk of immune suppression due to diabetes, human immunodeficiency virus, immunosuppressive drugs, and intravenous drug abuse[4].

Various procedures require invasive instruments for the gastrointestinal and genitourinary tracts, arteriovenous fistula for dialysis, pacemaker and defibrillator implantation, and immunosuppressive therapy[4]. Few cases (10–15%) reportedly required healthcare intervention[5] than IE due to rheumatic heart disease[4].

Fever, heart murmur, and splenomegaly should be considered highly suggestive of IE and lead to its early diagnosis[4].

Mailing Address: Shantanu P Sengupta •
senguptasp@gmail.com
Artigo recebido em 5/3/2022; revisado em 5/15/2022; aceito em 5/25/2022

DOI: 10.47593/2675-312X/20223502eed_15

The clinical presentation can vary but most often includes the following (in order of most common to least common): fever, chills or sweating, shortness of breath with a history of loss of appetite or weight, chest pain, and peripheral edema[6].

The microbiological profile involves a wide spectrum of species including staphylococci, streptococci, enterococci, *Streptococcus gallolyticus*, *Streptococci viridians, Streptococcus sanguis, Streptococcus bovis, Streptococcus mutans, Streptococcus mitis*, and others such as *Coxiellaburnetii*, *Legionella* spp., *Chlamydia*, *Mycoplasma* spp., *Streptobacillus moniliformis*, *Salmonella* spp., *Brucella* spp., *Bartonella* spp., *Tropheryma whippelei*, *Pseudomonas aeruginosa*, and the HACEK group (*Haemophilus, Aggregatibacter, Cardiobacterim, Eikenella,* and *Kingella*)[1,4].

After an 11-year study, Navneet et al. concluded that predominant sites affected by IE include the tricuspid valve, followed by the mitral valve and the aortic and pulmonary valves[6]. Multivalvular involvement is also encountered. Vegetations are commonly 10–30 mm in diameter[6]. Blood cultures using modified Duke`s criteria and two-dimensional echocardiography/TEE/transthoracic echocardiography (TTE) remain the principal diagnostic modalities. However, culture positivity rates vary widely nationwide (30–70%)[7,8]. Different non-invasive techniques such as multi-slice computed tomography, magnetic resonance imaging, and nuclear imaging such as ^{18}F-fluorodeoxyglucose positron emission tomography are gaining popularity[1]. Echocardiography can be useful for predicting complications based on vegetation size, mobility, extent, and consistency[4]. TTE is the procedure of choice[9]. TEE is better in cases of prosthetic valves since its image quality is superior due to higher transducer frequency and no interference of lung tissue[9]. Abscesses, vegetations, and destructive lesions are the anatomical features and main findings of IE on echocardiography[10]. Polymerase chain reaction (PCR) amplification of prokaryotic 165 rDNA (recombinant deoxyribonucleic acid) is helpful for demonstrating the presence of bacteria within the heart valve[4]. Newer PCR techniques include nested PCR, real-time PCR, and LightCycler technology[11], but the above techniques are not readily available or cost-effective in developing countries.

Medical management consists of various regimens including injectable vancomycin, gentamycin, ceftriaxone, nafcillin, oxacillin, cefazolin, and rifampin, which are used according to the organism isolated in culture. An increasing trend in surgical intervention is aiming to lower mortality rates. Shock, congestive heart failure, and staphylococcal endocarditis are associated with a higher mortality risk in India[7] as well as other parts of the world[8,12]. The disease profile of patients is shifting from young patients with rheumatic heart disease to those with prosthetic valves or underlying valvular disease[7].

Surgical management and timing are crucial in IE. Indications for surgery are heart failure, uncontrolled infection, and embolism risk[13]. Two major societies, the European Society of Cardiology(ESC) and the American Heart Association (AHA)/American College of Cardiology (ACC), agree on these indications but differ in some areas. The ESC proposes urgent/ emergent versus elective surgery, whereas the ACC/AHA recommends early surgery before antibiotics are stopped[13]. Surgery is recommended by the ACC/AHA for vegetations >10 mm versus by the ESC for those >30 mm[13].

The biggest challenge in the Indian subcontinent is obtaining sterile blood cultures since tested patients have likely already received antibiotics from their primary care physicians. Around 2.5–31% of cases in India are blood culture–negative IE due to the use of antibiotics before diagnosis and poor adherence to blood culture guidelines[4]. Strong suspicion, correlation between clinical findings and the history and work-up leads to early detection and better outcomes. Thus, the need for microbiology labs and echocardiography facilities across India for early detection is crucial. The second hurdle is a reluctance to receive surgical intervention; however, in-depth counseling can remedy this barrier. This response has ramped up in India over the past few decades. Early suspicion leads to early detection is seen, and increases in medical and surgical interventions are helping fight IE.

Conflict of interest

The author declares no conflicts of interest.

References

1. Habib G, Erba PA, Iung B, Donal E, Cosyns B, Laroche C, et al.; EURO-ENDO Investigators. Clinical presentation, aetiology and outcome of infective endocarditis. Results of the ESC-EORP EURO-ENDO (European infective endocarditis) registry: a prospective cohort study. Eur Heart J. 2019;40(39):3222-32. doi: https://doi.org/10.1093/eurheartj/ehz620. Erratum in: Eur Heart J. 2020;41(22):2091.

2. Sengupta SP, Prendergast B, Laroche C, Furnaz S, Ronderos R, Almaghraby A, et al.; EURO-ENDO Investigators Group. Socio-Economic Variations Determine the Clinical Presentation, Aetiology and Outcome of Infective Endocarditis: a Prospective Cohort Study from the ESC-EORP EURO-ENDO (European Infective Endocarditis) Registry. Eur Heart J Qual Care Clin Outcomes. 2022:qcac012. doi: https://doi.org/10.1093/ehjqcco/qcac012.

3. Gupta A, Gupta A, Kaul U, Varma A. Infective endocarditis in an Indian setup: Are we entering the 'modern' era? Indian J Crit Care Med. 2013;17(3):140-7. doi: https://doi.org/10.4103/0972-5229.117041.

4. Gupta R. Infective endocarditis: Indian scenario. India: API Text book of Medicine; 2013. p. 135-41. Available from: https://apiindia.org/wp-content/uploads/medicine_update_2013/chap29.pdf

5. R M, V R, Nambi PS, Ramakrishnan B, Gopalakrishnan R, Sathyamurthy. Profile of Infective Endocarditis: At a Tertiary Care Referral Centre. J Assoc Physicians India. 2018;66(6):60-5. PMID: 31331138.

6. Arora N, Panda PK, Cr P, Uppal L, Saroch A, Angrup A, et al. Changing spectrum of infective endocarditis in India: An 11-year experience from an academic hospital in North India. Indian Heart J. 2021;73(6):711-7. doi: https://doi.org/10.1016/j.ihj.2021.09.008

7. Abhilash KP, Patole S, Jambugulam M, Sathyendra S, Mitra S, Rebekah G, et al. Changing trends of infective endocarditis in India: a South Indian experience. Journal of Cardiovascular Disease Research. 2017;8;56-60. doi: https://doi.org/10.5530/jcdr.2017.2.13

8. Math RS, Sharma G, Kothari SS, Kalaivani M, Saxena A, Kumar AS, et al. Prospective study of infective endocarditis from a developing country. Am Heart J. 2011;162(4):633-8. doi: https://doi.org/10.1016/j.ahj.2011.07.014

9. Lindner JR, Case RA, Dent JM, Abbott D, Scheld WM, Kaul S. Diagnostic value of echocardiography in suspected endocarditis. Circulation. 1996;93:730-6. doi: https://doi.org/10.1161/01.CIR.93.4.730

10. Habib G, Badano L, Tribouilloy C, Vilacosta I, Zamorano JL, Galderisi M, et al.; European Association of Echocardiography. Recommendations for the practice of echocardiography in infective endocarditis. Eur J Echocardiogr. 2010;11(2):202-19. doi: https://doi.org/10.1093/ejechocard/jeq004

11. Fenollar F, Fournier PE, Raoult D. Molecular detection of Coxiella burnetii in the sera of patients with Q fever endocarditis or vascular infection. J Clin Microbiol. 2004;42(11):4919-24. doi: https://doi.org/10.1128/JCM.42.11.4919-4924.2004

12. Murdoch DR, Corey GR, Hoen B, Miró JM, Fowler VG Jr, Bayer AS, et al.; International Collaboration on Endocarditis-Prospective Cohort Study (ICE-PCS) Investigators. Clinical presentation, etiology, and outcome of infective endocarditis in the 21st century: the International Collaboration on Endocarditis-Prospective Cohort Study. Arch Intern Med. 2009;169(5):463-73. doi: https://doi.org/10.1001/archinternmed.2008.603

13. Wang A, Fosbøl EL. Current recommendations and uncertainties for surgical treatment of infective endocarditis: a comparison of American and European cardiovascular guidelines. Eur Heart J. 2022;43(17):1617-25. doi: https://doi.org/10.1093/eurheartj/ehab898.

My Approach to Imaging the Atrial Septal Defect by Three-Dimensional Echocardiography

Como Eu Faço a Avaliação Ecocardiográfica Tridimensional da Comunicação Interatrial

Dante Pazzanese Institute of Cardiology[1], São Paulo, SP, Brazil; Heart Institute of Hospital das Clínicas, School of Medicine, University of São Paulo (InCor-HCFMUSP)[2], São Paulo, SP, Brazil.

Daniela Lago Kreuzig[1,2]

Atrial septal defects (ASDs) correspond to 6–10% of all congenital heart diseases and are more prevalent in women; moreover, an estimated 60–75% of all cases correspond to ostium secundum (OS) ASDs, a defect affecting the intermediate septal region[1].

Transthoracic echocardiography (TTE) can be used to identify the defect, quantify the hemodynamic repercussions, estimate the pulmonary pressure, and identify other associated anomalies. Transesophageal echocardiography (TEE) is indicated for greater anatomical definitions, mainly in adults or in children with large defects in whom it is necessary to assess eligibility for percutaneous treatment.

Percutaneous treatment using a prosthesis is indicated in the following ASD cases: 1) OS type; 2) diameter less than 35 mm; 3) normal pulmonary venous drainage; 4) favorable borders around the defect (greater than 5 mm) except for the anterosuperior border, which may be absent; 5) hemodynamic repercussions (pulmonary and systemic flow ratio Qp/Qs > 1.5); 5) absence of fixed pulmonary hypertension; and 6) no other anomaly indicated for surgical treatment[1,2].

Three-dimensional (3D) echocardiography has become significantly relevant in this context of percutaneous treatment, since more than 90% of OS ASD cases are eligible for intervention. This technology is used in the echocardiography laboratory, mainly through transesophageal complementation in adults and patients weighting over 30 kg[3]. In our clinical practice, with the advent of more modern, smaller-caliber probes, we can perform this test in patients weighing more than 20 kg despite it not being recommended by the manufacturer.

However, the great advantage of the 3D technique is its use in the hemodynamics laboratory to guide closure of the OS ASD, which has a complex anatomy.

In my view, 3D acquisition in the pediatric population via the transthoracic window is very valuable for analyzing valves, performing volumetric assessments, and identifying particularities of complex heart diseases during surgical planning despite the limitations related to a high heart rate and breathing and movement artifacts. However, the specific anatomical detailing of the interatrial septum is usually insufficient and TEE resolution is superior considering its posterior location. Therefore, when treating a child with a large OS ASD, a candidate for percutaneous closure, I prefer to complement it with TEE, always under anesthesia, which results in a better quality test with fewer artifacts. Also, if the patient's weight allows it, we pass a 3D probe. Another issue of paramount importance is optimization of the two-dimensional (2D) image before 3D acquisition, which requires use of electrocardiography.

Next I will describe OS ASD assessment using the 3D technology aimed at percutaneous closure, i.e., via TTE and consider the different modes of acquisition, their advantages, and their use for this purpose.

Pre-procedural assessment

At the end of a detailed 2D TEE with a full septal analysis from the four-chamber view to bicaval section and color mapping, we commence the 3D image acquisition. The en-face projection of the ASD and the defect's positioning in the anatomic position provide valuable information from a single image: size, shape, location in the interatrial septum, characteristics of the defect's borders, and the presence of additional fenestration[3].

I usually start the 3D evaluation from the perspective of the right atrium to facilitate the identification of anatomical markers[2]. I acquire a medium angle block (3D or 4D zoom) or a large block (full-volume using the two-section tool) starting from an initial bicaval section and proceeding with approximate 90° rotation in the z-plane so that the superior and inferior vena cava are aligned in the vertical plane (i.e., superior vena cava at the 11 o'clock position) and the aorta in the anterior and superior region. I prefer not to use the narrow-angle mode for acquisition (live 3D or bird's eye

Keywords

Heart septal defects, atrial; Echocardiography, Three-Dimensional; Heart Defects, Congenital.

Mailing Address: Daniela Lago Kreuzig •
Avenida Dr. Dante Pazzanese, 500, Vila Mariana. CEP: 04012-909, São Paulo, SP, Brazil.
E-mail: danikreuzig@hotmail.com

Manuscript received 4/19/2022; revised 4/20/2022; accepted 4/26/2022.

DOI: 10.47593/2675-312X/20223502ecom32

view) or very high magnification due to a loss of anatomical references adjacent to the defect, which can interfere with this fundamental initial analysis[4]. From this reconstruction (Figure 1A), I can characterize the defect as unique, the OS type, having an oval shape, being central, being medium-sized, and having adequate borders. Video 1 shows the same ASD and allows assessment of the occurrence of dynamic variation in its dimension with the cardiac cycle.

We obtain the view of the left atrium[2] after 180° rotation on the axis of the AD panorama in an anatomical position (like turning the pages of a book) (Figure 1B, Video 2). The right superior pulmonary vein is adjacent to the superior vena cava (i.e., right superior pulmonary vein at the 1 o'clock position), the aorta is in a superior but leftward position, and the mitral valve is inferiorly and anteriorly located.

The ASD borders are classified to improve communication between the operator and the hemodynamics professional as follows: anteroinferior and superoposterior (in apical four-chamber view at 0°, border close to the atrioventricular valves and contralateral); anterosuperior and posterior (on the short axis of the aortic valve, at about 45°, border related to the aorta and contralateral); and, finally, posterosuperior and posteroinferior (in bicaval view at about 100° near the superior and inferior vena cava, respectively)[5,6].

Multiplanar reconstruction in three axes is possible after a high-quality 3D image is obtained to quantify measurements such as distance and/or area (Flexi-slice or 3DQ software). Thus, we obtain the true transverse plane of the defect (Figure 2), which allows us to make linear measurements comparable to those performed through standard 2D TEE

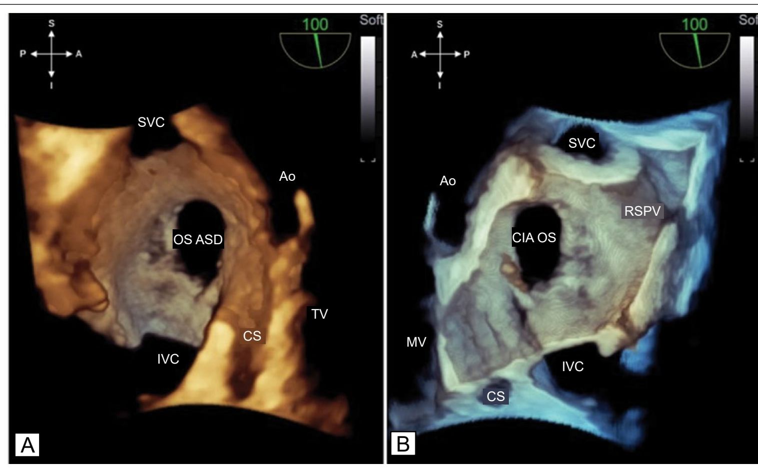

A, anterior; Ao, aorta; CS, coronary sinus; I, inferior; IVC, inferior vena cava; MV, mitral valve; OS ASD, ostium secundum atrial septal defect; P, posterior; RSPV, right superior pulmonary vein; S, superior; SVC, superior vena cava; and TV, tricuspid valve.

Figure 1 – *A) Three-dimensional image acquired by large block mode (full-volume) and manipulated by the two-sections tool starting from the bicaval section of the interatrial septum on transesophageal echocardiography. An en-face OS ASD is visible on the right atrial view in the anatomical position with adequate borders that is eligible for percutaneous closure. B) The same image taken from the left atrial perspective.*

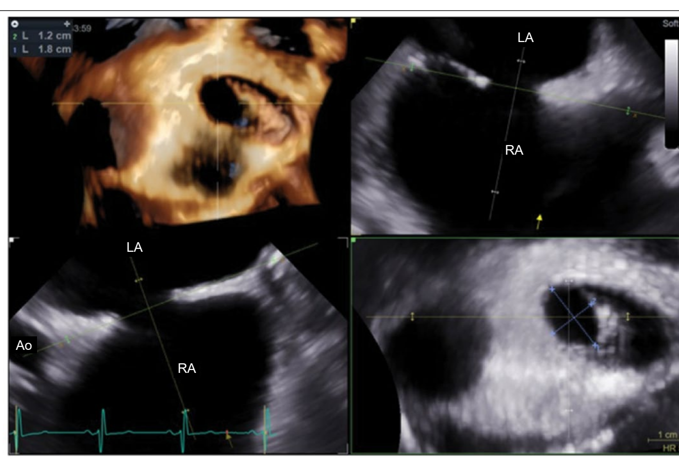

Ao, aorta; LA, left atrium; OS ASD, ostium secundum atrial septal defect; RA, right atrium.

Figure 2 – *Multiplanar reconstruction performed in three axes (flexi-slice) from a three-dimensional transesophageal echocardiography image taken in the true transverse plane of an OS ASD to measure the defect in its largest and smallest diameters (bottom right).*

sections[2]. Measuring the largest and smallest diameter of an ASD during atrial diastole is routinely performed. Handling the 3D image substantially improves the 2D understanding of septal defects with time and experience. Figure 3 compares the 3D image of two OS ASDs with their respective 2D sections and borders.

The most inferior and posterior region of the interatrial septum is the most difficult to access since it is closer to the transesophageal probe. However, most OS ASDs are located in the anterosuperior portion of the septum. It is mandatory to search for additional small defects in the presence of a larger anterosuperior OS ASD and a thin and redundant posterior or posteroinferior septum (even aneurysmal), which is present in an estimated 2.7% of cases[7].

Using this technology associated with color mapping (3D color view) to assess a simple OS ASD does not usually add information in the pre-assessment but substantially reduces the image frame rate. On the other hand, the tool with simultaneous 2D sections with color mapping (multidimensional or X-plane), which can be orthogonal in the presence of septa with several fenestrations, can help define the number, location, and proximity of fenestrations to one another.

Finally, the 3D assessment of an ASD is not time-consuming and image handling is concomitant with the test and performed by the device.

Intra-procedural assessment

The use of TEE to guide the percutaneous ASD closure requires knowledge of interatrial septal anatomy and the procedure's steps. The echocardiographer must help cross the defect with the catheter, position the guides and catheters in the pulmonary veins (usually in the left superior pulmonary vein), measure the defect in several planes, measure the diameter with a balloon catheter (as described later), open the left disk, waist, and right disk, position the device, and analyze the final result[5]. Videos 3, 4 and, 5 show 3D images of these steps. The imaging professional should inform the decision of which prosthesis is the best for the particular case.

A balloon catheter is usually passed through the ASD and slowly and progressively inflated during the echocardiographic evaluation with color mapping process. The outer to outer border of the balloon is measured at the moment the transseptal flow ceases (stop-flow technique)[2]. The chosen device is usually up to 2 mm above this measurement. Small fenestrations are commonly found in a thin redundant region of the septum (usually posteroinferiorly) after balloon inflation at the largest ASD. However, some hemodynamic professionals skip this step in the presence of a single OS ASD with thick and firm borders and opt for an overestimated prosthesis with a waist 20–30% larger than the baseline ASD measurement obtained by standard TEE sections[8].

The 3D complementation has great value in complex ASD cases such as an aneurysmal interatrial septum with multiple

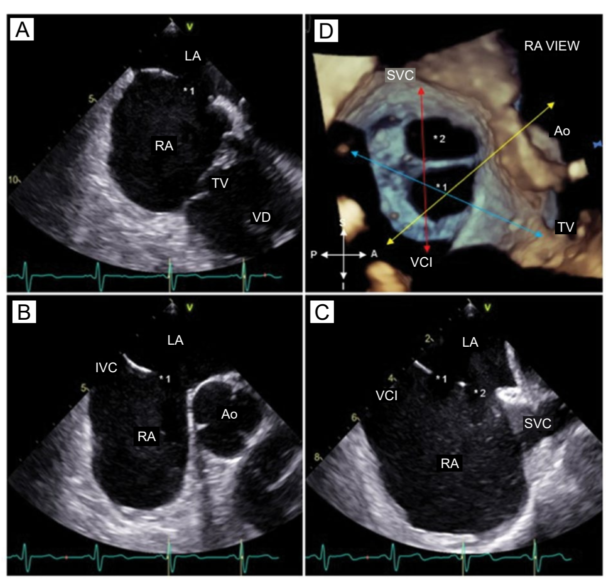

*A, anterior; Ao, aorta; CS, coronary sinus; I, inferior; IVC, inferior vena cava; LA, left atrium; OS ASDs, ostium secundum atrial septal defects; P, posterior; RA, right atrium; RV, right ventricle; S, superior; SVC, superior vena cava; TV, tricuspid valve; *1, most inferior OS ASD; *2, most superior OS ASD.*

Figure 3 – *Complex case of two OS ASDs assessed by two- and three-dimensional transesophageal echocardiography in the hemodynamics laboratory. A) Apical four-chamber view at 0° demonstrating the lowest ASD with adequate anteroinferior and superoposterior borders. Note that the border related to the atrioventricular valves is thicker and firmer. B) Short-axis view of the aortic valve at approximately 45° demonstrating only one of the ASDs with a deficient anterosuperior border. In this example, note that the inferior vena cava outflow is also considered in the section. C) The bicaval section at approximately 100°, with visualization of the two ASDs in two-dimensional view and posterosuperior and posteroinferior borders of appropriate dimensions. D) Three-dimensional view of the interatrial septum from the perspective of the right atrium showing the two large oval similarly sized ASDs, one superior to the other. Clearer anatomical definition was obtained by three-dimensional technology in this case. The colored arrows represent the corresponding two-dimensional sections: blue (A), yellow (B), and red (C).*

holes, two orifices distant from one another, the absence of one or more borders, and very large holes (>28 mm).

An aneurysmal interatrial septum must be very carefully analyzed and previous gain adjustments made to avoid misinterpretation of a drop-out image (due to a thin and mobile septum) as an additional ASD after 3D acquisition.

It is difficult to locate the hole through which guides or catheters can be passed in 2D tests in the presence of two or more holes, for example, considering that they may be superimposed. In this context, we can use two tricks of 3D technology. First, we can use two simultaneous 2D sections (multidimensional or X-plane) to distinguish the two holes with the advantage of the greater temporal and spatial resolution. Second, we can use the real-time image of a thin 3D slice with direct visualization of the material used by the hemodynamics professional passing through a certain hole. Figure 4 and Video 6 exemplify this procedure.

Another advantage of assessing the entire interatrial septum in the scenario of multiple defects is the decision to use a device for a septum with several fenestrations, a thin waist, or, in the case of defects that are quite distant from each other, the choice of two prostheses for the same patient. Figure 5 and Video 7 show the final result after the implantation of two prostheses in the same patient to close two large defects.

The conventional 2D technique associated with color mapping satisfactorily ensures prosthesis positioning, identifies borders between disks, and assesses heart valve and pericardial effusions at the end of the procedure.

ASDs with a more anterior and superior location in the absence of the aortic borders are more often associated with

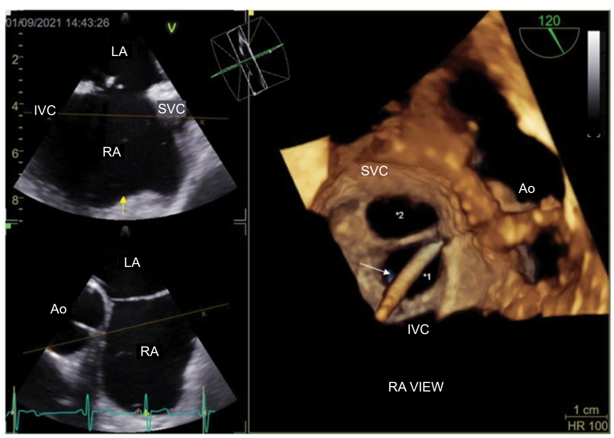

Ao, aorta; IVC: inferior vena cava, LA, left atrium; OS ASDs, ostium secundum atrial septal defects; RA, right atrium; RA VIEW, view of the right atrium; SVC, superior vena cava; *1, most inferior OS ASD; *2, most superior OS ASD.

Figure 4 – *Three-dimensional view of the interatrial septum from the right atrium showing two large OS ASDs and the catheter (arrow) passing through the most inferior ASD. Note the best anatomical detailing by three-dimensional transesophageal echocardiography technology to guide the interventional procedure of this complex case.*

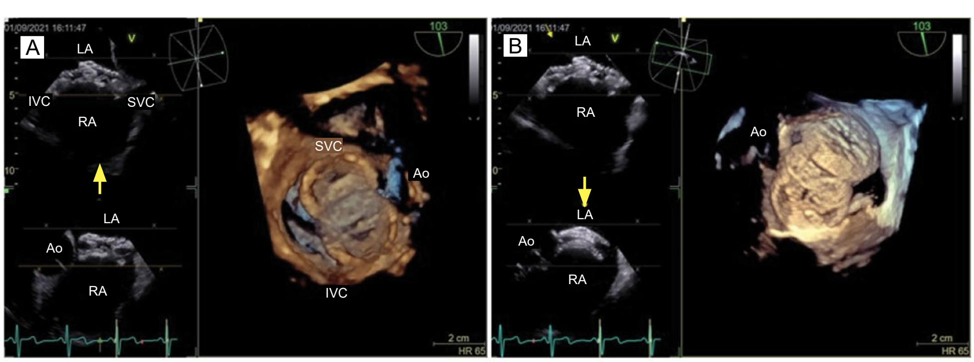

RA: right atrium; LA: left atrium; Ao: aorta; IVC: inferior vena cava; OS ASDs, ostium secundum atrial septal defects; SVC: superior vena cava.

Figure 5 – *A) Three-dimensional image of the interatrial septum with a right atrial view demonstrating the final result after the occlusion of both OS ASDs with two prostheses, in an anatomical position. B) Same image from left atrium perspective.*

aortic or atrial roof erosion. The 3D analysis of this region, including the transverse sinus, enables close follow-up due to the greater risk in such cases[2].

Device embolization is a rare (0.1–0.4%) but potentially serious event[1,2] that usually occurs early and requires re-catheterization or even surgery. The main cause of embolization is an undersized defect, especially in cases with redundant septa and the absence of one or more borders. Before releasing the device, any major and unusual movement can cause prosthesis instability and increase the risk of embolization.

The 3D assessments with color mapping are used in selected cases. In the presence of residual communication after closing the defect with a prosthesis, this technology defines flow size, shape, and proximity to the disk and estimates possible spontaneous closure during patient follow-up[2]. Another clinical condition is right or left ventricular diastolic dysfunction in which it is necessary to create a hole through the prosthesis to serve as a drain right after defect closure. In cases of congenital heart diseases such as pulmonary atresia with intact interventricular septum associated with OS ASD with repercussion, these holes allow some flow to be directed from the right to left atrium in the presence of diastolic right ventricular dysfunction, thus avoiding right heart failure due to unsaturation. On the other hand, in an older population already presenting with left ventricular diastolic dysfunction, the outflow would be from the left to right atrium to avoid abrupt volume overload in the left atrium and the potential for acute pulmonary edema. Figure 6 shows the case of an older patient with grade II diastolic dysfunction that persisted after an ASD occlusion test with a balloon catheter for ten minutes, during which it was decided to mechanically create two holes through the prosthesis mesh. These holes may close spontaneously during the normal prosthesis epithelialization process, but this benefit would be expected for a short time after the procedure.

Post-procedure assessment

TTE should be performed 24 hours after the procedure to assess device positioning and identify any pericardial effusions. It should then be repeated after 1, 3, 6, and 12 months and annually thereafter[1]. Transesophageal complementation is not necessary in cases of a normal progression and satisfactory acoustic window. The right heart chambers are significantly reduced and greater filling occurs of the left chambers, with cardiac remodeling evident at 3 months after the procedure. Small residual periprosthetic flows may disappear during the prosthesis epithelialization process that occurs during the first 6 months after catheterization. Acetylsalicylic acid anti-aggregation (3–5 mg/kg/day; maximum dose, 100 mg/day) is necessary during this period[8]. However, small residual flow persists in 3% of cases at 1 year after prosthesis implantation[2]. The prophylaxis for bacterial endocarditis should be extended if residual flow persists[8].

TEE is indicated in selected cases, such as in the presence of residual or additional ASD with hemodynamic repercussions. In this scenario, 3'D technology can be used to aggregate information for reintervention discussion purposes.

Final considerations

Percutaneous treatment is currently the treatment of choice for OS ASD with a favorable anatomy. The procedure-associated mortality rate is very low (0.05%), below that associated with surgery (0.13%)[2].

Echocardiography for interventional procedures is a growing and evolving area. The role of 3D echocardiography in the context of percutaneous OS ASD closure was highlighted here, especially in complex cases encountered in a hemodynamics laboratory.

Conflict of interest

The author declares a potential conflict of interest for being a consultant for Supri, Invasive, Tecmedic and Boynton.

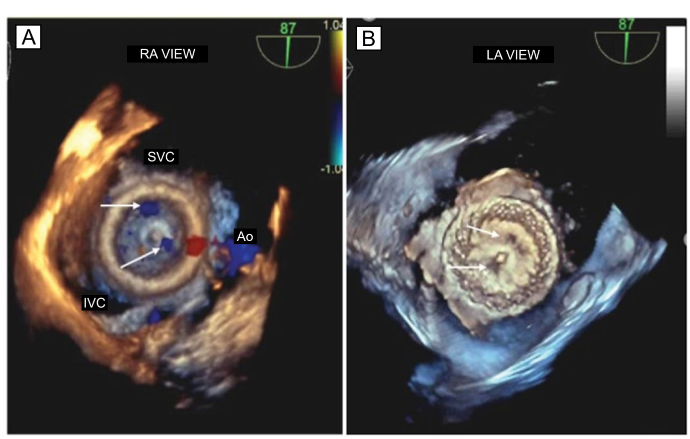

Ao, aorta; IVC, inferior vena cava; LA VIEW, view of the left atrium; RA VIEW, view of the right atrium; SVC, superior vena cava; white arrows: holes created in the prosthesis.

Figure 6 – *A) Three-dimensional view with color mapping of the interatrial septum in the anatomic position from the right atrial perspective after percutaneous occlusion of an OS ASD in an older patient with grade II diastolic dysfunction who had two holes created through the prosthesis mesh (white arrows). B) Left atrial view without color mapping.*

References

1. Silvestry FE, Cohen MS, Armsby LB, Burkule NJ, Fleishman CE, Hijazi ZM, et al.; American Society of Echocardiography; Society for Cardiac Angiography and Interventions. Guidelines for the Echocardiographic Assessment of Atrial Septal Defect and Patent Foramen Ovale: From the American Society of Echocardiography and Society for Cardiac Angiography and Interventions. J Am Soc Echocardiogr. 2015;28(8):910-58. doi: https://doi.org/10.1016/j.echo.2015.05.015

2. Bechis MZ, Rubenson DS, Price MJ. Imaging Assessment of the Interatrial Septum for Transcatheter Atrial Septal Defect and Patent Foramen Ovale Closure. Interv Cardiol Clin. 2017;6(4):505-524. doi: https://doi.org/10.1016/j.iccl.2017.05.004

3. Simpson J, Lopez L, Acar P, Friedberg MK, Khoo NS, Ko HH, et al. Three-dimensional Echocardiography in Congenital Heart Disease: An Expert Consensus Document from the European Association of Cardiovascular Imaging and the American Society of Echocardiography. J Am Soc Echocardiogr. 2017;30(1):1-27. doi: https://doi.org/10.1016/j.echo.2016.08.022

4. Saric M, Perk G, Purgess JR, Kronzon I. Imaging atrial septal defects by real-time three-dimensional transesophageal echocardiography: step-by-step approach. J Am Soc Echocardiogr. 2010;23(11):1128-35. doi: https://doi.org/10.1016/j.echo.2010.08.008

5. Vaidyanathan B, Simpson JM, Kumar RK. Transesophageal echocardiography for device closure of atrial septal defects: case selection, planning, and procedural guidance. JACC Cardiovasc Imaging. 2009;2(10):1238-42. doi: https://doi.org/10.1016/j.jcmg.2009.08.003.

6. Roldán FJ, Vargas-Barrón J, Vázquez-Antona C, Castellanos LM, Erdmenger-Orellana J, Romero-Cárdenas A, et al. Three-dimensional transesophageal echocardiography of the atrial septal defects. Cardiovasc Ultrasound. 2008;6:38. doi: https://doi.org/10.1186/1476-7120-6-38

7. Hahn RT, Saric M, Faletra FF, Garg R, Gillam LD, Horton K, et al. Recommended Standards for the Performance of Transesophageal Echocardiographic Screening for Structural Heart Intervention: From the American Society of Echocardiography. J Am Soc Echocardiogr. 2022;35(1):1-76. doi: https://doi.org/10.1016/j.echo.2021.07.006. Erratum in: J Am Soc Echocardiogr. 2022 Apr;35(4):447.

8. Ribeiro MS, Costa RN, Fernandes, SR, Pedra F, Kreuzig DL, Fontes VF et al. Estado Atual do Tratamento dos Defeitos do Septo Atrial. Rev Soc Cardiol Estado de São Paulo. 2017;27(1):39-48. doi: http://dx.doi.org/10.29381/0103-8559/2017270139-48.

My Approach to Echocardiography in Radiofrequency Ablation of Hypertrophic Obstructive Cardiomyopathy

Como Eu Faço Ecocardiograma na Ablação por Radiofrequência da Cardiomiopatia Hipertrófica Obstrutiva

Antonio Tito Paladino, Andrea de Andrade Vilela, Jorge Eduardo Assef, Bruno Pereira Valdigem

[1]Instituto Dante Pazzanese de Cardiologia, São Paulo, SP, Brazil; [2]Hospital SEPACO, São Paulo, SP, Brazil; [3]Hospital Vila Nova Star, São Paulo, SP, Brazil; [4]Grupo FLEURY, São Paulo, SP, Brazil; [5]Hospital São Luiz Jabaquara, São Paulo, SP, Brazil.

Introduction

Hypertrophic cardiomyopathy (HCM), an autosomal dominant genetic disease that affects one in 500 people,[1] is considered the most common isolated form of hereditary heart disease. HCM is characterized by varying degrees of ventricular hypertrophy, myocardial fiber disarray, interstitial fibrosis, and microvascular disease in the absence of cardiac or systemic conditions to justify these findings.[2]

Echocardiography, an invaluable tool for the diagnosis and follow-up of patients with HCM, is used to assess morphology, hemodynamic disorders, left ventricular (LV) function, and patient prognosis.[3] It also has a fundamental role in cases of hypertrophic obstructive cardiomyopathy (HOCM) in the indication of invasive treatments. Radiofrequency ablation (RFA) is a possible treatment under study.

After briefly reviewing HCM, we will describe the role of echocardiography in patient selection, intraprocedural RFA, and follow-up.

Genetic basis

HCM is caused by mutations in genes encoding the sarcomere protein, Z disk, or intracellular calcium modulators.[4] More than 1,500 mutations have been identified among more than 11 genes.[4]

Pathophysiological mechanisms

The combination of left ventricular outflow tract (LVOT) obstruction (LVOTO), mitral regurgitation (MR), diastolic dysfunction, and myocardial ischemia comprise the pathophysiological basis of HCM.[5]

The distinction between non-obstructive HCM and HOCM has great clinical importance, as the two conditions have different therapeutic strategies and prognosis.[6]

HOCM has a prevalence of one in 1,500 people. About one-third of patients with HCM have the non-obstructive form, one-third have significant obstruction at rest (defined as an instantaneous peak pressure gradient ≥ 30 mmHg), and one-third have latent obstruction (peak pressure gradient ≥ 30 mmHg after provocative maneuvers).[6] A pressure gradient ≥ 50 mmHg is considered hemodynamically important.

Obstruction is determined by an interaction between the septum, mitral valve, and subvalvular apparatus in addition to flow vectors generated in the ventricular cavity. The mechanisms responsible for LVOTO are: a) septal hypertrophy with LVOT narrowing, which increases the velocity and displaces the blood flow trajectory, which end up "dragging" the anterior mitral valve leaflets toward the interventricular septum[7] (Figure 1, Videos 1A and B); and b) morphological changes in the mitral valve apparatus (papillary muscles and anterior leaflet implantation and/or dimension) that may contribute to LVOTO.[8]

Left midventricular obstruction occurs in approximately 10% of patients with HCM; these patients often present with heart failure symptoms and are at increased risk of sudden death (SD) (Figure 2, Videos 2A and B).[10]

Mitral valve systolic anterior motion (SAM) is greater on the anterior versus posterior leaflet, resulting in coaptation distortion and dynamic mid-systolic regurgitation that is often directed to the lateral and posterior wall of the left atrium. The degree of MR varies according to the degree of LVOTO and the size of the posterior leaflet.[10]

The presence of a central or anterior jet should raise the suspicion of a primary mitral valve anomaly; in these cases, transesophageal echocardiography (TEE) is indicated to better elucidate the mechanism.[2]

The origins of the diastolic dysfunction and increased left ventricular filling pressures are multifactorial.[11] The hypertrophy, ischemia, and replacement fibrosis present in the myocardium are factors that increase myocardial stiffness and decrease compliance. The assessment of multiple parameters is recommended to define the degree of diastolic dysfunction (Figure 3). [12]

Diagnosis

The current diagnostic criteria for HCM are:

Maximum myocardial thickness measured in diastole > 15 mm of unexplained cause (in any LV segment); and

Septal and inferolateral wall thickness ratio > 1.3 in normotensive subjects or > 1.5 in hypertensive patients.[8]

Keywords

Echocardiography; Cardiac Hypertrophy; Ablation, Radio Frequency.

Mailing Address: Antonio Tito Paladino •

E-mail: atpf40@gmail.com

Manuscript received 3/16/2022; revised 3/17/2022; accepted 3/31/2022.

DOI: 10.47593/2675-312X/20223502ecom28

<< CONTENTS

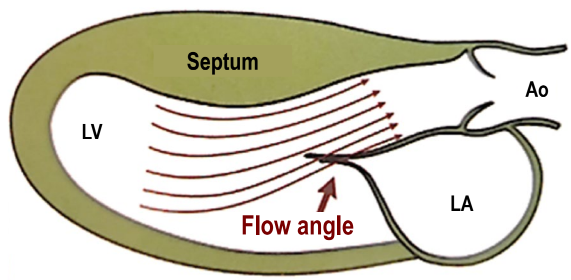

Source: Otto et al.[9]
LV: left ventricle; LA: left aorta; Ao: aorta.

Figure 1 – *Flow deviation caused by septal hypertrophy, generating an ejection flow angled in relation to the edges of the mitral valve that is ideal for "dragging" the leaflets toward the septum.*

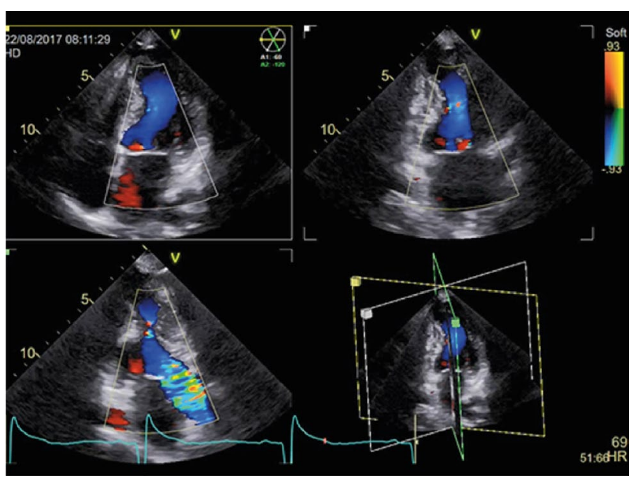

Source: Echocardiography Service of Instituto Dante Pazzanese de Cardiologia.

Figure 2 – *Hypertrophic cardiomyopathy with midventricular obstruction. Flow acceleration is visualized in three-chamber view (arrow).*

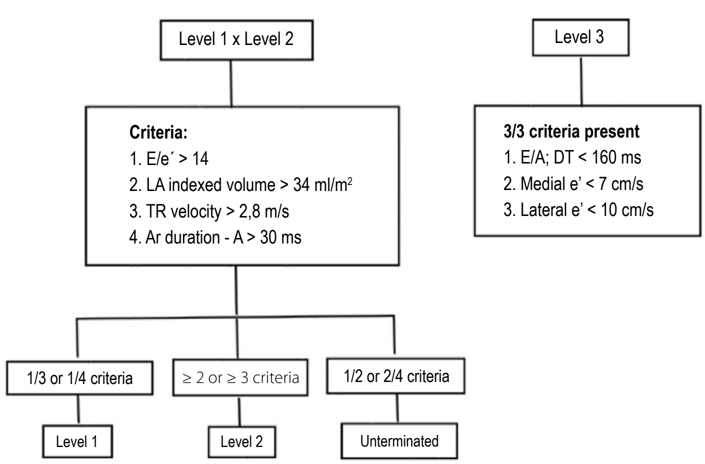

Ar-A, duration of the pulmonary reversal A wave – mitral A wave; DT, deceleration time; LA, left atrium; TR, tricuspid regurgitation. Source: Elliott PM et al.[2]

Figure 3 – *Algorithm used to determine the degree of diastolic dysfunction and filling pressures. It can be used regardless of the presence of LVOTO.*

A myocardial thickness ≥ 13 mm may be considered in the diagnosis of HCM in patients with a family history of HCM (especially if the electrocardiogram findings are abnormal). The distribution pattern of hypertrophy varies, with the asymmetric septal form being more common (70% of cases).[13]

Treatment

The pharmacological treatment of HCM is indicated in symptomatic patients. Beta-blockers are the first choice, disopyramide the second option, and verapamil is indicated for patients who are contraindicated to beta-blockers.[14]

In cases of significant obstruction (gradient > 50 mmHg at rest or after a provocative maneuver) with symptoms refractory to drug treatment, invasive measures may be necessary to alleviate symptoms and reduce the intraventricular gradient.[15]

Two invasive treatment methods are traditionally used to alleviate LVOT: surgical myectomy (SM) and alcohol septal ablation (ASA). SM is considered the gold standard and consists of partial resection of the hypertrophied septum, reducing the dynamic outflow tract obstruction.[2] ASA induces necrosis of the hypertrophied myocardium through the injection of alcohol into the septal perforating artery. Its use requires adequate anatomy, with the performance of contrast echocardiography being mandatory. If the contrast is not exclusively visualized in the basal septum, the procedure should be canceled.[2]

Recent articles on RFA reported favorable results.[16] RFA is an option in situations in which there are limitations to ASA and/or in midventricular obstructions. RFA is performed by electrophysiologists in a hemodynamics room and guided by a trained echocardiographer. Anatomical (place of greater thickness) and functional (place of greater velocity) information is analyzed on echocardiography, while electroanatomical mapping provides the other necessary information.[16] The patient is examined under general anesthesia in the supine position. The right femoral artery is punctured for retroaortic access to the septal region of the left ventricle, while the right femoral vein is punctured for the positioning of a quadripolar catheter in the right septum (to identify the bundle of His) and in the tip of the right ventricle. The therapeutic catheter is impacted at the point of greatest obstruction, where the radiofrequency is applied for 120 seconds (80 W and 60°C).

Role of echocardiography

In planning (preprocedural)

The purpose of the pre-RFA assessment is to determine the site of greatest myocardial thickness, assess the point of greatest flow obstruction (greater aliasing), record the maximum peak gradient, and identify changes in the mitral valve apparatus. The identification of the major primary or mixed MR makes SM more appropriate due to the possible need for mitral valve replacement. On the other hand, the identification of a significant midventricular gradient makes SM less indicated.

The morphofunctional analysis of the mitral cusps, subvalvular apparatus, and papillary muscles can elucidate the pathological mechanism mostly by TTE. TEE can be used in cases of limited acoustic window or uncertain mechanism of MR by TTE.

The LVOT flow assessment should consider the shape of the curve recorded by continuous Doppler, which typically resembles a dagger. This flow with peak mid-systolic velocity often varies with the Valsalva maneuver or physical exercise (Figures 4 and 5). Take care not to mismeasure MR as an intraventricular gradient.

During the procedure (intraprocedural)

The initial assessment is performed by TEE and aims to confirm the previously described findings: maximum peak gradient, greater aliasing point, and MR degree. Data on systolic function, left ventricular segmental contractility, and pericardial effusion are extremely important as they are compared with post-RFA findings (Figure 6).

Zero degree angles (in middle esophagus for five-chamber visualization), angles between 120° and 150°, and deep transgastric angles are the most commonly used to assess the site of greatest turbulence and measure maximum peak gradient. The gradient analysis should always consider the patient's blood pressure since, in cases of hypotension (very common during anesthesia), the value of the aorta-ventricle gradient may be higher than the one recorded in a previous examination.

The access route is usually retroaortic, but in cases in which passage of the catheter through the aortic valve is impossible (stenosis and significant calcification), access can occur via the transseptal route. The myocardium will be more echogenic (thermal injury) and slightly hypokinetic after the ablation

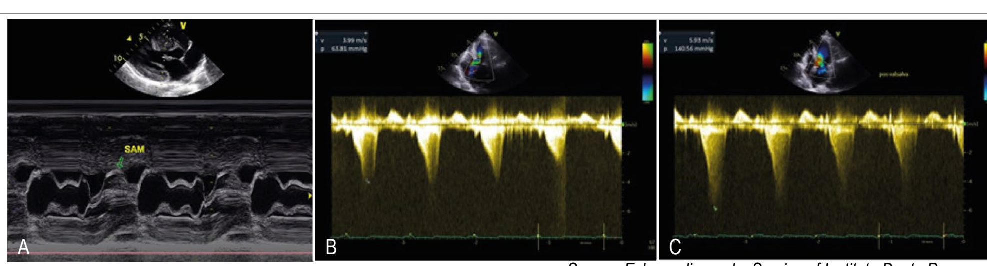

Source: Echocardiography Service of Instituto Dante Pazzanese de Cardiologia.

Figure 4 – *Preprocedural transthoracic echocardiogram: (A) M mode showing systolic anterior motion; (B) and (C) left ventricular outflow tract flows before and after the Valsalva maneuver.*

(Figure 7). A decreased SAM, and consequently a decreased degree of valve insufficiency, is an indicator of a good response to therapy (Figure 8,Table 1, Videos 3A and B).

In the follow-up period (postprocedural)

TTE should be performed 24–48 hours after the procedure to record the maximum peak gradient. During this period,

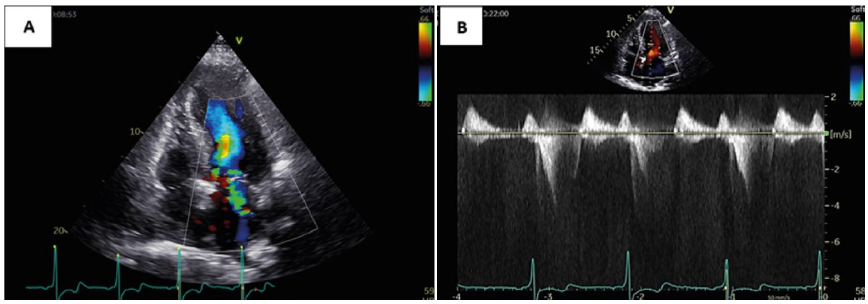

Source: Echocardiography Service of Instituto Dante Pazzanese de Cardiologia.

Figure 5 – *Preprocedural transthoracic echocardiogram: (A) four-chamber apical view with color flow mapping showing the site of greatest systolic flow turbulence. (B) left ventricular outflow tract mid-systolic flow was also recorded in the spectral recording of mitral regurgitation.*

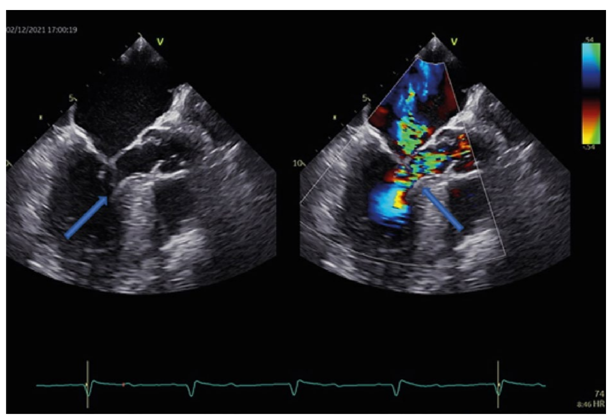

Source: Echocardiography Service of Instituto Dante Pazzanese de Cardiologia.

Figure 6 – *Intraprocedural transesophageal echocardiography with versus without color (at 150°): mitral valve assessment and systolic anterior motion identification and location. At this angle, we could more easily identify the site of greatest flow acceleration and the degree of mitral regurgitation.*

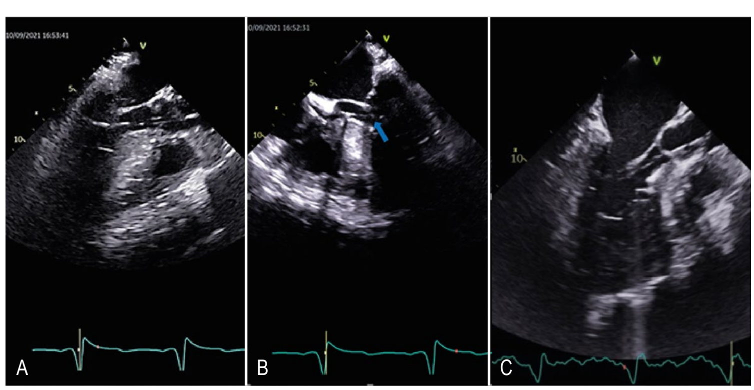

Source: Echocardiography Service of Instituto Dante Pazzanese de Cardiologia.

Figure 7 – *Intraprocedural transesophageal echocardiography at 120° (A) and 0° (B) showing the passage of the retroaortic catheter and its repositioning in the site of greatest flow obstruction. Catheter at 120° (C) during radiofrequency application the moment the myocardium becomes more echogenic and hypokinetic due to the thermal injury.*

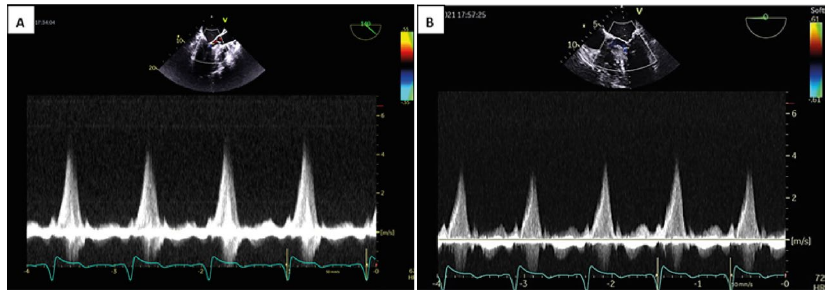

Source: Echocardiography Service of Instituto Dante Pazzanese de Cardiologia.

Figure 8 – *Intraprocedural transesophageal echocardiography with recording of maximum left ventricular outflow tract gradients before (A) and after (B) radiofrequency ablation with estimated values of 96 mmHg and 58 mmHg, respectively.*

Table 1 – Step-by-step echocardiography performed during the procedure.

Catheter access route and positioning
Step 1: Analyze gradients, valves, cavities, and pericardial space.
Step 2: Find where flow acceleration (SAM) occurs and what structures are involved.
Step 3: Guide the proper positioning of the ablation catheter (site of greatest acceleration).
During application
Step 1: Confirm that the catheter remains in the desired site.
Step 2: Confirm that the myocardium becomes hyperechoic, suggesting the therapy is effective.
Step 3: Confirm that the acceleration site changes with the application so that the catheter can be redirected, if necessary.
Step 4: Check the degree of MR, one indicator of therapeutic efficacy.
Step 5: Analyze the mitral and aortic valve apparatus to check if there was any damage during the procedure.

there are records of paradoxical gradient increase due to post-ablation wall edema.[15] The use of periprocedural dexamethasone seems to reduce the edema; however, further studies are required to assess its efficacy.

The literature reports progressively decreased gradients in up to a 1-year follow-up. TTE should be repeated after 3 months and annually thereafter if the clinical status shows no changes.[16]

Acknowledgments

Dr. Edileide de Barros Correia, responsible for the cardiomyopathies outpatient clinic at Instituto Dante Pazzanese de Cardiologia, for her attention and cordiality in choosing patients for our research.

Authors' contribution

Research creation and design: Paladino AT, VILELA, AA; Data acquisition: Paladino AT, Valdigem B; Manuscript writing: Paladino AT, VILELA, AA; Critical revision of the manuscript for important intellectual content: Assef JE.

Conflict of interest

The authors have declared that they have no conflict of interest.

References

1. Maron BJ. Hypertrophic cardiomyopathy. Lancet. 1997 Jul 12;350(9071):127-33. doi: https://doi.org/10.1016/S0140-6736(97)01282-8. Erratum in: Lancet 1997;350(9087):1330

2. Authors/Task Force members, Elliott PM, Anastasakis A, Borger MA, Borggrefe M, Cecchi F, et al. 2014 ESC Guidelines on diagnosis and management of hypertrophic cardiomyopathy: the Task Force for the Diagnosis and Management of Hypertrophic Cardiomyopathy of the European Society of Cardiology (ESC). Eur Heart J. 2014;35(39):2733-79. doi: https://doi.org/10.1093/eurheartj/ehu284

3. Afonso LC, Bernal J, Bax JJ, Abraham TP. Echocardiography in hypertrophic cardiomyopathy: the role of conventional and emerging technologies. JACC Cardiovasc Imaging. 2008;1(6):787-800. doi: https://doi.org/10.1016/j.jcmg.2008.09.002

4. Varma PK, Neema PK. Hypertrophic cardiomyopathy: part 1 - introduction, pathology and pathophysiology. Ann Card Anaesth. 2014;17(2):118-24. doi: https://doi.org/10.4103/0971-9784.129841

5. Bazan SG, Oliveira GO, Silveira CF, Reis FM, Malagutte KN, Tinasi LS, et al. Hypertrophic Cardiomyopathy: A Review. Arq Bras Cardiol. 2020;115(5):927-35. doi: https://doi.org/10.36660/abc.20190802

6. Maron MS, Olivotto I, Betocchi S, Casey SA, Lesser JR, Losi MA, Cecchi F, Maron BJ. Effect of left ventricular outflow tract obstruction on clinical outcome in hypertrophic cardiomyopathy. N Engl J Med. 2003 Jan 23;348(4):295-303. doi: 10.1056/NEJMoa021332.

7. Sherrid MV, Gunsburg DZ, Moldenhauer S, Pearle G. Systolic anterior motion begins at low left ventricular outflow tract velocity in obstructive hypertrophic cardiomyopathy. J Am Coll Cardiol. 2000;36(4):1344-54. doi: https://doi.org/10.1016/s0735-1097(00)00830-5

8. Silbiger JJ. Abnormalities of the Mitral Apparatus in Hypertrophic Cardiomyopathy: Echocardiographic, Pathophysiologic, and Surgical Insights. J Am Soc Echocardiogr. 2016;29(7):622-39. doi: https://doi.org/10.1016/j.echo.2016.03.003

9. Otto M, Netto F, Amorin I. Cardiomiopatia hipertrófica. In: Pena J, Vieira M, eds. Ecocardiografia e imagem cardiovascular. Rio de Janeiro: Thieme Revinter; 2021. p. 235-44.

10. Minami Y, Kajimoto K, Terajima Y, Yashiro B, Okayama D, Haruki S, et al. Clinical implications of midventricular obstruction in patients with hypertrophic cardiomyopathy. J Am Coll Cardiol. 2011;57(23):2346-55. doi: https://doi.org/10.1016/j.jacc.2011.02.033

11. Yang H, Carasso S, Woo A, Jamorski M, Nikonova A, Wigle ED, et al. Hypertrophy pattern and regional myocardial mechanics are related in septal and apical hypertrophic cardiomyopathy. J Am Soc Echocardiogr. 2010;23(10):1081-9. doi: https://doi.org/10.1016/j.echo.2010.06.006

12. Nagueh SF, Smiseth OA, Appleton CP, Byrd BF 3rd, Dokainish H, Edvardsen T, et al. Recommendations for the Evaluation of Left Ventricular Diastolic Function by Echocardiography: An Update from the American Society of Echocardiography and the European Association of Cardiovascular Imaging. J Am Soc Echocardiogr. 2016;29(4):277-314. doi: https://doi.org/10.1016/j.echo.2016.01.011

13. Maron MS, Olivotto I, Zenovich AG, Link MS, Pandian NG, Kuvin JT, et al. Hypertrophic cardiomyopathy is predominantly a disease of left ventricular outflow tract obstruction. Circulation. 2006;114(21):2232-9. doi: https://doi.org/10.1161/CIRCULATIONAHA.106.644682

14. Ommen SR, Mital S, Burke MA, Day SM, Deswal A, Elliott P, et al. 2020 AHA/ACC Guideline for the Diagnosis and Treatment of Patients With Hypertrophic Cardiomyopathy: Executive Summary: A Report of the American College of Cardiology/American Heart Association Joint Committee on Clinical Practice Guidelines. Circulation. 2020;142(25):e533-57. doi: https://doi.org/10.1161/CIR.0000000000000938

15. Cooper RM, Shahzad A, Hasleton J, Digiovanni J, Hall MC, Todd DM, et al. Radiofrequency ablation of the interventricular septum to treat outflow tract gradients in hypertrophic obstructive cardiomyopathy: a novel use of CARTOSound® technology to guide ablation. Europace. 2016;18(1):113-20. doi: https://doi.org/10.1093/europace/euv302

16. Valdigem BP, Correia EB, Moreira DA, Bihan D, Pinto IM, Abizaid AA, et al. Ablação septal com cateteres e radiofrequência guiada pela ecocardiografia para tratamento de pacientes com cardiomiopatia hipertrófica obstrutiva: experiência inicial. Arq Bras Cardiol. 2021;118(3). doi: https://doi.org/10.36660/abc.20201243

My Approach to Transseptal Mitral Valve-In-Valve

Como eu Faço Valve-in-Valve Mitral Via Transeptal

[1]Dante Pazzanese Cardiology Institute; [2]Institute of Cardiology and Transplantation of the Federal District; [3]Fleury Group; [4]Samaritano Hospital; [5]Vila Nova Star; [6]DF Star.

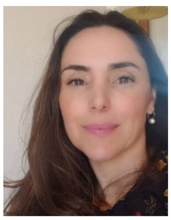

Andrea de Andrade Vilela[1,3]

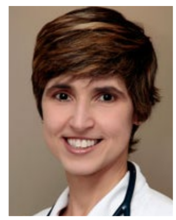

Maria Estefânia Bosco Otto[2,6]

Antonio Tito Paladino Filho[1,5]

Vanessa Andreoli Esmanhoto[1,4]

Introduction

The percutaneous treatment of heart valve disease is a subject of great interest in cardiology. Percutaneous aortic valve implantation, first performed in 2002 by Alan Cribier,[1] paved the way for transcatheter treatment of the mitral valve.

The first valve-in-valve (VIV) procedures were performed to treat deteriorated bioprosthetic valves in the aortic position.[2,3] In 2009, the group led by Dr. John Webb published the first successful case of mitral VIV.[4] Since then, mitral VIV has been performed in numerous centers worldwide.

Mitral valve disease has a significant prevalence worldwide,[5] particularly in Brazil. Its most frequent cause is rheumatic fever,[6] implying more severe valve diseases at a younger age that require early and repeated surgical procedures.[7] Knowing that bioprosthetic valve replacement is associated with high morbidity and mortality, VIV plays an extremely important role in avoiding or at least delaying surgery while improving patient quality of life.[5]

Keywords

Deart por Heart; Transthoracic Echocardiography; Treatment.

Mailing Address:

E-mail: andreadeandradevilela@gmail.com

Manuscript received 3/16/2022; revised 3/17/2022; accepted 3/31/2022.

DOI: 10.47593/2675-312X/20223502ecom24

Cardiovascular imaging multimodality is essential for transcatheter mitral valve interventions.[8] Here we will describe the role of echocardiography and computed tomography (CT) angiography in the different stages of evaluating mitral VIV.

Preprocedural assessment

Mitral VIV is a complex procedure that should only be performed after a careful heart team assessment to obtain better results.

The indication for mitral VIV depends on a series of data necessary to ensure its feasibility. Knowing the type and size of the implanted prosthesis is very useful for assessing the true internal diameter of the prosthesis and choosing the ideal endoprosthesis.[9] In the absence of information about surgical prosthesis type, fluoroscopy can provide important data for analyses of bioprosthetic valves.[10]

Role of echocardiography

Complete transthoracic echocardiography (TTE) followed by preprocedural transesophageal echocardiography (TEE) is essential, and the analysis main points include:

- Identify bioprosthesis failure mechanism and its quantification, including dysfunction type, degree, and, if possible, quantification;
- Rule out factors that contraindicate mitral VIV (Table 1)[11];

• Asses anatomical factors that predict left ventricular outflow tract (LVOT) obstruction (Table 2);

• Describe the characteristics of the interatrial septum, including the fact that the presence of extensive calcification, surgical patchs, thrombus, aneurysm, and exuberant lipomatous infiltration may hinder or prevent transseptal puncture;

• Analyse the hemodynamic repercussion of prosthetic dysfunction by assessing biventricular function and estimating pulmonary hypertension in which pulmonary dysfunction and hypertension worsen the outcome after surgical and/or percutaneous mitral valve treatment.[12,13]

Role of CT angiography

CT angiography is extremely important for analyzing the residual LVOT area after percutaneous prosthesis implantation (Figure 1) and the internal diameter of the annulus (Figure 2), which determines the implanted prosthesis size.[14,16]

The neo-LVOT area is calculated using an appropriate software that considers the LVOT measurement, the height of the percutaneous prosthesis, and the mitral-aortic angle, with the tolerated area to enable a VIV > 170 mm².[16]

As for the internal diameter of the prosthesis, the correct measurement is closely associated with the type of prosthesis implanted. In prostheses with internally sutured leaflets, the true diameter (true ID) of the annulus is 1 mm smaller than the measured value; prostheses with externally sutured leaflets have an internal diameter equal to that evaluated by CT angiography.[10,14]

Another relevant use of CT angiography is analyzing the coronary arteries, aorta, and lungs, adjuvant factors in the short- and long-term success of mitral VIV.[16]

Table 1 – Mitral valve-in-valve contraindications.

Absolute contraindication	Relative contraindication
Infectious endocarditis	Narrow left ventricular outflow tract
Prosthesis dehiscence	Paraprosthesis regurgitation
Extensive prosthesis thrombosis	Thrombus in the atrial cavity
Atrial septum thrombus	Major prosthesis-patient mismatch
Inferior vena cava interruption	Surgical repair of previous atrial septum
	Previous transseptal mitral valve repair

Source: Harloff et al.[11]

Table 2 – Anatomical factors predicting LVOT obstruction.

Echocardiography	Computed tomography
Basal septal hypertrophy	Estimated neo-outflow tract < 1.7 cm²
Small LV (<48 mm)	Less obtuse mitral-aortic angle (<115°)
Reduced distance from the IV septum to the mitral annulus (unfavorable if <17.8 mm)	

IV, interventricular; LV, left ventricle; LVOT, left ventricular outflow tract. Source: Pirelli et al.[14] e Yoon et al.[15]

Intraprocedural assessment

Mitral VIV should be performed in a hybrid operating room with the patient under general anesthesia (Figure 3). TEE plays a fundamental role in all the steps of the procedure as follows:

Initial assessment

TEE must be used to confirm the findings described in the preprocedural "Role of Echocardiography" assessment and rule out contraindications (Table 1).

Transseptal puncture orientation

This is a critical moment. The ideal for an appropriate puncture is the posteroinferior region of the lamina of the fossa ovalis. The use of 3D-TEE resources such as multi-D or X-plane are extremely important, as they provide optimal spatial orientation to the interventional physician, avoiding accidentally perforation of the aorta or heart cavity (Figure 4).[14]

RLVO, residual left ventricular outflow. Source: Internal archives from cardiac tomography and magnetic resonance of Dante Pazzanese Cardiology Institute.

Figure 1 – *Computed tomography image of estimated left ventricular outflow tract area with the implanted prosthesis chosen for the patient.*

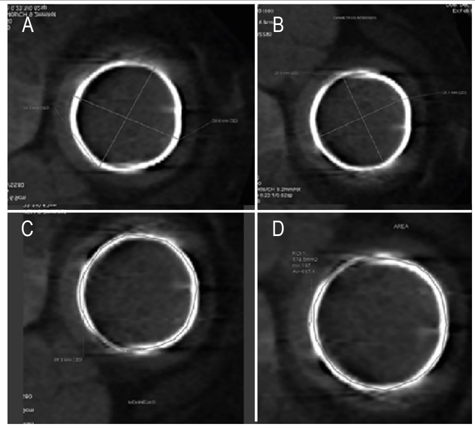

Source: Internal archives from cardiac tomography and magnetic resonance of Dante Pazzanese Cardiology Institute.

Figure 2 – *Tomography. (A) Measurement of the prosthesis' annulus. (B) Measurement of the prosthesis' internal diameter. (C) Measurement of the prosthesis' perimeter. (D) Measurement of the prosthesis' area.*

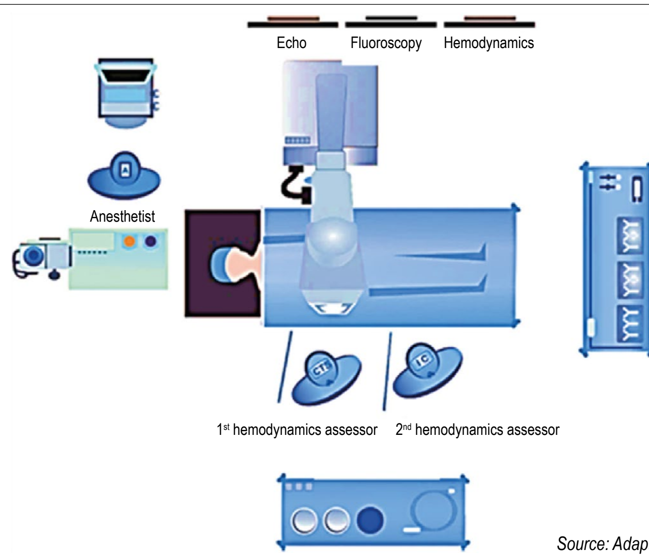

Source: Adapted from Harloff et al. Transseptal ViV-TMVR.[11]

Figure 3 – *hybrid operating room.*

Device position

The sequence of device positioning and release is detailed in Figure 5. The height of the percutaneous prosthesis implant is calculated by neo-LVOT on CT angiography.[14,16] The largest area usually occurs with 20% of the prosthesis in the atrial position and 80% in the ventricular position[14,16]; and postprocedural assessment must be performed systematically to ensure the absence of complications and to confirm the proper functioning of the new prosthesis.[16]

• Mitral endoprosthesis assessments are performed using 2D echocardiography (ECHO), 3D ECHO, and color flow mapping. The objective is to analyze whether the endoprosthesis is adequately expanded (circular shape, mobility, and adequate opening of leaflets) and identify the flow pattern (laminar or turbulent) in addition to the presence of central and/or paraprosthetic regurgitation and its quantification. The maximum and mean gradients of the endoprosthesis are recorded using continuous Doppler, while its area is defined using the continuity equation or 3D planimetry (figures 5 and 6 and video 1).

• LVOT assessment by color flow mapping and pulsed Doppler to detect high gradients. The technique of choice is deep transgastric view TEE at 0° or 5°, or even TTE (if flow alignment by TEE is inadequate). LVOT obstruction should be suspected in cases of hemodynamic deterioration immediately after endoprosthesis release and in the presence of turbulent outflow. These cases present an increase of ≥10 mmHg in mean LVOT gradient compared to the preprocedural assessment.[17]

• Ruling out the onset of pericardial effusion or changed left ventricular segmental contraction.

• Assessment of the atrial septum orifice status after puncture to determine its dimensions (orthogonal diameters and area,

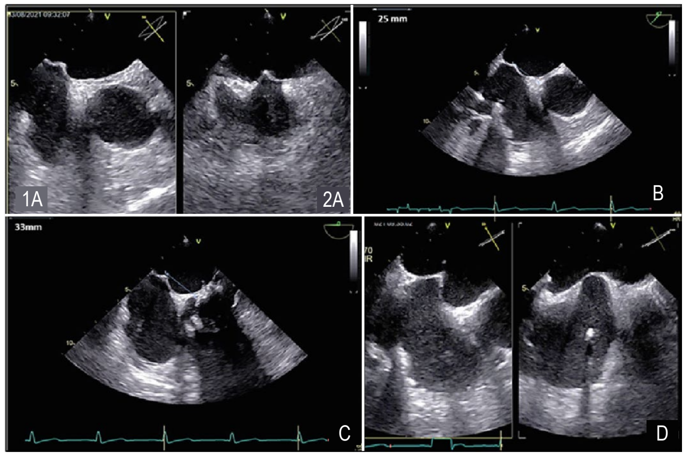

Source: Internal archive from Echocardiography division of Dante Pazzanese Institute of Cardiology.

Figure 4 – *Proper transseptal puncture sequence. Orthogonal multi-D three-dimensional transesophageal echocardiography images of the interatrial septum, its anterior (1A) and posterior (1B) portions with the image of a "tent" formed by the puncture needle. (B) The distance from the aortic puncture site should be assessed at 45°. (C) The puncture site must be a maximum of 35 mm away from the mitral annulus plane (performed at 0°). (D) Atrial septal transfixation by the puncture needle.*

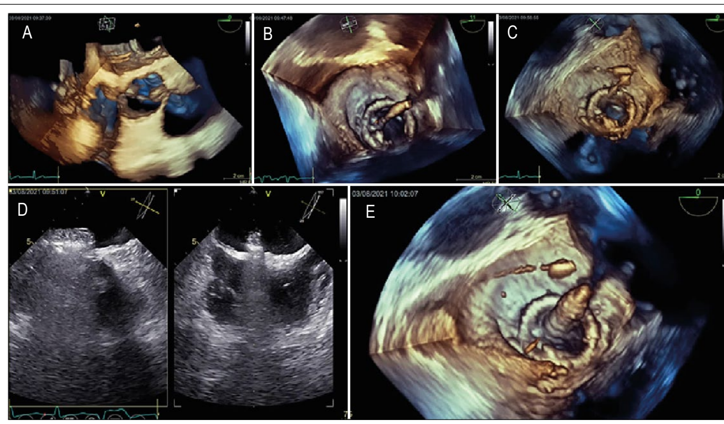

Source: Internal archive from Echocardiography division of Dante Pazzanese Institute of Cardiology.

Figure 5 – *Intraprocedural device positioning. (A) Passage of the catheter through the atrial septum. (B) Progression of the guide wire to the mitral prosthesis, passing into the left ventricle. (C) A rigid wire is passed to support release of the endoprosthesis. (D) At this time, the septal puncture orifice is usually dilated (to allow passage of the device delivery equipment). (E) Device position is evaluated (as central as possible to the bioprosthetic valve). Some degree of eccentricity is normally corrected with balloon inflation, which tends to naturally reposition the device in the center of the dysfunctional prosthesis.*

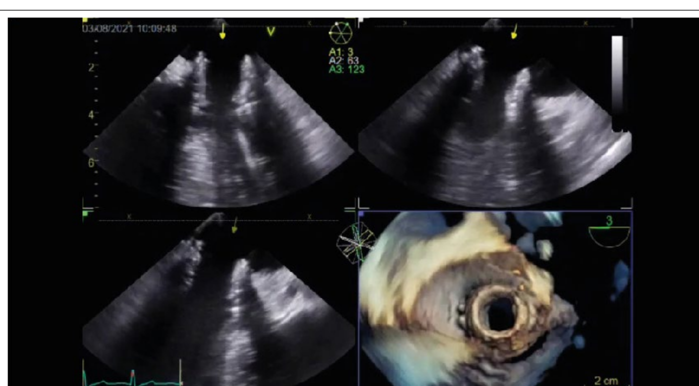

Source: Internal archive from Echocardiography division of Dante Pazzanese Institute of Cardiology.

Video 1 – *Endoprosthesis evaluation immediately after liberation.*

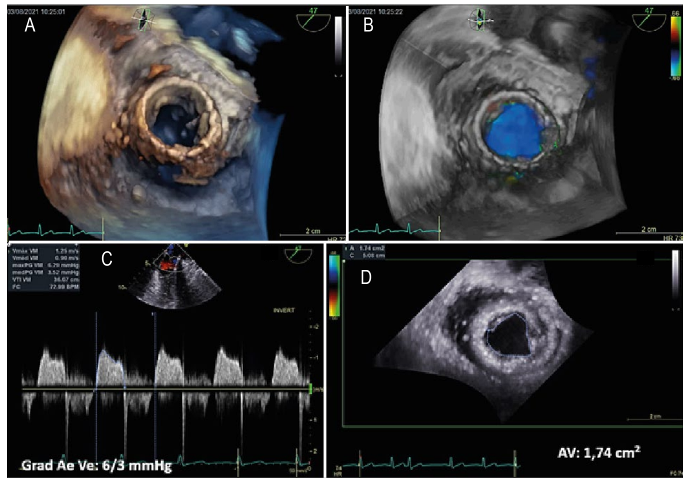

Source: Internal archive from Echocardiography division of Dante Pazzanese Institute of Cardiology.

Figure 6 – *Assessment after endoprosthesis release. (A) Three-dimensional echocardiogram (3D-ECHO) showing the endoprosthesis annulus inside the prosthetic annulus in diastole. (B) 3D-ECHO showing laminar flow delimiting the effective endoprosthesis orifice. (C) Left atrium-left ventricle gradient by continuous Doppler. (D) 3D planimetry used to estimate the endoprosthesis area.*

preferably by 3D ECHO) and the shunt direction through the orifice.

• Assessment of right ventricular function and tricuspid regurgitation and estimation of pulmonary artery systolic pressure.

Postprocedural assessment

Numbers of published cases and follow-up times remain small and limited. Simonato et al.[18] compiled a range of relevant information through a multicenter VIV and valve-in-ring registry (surgical ring endoprosthesis) in 90 different centers with 1,079 patients analyzed from 2006 to 2020, which can help the proper determination of long-term follow-up.[18] The results of this study are of great interest in the field of interventional cardiology and will be briefly summarized in this document. The long-term follow-up currently used at the Dante Pazzanese Cardiology Institute (*Instituto Dante Pazzanese de Cardiologia* - IDPC) is described in Table 3.

Key VIV registry findings: [18]

• Prosthesis stenosis was the most frequent failure in procedure success, occurring in 8.2% of VIV cases.

• The mean gradient of the analyzed prostheses was 5.7 mmHg; 61% of the patients had mean gradients above 5 mmHg, mainly when smaller devices were used or in patients with a larger body surface ares. Considering that the Mitral Valve Academic Research Consortium (mitral-VARC)[16] definition of stenosis is a mean gradient above 5 mmHg.

• The implications of these findings relate to suboptimal hemodynamic performance in mitral VIV prostheses, with a higher frequency of prosthesis–patient mismatch reported in 24.5% of cases and possible shorter durability.

Table 3 – Suggested IDPC valve-in-valve follow-up.

Follow-up steps
1. Register prosthesis type and size in the first follow-up report.
2. Pre-discharge: TTE with anatomical description, mean and maximum gradients, and effective orifice area.
3. Repeat follow-up at 3, 6, and 12 months with TTE and TEE.
4. What to evaluate on TTE: anatomy, maximum and mean gradients, and area by continuity equation.
5. What to evaluate on TEE: anatomy and presence of thrombi on the ventricular or atrial face of the valve, size and flow pattern in the ASD (normal being left to right).
6. Warning signs: ⇑ Man gradient > 5 mmHg ⇓ Effective orifice comparison ⇑ PASP ASD shunt changed direction (right to left)

ASD, atrial septal defect; IDPC, Instituto Dante Pazzanese de Cardiologia; PASP, pulmonary artery systolic pressure; TEE, transesophageal echocardiography; TTE, transthoracic echocardiography. Source: Follow up protocol described for randomized mitral VIV study on going SurVIV (NCT04402931).

Acknowledgment

Dr. Ibraim Masciarelli for cardiac tomography images and Dr. Dimitry Alexandre Alvim de Siqueira for performing the VIV procedures

Authors' contribution

Writing, preparing figures and videos and revisions: Vilela AA, Otto MEB, Paladino AT, Esmanhoto VA

Conflict of interest

The authors have declared that they have no conflict of interest.

References

1. Cribier A, Eltchaninoff H, Bash A, Borenstein N, Tron C, Bauer F, et al. Percutaneous Transcatheter Implantation of an Aortic Valve Prosthesis for Calcific Aortic Stenosis. Circulation. 2002;106(24):3006-8. doi: https://doi.org/10.1161/01.cir.0000047200.36165.b8.

2. Cribier A. The development of transcatheter aortic valve replacement (TAVR). Global Cardiology Science and Practice. 2017;2016(4). doi: https://doi.org/10.21542/gcsp.2016.32

3. Barbanti M, Webb J, Gilard M, Capodanno D, Tamburino C. Transcatheter aortic valve implantation in 2017: state of the art. EuroIntervention. 2017;13(AA):AA11-21. 10.4244/EIJ-D-17-00567

4. Cheung A, Webb JG, Wong DR, Ye J, Masson JB, Carere RG, et al. Transapical transcatheter mitral valve-in-valve implantation in a human. The Annals of Thoracic Surgery. 2009;87(3):e18-20. doi: https://doi.org/10.1016/j.athoracsur.2008.10.016

5. Otto CM, Nishimura RA, Bonow RO, Carabello BA, Erwin JP 3rd, Gentile F, et al. 2020 ACC/AHA Guideline for the Management of Patients With Valvular Heart Disease: A Report of the American College of Cardiology/American Heart Association Joint Committee on Clinical Practice Guidelines. Circulation. 2021;143(5):e72-e227. doi: https://doi.org/10.1161/CIR.0000000000000923. Erratum in: Circulation. 2021;143(5):e229

6. Tarasoutchi F, Montera MW, Ramos AI, Sampaio RO, Rosa VE, Accorsi TA, et al. Update of the Brazilian Guidelines for Valvular Heart Disease - 2020. Arq Bras Cardiol. 2020;115(4):720-775. doi: https://doi.org/10.36660/abc.20201047

7. Chan V, Malas T, Lapierre H, Boodhwani M, Lam BK, Rubens FD, et al. Reoperation of left heart valve bioprostheses according to age at implantation. Circulation. 2011;124(11_suppl_1). doi:10.1161/CIRCULATIONAHA.110.011973

8. Blanke P, Naoum C, Webb J, Dvir D, Hahn RT, Grayburn P, et al. Multimodality Imaging in the Context of Transcatheter Mitral Valve Replacement. JACC: Cardiovascular Imaging. 2015;8(10):1191-208. doi: https://doi.org/10.1016/j.jcmg.2015.08.004.

9. Bapat VN, Attia R, Thomas M. Effect of valve design on the stent internal diameter of a bioprosthetic valve: a concept of true internal diameter and its implications for the valve-in-valve procedure. JACC Cardiovasc Interv. 2014;7(2):115-127. doi: https://doi.org/10.1016/j.jcin.2013.10.012.

10. Bapat V, Mydin I, Chadalavada S, Tehrani H, Attia R, Thomas M. A guide to fluoroscopic identification and design of bioprosthetic valves: A reference for valve-in-valve procedure. Catheterization and Cardiovascular Interventions. 2013;81(5):853-61. doi: https://doi.org/10.1002/ccd.24419.

11. Harloff MT, Chowdhury M, Hirji SA, Percy ED, Yazdchi F, Shim H, et al. A step-by-step guide to transseptal valve-in-valve transcatheter mitral valve replacement. Ann Cardiothorac Surg. 2021;10(1):113-121. doi: https://doi.org/10.21037/acs-2020-mv-104

12. Sengupta A, Yazdchi F, Alexis SL, Percy E, Premkumar A, Hirji S, et al. Reoperative mitral surgery versus transcatheter mitral valve replacement: a systematic review. J Am Heart Assoc. 2021;10(6):e019854. doi: https://doi.org/10.1161/JAHA.120.019854

13. Yucel E, Al-Bawardy R, Bertrand PB. Pulmonary Hypertension in Patients Eligible for Transcatheter Mitral Valve Repair: Prognostic Impact and Clinical Implications. Curr Treat Options Cardiovasc Med. 2019;21(10):60. doi: https://doi.org/10.1007/s11936-019-0768-6

14. Pirelli L, Hong E, Steffen R, Vahl TP, Kodali SK, Bapat V. Mitral valve-in-valve and valve-in-ring: tips, tricks, and outcomes. Ann Cardiothorac Surg. 2021;10(1):96-112. doi: https://doi.org/10.21037/acs-2019-mv-169.

15. Yoon SH, Bleiziffer S, Latib A, Eschenbach L, Ancona M, Vincent F, et al. Predictors of Left Ventricular Outflow Tract Obstruction After Transcatheter Mitral Valve Replacement. JACC Cardiovasc Interv. 2019;12(2):182-193. doi: https://doi.org/10.1016/j.jcin.2018.12.001

16. Little SH, Bapat V, Blanke P, Guerrero M, Rajagopal V, Siegel R. Imaging Guidance for Transcatheter Mitral Valve Intervention on Prosthetic Valves, Rings, and Annular Calcification. JACC Cardiovasc Imaging. 2021;14(1):22-40. doi: https://doi.org/10.1016/j.jcmg.2019.10.027.

17. Stone GW, Adams DH, Abraham WT, Kappetein AP, Généreux P, Vranckx P, et al.; Mitral Valve Academic Research Consortium (MVARC). Clinical Trial Design Principles and Endpoint Definitions for Transcatheter Mitral Valve Repair and Replacement: Part 2: Endpoint Definitions: A Consensus Document From the Mitral Valve Academic Research Consortium. J Am Coll Cardiol. 2015;66(3):308-321. doi: https://doi.org/10.1016/j.jacc.2015.05.049

18. Simonato M, Whisenant B, Ribeiro HB, Webb JG, Kornowski R, Guerrero M, et al. Transcatheter Mitral Valve Replacement After Surgical Repair or Replacement: Comprehensive Midterm Evaluation of Valve-in-Valve and Valve-in-Ring Implantation From the VIVID Registry. Circulation. 2021;143(2):104-116. doi: https://doi.org/10.1161/CIRCULATIONAHA.120.049088

What do Cardiologists Expect from the Echocardiogram in Heart Failure with Reduced Ejection Fraction?

O que o Cardiologista Espera do Ecocardiograma na Insuficiência Cardíaca com Fração de Ejeção Reduzida?

[1]Heart Institute (InCor), Hospital das Clínicas, School of Medicine, University of São Paulo; [2]São José dos Campos Regional Hospital.

Ciro Mancilha Murad[1]

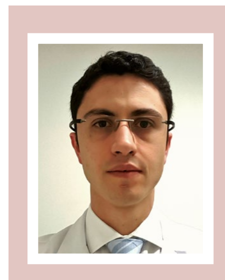

Danilo Bora Moleta[2]

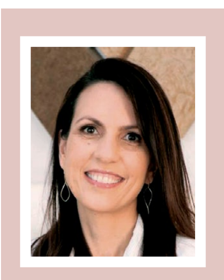

Fabiana Goulart Marcondes-Braga[1]

Introduction

The echocardiogram plays a central role in assessments of patients with heart failure (HF), contributing to its classification, etiology definition, severity stratification, hemodynamic assessment, and clinical follow-up.[1] HF has been historically divided according to the echocardiographic parameter left ventricular ejection fraction (LVEF). The most recent classification divided it into preserved (≥50%), reduced (≤40%), and slightly reduced LVEF (41–49%).[1,2] Different societies have recently proposed a universal definition of HF that involves the presence of symptoms and signs caused by structural and/or functional cardiac changes associated with increased natriuretic peptide levels or objective evidence of congestion. The authors also highlight the importance of classifying HF according to LVEF.[2] (Figure 1) This article will describe the main parameters which the clinical cardiologist should pay attention on the echocardiogram of patients with HF with reduced ejection fraction (HFrEF) and how best to use them in clinical practice.

Keywords

Heart Failure; Stroke volume; Echocardiography.

Mailing Address: Fabiana Goulart Marcondes-Braga •

E-mail: fgmarcondes@yahoo.com.br/fgmarcondes@gmail.com

Manuscript received 3/31/2022; revised 4/12/2022; accepted 4/26/2022

DOI: 10.47593/2675-312X/20223502ecard06

Etiological assessment

The echocardiogram may be the first method used to define the etiology of HFrEF (Figure 2). Segmental contractility changes suggest ischemic etiology, especially if associated with inactive electrical areas on the electrocardiogram. However, they can also occur in other heart diseases. Severe valvular dysfunction associated with morphological changes suggests a valvular etiology. The presence of a digitiform apical aneurysm, inferior or inferolateral contractility changes, and right ventricular dysfunction are frequent in Chagas heart disease. Echocardiographic parameters can also be useful to define the etiology of resctrictive cardiomyopathies, which may present with decreased LVEF in advanced stages. Right and left ventricular wall thickening and a myocardium with a granular aspect and preserved apical contractility are suggestive of amyloidosis. The presence of posterior and/or septal wall thickening with mitral regurgitation and a left ventricular outflow tract obstruction suggest hypertrophic cardiomyopathy, especially when the degree of hypertrophy is not explained by arterial hypertension. Finally, increased lateral and apical trabeculations are suggestive of noncompaction cardiomyopathy.

What do Cardiologists Expect

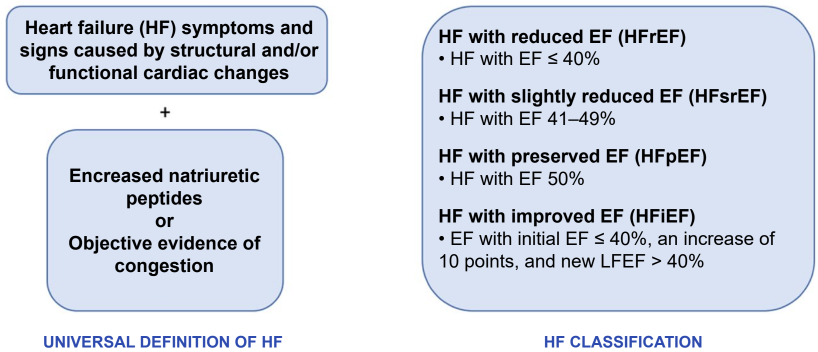

IC: insuficiência cardíaca; ICFER: insuficiência cardíaca com fração de ejeção reduzida; ICFElr: insuficiência cardíaca com fração de ejeção levemente reduzida; ICFEP: insuficiência cardíaca com fração de ejeção preservada; ICFEme: insuficiência cardíaca com fração de ejeção melhorada; FEVE: fração de ejeção do ventrículo esquerdo.

Figure 1 – *Universal definition and new classification of HF.*

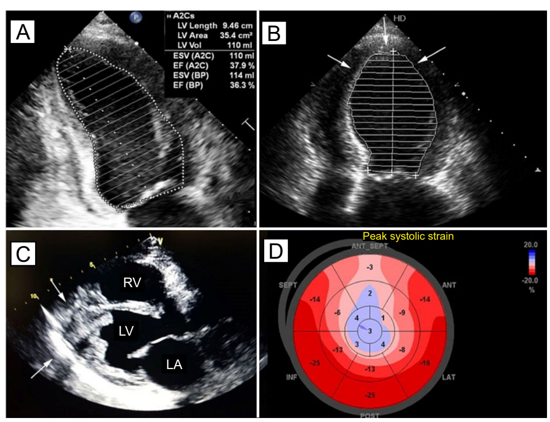

GLS, global longitudinal strain; HF, heart failure; LA, left atrium; LV, left ventricle; LVEF, left ventricular ejection fraction.

Figura 2 – *Use of echocardiography to classify and define the etiology of HF. A: LVEF calculation by the Simpson's method. Apical two-chamber view, final biplane LVEF of 36.3%. B, C, and D: Examples of the use of echocardiography to define HF etiologies. B: Apical two-chamber window demonstrating the apical "ballooning" pattern of a patient with Takotsubo syndrome. C: Long-axis parasternal window demonstrating apical obliteration in a patient with endomyocardial fibrosis. D: Left-ventricular GLS final polar map (bull's eye) demonstrating segmental heart disease in the territory of the anterior descending artery.*

Prognostic assessment

LVEF is one of the best-known prognostic factors for HFrEF. Several studies reported lower survival rates among patients with a lower LVEF.[3,4] A sub-analysis of patients in the Candesartan in Heart failure: Assessment of Reduction in Mortality and Morbidity (CHARM) program showed that the risk of death from all causes increased by 39% for every 10% decrease in LVEF, starting from a 45% LVEF.[4] An LVEF below 30% is also one of the criteria used by the European Society of Cardiology and the Brazilian Society of Cardiology to define advanced HF, i.e., it helps identify patients who would benefit most from treatments such as heart transplantation or long-term circulatory support devices.[5,6] Right ventricular dysfunction associated with HFrEF is also considered a marker of adverse prognosis and signals advanced-stage disease.[7,8] A recent study reported that right ventricular global longitudinal strain (GLS) was the best predictor of adverse outcomes, even compared to cardiac magnetic resonance imaging parameters.[7] On the other hand, simpler parameters such as the tricuspid annular plane systolic excursion (TAPSE) and the TAPSE/pulmonary artery systolic pressure (PASP) ratio are also related to worse prognosis and may be useful in clinical practice.[8] Cardiac chamber size, the presence of pulmonary hypertension, and secondary mitral regurgitation are also recognized predictors of adverse prognosis in HFrEF.[3,9-10]

Hemodynamic and fluid overload assessment

In addition to classification, signaling possible etiologies, and assessing prognosis, echocardiography plays a key role in hemodynamic assessments and por volemia definition in

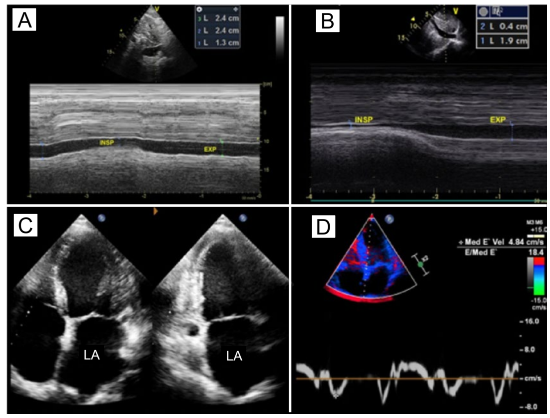

LA, left atrium.

Figure 3 – *Use of echocardiography to define HF etiology. A: Two-dimensional M-mode echocardiogram demonstrating an inferior vena cava measuring 2.4 cm without significant inspiratory collapse suggestive of an increased right atrial filling pressure. B: Inferior vena cava collapsing on inspiration suggestive of a low right atrial filling pressure. C: Apical four- and two-chamber windows demonstrating left atrial dilation. D: Tissue Doppler demonstrating an increased E/e' ratio suggestive of an increased left atrial filling pressure.*

HFrEF (Figure 3). Right atrial pressure (RAP) can be estimated noninvasively by assessment of the diameter and respiratory variation of the inferior vena cava.[11] A diameter < 2.1 cm with a respiratory variation > 50% correlates with a RAP of 0–5 mmHg, while a diameter > 2.1 cm with a variation < 50% correlates with a RAP of 10–20 mmHg.[11] The absence of hepatic vein inspiratory collapse, right atrial dilation with left interatrial septum deviation, and tricuspid valve E/e' ratio > 6 are adjuvant parameters also correlated with a higher RAP.[11] These data may indicate systemic congestion in clinical practice and thus help with its clinical management.

Increased left-atrial filling pressures suggest pulmonary edema and can be noninvasively estimated by echocardiography. A study of intensive care unit patients correlated a mitral valve E/e' ratio > 15 with a pulmonary capillary pressure (PCP) > 15 with 86% sensitivity and 88% specificity.[12] However, this method is less accurate in patients with valve disease or mitral calcification, left bundle branch block, or under resynchronization therapy. Anderson et al. developed an algorithm to estimate left-chamber filling pressures with better accuracy than the use of isolated variables alone.[13] In this algorithm, a mitral valve E/A ratio ≥ 2 or two changed parameters (maximum indexed left atrial volume > 34 mL/m^2, peak tricuspid regurgitation velocity > 2.8 m/s, E/e' > 14) have 87% accuracy for predicting a PCP > 12 mmHg[13]. In addition, cardiac output can be estimated by pulsed Doppler in the left ventricular outflow tract, which has been increasingly used at the bedside to assess and adjust cardiogenic shock therapy.[14]

New echocardiographic techniques

New techniques for potential use in HFrEF have recently been described. One such technique is the strain measurement or myocardial strain index. Some studies already showed that left ventricle GLS is a better predictor of mortality than LVEF and other echocardiographic parameters.[15,16] It can also be used for cardiotoxicity monitoring and the diagnostic evaluation of some cardiomyopathies (e.g., the standard apical-sparing pattern in amyloidosis can be easily identified through a strain echocardiogram). Three-dimensional echocardiography is also more accurate for determining cardiac chamber volumes and function, including from the right ventricle, which has limited assessment on two-dimensional echocardiography.[17,18] It has already been used in clinical practice for cardiotoxicity monitoring and during invasive procedures such as the MitraClip®.

Conclusion and perspectives

We believe that the role of echocardiography in HFrEF extends beyond LVEF and cavity size assessments (Figure 4). It is a widely available, noninvasive method that provides a vast set of information about the clinical condition of patients with HFrEF. The knowledge and correct interpretation of different echocardiographic parameters improves the diagnosis, prognostic assessment, treatment, and clinical follow-up of these patients.

Authors' contributions

Research creation and design: Marcondes-Braga, FG; Murad, CM. Data acquisition: Boleta, DB. Redação do manuscrito: Murad, CM; Marcondes-Braga, FG. Critical revision of the manuscript for important intellectual content: Marcondes-Braga, FG; Boleta, DB.

Conflict of interest

The authors have declared that they have no conflict of interest.

What do Cardiologists Expect

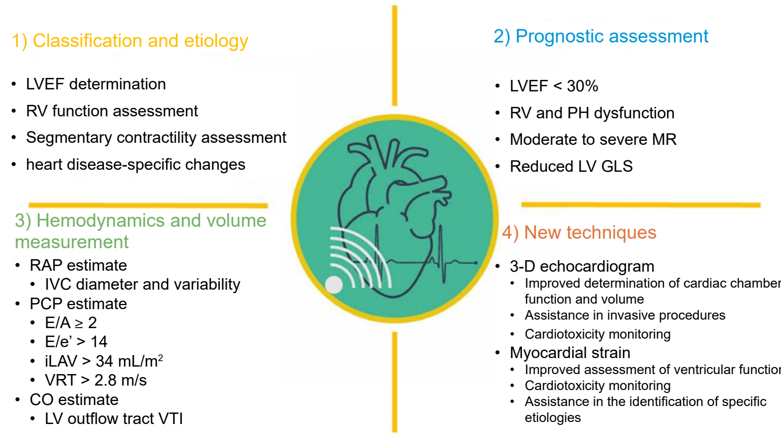

CO, cardiac output; E/A, early/late mitral transvalvular flow velocity; E/e', early transmitral velocity/early mitral annulus diastolic velocity; GLS, global longitudinal strain; iLAV, indexed left atrial volume; IVC, inferior vena cava; LV, left ventricular; LVEF, left ventricular ejection fraction; MR, mitral regurgitation; PCP, pulmonary capillary pressure; PH, pulmonary hypertension; RAP, right atrial pressure; RV, right ventricle; VRT, peak tricuspid regurgitation velocity; VTI, velocity time integral.

Figure 4 – *Central role of echocardiography in HF.*

References

1. McDonagh TA, Metra M, Adamo M, Gardner RS, Baumbach A, Böhm M, et al.; ESC Scientific Document Group. 2021 ESC Guidelines for the diagnosis and treatment of acute and chronic heart failure. Eur Heart J. 2021;42(36):3599-726. doi: 10.1093/eurheartj/ehab368. Erratum in: Eur Heart J. 2021 Oct 14;: PMID: 34447992.
2. Bozkurt B, Coats AJ, Tsutsui H, Abdelhamid CM, Adamopoulos S, Albert N, et al. Universal definition and classification of heart failure: a report of the Heart Failure Society of America, Heart Failure Association of the European Society of Cardiology, Japanese Heart Failure Society and Writing Committee of the Universal Definition of Heart Failure: Endorsed by the Canadian Heart Failure Society, Heart Failure Association of India, Cardiac Society of Australia and New Zealand, and Chinese Heart Failure Association. Eur J Heart Fail. 2021;23(3):352-80. doi: 10.1002/ejhf.2115
3. Quiñones MA, Greenberg BH, Kopelen HA, Koilpillai C, Limacher MC, Shindler DM, et al. Echocardiographic predictors of clinical outcome in patients with left ventricular dysfunction enrolled in the SOLVD registry and trials: significance of left ventricular hypertrophy. Studies of Left Ventricular Dysfunction. J Am Coll Cardiol. 2000;35(5):1237-44. doi: 10.1016/s0735-1097(00)00511-8
4. Solomon SD, Anavekar N, Skali H, McMurray JJ, Swedberg K, Yusuf S, et al.; Candesartan in Heart Failure Reduction in Mortality (CHARM) Investigators. Influence of ejection fraction on cardiovascular outcomes in a broad spectrum of heart failure patients. Circulation. 2005;112(24):3738-44. doi: 10.1161/CIRCULATIONAHA.105.561423
5. Crespo-Leiro MG, Metra M, Lund LH, Milicic D, Costanzo MR, Filippatos G, et al. Advanced heart failure: a position statement of the Heart Failure Association of the European Society of Cardiology. Eur J Heart Fail. 2018;20(11):1505-35. doi: 10.1002/ejhf.1236
6. Marcondes-Braga FG, Moura LA, Issa VS, Vieira JL, Rohde LE, Simões MV, et al. Emerging Topics Update of the Brazilian Heart Failure Guideline - 2021. Arq Bras Cardiol. 2021;116(6):1174-212. English, Portuguese. doi: 10.36660/abc.20210367
7. Houard L, Benaets MB, de Meester de Ravenstein C, Rousseau MF, Ahn SA, Amzulescu MS, et al. Additional Prognostic Value of 2D Right Ventricular Speckle-Tracking Strain for Prediction of Survival in Heart Failure and Reduced Ejection Fraction: A Comparative Study With Cardiac Magnetic Resonance. JACC Cardiovasc Imaging. 2019;12(12):2373-85. doi: 10.1016/j.jcmg.2018.11.028
8. Bosch L, Lam CSP, Gong L, Chan SP, Sim D, Yeo D, et al. Right ventricular dysfunction in left-sided heart failure with preserved versus reduced ejection fraction. Eur J Heart Fail. 2017;19(12):1664-71. doi: 10.1002/ejhf.873
9. Ghio S, Gavazzi A, Campana C, Inserra C, Klersy C, Sebastiani R, et al. Independent and additive prognostic value of right ventricular systolic function and pulmonary artery pressure in patients with chronic heart failure. J Am Coll Cardiol. 2001;37(1):183-8. doi: 10.1016/s0735-1097(00)01102-5
10. Sannino A, Smith RL 2nd, Schiattarella GG, Trimarco B, Esposito G, Grayburn PA. Survival and Cardiovascular Outcomes of Patients With Secondary Mitral Regurgitation: A Systematic Review and Meta-analysis. JAMA Cardiol. 2017;2(10):1130-9. doi: 10.1001/jamacardio.2017.2976
11. Beigel R, Cercek B, Luo H, Siegel RJ. Noninvasive evaluation of right atrial pressure. J Am Soc Echocardiogr. 2013;26(9):1033-42. doi: 10.1016/j.echo.2013.06.004
12. Dokainish H, Zoghbi WA, Lakkis NM, Al-Bakshy F, Dhir M, Quinones MA, et al. Optimal noninvasive assessment of left ventricular filling pressures: a comparison of tissue Doppler echocardiography and B-type natriuretic peptide in patients with pulmonary artery catheters. Circulation. 2004;109(20):2432-9. doi: 10.1161/01.CIR.0000127882.58426.7A
13. Andersen OS, Smiseth OA, Dokainish H, Abudiab MM, Schutt RC, Kumar A, et al. Estimating Left Ventricular Filling Pressure by Echocardiography. J Am Coll Cardiol. 2017;69(15):1937-48. doi: 10.1016/j.jacc.2017.01.058
14. Price S, Platz E, Cullen L, Tavazzi G, Christ M, Cowie MR, et al.; Acute Heart Failure Study Group of the European Society of Cardiology Acute Cardiovascular Care Association. Expert consensus document: Echocardiography and lung ultrasonography for the assessment and management of acute heart failure. Nat Rev Cardiol. 2017;14(7):427-40. doi: 10.1038/nrcardio.2017.56
15. Sengeløv M, Jørgensen PG, Jensen JS, Bruun NE, Olsen FJ, Fritz-Hansen T, et al. Global Longitudinal Strain Is a Superior Predictor of All-Cause Mortality in Heart Failure With Reduced Ejection Fraction. JACC Cardiovasc Imaging. 2015;8(12):1351-9. doi: 10.1016/j.jcmg.2015.07.013
16. Park JJ, Park JB, Park JH, Cho GY. Global Longitudinal Strain to Predict Mortality in Patients With Acute Heart Failure. J Am Coll Cardiol. 2018;71(18):1947-57. doi: 10.1016/j.jacc.2018.02.064
17. Dorosz JL, Lezotte DC, Weitzenkamp DA, Allen LA, Salcedo EE. Performance of 3-dimensional echocardiography in measuring left ventricular volumes and ejection fraction: a systematic review and meta-analysis. J Am Coll Cardiol. 2012;59(20):1799-808. doi: 10.1016/j.jacc.2012.01.037
18. Leibundgut G, Rohner A, Grize L, Bernheim A, Kessel-Schaefer A, Bremerich J, et al. Dynamic assessment of right ventricular volumes and function by real-time three-dimensional echocardiography: a comparison study with magnetic resonance imaging in 100 adult patients. J Am Soc Echocardiogr. 2010;23(2):116-26. doi: 10.1016/j.echo.2009.11.016

Left Atrial Function Analysis in Patients with Functional Mitral Regurgitation Associated with Dilated Cardiomyopathy

Análise da Função Atrial Esquerda em Pacientes com Insuficiência Mitral Funcional Associada à Miocardiopatia Dilatada

Stephanie Macedo Andrade[1], Rodrigo Bellio de Mattos Barretto[2], Francisco Thiago Tomaz de Sousa[1], David Costa de Souza Le Bihan[2]

[1]Dante Pazzanese Institute of Cardiology, São Paulo, SP, Brazil. [2]InCor Heart Institute, Medical School, University of São Paulo, São Paulo, SP, Brazil.

Abstract

Background: Functional mitral regurgitation (FMR) is associated with dilated cardiomyopathy (DC), heart failure (HF) and worsening left atrial function (LAF). Patients with DC and FMR may present left atrial dysfunction resulting from both ventricular dysfunction and valve disease, but it is unknown whether the presence of valve disease will lead to greater LAF impairment.

Objective: This study aimed to evaluate the relationship between LAF parameters and FMR degree in patients with DC.

Methods: This cross-sectional observational study included 214 patients with DC, 46 without FMR (control group) and 168 with mild, moderate or severe FMR. An LAF analysis was performed by speckle tracking echocardiography (STE) and atrial volumetric variation.

Results: LAF analyzed by STE by means of reservoir strain, conduit strain and active contraction strain was reduced in the sample, with values of 14.3%, 8.49% and 5.92%, respectively. FMR degree was significantly associated with reservoir strain (0.27 ± 0.16 versus 0.15 ± 0.09; $p < 0.001$) and contraction strain (19.2 ± 7.3 versus 11.2 ± 2.7; $p < 0.001$). FMR was also associated with a reduced LAF assessed by volumetric analysis: total atrial emptying fraction of 0.51 ± 0.13 versus 0.34 ± 0.11 and active atrial emptying fraction of 0 .27 ± 0.16 versus 0.15 ± 0.09 ($p < 0.001$).

Conclusion: In a population with DC, FMR was associated with reduced LAF assessed by STE and atrial volume variation.

Keywords: Atrial Function, Left; Mitral Valve Insufficiency; Cardiomyopathy, Dilated; Echocardiography.

Resumo

Fundamento: *A insuficiência mitral funcional (IMF) está associada à miocardiopatia dilatada (MD), à insuficiência cardíaca (IC) e à piora da função atrial esquerda (FAE). A FAE pode decair tanto pela disfunção ventricular quanto pela valvopatia, mas não se sabe se esta leva a um prejuízo maior da FAE.*

Objetivo: *Avaliar a relação entre a piora de parâmetros de FAE com o grau de IMF, em pacientes com MD.*

Métodos: *Trata-se de estudo observacional transversal, que incluiu 214 pacientes com MD, sendo 46 sem IMF (controle) e 168 com IMF discreta, moderada ou grave. A análise da FAE foi realizada por ecocardiografia por speckle tracking (STE) e por variação volumétrica atrial.*

Resultados: *A FAE, analisada por STE– por meio do strain de reservatório, conduto e contração ativa – encontrou-se reduzida na amostra, com valores respectivos de 14,3%, 8,49% e 5,92%. O grau de IMF associou-se significativamente com os valores do strain de reservatório (0,27±0,16 versus 0,15±0,09; p <0,001) e de contração (19,2±7,3 versus 11,2±2,7; p <0,001). A IMF também apresentou correlação com a redução da FAE avaliada por análise volumétrica, observada pela medida da fração de esvaziamento atrial total (FEAT): 0,51±0,13 versus 0,34±0,11 e da fração de esvaziamento atrial ativa (FEAA): 0,27±0,16 versus 0,15±0,09 com p <0,001.*

Conclusão: *Em uma população com MD, a presença de IMF associa-se à redução da FAE de reservatório e de contração, avaliada por STE e pela variação volumétrica atrial.*

Palavras-chave: *Função do átrio esquerdo; Insuficiência da valva mitral; Cardiomiopatia dilatada; Ecocardiografia.*

Mailing Address: Stephanie Macedo Andrade •
Rua José Antônio Coelho, 750, Vila Mariana. CEP: 04011-062 – São Paulo, SP, Brazil.
E-mail: stephaniemandrade@hotmail.com

Manuscript received 1/3/2022; revised 3/18/2022; accepted 5/11/2022

DOI: 10.47593/2675-312X/20223502eabc281

Introduction

Mitral regurgitation (MR) is characterized by blood regurgitation into the left atrium (LA) during ventricular systole. Functional MR (FMR) results from valve geometry changes induced by left ventricular (LV) dilation that separates the papillary muscles, or from annulus dilation due to atrial enlargement that creates a central area of poor valve leaflet coaptation and, subsequently, reflux into the LA. The most common causes of FMR are myocardial ischemia and dilated cardiomyopathy (DCM).[1-3]

It is difficult to estimate the epidemiology of FMR due to differences in definitions in the literature, but some studies suggest that about 40% of patients with DCM will develop FMR.[4-6] Data on the Brazilian population show that the main etiologies of DCM are ischemic, hypertensive, and dilated idiopathic heart failure (HF), which affect 30.1%, 20.3% and 14.6% of patients, respectively.[7]

The LA is a functional cavity that works as a volume reservoir and contractile myocardium and plays a crucial role in cardiac performance.[8] LA function (LAF) is classically divided into three phases (reservoir, conduit, and active contraction), which can be obtained through two-dimensional echocardiography by speckle tracking (STE) or atrial volume variation.[9-11] Good LA functioning is even more important in patients with HF since atrial output can correspond to up to 30% of cardiac output, something relevant in patients with LV dysfunction.[10]

Patients with DCM and FMR may have atrial dysfunction resulting from ventricular dysfunction and valvular heart disease, but whether the presence of valvular heart disease leads to greater LAF impairment it is unknown. This study aimed to evaluate the correlation between LAF worsening assessed by STE and phasic volumetric variation and the degree of FMR in patients with DCM.

Method

Population

This cross-sectional observational study enrolled patients who underwent HF treatment in a specialized tertiary hospital in 2007–2011. The inclusion criteria were sinus rhythm; left ventricular ejection fraction (LVEF) < 40%; and mild, moderate, or severe MR with functional characteristics on two-dimensional echocardiography. The exclusion criteria were history of acute myocardial infarction or unstable angina less than 90 days before the examination; acute myocarditis; history of organic (primary) valve disease or previous valve surgery; or echocardiographic image of inadequate quality. All participants signed an informed consent form, and the institution's research ethics committee approved the study. Of the 280 patients who met the inclusion criteria, 25 were excluded due to inadequate image quality or echocardiographic monitoring, leaving 255 participants for the analysis. Of them, data were available for FMR assessment for only 214: 46 had no FMR (control group), 124 had mild FMR, 29 had moderate FMR, and 15 had severe FMR.

Echocardiography

Echocardiographic images were acquired using Vivid 7 and Vivid E9 devices (GE Healthcare), and images were analyzed by advanced techniques (STE) on an appropriate workstation using EchoPAC PC® software version 6.0.1 (GE Healthcare).

Echocardiography was performed with electrocardiographic monitoring following American Society of Echocardiography guidelines.[12,13] FMR degree was assessed following the same guidelines, favoring quantitative measures such as effective regurgitant orifice (ERO; cm^2) and regurgitant volume (RV; mL).[14,15]

Images were obtained in different phases of the cardiac cycle for LA volume measurements as recommended by Abhayaratna et al.[16] Three volumes were obtained in apical four- and two-chamber windows: maximum volume (at the end of ventricular systole), pre-P-wave volume (immediately before the P-wave on electrocardiography), and minimum volume (at the end of ventricular diastole). The reservoir function is represented by the total atrial emptying fraction (TAEF) and active contraction function by the active atrial emptying fraction (AAEF). TAEF is calculated as (maximum volume - minimum volume)/maximum volume. AAEF is calculated as (pre-P volume - minimum volume)/pre-P volume.

LA strain was analyzed by STE using the software originally developed for LV assessment. This evaluation was performed in apical four- and two-chamber views with six different segments analyzed in each. Each segment generated a regional atrial strain curve. The mean between these curves in both acquisitions was used to measure the reservoir function, which corresponds to the greatest positive longitudinal strain measured after the T wave by electrocardiography and the contraction function, which corresponds to the ascending P-wave strain. The conduit function corresponds to the difference between these values (Figure 1).[17]

Statistical analysis

Quantitative variables were subjected to the Kolmogorov-Smirnov test for a normality assessment. Normally distributed variables are presented as mean and standard deviation. Non-normally distributed variables are described as median and interquartile range (Q1–Q3). Categorical variables are presented as percentages.

The Pearson's and Spearman's methods were used to assess the correlation between the variables representing LA function, the quantitative variables for FMR grading, and LVEF.

Analysis of variance was used to assess the association between atrial emptying volumes and fractions and reservoir, conduit, and contraction atrial strain values by FMR (mild, moderate, and severe).

Values of $p < 0.05$ were defined as significant in all analyses performed using SPSS software for Windows (version 20.0; IBM) and tabulated using Microsoft Excel 2003 software.

Results

Clinical characteristics

Most patients were men (62%), with a mean age of 59 ± 13 years and New York Heart Association functional classes II

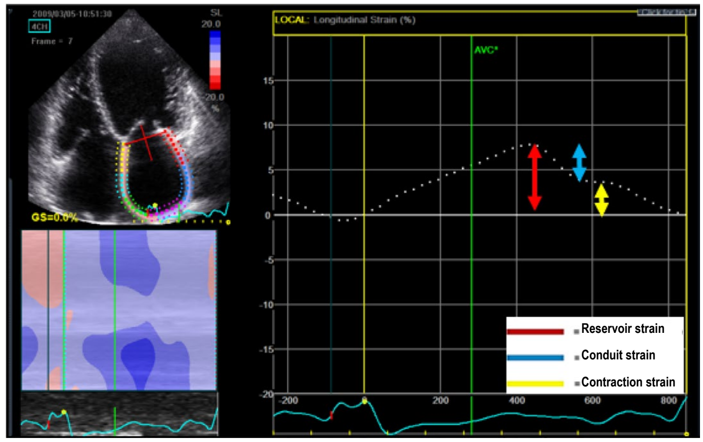

Source: Study patient image.

Figure 1 – *Atrial strain phases by two-dimensional speckle tracking echocardiography in apical four-chamber view synchronized by QRS. The dotted curve in the center represents the mean between the regional strain curves with their reservoir and contraction strain peaks. The difference between them represents the conduit strain.*

and III. The most frequent comorbidities were arterial hypertension (62.7%), coronary artery disease (32.9%), and previous infarction (38.4%).

Most patients were on optimized treatment for HF, with angiotensin-converting enzyme inhibitors being used by 65.7%, angiotensin 2 receptor blockers by 25.7%, beta-blockers by 89.8%, and spironolactone by 72%.

Table 1 demonstrates the clinical characteristics of the study population.

Echocardiographic characteristics

Most patients in the study had significant LV dysfunction, with a mean LVEF of 29.7 ± 6.4%. The main echocardiographic variables are described in Table 2.

LA function

All atrial function components – reservoir, conduit and active contraction – measured by STE were significantly reduced in the sample by 14.3%, 8.49%, and 5.92%, respectively. LA volumes increased, with a mean of 45.3 ± 17.2 mL/m² at maximum volume. The atrial function variables are described in Table 3.

The analysis of ischemic versus non-ischemic etiology showed no difference except for the maximum LA volume, which was greater in non-ischemic patients (Table 4).

Mitral regurgitation

FMR degree was significantly correlated with LAF assessed by a volume analysis using the total and active emptying fractions. The STE analysis showed that FMR degree was associated with reservoir and contraction strain. FMR degree was directly associated with increased LA volume and inversely related to LVEF. Table 5 shows the analysis of these data.

As for FMR quantitative variables, ERO and RV were directly correlated with atrial volume and inversely corelated with atrial function. LVEF showed the same correlation pattern but with a less strong association (Table 6).

Discussion

Two findings were especially relevant in this study: variables related to LAF reservoir and contraction were reduced in this sample of patients with DCM; and FMR degree was significantly associated with most echocardiographic parameters related to volume and LAF.

Ischemic MR severity was associated with all variables related to left atrial volume, atrial emptying fractions, and reservoir and active contraction strain, possibly due to MR pathophysiology in which the blood returns to the LA, increasing its pressure and dimensions and, consequently, reducing its function. The literature reports the same finding, mostly related to organic MR as no studies on FMR are currently available. A study of 144 patients with FMR subdivided into groups 1 (absent or mild MR) and 2 (moderate or severe MR) reported a correlation between degree of regurgitation and left atrial volume, but parameters related to atrial function were not analyzed.[18]

As for prognosis, FMR is classically one factor associated with lower survival, worse functional class, and greater morbidity in DCM.[19-23] However, it is unclear whether atrial dysfunction associated with this condition represents an additional adverse prognostic factor.

LA volume has been extensively studied and is currently a more reliable LA dimension measurement than anteroposterior diameter.[24-27] In fact, it has prognostic value in several cardiovascular diseases.[28-37]

A European multicenter study of 371 healthy participants reported indexed LA volume, TAEF, and AAEF values of 26.3 mL/m², 68.5%, and 43.1%, respectively.[38] In our study, the atrial volumes were increased and the phasic function variables were decreased. Indexed LA volume, TAEF, and AAEF values were 45.3 ± 17 mL/m², 42 ± 15%, and 22 ± 14%, respectively.

Table 1 - Clinical characteristics of the population.

Variable	Value (N = 255)
Sex	
Male	158 (62)
Female	97 (38)
Age, years	59 ± 13
NYHA functional class	
I	24 (9.4)
II	112 (43.9)
III	82 (32.2)
IV	37 (14.5)
Heart rate, bpm	68.9 ± 12.3
DM	
No	189 (74.1)
Yes	66 (25.9)
SAH	
No	95 (37.3)
Yes	160 (62.7)
CAD	
No	150 (58.8)
Yes	105 (41.2)
Previous AMI	
No	157 (61.6)
Yes	98 (38.4)
Chagas	
No	225 (88.2)
Yes	30 (11.8)
Myocarditis	
No	241 (94.5)
Yes	14 (5.5)
Previous rheumatic disease	
No	254 (99.6)
Yes	1 (0.4)
Alcoholism	
No	235 (92.2)
Yes	20 (7.8)
Other comorbidities	
No	200 (78.4)
Yes	55 (21.6)
Drugs	
Digoxin	68 (26.8)
Loop diuretic	200 (78.7)
Thiazide diuretic	22 (8.7)
Spironolactone	183 (72)
Angiotensin-converting enzyme inhibitors	167 (65.7)
Angiotensin 2 receptor blockers	65 (25.7)
Beta-blocker	228 (89.8)
Calcium channel blocker	15 (5.9)
Nitrate	39 (15.4)
Hydralazine	10 (3.9)
ASA	148 (58.3)
Statin	128 (50.4)
Other drug	122 (48.6)

AMI, acute myocardial infarction; ASA, acetylsalicylic acid; BMI, body mass index; BPM, beats per minute; CAD, coronary artery disease; DM, diabetes mellitus; NYHA, New York Heart Association; SAH, systemic arterial hypertension; SD, standard deviation. Values are shown as n (%) or mean ± standard deviation.

Table 2 - Echocardiographic characteristics of the population.

Variable	Value
LA diameter, cm	(n = 214)
Mean ± SD	4.65 ± 0.67
Median (min, max)	4.6 (2.8; 6.9)
VE end-diastolic volume, mL	(n = 214)
Mean ± SD	196.9 ± 73.3
LV end systolic volume, mL	(n = 214)
Mean ± SD	140.5 ± 59.3
LVEF (Simpson's method), %	(n = 214)
Mean ± SD	29.7 ± 6.4
Median (min, max)	0.3 (0.15; 0.4)
LV global longitudinal strain, %	(n = 203)
Mean ± SD	-8.14 ± 2.56
Diastolic dysfunction	(n = 213)
I	59 (27.7)
II	43 (20.2)
III/IV	97 (45.5)
Inconclusive	14 (6.6)
Mitral regurgitant volume, mL	(n = 214)
Mean ± SD	22.7 ± 17.3
Mitral regurgitation ERO, cm²	(n = 214)
Mean ± SD	0.15 ± 0.12
Mitral regurgitation	(n = 214)
Absent	46 (21.5)
Mild	124 (57.9)
Moderate	29 (13.6)
Severe	(7)

ERO, effective regurgitant orifice; LA, left atrium; LV, left ventricle; LVEF, left ventricular ejection fraction; SD, standard deviation.

Table 3 - Atrial function variables and synchrony.

Variable	Description
Maximum LA volume, mL/m²	(n = 214)
Mean ± SD	45.3 ± 17.2
Minimum LA volume, mL/m²	(n = 214)
Mean ± SD	27.6 ± 15.3
Pre-P LA volume, mL/m²	(n = 214)
Mean ± SD	36.7 ± 15.8
Total atrial emptying fraction, %	(n = 214)
Mean ± SD	42 ± 15
Active atrial emptying fraction, %	(n = 214)
Mean ± SD	22 ± 14
LA reservoir strain, %	(n = 182)
Mean ± SD	14.3 ± 6.6
LA contraction strain, %	(n = 181)
Mean ± SD	8.49 ± 5.01
LA conduit strain, %	(n = 181)
Mean ± SD	5.92 ± 3.32

LA, left atrium; SD, standard deviation.

Table 4 - Atrial function and synchrony variables according to myocardial disease etiology.

Variable	Etiology		P
	Non-ischemic	Ischemic	
Maximum LA volume, mL/m^2			0.029
Mean ± SD	47.4 ± 18	42.1 ± 15.6	
Minimum LA volume, mL/m^2			0.238
Mean ± SD	28.6 ± 16.1	26.2 ± 13.9	
Pre-P LA volume, mL/m^2			0.083
Mean ± SD	38.2 ± 16.3	34.4 ± 14.7	
Total atrial emptying fraction, %			0.193
Mean ± SD	0.43 ± 0.15	0.4 ± 0.14	
Active atrial emptying fraction, %			0.358
Mean ± SD	0.23 ± 0.15	0.21 ± 0.12	
LA reservoir strain, %			0.259
Mean ± SD	14.8 ± 7.1	13.7 ± 5.8	
LA contraction strain, %			0.407
Mean ± SD	8.8 ± 5.5	8.2 ± 4.4	
LA conduit strain, %			0.207
Mean ± SD	6.2 ± 3.5	5.6 ± 3.1	

Student's t-test. LA, left atrium; SD, standard deviation.

These values tend to be lower in populations with DCM and LV systolic dysfunction. Triposkiadis *et al*. reported a correlation between AAEF reduction in idiopathic DCM and between a ischemic and control group (18 ± 10% vs. 32 ± 10% vs. 36 ± 10%, respectively; p = 0.05).[39] D'Andrea *et al*. reproduced this finding with an AAEF of 22.5 ± 10% for idiopathic DCM and 33.1 ± 9.3% for ischemic DCM.[40] In our study, atrial function was reduced in the entire group and no differences were observed between the ischemic and non-ischemic etiologies.

STE LAF values in patients with HF with reduced EF tend to be reduced as evaluated by Cameli *et al.*, who found values of 13 ± 11.3% for reservoir strain and of 5.26 ± 5.54% for contraction strain in a group of patients with an LVEF < 30%.[41] Another study with a population with DCM and LVEF < 40% reported reservoir and contraction strain values of 12.3 ± 3.6% and 6.2 ± 1.6% in patients with increased LV filling pressures, respectively.[42] In our sample, reservoir, contraction, and conduit functions assessed by two-dimensional strain were also decreased at 14.3%, 8.49%, and 5.92%, respectively.

Table 5 - Echocardiographic parameters by degree of mitral regurgitation.

Variable	Mitral regurgitation				r	p
	Absent	Discrete	Moderate	Severe		
Maximum LA volume, mL/m^2					0.495	< 0.001
Mean ± SD	33.7 ± 11.6	44.5 ± 14	54.7 ± 19.9	68.8 ± 18.6		
Minimum LA volume, mL/m^2					0.515	< 0.001
Mean ± SD	17.2 ± 8.9	27 ± 13.1	37.7 ± 17.6	45.7 ± 15.5		
Pre-P LA volume, mL/m^2					0.512	< 0.001
Mean ± SD	25.6 ± 9.5	36.4 ± 13.4	46 ± 18.9	55.4 ± 15.4		
Total atrial emptying fraction, %					-0.396	< 0.001
Mean ± SD	0.51 ± 0.13	0.41 ± 0.15	0.33 ± 0.11	0.34 ± 0.11		
Active atrial emptying fraction, %					-0.271	< 0.001
Mean ± SD	0.27 ± 0.16	0.23 ± 0.13	0.16 ± 0.09	0.15 ± 0.09		
LA reservoir strain, %					-0.324	< 0.001
Mean ± SD	19.2 ± 7.3	13.5 ± 6.3	12.2 ± 5.1	11.2 ± 2.7		
LA contraction strain, %					-0.408	< 0.001
Mean ± SD	12.25 ± 5.19	8.11 ± 4.58	6 ± 3.87	5.65 ± 2.42		
LA conduit strain, %					-0.007	0.932
Mean ± SD	6.98 ± 4.23	5.58 ± 3.42	6.21 ± 2.74	5.51 ± 1.96		
LVEF (Simpson's method), %					-0.299	< 0.001
Mean ± SD	32.4 ± 5.4	29.3 ± 5.7	26.6 ± 4.9	28.1 ± 5.7		

Spearman correlation. LA, left atrium; LVEF, left ventricular ejection fraction; SD, standard deviation.

Table 6 - Atrial function variables, left ventricular ejection fraction, and quantitative parameters of mitral regurgitation.

Variable	MR ERO		MR RV		LVEF (Simpson's)	
	Correlation	p	Correlation	p	Correlation	p
Maximum LA volume, mL/m^2	0.516	<0.001	0.521	<0.001	-0.254	<0.001
Minimum LA volume, mL/m^2	0.502	<0.001	0.506	<0.001	-0.265	<0.001
Pre-P LA volume, mL/m^2	0.480	<0.001	0.497	<0.001	-0.285	<0.001
Total atrial emptying fraction, %	-0.373	<0.001	-0.381	<0.001	0.234	0.001
Active atrial emptying fraction, %	-0.311	<0.001	-0.289	<0.001	0.088	0.202
LA reservoir strain, %	-0.390	<0.001	-0.334	<0.001	0.344	<0.001
LA contraction strain, %	-0.451	<0.001	-0.379	<0.001	0.275	0.001
LA conduit strain, %	-0.109	0.189	-0.112	0.176	0.274	0.001

Pearson's correlation. ERO, effective regurgitant orifice; LA, left atrium; LVEF, left ventricular ejection fraction; MR, mitral regurgitation, RV, regurgitant volume.

No studies correlating these variables with the presence of FMR have been published.

The fact that we observed an association between LAF variables expressing reservoir and contraction functions and not between FMR and the conduit function may be because the latter is physiologically related to LV compliance and relaxation, which were likely to be homogeneously reduced in this DCM population regardless of FMR degree.

Further studies are needed to understand the prognostic impact of atrial dysfunction in the population with DCM and FMR, especially in terms of the genesis of atrial fibrillation, which has high morbidity and mortality rates among DCM patients.

Conclusions

Patients with myocardial ischemia and dilated cardiomyopathy (DCM) and Functional mitral regurgitation (FMR) present global left atrium function (LAF) impairment.

FMR is associated with increased atrial volumes and reduced phasic reservoir function and atrial contraction parameters.

Authors' contribution

Research conception and design: Le Bihan DCS; Data collection: Andrade SM, Barretto RBM, Sousa FTT; Data analysis and interpretation: Andrade SM, Barretto RBM, Le Bihan DCS; Statistical analysis: Le Bihan DCS, Andrade SM; Manuscript writing: Andrade SM; Critical review of the manuscript for important intellectual content: Le Bihan DCS.

Conflict of interest

The authors have declared that they have no conflict of interest.

Referências

1. Schmitto JD, Lee LS, Mokashi SA, Bolman RM 3rd, Cohn LH, Chen FY. Functional mitral regurgitation. Cardiol Rev. 2010;18(6):285-91. doi: https://doi.org/10.1097/CRD.0b013e3181e8e648
2. Tarasoutchi F, Montera MW, Ramos AI, Sampaio RO, Rosa VE, Accorsi TA, et al. Atualização das Diretrizes Brasileiras de Valvopatias: Abordagem das Lesões Anatomicamente Importantes. Arq Bras Cardiol. 2017;109(6 suppl 2):1-34. doi: https://doi.org/10.5935/abc.20180007. Erratum in: Arq Bras Cardiol. 2018;110(5):497.
3. Tarasoutchi F, Montera MW, Ramos AI, Sampaio RO, Rosa VE, Accorsi TA, et al. Update of the Brazilian Guidelines for Valvular Heart Disease - 2020. Arq Bras Cardiol. 2020;115(4):720-75. doi: https://doi.org/10.36660/abc.20201047
4. Iung B. Management of ischaemic mitral regurgitation. Heart. 2003;89(4):459-64. doi: https://doi.org/10.1136/heart.89.4.459
5. Miller DC. Ischemic mitral regurgitation redux--to repair or to replace? J Thorac Cardiovasc Surg. 2001;122(6):1059-62. doi: https://doi.org/10.1067/mtc.2001.120341
6. Vahanian A, Alfieri O, Andreotti F, Antunes MJ, Barón-Esquivias G, Baumgartner H, et al.; ESC Committee for Practice Guidelines (CPG); Joint Task Force on the Management of Valvular Heart Disease of the European Society of Cardiology (ESC); European Association for Cardio-Thoracic Surgery (EACTS). Guidelines on the management of valvular heart disease (version 2012): the Joint Task Force on the Management of Valvular Heart Disease of the European Society of Cardiology (ESC) and the European Association for Cardio-Thoracic Surgery (EACTS). Eur J Cardiothorac Surg. 2012;42(4):S1-44. doi: https://doi.org/10.1093/ejcts/ezs455
7. Albuquerque DC, Neto JD, Bacal F, Rohde LE, Bernardez-Pereira S, Berwanger O, et al.; Investigadores Estudo BREATHE. I Brazilian Registry of Heart Failure - Clinical Aspects, Care Quality and Hospitalization Outcomes. Arq Bras Cardiol. 2015;104(6):433-42. doi: https://doi.org/10.5935/abc.20150031. Erratum in: Arq Bras Cardiol. 2015;105(2):208.
8. Sousa FT. Avaliação ecocardiográfica da função do átrio esquerdo como marcadora de eventos em pacientes com insuficiência cardíaca [Doutorado]. São Paulo: Universidade de São Paulo; 2017 [citado 2022 Mai 25]. Disponível em: https://www.teses.usp.br/teses/disponiveis/98/98131/tde-02012018-133920/pt-br.php
9. Cameli M, Caputo M, Mondillo S, Ballo P, Palmerini E, Lisi M, et al. Feasibility and reference values of left atrial longitudinal strain imaging by two-dimensional speckle tracking. Cardiovasc Ultrasound. 2009;7:6. doi: https://doi.org/10.1186/1476-7120-7-6
10. Mehrzad R, Rajab M, Spodick DH. The three integrated phases of left atrial macrophysiology and their interactions. Int J Mol Sci. 2014;15(9):15146-60. doi: https://doi.org/10.3390/ijms150915146
11. Sirbu C, Herbots L, D'hooge J, Claus P, Marciniak A, Langeland T, Bijnens B, et al. Feasibility of strain and strain rate imaging for the assessment of regional left atrial deformation: a study in normal subjects. Eur J Echocardiogr. 2006;7(3):199-208. doi: https://doi.org/10.1016/j.euje.2005.06.001
12. Lang RM, Badano LP, Mor-Avi V, Afilalo J, Armstrong A, Ernande L, et al. Recommendations for cardiac chamber quantification by echocardiography in adults: an update from the American Society of Echocardiography and the European Association of Cardiovascular Imaging. J Am Soc Echocardiogr. 2015;28(1):1-39.e14. doi: https://doi.org/10.1016/j.echo.2014.10.003
13. Picard MH, Adams D, Bierig SM, Dent JM, Douglas PS, Gillam LD, et al; American Society of Echocardiography. American Society of Echocardiography recommendations for quality echocardiography laboratory operations. J Am Soc Echocardiogr. 2011;24(1):1-10. doi: https://doi.org/10.1016/j.echo.2010.11.006
14. Lancellotti P, Moura L, Pierard LA, Agricola E, Popescu BA, Tribouilloy C, et al.; European Association of Echocardiography. European Association of Echocardiography recommendations for the assessment of valvular regurgitation. Part 2: mitral and tricuspid regurgitation (native valve disease). Eur J Echocardiogr. 2010;11(4):307-32. doi: https://doi.org/10.1093/ejechocard/jeq031
15. Zoghbi WA, Enriquez-Sarano M, Foster E, Grayburn PA, Kraft CD, Levine RA, et al.; American Society of Echocardiography. Recommendations for evaluation of the severity of native valvular regurgitation with two-dimensional and Doppler echocardiography. J Am Soc Echocardiogr. 2003;16(7):777-802. doi: https://doi.org/10.1016/S0894-7317(03)00335-3
16. Abhayaratna WP, Seward JB, Appleton CP, Douglas PS, Oh JK, Tajik AJ, et al. Left atrial size: physiologic determinants and clinical applications. J Am Coll Cardiol. 2006;47(12):2357-63. doi: https://doi.org/10.1016/j.jacc.2006.02.048
17. Vieira MJ, Teixeira R, Gonçalves L, Gersh BJ. Left atrial mechanics: echocardiographic assessment and clinical implications. J Am Soc Echocardiogr. 2014;27(5):463-78. doi: https://doi.org/10.1016/j.echo.2014.01.021
18. Park SM, Park SW, Casaclang-Verzosa G, Ommen SR, Pellikka PA, Miller FA Jr, et al. Diastolic dysfunction and left atrial enlargement as contributing factors to functional mitral regurgitation in dilated cardiomyopathy: data from the Acorn trial. Am Heart J. 2009;157(4):762.e3-10. doi: https://doi.org/10.1016/j.ahj.2008.12.018
19. Cioffi G, Tarantini L, De Feo S, Pulignano G, Del Sindaco D, Stefenelli C, et al. Functional mitral regurgitation predicts 1-year mortality in elderly

patients with systolic chronic heart failure. Eur J Heart Fail. 2005;7(7):1112-7. doi: https://doi.org/10.1016/j.ejheart.2005.01.016

20. Crawford MH, Souchek J, Oprian CA, Miller DC, Rahimtoola S, Giacomini JC, et al. Determinants of survival and left ventricular performance after mitral valve replacement. Department of Veterans Affairs Cooperative Study on Valvular Heart Disease. Circulation. 1990;81(4):1173-81. doi: https://doi.org/10.1161/01.cir.81.4.1173

21. Hickey MS, Smith LR, Muhlbaier LH, Harrell FE Jr, Reves JG, Hinohara T, et al. Current prognosis of ischemic mitral regurgitation. Implications for future management. Circulation. 1988;78(3 Pt 2):I51-9.

22. Lee R, Haluska B, Leung DY, Case C, Mundy J, Marwick TH. Functional and prognostic implications of left ventricular contractile reserve in patients with asymptomatic severe mitral regurgitation. Heart. 2005;91(11):1407-12. doi: https://doi.org/10.1136/hrt.2004.047613

23. Trichon BH, Felker GM, Shaw LK, Cabell CH, O'Connor CM. Relation of frequency and severity of mitral regurgitation to survival among patients with left ventricular systolic dysfunction and heart failure. Am J Cardiol. 2003;91(5):538-43. doi: https://doi.org/10.1016/s0002-9149(02)03301-5

24. Jenkins C, Bricknell K, Marwick TH. Use of real-time three-dimensional echocardiography to measure left atrial volume: comparison with other echocardiographic techniques. J Am Soc Echocardiogr. 2005;18(9):991-7. doi: https://doi.org/10.1016/j.echo.2005.03.027

25. Le Bihan DC, Della Togna DJ, Barretto RB, Assef JE, Machado LR, Ramos AI, et al. Early improvement in left atrial remodeling and function after mitral valve repair or replacement in organic symptomatic mitral regurgitation assessed by three-dimensional echocardiography. Echocardiography. 2015;32(7):1122-30. doi: https://doi.org/10.1111/echo.12817

26. Lester SJ, Ryan EW, Schiller NB, Foster E. Best method in clinical practice and in research studies to determine left atrial size. Am J Cardiol. 1999;84(7):829-32. doi: https://doi.org/10.1016/s0002-9149(99)00446-4

27. Messika-Zeitoun D, Bellamy M, Avierinos JF, Breen J, Eusemann C, Rossi A, et al. Left atrial remodelling in mitral regurgitation--methodologic approach, physiological determinants, and outcome implications: a prospective quantitative Doppler-echocardiographic and electron beam-computed tomographic study. Eur Heart J. 2007;28(14):1773-81. doi: https://doi.org/10.1093/eurheartj/ehm199

28. Aurigemma GP, Gottdiener JS, Arnold AM, Chinali M, Hill JC, Kitzman D. Left atrial volume and geometry in healthy aging: the Cardiovascular Health Study. Circ Cardiovasc Imaging. 2009;2(4):282-9. doi: https://doi.org/10.1161/CIRCIMAGING.108.826602

29. Moller JE, Hillis GS, Oh JK, Seward JB, Reeder GS, Wright RS, et al. Left atrial volume: a powerful predictor of survival after acute myocardial infarction. Circulation. 2003;107(17):2207-12. doi: https://doi.org/10.1161/01.CIR.0000066318.21784.43

30. Tsang TS, Barnes ME, Gersh BJ, Bailey KR, Seward JB. Risks for atrial fibrillation and congestive heart failure in patients >/=65 years of age with abnormal left ventricular diastolic relaxation. Am J Cardiol. 2004;93(1):54-8. doi: https://doi.org/10.1016/j.amjcard.2003.09.012

31. Kottkamp H. Fibrotic atrial cardiomyopathy: a specific disease/syndrome supplying substrates for atrial fibrillation, atrial tachycardia, sinus node disease, AV node disease, and thromboembolic complications. J Cardiovasc Electrophysiol. 2012;23(7):797-9. doi: https://doi.org/10.1111/j.1540-8167.2012.02341.x

32. Flaker GC, Fletcher KA, Rothbart RM, Halperin JL, Hart RG. Clinical and echocardiographic features of intermittent atrial fibrillation that predict recurrent atrial fibrillation. Stroke Prevention in Atrial Fibrillation (SPAF) Investigators. Am J Cardiol. 1995;76(5):355-8. doi: https://doi.org/10.1016/s0002-9149(99)80100-3

33. Bolca O, Akdemir O, Eren M, Dagdeviren B, Yildirim A, Tezel T. Left atrial maximum volume is a recurrence predictor in lone atrial fibrillation: an acoustic quantification study. Jpn Heart J. 2002;43(3):241-8. doi: https://doi.org/10.1536/jhj.43.241

34. Barnes ME, Miyasaka Y, Seward JB, Gersh BJ, Rosales AG, Bailey KR, et al. Left atrial volume in the prediction of first ischemic stroke in an elderly cohort without atrial fibrillation. Mayo Clin Proc. 2004;79(8):1008-14. doi: https://doi.org/10.4065/79.8.1008

35. Benjamin EJ, D'Agostino RB, Belanger AJ, Wolf PA, Levy D. Left atrial size and the risk of stroke and death. The Framingham Heart Study. Circulation. 1995;92(4):835-41. doi: https://doi.org/10.1161/01.cir.92.4.835

36. Lønborg JT, Engstrøm T, Møller JE, Ahtarovski KA, Kelbæk H, Holmvang L, et al. Left atrial volume and function in patients following ST elevation myocardial infarction and the association with clinical outcome: a cardiovascular magnetic resonance study. Eur Heart J Cardiovasc Imaging. 2013;14(2):118-27. doi: https://doi.org/10.1093/ehjci/jes118

37. Tsang TS, Barnes ME, Gersh BJ, Takemoto Y, Rosales AG, Bailey KR, et al. Prediction of risk for first age-related cardiovascular events in an elderly population: the incremental value of echocardiography. J Am Coll Cardiol. 2003;42(7):1199-205. doi: https://doi.org/10.1016/s0735-1097(03)00943-4

38. Sugimoto T, Robinet S, Dulgheru R, Bernard A, Ilardi F, Contu L, et al.; NORRE Study. Echocardiographic reference ranges for normal left atrial function parameters: results from the EACVI NORRE study. Eur Heart J Cardiovasc Imaging. 2018;19(6):630-8. doi: https://doi.org/10.1093/ehjci/jey018

39. Triposkiadis F, Moyssakis I, Hadjinikolaou L, Makris T, Zioris H, Hatzizaharias A, et al. Left atrial systolic function is depressed in idiopathic and preserved in ischemic dilated cardiomyopathy. Eur J Clin Invest. 1999;29(11):905-12. doi: https://doi.org/10.1046/j.1365-2362.1999.00563.x

40. D'Andrea A, Caso P, Romano S, Scarafile R, Cuomo S, Salerno G, et al. Association between left atrial myocardial function and exercise capacity in patients with either idiopathic or ischemic dilated cardiomyopathy: a two-dimensional speckle strain study. Int J Cardiol. 2009;132(3):354-63. doi: https://doi.org/10.1016/j.ijcard.2007.11.102

41. Cameli M, Sparla S, Losito M, Righini FM, Menci D, Lisi M, et al. Correlation of Left Atrial Strain and Doppler Measurements with Invasive Measurement of Left Ventricular End-Diastolic Pressure in Patients Stratified for Different Values of Ejection Fraction. Echocardiography. 2016;33(3):398-405. doi: https://doi.org/10.1111/echo.13094

42. Guler A, Tigen KM, Dundar C, Karaahmet T, Karabay CY, Aung SM, et al. Left atrial deformation and nonischemic dilated cardiomyopathy. A 2D speckle-tracking imaging study. Herz. 2014;39(2):251-7. doi: https://doi.org/10.1007/s00059-013-3817-z.

Original article

Left Ventricular Longitudinal Linear Displacement Versus Global Longitudinal Strain on Cardiovascular Magnetic Resonance

Deslocamento Linear Longitudinal do Ventrículo Esquerdo Comparado ao Strain Longitudinal Global por Ressonância Magnética Cardiovascular

Rafael Almeida Fonseca[1], Sergio Marrone Ribeiro[2], Clerio Francisco de Azevedo Filho[3], Roney Sampaio[1], Flávio Tarasoutchi[1], Carlos Eduardo Rochitte[1]

[1]Heart Institute (InCor), Hospital das Clínicas, School of Medicine, University of São Paulo, São Paulo, SP, Brazil. [2]Botucatu School of Medicine, Paulista State University, UNESP, Botucatu, SP, Brazil. [3]Department of Cardiology, Duke University Medical Center, Durham, NC, USA.

Abstract

Background: Left ventricular (LV) systolic diastolic function is prognostic in cardiovascular diseases and can be assessed via global longitudinal strain (GLS) on echocardiography and cardiac magnetic resonance (CMR). However, GLS by CMR requires the use of expensive software. Longitudinal linear displacement (LLD) may be a simple and inexpensive alternative to GLS, but the two have not been systematically compared.

Objective: To compare LLD with GLS and LV ejection fraction (LVEF) in aortic valve disease patients and controls.

Methods: We included 44 participants (26 with aortic valve disease, 19 controls). GLS was determined using CVI42 software (Circle Cardiovascular Imaging), while the LLD linear measurements of the distance between the base/apex of the LV included maximum displacement (MD), maximum velocity in early diastole (MVED), atrioventricular junction velocity in diastasis (VDS), and VDS/MVED ratio.

Results: DM and MVED were correlated with GLS (r=0.69 and r=0.65, respectively) and LVEF (r=0.47 and r=0.57, p<0.001 for both). DM and MVED showed areas under the receiver operating characteristic curve (AUC) of 0.88 and 0.91, and at the best cut-off point (-0.13 and 0.66), sensitivities of 72.43% and 57.14% and specificities of 80.65% and 87.10%, respectively, compared to GLS. Using LVEF as a reference, we obtained AUC of 0.70 and 0.82, and at the best cut-off point (-0.11 and 0.61), sensitivities of 75.00% and 50.00% and specificities of 72.97% and 78.38%, respectively.

Conclusion: LLD demonstrated similar performance to that of GLS. MD derived from LLD was the best parameter during systole, while MVED was the best during diastole. Our findings demonstrate the routine, quick, and inexpensive assessment of diastolic function on CMR.

Keywords: Magnetic Resonance; Myocardial Contraction; Aortic Valve Stenosis; Aortic Valve Insufficiency; Diastole.

Resumo

Introdução: A função sistodiastólica do ventrículo esquerdo é prognóstica nas doenças cardiovasculares e pode ser avaliada por *strain* longitudinal global por meio de ecocardiografia e de ressonância magnética cardíaca. O *strain longitudinal global* pela ressonância magnética cardíaca exige a utilização de *software* de alto custo. O deslocamento linear longitudinal do ventrículo esquerdo pode ser uma alternativa simples e barata ao *strain* longitudinal global, porém eles não foram ainda comparados sistematicamente.

Objetivo: Comparar o deslocamento linear longitudinal com o *strain* longitudinal global e fração de ejeção do ventrículo esquerdo em valvopatas aórticos e controles.

Métodos: Incluímos 44 participantes (26 valvopatas aórticos/19 controles). O *strain* longitudinal global utilizou *software* específico (*Circle Cardiovascular Imaging* 42) e o deslocamento linear longitudinal apenas medidas lineares de distância entre a base e o ápex do ventrículo esquerdo, gerando deslocamento máximo, velocidade máxima no início da diástole, velocidade na diástase e a relação entre velocidade na diástase e velocidade máxima no início da diástole.

Resultados: Deslocamento máximo e velocidade máxima no início da diástole correlacionaram-se com *strain* longitudinal global (r=0,69 e r=0,65 respectivamente) e com a fração de ejeção do ventrículo esquerdo (r=0,47 e r=0,57, p<0,001 para ambos). Deslocamento

Mailing Address: Carlos Eduardo Rochitte •
Instituto do Coração, Faculdade de Medicina, Universidade de São Paulo, Avenida Dr. Enéas de Carvalho Aguiar, 44, Andar AB, Cerqueira César.
CEP: 05403-000 – São Paulo, SP, Brazil.
E-mail: rochitte@incor.usp.br
Manuscript received 5/11/2022; revised 5/18/2022; accepted 5/25/2022

DOI: 10.47593/2675-312X/20223502eabc304

máximo e velocidade máxima no início da diástole apresentaram área sob a curva Característica de Operação do Receptor de 0,88 e 0,91 e, no melhor ponto de corte (-0,13 e 0,66), sensibilidade de 72,43% e 57,14% e especificidade 80,65% e 87,10%, respectivamente, quando comparados ao *strain* longitudinal global. Utilizando a fração de ejeção do ventrículo esquerdo como referência, foram obtidos 0,70 e 0,82, e, no melhor ponto de corte (-0,11 e 0,61), sensibilidade de 75,00% e 50,00% e especificidade 72,97% e 78,38%, respectivamente.

Conclusão: O deslocamento linear longitudinal foi semelhante ao *strain* longitudinal global. O deslocamento máximo derivado do deslocamento linear longitudinal foi o melhor parâmetro na sístole, enquanto a velocidade máxima no início da diástole foi o melhor na diástole, o que possibilita a avaliação da função diastólica pela ressonância magnética cardíaca na rotina clínica de forma rápida e sem custo adicional.

Palavras-chave: Ressonância Magnética; Contração Miocárdica; Estenose da Valva Aórtica; Insuficiência da Valva Aórtica; Diástole.

Introduction

Systolic and diastolic dysfunction are important markers of several cardiovascular diseases in clinical practice.[1] Studies evaluating myocardial strain demonstrated high ability for the early detection of contractile dysfunction in several cardiovascular diseases.[2] The myocardial strain technique is based on myocardial architecture analysis and evaluates three distinct layers: subendocardial, formed by longitudinal fibers oriented from the base to the apex; middle of the wall, with circumferential fibers; and subepicardial, with longitudinal fibers oriented from the apex to the base.[2]

The strain is often measured by two modalities, speckle tracking by echocardiography (ECHO) and feature tracking imaging (FTI) by cardiac magnetic resonance imaging (CMRI).[3,4] ECHO, which analyzes small groups of pixels in the myocardium created by the interaction of ultrasonic beams and the heart muscle with specific grayscale characteristics, is the most widely used modality in clinical practice. CMRI can assess GLS via two techniques. The first technique is myocardial tissue tagging, which identifies simple linear or grid patterns applied to the CMRI image during its acquisition and is considered the gold standard for assessing GLS against which ECHO was validated.[5] However, this technique requires the acquisition of specific tagging images, demanding additional time for CMRI study.

The new FTI technique was recently developed for GLS assessments using conventional cine-MRI. This technique uses principles similar to speckle-tracking used in ECHO but that are applied to CMRI to track specific pixels characteristics throughout the cardiac cycle.[6] Studies of patients developing diastolic dysfunction in pathologies such as aortic stenosis (AoS) and aortic insufficiency (AoI) demonstrated a left ventricular (LV) ejection fraction (LVEF) within the normal range and changed strain, indicating the presence of a diastolic dysfunction component in addition to the incipient contractile dysfunction not detected by LVEF. These data indicate that GLS, which incorporates systolic and diastolic function, is more sensitive than LVEF for assessing ventricular contraction mechanics.[7,8]

GLS is not usually assessed by FTI CMRI in clinical routine, as it requires additional post-processing time and specialized and expensive software. This technique requires the acquisition of endocardial and epicardial contours for all cardiac phases on a cine-MRI scan. Our group evaluated a new technique that is simple to apply, requires no specialized software, and can be performed using simple and free image viewer software. This technique is based on LV longitudinal linear displacement (LLD), more specifically on the linear basal-apical shortening of the LV. In this previous study, longitudinal shortening detected systolic and diastolic function changes in patients with aortic valve disease (AVD) versus normal controls.

Although LLD was already compared with diastolic dysfunction by ECHO[9] and in specific groups of patients with proven diastolic dysfunction,[10] it has not yet been compared with GLS by FTI CMRI. Thus, this study aimed to compare LLD and GLS measured by the FTI technique.

Methods

Study population

This study included 26 patients with severe AVD eligible for aortic valve replacement surgery with LVEF within the normal range who underwent CMRI as part of their clinical evaluation. It also included 19 healthy controls. Of the patients with AVD, 11 (42.3%) had aortic regurgitation and 15 (57.7%) had AoS. The exclusion criteria were age below 18 and above 85 years, diabetes mellitus, systemic arterial hypertension, dyslipidemia, or significant concomitant coronary disease. All patients aged over 40 years underwent coronary angiography, and those with significant coronary artery disease (luminal stenosis > 50%) were excluded. Patients with concomitant mitral valve disease, previous cardiac surgery, or contraindications to CMRI; who were using pacemakers, metal clips, or other ferromagnetic structures; or who had claustrophobia were also excluded.

Baseline GLS and LLD were established in 19 healthy volunteers with no significant medical history. Patients underwent CMRI with a 1.5 Tesla clinical magnet (Signa CV/i; GE Medical Systems, Waukesha, WI, USA) and dedicated cardiac coil. After the heart was located, 8–12 contiguous short-axis slices covering the entire LV (8-mm slice thickness and 2-mm inter-slice interval) and long-axis slices (two- and four-chamber planes and LV outflow tract) were prescribed. Cine-MRI scans were acquired with a steady-state free precession pulse sequence with high temporal resolution (<50 ms between phases) and with other conventional parameters: TR, 3.9 ms; TE, 1.8 ms; flip angle, 45°; receiver bandwidth, ±125 kHz; field of view, 34 × 34 cm; 256 × 160 matrix; and voxel size, 1.3 × 2.1 × 8.0 mm.

Image analysis using feature tracking imaging technique to obtain GLS

Global longitudinal strain was analyzed using cine-MRI images in four-chamber long-axis view and along 20 cardiac phases. CVI42 software (Circle Cardiovascular Imaging, Calgary, Canada) and the Tissue Tracking tool were used to identify the diastolic phase, with manual definition of the endocardial and epicardial contours, which are automatically propagated by the software to the other cardiac phases. Subsequently, myocardial GLS was automatically calculated by the software using a Eulerian mathematical principle that represents a measure of ventricular strain (Figure 1).[11] GLS numerical data were stored in the software and exported to data sheets for further analysis.

Image analysis using the longitudinal linear displacement (LLD) technique

As in GLS analysis, LLD was performed on cine-MRI images in four-chamber long-axis view. The basal atrioventricular junction (AVJ) position was defined in end-diastole and its longitudinal displacement was measured in relation to a reference line drawn between the LV apex (epicardium contour, low-intensity line corresponding to the myocardial and epicardial fat interface) and the lower limit (low-intensity line) of the coronary sinus running along the atrioventricular groove immediately lateral to the AVJ. A simple straight line was traced through the cardiac cycle along all phases between the basal and apical landmarks using a DICOM Webpax visualization platform (Heart Imaging Technologies, LLC, Durham, NC, USA) (Figure 2). Phase-by-phase LV longitudinal measurements were subsequently divided by the longitudinal length at end-diastole (maximum length) to provide percentage AVJ displacement values during the 20 phases.

(AVJ dis.%). $$AVJ\ dis.(\%) = \frac{LM(phase)}{CM}$$

Longitudinal displacement (D) versus time was analyzed by subtracting the maximum percentage AVJ displacement (max AVJ des. %) by the minimum for each phase (min. phase) divided by the max AVJ des. % as shown in the equation below.

$$D = \frac{AVJ\ dis.(\%)Max - Min(phase)}{Max\ AVJ\ dis.(\%)}$$

LLD parameters were extracted from the generated longitudinal displacement (D) versus time graph: maximum displacement (MD), maximum velocity in early diastole (MVED), best-fit line of normalized AVJ velocity in diastasis (VDS), and VDS/MVED ratio. MD was extracted through the minimum over the data range obtained from D as shown in the equation below.

$$MD = Minimum\ D\ (phase\ by\ phase)$$

The MVED of each participant was acquired through a regression slope on the displacement versus time graph adjusted for early diastole (Figure 2). The same method was used for VDS considering the time of diastasis.

Statistical analysis

Sample size was related to the number of patients with a confirmed diagnosis available for analysis (convenience sample), which corroborates the literature in the area.[10,12] Normality was assessed by the Shapiro-Wilk test. Simple linear regression analyses were performed for each of the LLD parameters (MVED, VDS, MD, and VDS/MVED) with GLS and LVEF. A GLS cutoff point of -13%, which corresponds to the 99th percentile of the values measured in the control group, was used as the limit of normality. A normal LVEF was considered those greater than or equal to 55%. We evaluated the accuracy, sensitivity, and specificity of the LLD parameters (MVED, VDS, MD, and VDS/MVED) using FTI GLS and LVEF with the normality thresholds defined above as the reference method. The receiver operating characteristic (ROC) curves and the cut-point test were used to define the optimal sensitivity and specificity threshold. Stata software version 13 for Macintosh was used for the statistical analysis considering values of $p < 0.05$ as statistically significant.

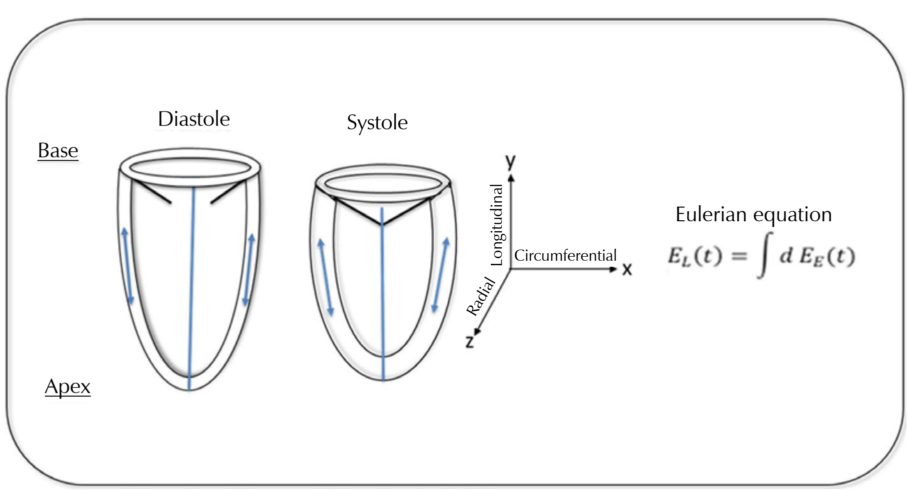

Figure 1 – *Illustration of myocardial deformation by the Eulerian equation used to extract the global longitudinal strain values used in our study using CVI 42 software.*

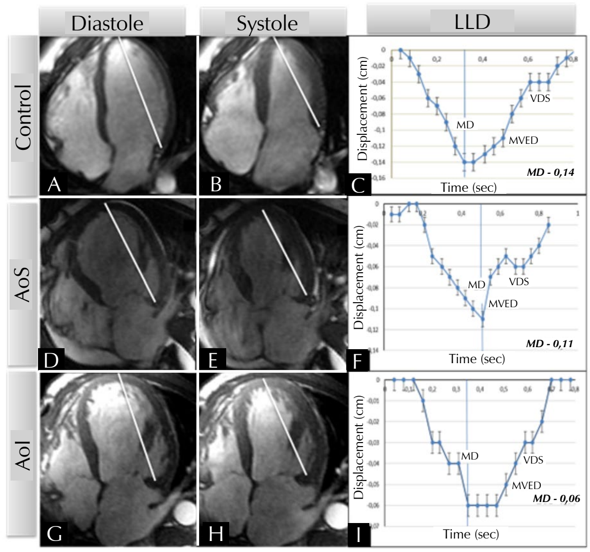

AoI: aortic insufficiency; AoS: aortic stenosis; LLD: longitudinal linear displacement.

Figure 2 – *Panel demonstrating longitudinal linear displacement (LLD) analysis in patients with valve disease and normal controls. (A) and (B) represent the cardiac cycle phase. (C) represents the LLD parameter curve.*

Results

Population characteristics

The group of healthy volunteers included 10 men and nine women with a mean age of 43.1 ± 11.8 years (range, 24–58 years). The patient group included 19 men and seven women with a mean age of 46.8 ± 13.7 years (range, 26–72 years). The participants' clinical characteristics including cardiovascular history, risk factors, and CMRI data are presented in Table 1.

Cardiovascular magnetic resonance imaging

Table 2 shows the results of GLS, morphology, volume, and global LV function measurements for all groups. Figure 3 shows sample GLS analyses in each group and endocardial and epicardial contours.

The MVED, MD, VDS, and VDS/MVED correlation coefficients (r) and (p) are presented in Table 3. MD and MVED showed strong and significant correlations compared with the GLS approach for both the total sample and for only patients with AVD. Compared with LVEF, the correlations were more evident and significant for all participants (Table 3). The linear regression of MD versus GLS showed a positive correlation with an $r = 0.69$ and $p < 0.001$ for the total sample and an $r = 0.66$ and $p < 0.001$ for patients with AVD (Figure 4). Comparison of MD and LVEF resulted in an $r = 0.47$ and $p < 0.001$ (Figure 4).

The linear regression of MVED versus GLS showed a negative correlation of an $r = -0.65$ and $p < 0.001$ for the total sample and an $r = -0.53$ and $p < 0.005$ for patients with AVD (Figure 5). MVED is positively correlated with LVEF and showed an $r = 0.57$ and $p < 0.001$ for all participants.

The evaluation of VDS and VDS/MVED with GLS and LVEF

Table 1 – Patients' clinical characteristics.

Característica	OAI	AoS	Controls	p/p*
Demographics				
Total (N = 45)	11 (42.3)	15 (57.7)	19	
Men	10 (90.9)	9 (60.0)	10 (52.6)	0.079/0.101
Age, years	46.0±15.7	48±11.3	38.1±10.5	0.610/0.039
Weight, kg	76.6±10.6	71.2±11.9	67.9±15.3	0.336/0.356
BMI, kg/m^2	27.9±3.5	26.3±3.8	23.5±3.6	0.382/0.021
BSA, m^2	1.8±3.5	1.7±0.1	1.47±0.2	0.209/0.696
Rheumatic	9 (81.8)	3 (20.0)	-	
Bicuspid	2 (18.2)	8 (53.3)	-	
Degeneration/calcification	0	4 (26.7)	-	
Heart rate, bpm	65.0±11.9	81.5±20.7	70.1±10.6	0.027/0.019
SBP	126.7±11.9	121.5±15.2	111.6±8.9	0.505/0.018
DBP	80±8.9	71.8±12.8	71.3±6.6	0.183/0.143
Risk factors and cardiovascular history				
Angina	0 (0.0)	1 (6.7)	-	0.465
Hypertension	6 (54.6)	1 (6.7)	-	0.465
Syncope	0	6 (40.0)	-	0.100
Diabetes	0	1 (13.3)	-	0.342
Hypercholesterolemia	0	0	-	-
Smoker	0 (0.0)	5 (33.3)	-	0.100
Family history and CAD	4 (34.4)	3 (20.0)		0.190
NYHA classification > I (II and III)	11 (100.0)	15 (100.0)	19 (100.0)	0.526

*Absolute values and percentages in parentheses, n (%). AoI, aortic insufficiency; AoS, aortic stenosis; BMI, body mass index; BSA, body surface area; CAD, coronary artery disease; DBP, diastolic blood pressure; EDV, end-diastolic volume; ESV, end-systolic volume; GLS, global longitudinal strain; LV, left ventricle; LVEF, left ventricular ejection fraction; NYHA, New York Heart Association; SBP, systolic blood pressure. *Comparison between three groups, including controls; remaining p values for comparison between aortic insufficiency and stenosis. The criteria for defining concentric hypertrophy are LV mass/EDV ratio > 1.16 g/mL). Ref: Dweck MR et al. J Cardiovasc Magn Reson 2012.*

showed weak correlations or discrete associations, some of which were not statistically significant for the total sample or patients with AVD (Table 3).

Table 4 shows the diagnostic performance analysis data for MVED, MD, VDS, and VDS/MVED measures to predict GLS and LVEF. MD and MVED again demonstrated better diagnostic performance than LVEF and GLS. The MD versus GLS longitudinal axis presented an area under the ROC curve of 0.88. When the best cutoff point (-0.13) was defined, MD demonstrated 72.43% sensitivity and 86.65% specificity (Figure 6). The analysis with LVEF showed an area of 0.70, sensitivity of 75.00%, and specificity of 72.97% (at the best cutoff point under the ROC curve, -0.11) (Figure 6). MVED versus GLS showed an area of 0.91, sensitivity of 57.14%, and specificity of 87.10% (cutoff point of 0.53). The analysis of MVED and LVEF resulted in an area of 0.82, sensitivity of 50.00%, and specificity of 78.38% (at the best cutoff point of 0.61) (Figure 7). VDS and VDS/MVED demonstrated inferior diagnostic performance (Table 4).

Discussion

This study demonstrated that the assessment of LV diastolic

Table 2 – Cardiac magnetic resonance imaging data by study group.

Characteristic	IAo	EAo	Controles	p/p*
GLS	-10.7±2.3	-13.0±3.2	15.9±1.7	<0.001
LVEDV, mL	29.6±68.5	179.99±42.1	129.5±24.7	<0.001
LVESV, mL	148.9±60.4	82.0±28.7	45.5±9.4	<0.001
LVEF, %	51.7±11.4	55.1±9.1	64.7±5.3	<0.001
LV mass, g	264.2±42.4	272.8±45.5	118.1±40.5	<0.001
Eccentric hypertrophy	10 (90.9)	1 (6.7)		
Concentric hypertrophy	1 (9.1)	14 (93.30		
MD	-0.09	0.12	0.16	
MVED	0.47	0.78	1.43	
VDS	0.09	0.31	0.28	
VDS/MVED	0.44	0.23	0.21	

AoI, aortic insufficiency; AoS, aortic stenosis; GLS, global longitudinal strain; LVEDV, left ventricular end-diastolic volume; LVEF, left ventricular ejection fraction; LVESV, left ventricular end-systolic volume; MD, maximum displacement; MVED, maximum velocity in early diastole, VDS, best-fit line of normalized atrioventricular junction velocity in diastasis. All indicates AoI, AoS, and controls.

Table 3 – Linear regression analysis of MD, MVED, VDS, and VDS/MVED.

All	Strain (%)		LVEF (%)	
MD, cm	0.69	<0.001	0.47	<0.001
MVED, s^{-1}	0.65	<0.001	0.57	<0.001
VDS, s^{-1}	0.01	<0.920	0.09	<0.559
VDS/MVED	0.31	<0.035	0.43	<0.003
Aortic valve disease r,(p)				
MD, cm	0.66	<0.001	0.23	<0.244
MVED, s^{-1}	0.53	<0.005*	0.39	<0.049
VDS, s^{-1}	0.43	<0.027	0.25	<0.215
VDS/MVED	0.04	<0.837	0.18	<0.378

LVEF, left ventricular ejection fraction; MD, maximum displacement; MVED, maximum velocity in early diastole, VDS, best-fit line of normalized atrioventricular junction velocity in diastasis. All indicates AoI, AoS, and controls.

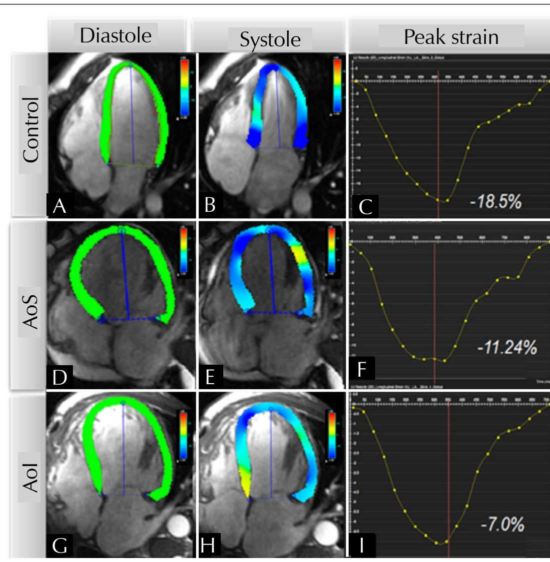

AoI:aortic insufficiency; AoS: aortic stenosis.

Figure 3 – *Panel demonstrating global longitudinal strain analyses detailing endocardial and epicardial contours. Peak strain is shown. (A) and (B) represent the analyses of normal control volunteers with peak stain of 18.5% (C). (D) and (E) show the analyses of patients with aortic stenosis and a strain peak of 7.0% (G). (F) and (H) present the strain of patients with aortic insufficiency and a peak strain of 11.0% (I).*

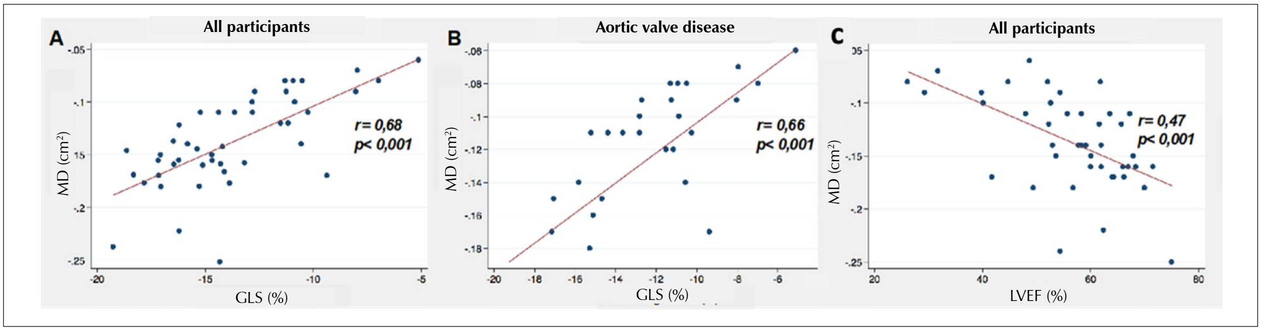

Figure 4 – *(A) and (B) show the correlation between maximum atrioventricular junction displacement and global longitudinal strain. (A) shows the analysis of all patients. (B) shows the regression of patients with aortic valve disease.*

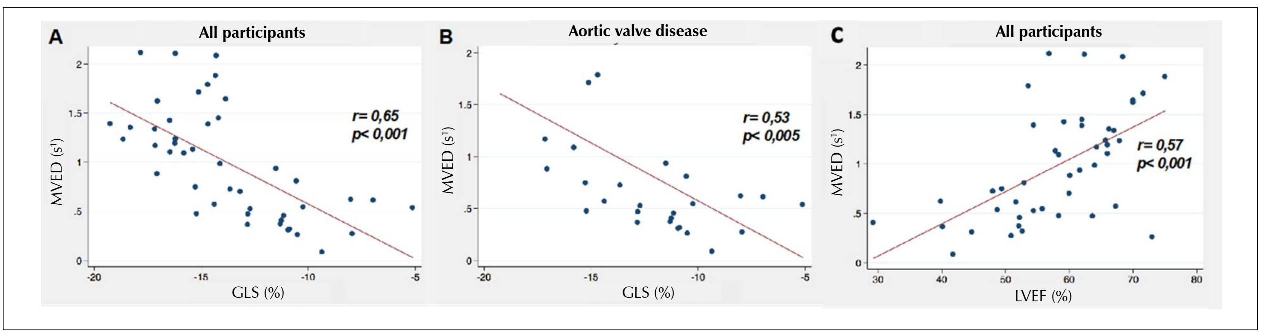

Figure 5 – *(A) and (B) show the correlation between maximum atrioventricular junction displacement and left ventricular ejection fraction. (A) shows the analysis of all patients. (B) shows the regression of patients with aortic valve disease.*

Table 4 – Diagnostic performance of MD, MVED, VDS, and VDS/MVED on the receiver operating characteristic curve.

	AUC	Sensitivity	Specificity	PPV	NPV
Strain, %					
MD, cm	0.88	72.43	80.65	62.50	86.21
MVED, s^{-1}	0.91	57.14	87.10	66.67	81.82
VDS, s^{-1}	0.56	57.14	64.52	42.11	76.92
VDS/MVED	0.68	78.57	58.06	45.83	85.71
LVEF (%)					
MD, cm	0.70	75.00	72.97	37.50	93.10
MVED, s^{-1}	0.82	50.00	78.38	33.33	87.88
VDS, s^{-1}	0.67	62.50	62.16	26.32	88.46
VDS/MVED	0.82	100.00	56.76	33.33	100.00

AUC, area under the receiver operating characteristic curve; LVEF, left ventricular ejection fraction; MD, maximum displacement; MVED, maximum velocity in early diastole; NPV, negative predictive value; PPV, positive predictive value; VDS, best-fit line of normalized atrioventricular junction velocity in diastasis.

dysfunction using linear CMRI parameters (MD and MVED) has statistically high correlation and diagnostic accuracy to that of GLS measured by FTI and LVEF in patients with AoS and AoI as well as in normal controls.

These data corroborate and reinforce the results of the study by Ribeiro et al., in which LV linear measurements (MVED, MD, VDS, and VDS/MVED) differed significantly between patients with AVD and normal controls. In our study, we validated linear measurements derived from LLD versus GLS measured by specific FTI software and LVEF. Saba et al. used a similar technique and obtained slightly higher linear measurements in the normal control group than in that of our study (-0.165).[9] This is probably due to the use of a less lateral anatomical landmark and, therefore, a lower diastolic value of this distance that results in a greater percentage variation with the systolic linear measurement. The most lateral point chosen in the present study increased the precision and reproducibility of its visual definition by the observer. On cine-MRI, coronary sinus interface in the atrioventricular groove is better defined than the junction of the mitral valve leaflets in the mitral fibrous annulus. We used only one AVJ displacement measurement, with a better defined reference point on the AVJ lateral wall instead of two, thus simplifying and making the measurements faster and more practical.

Saba et al. validated linear measurements with peak systolic strain using tissue Doppler to assess diastolic function; however, our study demonstrated a statistically significant correlation between MD and GLS by FTI CMRI. These data reinforce the relevance of MD on CMRI in the assessment of systolic dysfunction. Furthermore, the area under the ROC curve of MD versus GLS showed high accuracy (0.88) for assessing systolic function. MVED demonstrated high accuracy when correlated with GLS (0.91). For the first time, this information allows the use of a method to analyze

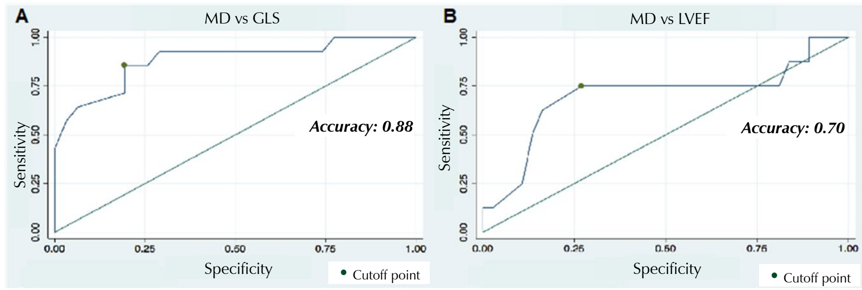

MD: maximum displacement; LVEF: left ventricular ejection fraction.

Figure 6 – *(A) Receiver operating characteristic curve between global longitudinal strain and maximum velocity in early diastole indicating the best cutoff point. (B) Atrioventricular junction velocity in diastasis and left ventricular ejection fraction performance.*

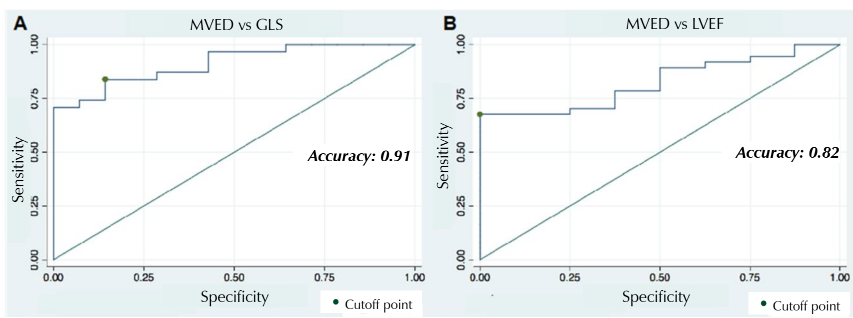

VMED: maximum velocity in early diastole LVEF: left ventricular ejection fraction.

Figure 7 – *(A) Receiver operating characteristic curve of global longitudinal strain and maximum atrioventricular junction displacement indicating the best cutoff point. (B) Maximum atrioventricular junction displacement and left ventricular ejection fraction performance.*

diastolic function by CMRI that, associated with its practical performance of both MD and MVED, can be considered a promising method for routine clinical use.

AVD presents with diastolic function disorders that precede evident LV systolic function changes that have important implications for morbidity and mortality before and after aortic valve replacement.[13–15] Several studies reported that LVEF is not affected early in groups of patients with AVD. A deteriorated ejection fraction in the clinical setting was considered a sign of severe and advanced AVD.[16–18] Several studies reported changed GLS and preserved LVEF in patients with AVD.[19–22]

GLS analysis after aortic valve replacement detected improved LV diastolic function measured by transmitral flow on ECHO. Similar studies also showed that GLS analysis after valve replacement indicated improved ventricular function.[23] GLS also showed less dependence on hemodynamic load conditions than LVEF, thus detecting more subtle changes in the underlying myocardial substrate.[24–26] Greater sensitivity for diagnosing diastolic dysfunction was observed after GLS evaluations in patients with AoS and AoI compared with conventional methods.[27] Analysis of the diagnostic performance of LLD parameters (MD and MVED) detects diastolic dysfunction in patients with AVD versus normal controls with a sensitivity similar to that of GLS. Diastolic function is rarely evaluated on CMRI because it depends on mitral, pulmonary vein, and myocardial flow velocity acquisition by cine-MRI with flow map (phase-contrast). Simple and practical MD and VDS measurements, especially the latter, represent a promising option for the diagnosis of diastolic dysfunction by CMRI that was validated in this study for patients with AVD.

VDS measurements and the VDS/MVED ratio also showed significant differences between pathological patients and normal controls, providing additional data in the assessment of diastolic dysfunction. However, the differences were smaller compared to those of MD and MVED, probably indicating less potential for their clinical application.

Limitations

This was a retrospective study with a relatively small number of patients. We also did not correlate LLD and GLS by ECHO; however, these parameters were validated by the CMRI myocardial tagging, a technique similar to the FTI used in this study as a reference, which mitigates this limitation. Finally, our new LLD method was validated only in patients with AVD; thus, future studies are needed to validate its use in patients with other diseases.

Conclusion

This study validated the LLD technique against GLS measured by FTI using CMRI. LLD parameters were obtained using only two linear measurements, which is possible with most image visualization software. Of the LLD parameters that assess systolic-diastolic function, MD showed better accuracy for assessing systolic function (normal values, less than -0.13), while MVED showed better accuracy for assessing diastolic function by CMRI (normal values, greater than 0.66). These parameters can improve the assessment of systolic-diastolic contractility in the clinical CMRI routine.

Acknowledgments

The authors thank the Zerbini Foundation for providing institutional support of this research project and Mrs. Lenira Cipriano for her support of the manuscript writing process.

Academic affiliation

This article represents scientific writing as a requirement to finish the internship project in scientific initiation of Rafael Almeida Fonseca, biomedicine student at Anhembi Morumbi University, held at the Cardiovascular Magnetic Resonance Sector of the Heart Institute (*Instituto do Coração* - InCor) of the School of Medicine, University of São Paulo (USP).

Ethical approval and consent information

This article is a sub-study of the project approved by the Research Ethics Committee of Hospital das Clínicas, School of Medicine, University of São Paulo (*Hospital das Clínicas da Faculdade de Medicina da Universidade de São Paulo* - HC FMUSP; no. 214,311). Due to the study's retrospective nature, the requirement for written informed consent was waived.

Authors' contribution

Fonseca RA, Ribeiro SM, Azevedo CF, Sampaio R, Tarasoutchi F, Rochitte CE contributed substantially to the study conception and design, data collection and analysis, and manuscript writing.

Conflict of interest

The authors have declared that they have no conflict of interest.

References

1. Del Castillo JM, Albuquerque ES, Silveira CA, Lamprea DP, Sena AD. Diastolicfunction assessment with doppler echocardiography and two-dimensional strain. Arq Bras Cardiol: Imagem cardiovasc 2017; 30(2): 46-53. DOI: 10.5935/2318-8219.20170012
2. Scatteia A, Baritussio A, Bucciarelli-Ducci C. Strain imaging using cardiac magnetic resonance. Heart Fail Rev. 2017;22(4):465-76. doi: https://doi.org/10.1007/s10741-017-9621-8
3. Claus P, Omar AM, Pedrizzetti G, Sengupta PP, Nagel E. Tissue Tracking Technology for Assessing Cardiac Mechanics: Principles, Normal Values, and Clinical Applications. JACC Cardiovasc Imaging. 2015;8(12):1444-60. doi: https://doi.org/10.1016/j.jcmg.2015.11.001
4. Pryds K, Larsen AH, Hansen MS, Grøndal AYK, Tougaard RS, Hansson NH, et al. Myocardial strain assessed by feature tracking cardiac magnetic resonance in patients with a variety of cardiovascular diseases - A comparison with echocardiography. Sci Rep. 2019;9(1):11296. doi: https://doi.org/10.1038/s41598-019-47775-4
5. Amundsen BH, Helle-Valle T, Edvardsen T, Torp H, Crosby J, Lyseggen E, et al. Noninvasive myocardial strain measurement by speckle tracking echocardiography: validation against sonomicrometry and tagged magnetic resonance imaging. J Am Coll Cardiol. 2006;47(4):789-93. doi: https://doi.org/10.1016/j.jacc.2005.10.040
6. Lopez-Candales A, Hernandez-Suarez DF. Strain Imaging Echocardiography: What Imaging Cardiologists Should Know. Curr Cardiol Rev. 2017;13(2):118-29. doi: https://doi.org/10.2174/1573403X12666161028122649
7. Mangion K, Burke NM, McComb C, Carrick D, Woodward R, Berry C. Feature-tracking myocardial strain in healthy adults- a magnetic resonance study at 3.0 tesla. Sci Rep. 2019;9(1):3239. doi: https://doi.org/10.1038/s41598-019-39807-w
8. Nagueh SF, Smiseth OA, Appleton CP, Byrd BF 3rd, Dokainish H, Edvardsen T, et al. Recommendations for the Evaluation of Left Ventricular Diastolic Function by Echocardiography: An Update from the American Society of Echocardiography and the European Association of Cardiovascular Imaging. J Am Soc Echocardiogr. 2016;29(4):277-314. doi: https://doi.org/10.1016/j.echo.2016.01.011
9. Saba SG, Chung S, Bhagavatula S, Donnino R, Srichai MB, Saric M, et al. A novel and practical cardiovascular magnetic resonance method to quantify mitral annular excursion and recoil applied to hypertrophic cardiomyopathy. J Cardiovasc Magn Reson. 2014;16(1):35. doi: https://doi.org/10.1186/1532-429X-16-35
10. Ribeiro SM, Azevedo Filho CF, Sampaio R, Tarasoutchi F, Grinberg M, Kalil-Filho R, et al. Longitudinal Shortening of the Left Ventricle by Cine-CMR for Assessment of Diastolic Function in Patients with Aortic Valve Disease. Arq Bras Cardiol. 2020;114(2):284-92. doi: https://doi.org/10.5935/abc.20190193
11. Simpson RM, Keegan J, Firmin DN. MR assessment of regional myocardial mechanics. J Magn Reson Imaging. 2013;37(3):576-99. doi: https://doi.org/10.1002/jmri.23756
12. Chen Q, Gan Y, Li ZY. Left ventricular diastolic dysfunction in type 2 diabetes patients: a novel 2D strain analysis based on cardiac magnetic resonance imaging. Comput Methods Biomech Biomed Engin. 2016;19(12):1330-8. doi: https://doi.org/10.1080/10255842.2016.1139093
13. Kumpuris AG, Quinones MA, Waggoner AD, Kanon DJ, Nelson JG, Miller RR. Importance of preoperative hypertrophy, wall stress and end-systolic dimension as echocardiographic predictors of normalization of left ventricular dilatation after valve replacement in chronic aortic insufficiency. Am J Cardiol. 1982;49(5):1091-100. doi: https://doi.org/10.1016/0002-9149(82)90032-7
14. Villari B, Hess OM, Kaufmann P, Krogmann ON, Grimm J, Krayenbuehl HP. Effect of aortic valve stenosis (pressure overload) and regurgitation (volume overload) on left ventricular systolic and diastolic function. Am J Cardiol. 1992;69(9):927-34. doi: https://doi.org/10.1016/0002-9149(92)90795-z
15. Bech-Hanssen O, Wallentin I, Houltz E, Beckman Suurküla M, Larsson S, Caidahl K. Gender differences in patients with severe aortic stenosis: impact on preoperative left ventricular geometry and function, as well as early postoperative morbidity and mortality. Eur J Cardiothorac Surg. 1999;15(1):24-30. doi: https://doi.org/10.1016/s1010-7940(98)00268-1
16. Lamb HJ, Beyerbacht HP, de Roos A, van der Laarse A, Vliegen HW, Leujes F, et al. Left ventricular remodeling early after aortic valve replacement: differential effects on diastolic function in aortic valve stenosis and aortic regurgitation. J Am Coll Cardiol. 2002;40(12):2182-8. doi: https://doi.org/10.1016/s0735-1097(02)02604-9
17. Faggiano P, Rusconi C, Ghizzoni G, Sabatini T. Left ventricular remodeling and function in adult aortic stenosis. Angiology. 1994;45(12):1033-8. doi: https://doi.org/10.1177/000331979404501206

18. Lund O, Flø C, Jensen FT, Emmertsen K, Nielsen TT, Rasmussen BS, et al. Left ventricular systolic and diastolic function in aortic stenosis. Prognostic value after valve replacement and underlying mechanisms. Eur Heart J. 1997;18(12):1977-87. doi: https://doi.org/10.1093/oxfordjournals.eurheartj.a015209

19. Vollema EM, Sugimoto T, Shen M, Tastet L, Ng AC, Abou R, et al. Association of Left Ventricular Global Longitudinal Strain With Asymptomatic Severe Aortic Stenosis: Natural Course and Prognostic Value. JAMA Cardiol. 2018;3(9):839-47. doi: https://doi.org/10.1001/jamacardio.2018.2288

20. Ng AC, Delgado V, Bertini M, Antoni ML, van Bommel RJ, van Rijnsoever EP, et al. Alterations in multidirectional myocardial functions in patients with aortic stenosis and preserved ejection fraction: a two-dimensional speckle tracking analysis. Eur Heart J. 2011;32(12):1542-50. doi: https://doi.org/10.1093/eurheartj/ehr084

21. Klaeboe LG, Haland TF, Leren IS, Ter Bekke RMA, Brekke PH, Røsjø H, et al. Prognostic Value of Left Ventricular Deformation Parameters in Patients with Severe Aortic Stenosis: A Pilot Study of the Usefulness of Strain Echocardiography. J Am Soc Echocardiogr. 2017;30(8):727-735.e1. doi: https://doi.org/10.1016/j.echo.2017.04.009.

22. Kusunose K, Goodman A, Parikh R, Barr T, Agarwal S, Popovic ZB, et al. Incremental prognostic value of left ventricular global longitudinal strain in patients with aortic stenosis and preserved ejection fraction. Circ Cardiovasc Imaging. 2014;7(6):938-45. doi: https://doi.org/10.1161/CIRCIMAGING.114.002041

23. Lamb HJ, Beyerbacht HP, de Roos A, van der Laarse A, Vliegen HW, Leujes F, Bax JJ, et al. Left ventricular remodeling early after aortic valve replacement: differential effects on diastolic function in aortic valve stenosis and aortic regurgitation. J Am Coll Cardiol. 2002;40(12):2182-8. doi: https://doi.org/10.1016/s0735-1097(02)02604-9

24. Erley J, Genovese D, Tapaskar N, Alvi N, Rashedi N, Besser SA, et al. Echocardiography and cardiovascular magnetic resonance based evaluation of myocardial strain and relationship with late gadolinium enhancement. J Cardiovasc Magn Reson. 2019;21(1):46. doi: https://doi.org/10.1186/s12968-019-0559-y

25. Knappe D, Pouleur AC, Shah AM, Cheng S, Uno H, Hall WJ, et al.; Multicenter Automatic Defibrillator Implantation Trial-Cardiac Resynchronization Therapy Investigators. Dyssynchrony, contractile function, and response to cardiac resynchronization therapy. Circ Heart Fail. 2011;4(4):433-40. doi: https://doi.org/10.1161/CIRCHEARTFAILURE.111.962902

26. Smedsrud MK, Pettersen E, Gjesdal O, Svennevig JL, Andersen K, Ihlen H, et al. Detection of left ventricular dysfunction by global longitudinal systolic strain in patients with chronic aortic regurgitation. J Am Soc Echocardiogr. 2011;24(11):1253-9. doi: https://doi.org/10.1016/j.echo.2011.08.003

27. Giritharan S, Cagampang F, Torrens C, Salhiyyah K, Duggan S, Ohri S. Aortic Stenosis Prognostication in Patients With Type 2 Diabetes: Protocol for Testing and Validation of a Biomarker-Derived Scoring System. JMIR Res Protoc. 2019;8(8):e13186. doi: https://doi.org/10.2196/13186

Original article

Is Paclitaxel Less Cardiotoxic in the Treatment of Breast Cancer Before or After Doxorubicin?

Qual Estratégia Terapêutica é Menos Cardiotóxica no Tratamento do Câncer De Mama: Uso de Paclitaxel Antes ou Depois da Doxorrubicina?

André Luiz Cerqueira de Almeida[1], Edval Gomes dos Santos Júnior[2], Aluísio José de Oliveira Monteiro Neto[3], Thyago Monteiro do Espírito Santo[1], Paulo André A. Almeida[4], Samuel Oliveira Affonseca[1], Caroline de Souza Almeida[1], Matheus Pamponet Freitas[1], Cecília Lopes Viana Santos[1], Vitória Régia Beserra Barbosa Ximenes[1], Mariana Andrade Falcão[1], Israel Costa Reis[1], Suzane Pereira de Souza[2], Maurício Gomes da Silva Serra[2], Ana Beatriz Menezes de Oliveira[2], Tayla Silva Santos[1], Nilson Lima Lopes[1], Marcelo Dantas Tavares de Melo[3]

[1]Santa Casa de Misericórdia of Feira de Santana, Feira de Santana, BA - Brazil. [2]State University of Feira de Santana, Feira de Santana, BA - Brazil. [3]Federal University of Paraíba, João Pessoa, PB - Brazil. [4]UNIFACS Course of Medicine, Salvador, BA - Brazil.

Abstract

Background: The combination of doxorubicin (DOX) with paclitaxel (PTX) effectively treats breast cancer (BC). However, DOX-associated cardiotoxicity (CTX) is aggravated by the use of PTX. Consensus is lacking about which drug sequence involves the most CTX.

Objectives: To evaluate whether DOX followed by PXT or the reverse sequence has the greatest cardiotoxic potential in the treatment of BC.

Methods: Prospective study of women with primary BC who received four cycles of DOX and 12 infusions of PTX. Participants were divided into Group 1 (G1; PXT before DOX) and Group 2 (G2; DOX before PXT) at the discretion of the oncologist. CTX was defined as an absolute reduction in left ventricular ejection fraction (LVEF) > 10% to a value <53%. Patients underwent clinical evaluations and echocardiography before treatment (Phase 1) and one year after treatment (Phase 2).

Results: Sixty-nine women were evaluated: 19 in G1 and 50 in G2. The groups had similar clinical characteristics. The doses of radiation, DOX, and PTX used were similar. Eight (11.6%) patients developed CTX: two (10.5%) in G1 and six (12.0%) in G2 (p=0.62). The mean LVEF was similar between groups in Phase 1 (G1=65.1±3.5%; G2=65.2±3.9%; p=0.96), with a significant reduction noted after one year in both groups: G1=61.4±8.1% (p=0.021) and G2=60.8±7.6% (p<0.001). Although lower, mean LVEF remained similar between groups after Phase 2 (p=0.79).

Conclusions: In women with BC who underwent chemotherapy, the incidence of CTX at the end of the first year of treatment was similar regardless of whether DOX was used before or after PTX.

Keywords: Cardiotoxicity, Paclitaxel, Doxorubicin, Breast neoplasm.

Resumo

Fundamento: *A combinação de doxorrubicina com paclitaxel é eficaz no tratamento do câncer de mama. No entanto, a cardiotoxidade associada à doxorrubicina é agravada pelo uso do paclitaxel. Não há consenso sobre qual sequência é mais segura.*

Objetivos: *Avaliar qual sequência tem maior potencial cardiotóxico no tratamento do câncer de mama: doxorrubicina seguida de paclitaxel ou o inverso.*

Métodos: *Estudo prospectivo de mulheres com câncer de mama primário. Todos os participantes receberam quatro ciclos de doxorrubicina e 12 infusões de paclitaxel. Os participantes foram divididos em dois grupos, a critério do oncologista: Grupo 1, que recebeu paclitaxel antes da doxorrubicina, e Grupo 2, que teve doxorrubicina antes do paclitaxel. Definiu-se cardiotoxicidade como uma redução absoluta na fração de ejeção ventricular esquerda >10% para <53%. Os pacientes foram submetidos a avaliação clínica e ecocardiografia antes do tratamento (fase 1) e 1 ano após o tratamento (fase 2).*

Resultados: *Foram avaliadas 69 mulheres: 19 no Grupo 1 e 50 no Grupo 2. Os grupos apresentavam características clínicas semelhantes. As doses*

Mailing Address: Marcelo Dantas Tavares de Melo •

E-mail: marcelot@alumni.usp.br

Manuscript received 2/6/2022; revised 3/16/2022; accepted 4/12/2022

DOI: 10.47593/2675-312X/20223502eabc289

de radiação, doxorrubicina e paclitaxel utilizadas foram semelhantes. Oito (11,6%) pacientes desenvolveram cardiotoxicidade: dois (10,5%) no Grupo 1 e seis (12,0%) no Grupo 2 (p=0,62). A fração de ejeção ventricular esquerda se mostrou semelhante entre os grupos da fase 1 (Grupo 1 = 65,1±3,5; Grupo 2=65,2±3,9; p=0,96), com redução significativa após 1 ano em ambos os grupos: Grupo 1 = 61,4±8,1% (p=0,021) e Grupo 2 = 60,8±7,6% (p<0,001). Embora menor, a fração de ejeção ventricular esquerda permaneceu semelhante entre os grupos após a Fase 2 (p=0,79).

Conclusão: *Nas mulheres com câncer de mama submetidas à quimioterapia, a incidência de cardiotoxicidade ao final do primeiro ano de tratamento foi semelhante, independentemente do uso de doxorrubicina antes ou após o paclitaxel.*

Palavras-chave: *Cardiotoxicidade; Paclitaxel; Doxorrubicina; Neoplasias de mama.*

Introduction

Approximately 1.7 million new cases of cancer will be diagnosed in the United States in 2019. Of them, 270,000 will be breast cancer (BC)[1,2]. In Brazil, the National Cancer Institute estimates approximately 600,000 new cases of cancer in 2019, including 60,000 of BC[3]. From 1991 to 2016, the overall cancer mortality rate steadily declined in the US by 27%, translating into approximately 2.6 million fewer cancer deaths than would be expected had mortality rates remained at their peak[2]. The mean 5-year survival rate of patients with BC is approximately 90%[2]. The causes of this improvement in survival are multifactorial. Advances in antineoplastic therapy play an important role in this favorable outcome, but this type of therapy is also associated with undesirable cardiotoxic effects[4].

Doxorubicin (DOX) and paclitaxel (PTX) are potent chemotherapeutic drugs that were introduced in the therapeutic arsenal in the 1960s and 1980s, respectively[5]. The combination of DOX with PTX is widely used in BC patients because of its efficacy against cancer cells[6]. DOX is a chemotherapeutic agent of the anthracycline class that, depending on the dose used, may feature left ventricular (LV) dysfunction as a side effect in 3–48% of cases[4]. PTX and DOX belong to the taxane class (antimicrotubule agents), which have an incidence of cardiotoxicity (CTX) of 1–13%[4]. DOX-associated CTX is aggravated by PTX use[6-10]. In experimental study models, PTX may synergistically aggravate DOX-induced CTX. This result is reportedly more pronounced when PTX is used 24 hours after DOX[11]. Data from the FinHer trial, in contrast, suggested that CTX may remain low when a taxane (docetaxel) is given prior to the anthracycline[12]. Whether due to the therapeutic benefits or possible side effects, consensus is lacking about which drug should be used first in the treatment of BC patients[6,13].

Echocardiography is an important tool in the follow-up of patients who are antineoplastic therapy candidates. In this scenario, left ventricular ejection fraction (LVEF) is the most commonly used echocardiographic parameter for monitoring ventricular function[14]. Although useful, LVEF has low sensitivity for detecting small changes in ventricular function. The evaluation of myocardial deformation through the study of strain by the speckle tracking technique allows detection of subclinical LV dysfunction in several scenarios[15]. The reduction in global longitudinal strain (GLS) in patients undergoing chemotherapy is a sign of subclinical myocardial alterations that occur secondary to cancer therapy[16]. The change in GLS in this scenario usually occurs before any change in LVEF is detected[16,17].

The primary objective of this study was to evaluate which sequence has greater cardiotoxic potential in the treatment of BC patients: DOX followed by PTX or the reverse order. The secondary objective was to evaluate GLS and LVEF at the end of the first year of treatment of BC patients undergoing chemotherapy and compare GLS and LVEF between the DOX and PTX use sequences.

Methods

This prospective study included women diagnosed with BC indicated for treatment with DOX and PTX who were admitted to the oncology service of our hospital for chemotherapy during the period of 06/2014 to 07/2015. The exclusion criteria were an LVEF < 55%, previous cancer treatment, segmental dysfunction detected on echocardiography, diagnosis of heart failure by the Framingham criteria, inadequate echocardiographic window for GLS analysis, complex arrhythmia, valvular heart disease, any type of cardiomyopathy, and LV hypertrophy greater than discrete. All patients received four cycles of DOX (60 mg/m^2) with intervals of three weeks between cycles and 12 weekly infusions of PTX (80 mg/m^2). The sequence of use of both drugs was at the discretion of the treating oncologist. Participants were divided into Group 1 (PTX before DOX) and Group 2 (DOX before PTX). Patients underwent clinical evaluation and echocardiography prior to treatment initiation (Phase 1) and one year after initiation of DOX (Phase 2). CTX was defined as an absolute reduction in LVEF>10%, to a value <53%, one year after starting DOX[14]. The study was approved by our institution's research ethics committee. All patients signed an informed consent form.

Echocardiography

Transthoracic echocardiography was performed using a Vivid 6 or Vivid I cardiovascular ultrasound system (GE Healthcare, Milwaukee, WI, USA). All echocardiographic variables were analyzed off-line at the workstation of our service's echocardiography laboratory. EchoPAC software version 112.0.x (GE Healthcare) was used for these analyses. LVEF was calculated using the modified biplane Simpson method with four- and two-chamber apical views of the LV. The other echocardiographic measurements were calculated based on American Society of Echocardiography guidelines[18].

Grayscale images of the two-dimensional echocardiograms were obtained in four-, three-, and two-chamber apical views for the measurement of the LV subjective global assessment (SGA). The aortic valve closure time was obtained using pulsed Doppler flow tracing in the aortic valve synchronized with the electrocardiogram.

The professionals involved in the strain image acquisition received previous training to ensure the acquisition of adequate images for GLS analysis. The images corresponding to the GLS measurement were acquired with a frame rate of 50–80 cycles/s in three total cycles for each image. Proper tracking of points was checked and adjusted manually if necessary.

The LV SGA was calculated by the mean longitudinal strain values in the basal, mid-, and apical segments obtained in the four-, three-, and two-chamber LV apical views (Figure 1). To avoid confusion and following previous recommendations, GLS is expressed as the absolute value (aGLS), thus eliminating the negative sign[18,19].

Reproducibility

To determine intraobserver variability, echocardiograms from 20 randomly selected patients were retested by the same evaluator (FTAA) six months after the initial analysis. To determine interobserver variability, the data of these 20 patients were analyzed by a second evaluator (VRBBX) using the same exams and the same cycles for each.

Statistical analysis

The statistical analysis was performed using SPSS 2.0. The distribution of the studied variables was analyzed using the Shapiro-Wilk test. Quantitative variables are expressed as mean ± standard deviation and were compared by the *t* test for independent samples or Wilcoxon signed-rank test, while qualitative variables are expressed as frequency and percentage and were compared by the chi-square test or Fisher's exact test. The paired *t* test was used to determine if the mean of the differences between two paired samples differed from zero. The interobserver and intraobserver agreements were evaluated by the intraclass correlation coefficient (ICC) with 95% confidence interval (CI). Values of $p<0.05$ were considered statistically significant.

RESULTS

Sample

A total of 76 women with BC were treated with DOX and PTX during the study period. Of them, seven were excluded: two who requested exclusion and five who died before the evaluation in Phase 2 (two of sepsis, one of brain metastasis, one of sudden death, and of unknown cause). Of the 69 patients who composed the sample, 19 (27.5%) were treated with PTX before DOX (Group 1) and 50 (72.5%) were treated with DOX before PTX (Group 2).

The patients' main characteristics are summarized in Table 1. At the start of the study, the two groups were similar in age, systolic blood pressure, diastolic blood pressure, body mass index, and waist circumference. The same was observed in terms of the main cardiovascular risk factors and the use of cardiovascular drugs.

Table 1 – Patient characteristics by group.

Variable	Group 1 (n=19)	Group 2 (n=50)	P value
Age (years)	50±13	49±13	0.76
SBP (mmHg)	133±18	131±26	0.79
DBP (mmHg)	83±12	81±13	0.63
BMI (kg/m²)	26.9±5.1	27.3±4.7	0.74
Waist circumference (cm)	90±12	88±14	0.71
Cardiovascular risk factors, n (%)			
Hypertension	9 (47)	20 (41)	0.63
Diabetes	4 (21.1)	4 (8.5)	0.21
Smoking	0 (0)	3 (6.5)	0.55
Sedentary lifestyle	15 (83.3)	36 (81.8)	1.0
Dyslipidemia	1 (5.3)	3 (6.5)	1.0
Radiation therapy	16 (84.2)	40 (80)	1.0
Trastuzumab	3 (15.8)	14 (28)	0.36
Cardiovascular medication, n (%)			
ACEI	2 (13.3)	8 (22.2)	0.70
Beta-blocker	0 (0)	2 (5.6)	1.0
ARB	5 (33.3)	5 (13.2)	0.09
Antineoplastic treatment (n of doses)			
DOX (mg/m²)	240±11	237±14	0.38
PTX (mg)	1570±138	1567±236	0.96
Radiation (Gy)	58±5	56±6	0.39

Continuous variables are presented as mean ± standard deviation, while categorical variables are shown as frequency (percentage). ACEI, angiotensin-converting enzyme inhibitor; ARB, angiotensin receptor blocker; BMI, body mass index; DBP, diastolic blood pressure; DOX, doxorubicin; PTX, paclitaxel; SBP, systolic blood pressure.

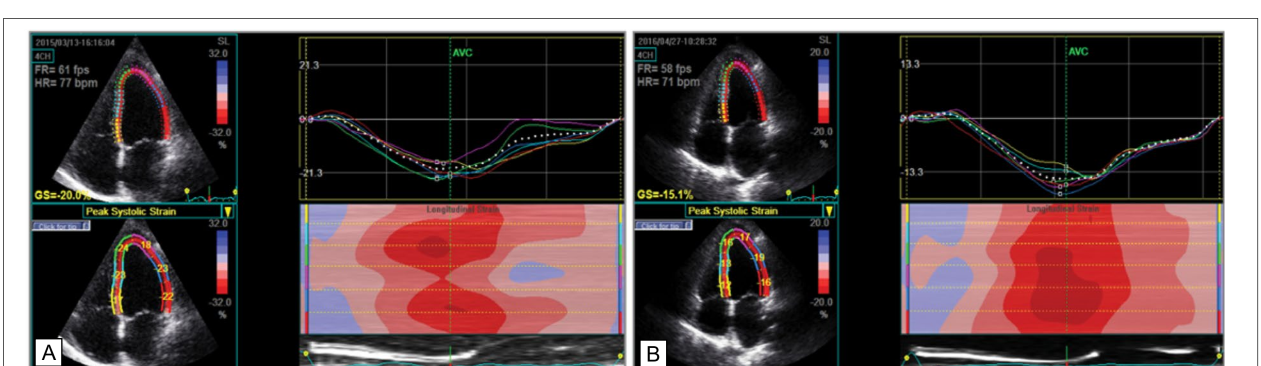

Figure 1 – *Normal longitudinal strain before chemotherapy (A) and decreased longitudinal strain after chemotherapy (B).*

One patient (1.4%) in Group 2 had bilateral BC. Of the others, 34 (49.3%) had right BC, and 34 (49.3%) had left BC. Seven (37%) Group 1 patients had right BC, while 27 (54%) Group 2 patients had right BC (p=0.18).

Eight patients (11.6%) developed CTX by the end of the study: two (10.5%) in Group 1 and six (12.0%) in Group 2 (p=0.62) (Figure 2).

Antineoplastic treatment

The cumulative dose of DOX and the total dose of PTX did not differ between groups (p=0.38 and p=0.96 for Groups 1 and 2, respectively; Table 1).

Radiation therapy was used in 16 (84.2%) patients in Group 1 and 40 (80%) patients in Group 2 (p=1.0). There was no intergroup difference in the radiation dose used (p=0.39; Table 1).

Seventeen (24.6%) patients were classified as being *HER2*-positive and, therefore, were treated with trastuzumab: 3 (15.8%) in Group 1 and 14 (28%) in Group 2 (p=0.36; Table 1).

Echocardiographic variables

The main echocardiographic variables in Phases 1 and 2 are presented in Table 2.

LVEF at baseline was similar between groups (Group 1, 65.1±3.5% versus Group 2, 65.2±3.9%; p=0.96; Table 3). There was a significant decrease in LVEF after one year in both groups (Table 2). The LVEF decreased by 3.7% in Group 1 (from 65.1±3.5% to 61.4±8.1%; p=0.021) and by 4.4% in Group 2 (from 65.2±3.9% to 60.8±7.6%; p<0.001). One year after treatment, although lower, LVEF remained similar between groups (Group 1, 61.4±8.1% versus Group 2, 60.8±7.6%; p=0.79; Table 3).

The aGLS results were similar to the LVEF results. There was no intergroup difference in aGLS before treatment (Group 1, 19.9±2.0% versus Group 2, 20.0±2.4%; p=0.90; Table 3). A significant decrease in aGLS was noted in both groups at the end of the first year of chemotherapy (Table 2), but the decreases were similar between them (Table 3).

Other variables associated with LV systolic function (mitral annular plane systolic excursion [MAPSE], mitral S′ wave, and systolic longitudinal strain rate [LSRs]) followed the same pattern as LVEF and aGLS (Table 2). The same occurred in the ratio of early diastolic transmitral velocity-to-early diastolic tissue velocity ratio (E/E′ ratio), a variable related

Table 2 - Echocardiographic parameters by group and study phase.

Variable	Group 1 (n=19)		Group 2 (n=50)	
	Phase 1	Phase 2	Phase 1	Phase 2
LVDD (mm)	44.7±3.8	44.2±5.6	44.8±3.9	45.5±4.8
LVSD (mm)	28.8±3.0	29.3±5.9	29.0±3.0	30.1±4.9*
LVEF (%)	65.1±3.5	61.4±8.1†	65.2±3.9	60.8±7.6*
E/A ratio	1.12±0.40	1.09±0.32	1.09±0.33	1.09±0.37
E/E' ratio	8.6±2.7	9.9±3.4†	7.9±2.6	9.5±3.1*
Mitral S' wave (cm/s)	6.7±1.0	6.0±1.1†	7.2±1.3	6.3±1.3*
MAPSE (mm)	13.2±1.3	12.2±2.3†	13.4±1.8	12.2±1.7*
aGLS (%)	19.9±2.0	18.4±2.3†	20.0±2.4	18.9±2.7*
LSRs $^{(-1)}$	1.00±0.15	-0.90±0.13†	-1.02±0.17	-0.95±0.22*

*aGLS, absolute global longitudinal left ventricular strain; LSRs, systolic longitudinal strain rate; LVDD, left ventricular diastolic diameter; LVSD, left ventricular systolic diameter; LVEF, left ventricular ejection fraction; MAPSE, mitral annular plane systolic excursion. *p<0.05 versus Phase 1 results. #p<0.05 versus Phase 1 results.*

Table 3 - LVEF and global longitudinal strain.

Variable	Group 1 (n=19)	Group 2 (n=50)	P value
	Phase 1, %		
LVEF (%)	65,1±3,5	65,2±3,9	0,96
aGLS (%)	19,9±2,0	20,0±2,4	0,90
	Phase 2, %		
LVEF (%)	61,4±8,1	60,8±7,6	0,79
aGLS (%)	18,4±2,3	18,9±2,7	0,48

Data are presented as mean ± standard deviation. aGLS, absolute global longitudinal strain of the left ventricle; LVEF, left ventricular ejection fraction

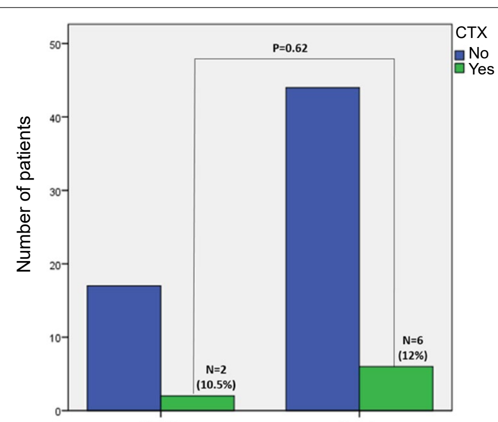

CTX: cardiotoxidade.

Figure 2 – *Cardiotoxicity after 1 year.*

to LV diastolic function. However, no change was noted in the early-to-late diastolic transmitral flow velocity ratio (E/A ratio) of mitral flow.

Reproducibility

There was excellent intraobserver agreement in aGLS (ICC, 0.94; 95% CI, 0.84–0.98) and interobserver (ICC, 0.92; 95% CI, 0.80–0.97).

Discussion

The present study demonstrated no difference in the incidence of CTX when DOX followed PTX or, conversely, when PTX followed DOX in the treatment of BC patients. Despite this, a significant decrease in aGLS and LVEF was noted at the end of the first year of chemotherapy. This decrease, however, was similar between the two groups regardless of the drug use sequence.

Other variables evaluated in our study, such as MAPSE, mitral annulus S′ wave, and LSRs, followed the pattern observed for LVEF and aGLS. These data confer greater robustness to our results because they also provide important information about LV systolic function.[14] In addition, because it is not possible to evaluate aGLS by using the speckle tracking technique, MAPSE and mitral annulus S′ wave are the variables recommended to ensure an adequate evaluation of LV longitudinal function[14].

DOX-associated CTX is aggravated by PTX treatment[6-9]. The latter increases the plasma concentration of the former[8,9]. PTX also stimulates the formation of DOX metabolites, which play a key role in the mechanism of CTX[9]. The effect of PTX on DOX metabolites can reportedly be attributed to interference by the PTX carrier in the biliary elimination of the anthracycline molecule, explaining the greater toxicity of the PTX-DOX association versus DOX alone[7]. Studies in laboratory animals have shown that PTX can aggravate DOX-induced CTX, especially when a taxane (paclitaxel) is used after DOX[11]. Another chemotherapeutic taxane, docetaxel, has effects similar to those of PTX[9]. However, the FinHer study showed that docetaxel, when used before DOX, was associated with low CTX rates[12]. Focan et al.[20] demonstrated that the use of an anthracycline (epirubicin) on day 1 followed by a taxane (PTX) on day 2 decreased the risks of hematological complications, especially neutropenia. However, the CTX, as in our study, did not change regardless of drug sequence[20].

The incidence of CTX in our sample was low (11.6%), similar to the 9% reported by Cardinale et al.[21] but lower than those of other reports in the literature[4,22]. This relatively low incidence of CTX may be attributed to the low dose of DOX used by our patients (238±13 mg/m^2). Higher rates are usually seen with higher doses. The increase in CTX related to the DOX-PTX combination is currently prevented by limiting the cumulative dose of DOX to 360 mg/m^2 or separating the infusion of the two drugs by an interval of more than four hours[8]; both approaches were used with our patients. Our patients were at low risk of developing CTX, and some were already using cardioprotective drugs. These factors may also be associated with the low incidence of CTX in our sample.

The use of more sensitive methods for detecting subclinical ventricular dysfunction, such as GLS, has been very useful for monitoring patients undergoing chemotherapy[14]. The data are very consistent regarding the diagnostic value of GLS in CTX screenings among these patients. A relative reduction in aGLS > 15% compared to baseline is strong evidence of subclinical ventricular dysfunction in patients undergoing chemotherapy; furthermore, it is a predictor of an LVEF decrease and subsequent development of heart failure[14]. Charbonnel et al.[23] demonstrated that even at low doses of DOX (150 mg/m^2), aGLS was an independent predictor of future CTX associated with anthracycline use. Our study demonstrated a decrease in aGLS at one year after the start of DOX treatment, a finding that did not depend on the sequence of DOX and PTX use. The patients who composed the sample in our study continue to be followed up to enable the future analysis of the prognostic value of aGLS in patients at high risk for cardiovascular events.

The choice of the sequence of anthracycline and taxane administration in BC patients is currently based on classical biological factors as well as clinical and demographic factors associated with the risk of disease recurrence[6]. It is customary to use an anthracycline followed by a taxane based on the above information and on historical development, as anthracyclines were introduced first in clinical practice. This influences the routine of many services. However, recent studies reported using taxanes before anthracyclines[24], which has served as an example for other centers. Virtually all of these studies had the main objective of evaluating the therapeutic efficacy of the drugs; in most of them, there was no specific design to evaluate the cardiotoxic potential associated with the anthracycline and taxane administration sequences. Focan et al.[20] was one of the few that made this evaluation; epirubicin was the anthracycline used. Our study also performed this evaluation, but we used DOX instead. Based on our results, either sequence of DOX and PTX administration is safe from a cardiovascular standpoint since neither increases the risk of CTX in patients with BC. This information can give peace of mind to oncology services when choosing the treatment sequence. However, further studies are needed with larger numbers of patients that use the currently recommended doses and evaluate the CTX potential of possible anthracycline and taxane administration sequences in BC patients.

Limitations

Our study has some limitations. Its relatively small number of patients may have contributed to the lack of statistically significant intergroup differences. As the number of patients who developed CTX was small, our findings require confirmation in a larger sample. The fact that the patients come from a single center raises the possibility of selection bias. This issue is attenuated by the fact that the sample comprised all the women who met the study inclusion criteria within one year and were admitted to our hospital's oncology department for chemotherapy. Due to the variability in GLS among the different manufacturers of echocardiography devices, we cannot guarantee that our results can be replicated with devices of brands other than the one used here. The professionals who acquired the echocardiogram images were not blinded to the examination phase, which may have led to observation bias. And finally, it was not possible to measure biomarker levels, but this was not the objective of our study.

Conclusion

In the present sample of BC patients referred to begin chemotherapy, the incidence of CTX at the end of the first year of treatment was similar regardless of whether DOX was used before or after PTX. The study also showed significant and similar decreases in aGLS and LVEF at the end of the first year of treatment regardless of the chemotherapeutic agent use sequence.

Author contributions

Conception and design: Almeida ALC, Melo MDT; Data collection: Melo MDT, Santo TME, Monteiro Neto AJO, Almeida CS, Santos CLV, Souza SP, Serra MGS, Oliveira ABM, Santos TS, Lopes NL, Ximenes VRBB, Lopes NL, Reis IC; Data analysis and interpretation: Santos Junior EG, Affonseca SO, Santo TM, Melo MDT, Almeida ALC; Statistical analysis: Santos Junior EG, Almeida ALC; Writing the manuscript: Almeida ALC, Monteiro Neto AJO, Melo MDT, Almeida PAA; Critical review for intellectual content: Melo MDT, Santos Júnior EGS, Almeida ALC, Affonseca SO.

Conflict of interest

The authors have declared that they have no conflict of interest.

References

1. American Cancer Society. Cancer facts & figures 2018. Atlanta: American Cancer Society; 2018.
2. Siegel RL, Miller KD, Jemal A. Cancer statistics, 2019. CA Cancer J Clin. 2019;69(1):7-34. doi: https://doi.org/10.3322/caac.21551
3. Estimativa 2018: incidência de câncer no Brasil. Instituto Nacional de Câncer José Alencar Gomes da Silva/ Ministério da Saúde; 2017. Available at: http://www.inca.gov.br/estimativa/2018
4. Zamorano JL, Lancellotti P, Rodriguez Muñoz D, Aboyans V, Asteggiano R, Galderisi M, et al.; ESC Scientific Document Group. 2016 ESC Position Paper on cancer treatments and cardiovascular toxicity developed under the auspices of the ESC Committee for Practice Guidelines: The Task Force for cancer treatments and cardiovascular toxicity of the European Society of Cardiology (ESC). Eur Heart J. 2016;37(36):2768-2801. doi: https://doi.org/10.1093/eurheartj/ehw211. Erratum in: Eur Heart J. 2016 Dec 24; PMID: 27567406
5. de Moor JS, Mariotto AB, Parry C, Alfano CM, Padgett L, Kent EE, et al. Cancer survivors in the United States: prevalence across the survivorship trajectory and implications for care. Cancer Epidemiol Biomarkers Prev. 2013;22(4):561-70. doi: https://doi.org/10.1158/1055-9965.EPI-12-1356
6. Bines J, Earl H, Buzaid AC, Saad ED. Anthracyclines and taxanes in the neo/adjuvant treatment of breast cancer: does the sequence matter? Ann Oncol. 2014;25(6):1079-85. doi: https://doi.org/10.1093/annonc/mdu007
7. Gianni L, Viganò L, Locatelli A, Capri G, Giani A, Tarenzi E, et al. Human pharmacokinetic characterization and in vitro study of the interaction between doxorubicin and paclitaxel in patients with breast cancer. J Clin Oncol. 1997;15(5):1906-15. doi: https://doi.org/10.1200/JCO.1997.15.5.1906
8. Gianni L, Salvatorelli E, Minotti G. Anthracycline cardiotoxicity in breast cancer patients: synergism with trastuzumab and taxanes. Cardiovasc Toxicol. 2007;7(2):67-71. doi: https://doi.org/10.1007/s12012-007-0013-5
9. Salvatorelli E, Menna P, Cascegna S, Liberi G, Calafiore AM, Gianni L, et al. Paclitaxel and docetaxel stimulation of doxorubicinol formation in the human heart: implications for cardiotoxicity of doxorubicin-taxane chemotherapies. J Pharmacol Exp Ther. 2006;318(1):424-33. doi: https://doi.org/10.1124/jpet.106.103846
10. Gianni L, Dombernowsky P, Sledge G, Martin M, Amadori D, Arbuck SG, et al. Cardiac function following combination therapy with paclitaxel and doxorubicin: an analysis of 657 women with advanced breast cancer. Ann Oncol. 2001;12(8):1067-73. doi: https://doi.org/10.1023/a:1011655503511
11. Saad SY, Najjar TA, Alashari M. Cardiotoxicity of doxorubicin/paclitaxel combination in rats: effect of sequence and timing of administration. J Biochem Mol Toxicol. 2004;18(2):78-86. doi: https://doi.org/10.1002/jbt.20012
12. Joensuu H, Bono P, Kataja V, Alanko T, Kokko R, Asola R, et al. Fluorouracil, epirubicin, and cyclophosphamide with either docetaxel or vinorelbine, with or without trastuzumab, as adjuvant treatments of breast cancer: final results of the FinHer Trial. J Clin Oncol. 2009;27(34):5685-92. doi: https://doi.org/10.1200/JCO.2008.21.4577
13. Wildiers H, Forceville K, Paridaens R, Joensuu H. Taxanes and anthracyclines in early breast cancer: which first? Lancet Oncol. 2010;11(3):219-20. doi: https://doi.org/10.1016/S1470-2045(10)70025-5
14. Plana JC, Galderisi M, Barac A, Ewer MS, Ky B, Scherrer-Crosbie M, et al. Expert consensus for multimodality imaging evaluation of adult patients during and after cancer therapy: a report from the American Society of Echocardiography and the European Association of Cardiovascular Imaging. Eur Heart J Cardiovasc Imaging. 2014;15(10):1063-93. doi: https://doi.org/10.1093/ehjci/jeu192.
15. Geyer H, Caracciolo G, Abe H, Wilansky S, Carerj S, Gentile F, et al. Assessment of myocardial mechanics using speckle tracking echocardiography: fundamentals and clinical applications. J Am Soc Echocardiogr. 2010;23(4):351-69; quiz 453-5. doi: https://doi.org/10.1016/j.echo.2010.02.015. Erratum in: J Am Soc Echocardiogr. 2010;23(7):734
16. Thavendiranathan P, Poulin F, Lim KD, Plana JC, Woo A, Marwick TH. Use of myocardial strain imaging by echocardiography for the early detection of cardiotoxicity in patients during and after cancer chemotherapy: a systematic review. J Am Coll Cardiol. 2014;63(25 Pt A):2751-68. doi: https://doi.org/10.1016/j.jacc.2014.01.073
17. Almeida AL, Silva VA, de Souza Filho AT, Rios VG, Lopes JR, de Afonseca SO, et al. Subclinical ventricular dysfunction detected by speckle tracking two years after use of anthracycline. Arq Bras Cardiol. 2015;104(4):274-83. doi: https://doi.org/10.5935/abc.20140209
18. Lang RM, Badano LP, Mor-Avi V, Afilalo J, Armstrong A, Ernande L, et al. Recommendations for cardiac chamber quantification by echocardiography in adults: an update from the American Society of Echocardiography and the European Association of Cardiovascular Imaging. J Am Soc Echocardiogr. 2015;28(1):1-39.e14. doi: https://doi.org/10.1016/j.echo.2014.10.003.
19. Feigenbaum H, Mastouri R, Sawada S. A practical approach to using strain echocardiography to evaluate the left ventricle. Circ J. 2012;76(7):1550-5. doi: https://doi.org/10.1253/circj.cj-12-0665.
20. Focan C, Graas MP, Beauduin M, Canon JL, Salmon JP, Jerusalem G, et al. Sequential administration of epirubicin and paclitaxel for advanced breast cancer. A phase I randomised trial. Anticancer Res. 2005;25(2B):1211-7.

21. Cardinale D, Colombo A, Bacchiani G, Tedeschi I, Meroni CA, Veglia F, et al. Early detection of anthracycline cardiotoxicity and improvement with heart failure therapy. Circulation. 2015;131(22):1981-8. doi: https://doi.org/10.1161/CIRCULATIONAHA.114.013777

22. Sawaya H, Sebag IA, Plana JC, Januzzi JL, Ky B, Tan TC, et al. Assessment of echocardiography and biomarkers for the extended prediction of cardiotoxicity in patients treated with anthracyclines, taxanes, and trastuzumab. Circ Cardiovasc Imaging. 2012;5(5):596-603. doi: https://doi.org/10.1161/CIRCIMAGING.112.973321

23. Charbonnel C, Convers-Domart R, Rigaudeau S, Taksin AL, Baron N, Lambert J, et al. Assessment of global longitudinal strain at low-dose anthracycline-based chemotherapy, for the prediction of subsequent cardiotoxicity. Eur Heart J Cardiovasc Imaging. 2017;18(4):392-401. doi: https://doi.org/10.1093/ehjci/jew223

24. Bear HD, Tang G, Rastogi P, Geyer CE Jr, Robidoux A, Atkins JN, et al. Bevacizumab added to neoadjuvant chemotherapy for breast cancer. N Engl J Med. 2012;366(4):310-20. doi: https://doi.org/10.1056/NEJMoa1111097.

Assessing Myocardial Viability in Clinical Practice

Viabilidade Miocárdica na Prática Clínica

Miriana Basso Gomes[1,2,3]

[1]*Institute of Cardiology/University Foundation of Cardiology, Porto Alegre, RS, Brazil.* [2]*Master's student at the Postgraduate Program in Health Sciences: Cardiology and Cardiovascular Sciences at the Federal University of Rio Grande do Sul, Porto Alegre, RS, Brazil.* [3]*Cardionuclear Clinic, Porto Alegre, RS, Brazil.*

Abstract

Although assessing myocardial viability is a common cardiology practice, many physicians question the results of diagnostic methods. Nuclear medicine plays an important role in viability studies, but the reports require interpretation in a clinical and pathophysiological context. this article was aimed at reviewing the origin and evolution of myocardial viability. Here we present diagnostic methods by emphasizing nuclear medicine and provide a functional explanation of each test type using example images. We also propose how to act in these cases based on clinic examination findings, the percentage of affected myocardium, and coronary lesion topography (proximal or distal).

"Do not declare that the stars are dead just because the sky is cloudy."

Arabic proverb

Introduction

The most common question in the cardiologist's daily routine regarding interventions in patients with a previous history of infarction or left ventricular dysfunction is as follows: Is the myocardium viable or unviable? However, answering this question is not so simple. In addition to a variety of methods of assessing viability, there are several anatomical possibilities for lesions within the same muscle area. Cases referred by the physician for a viability test are usually complex to diagnose. As René Descartes said: "There are no easy methods to solve difficult problems." Thus, this review aimed at explaining the principles of viability, especially those used in nuclear medicine tests.

Theoretical background

The concept of myocardial viability emerged in the early 1980s. Prior to that point, left ventricular dysfunction was considered an "irreversible" process. The term "hibernating myocardium" was created after the perception that some patients had improved ejection fractions after coronary artery bypass graft surgery.[1]

Keywords

Myocardial Viability; Myocardial Infarction; Cardiology; Nuclear Medicine.

Mailing Address: Miriana Basso Gomes •
Instituto de Cardiologia/Fundação Universitária de Cardiologia – Avenida Princesa Isabel, 395, Santana. CEP 90040-371 – Porto Alegre, RS, Brazil.
E-mail: mirianab.gomes@hotmail.com
Manuscript received 10/17/2021; revised 11/9/2021; accepted 4/12/2022

DOI: 10.47593/2675-312X/20223502eabc264

An important study at that time was the Coronary Artery Surgery Study (CASS),[2] which divided 780 three-vessel disease patients with left ventricular dysfunction into two treatment groups: 1) clinical and 2) surgical. The CASS study showed a significant advantage of surgical therapy. The survival rate was 88% for the surgical group versus 65% for the clinical group ($p = 0.009$). The pharmacological treatment used at the time of the CASS included no beta-blockers, statins, and angiotensin-converting-enzyme (ACE) inhibitors; moreover, no mammary grafts were used (only saphenous). Thus, the results cannot be fully extrapolated to the present day, although the concept of left ventricular dysfunction and three-vessel disease are still considered by many as synonymous with surgical therapy.

But why do patients with coronary lesions develop left ventricular dysfunction? Contractility loss is part of what we call "programmed cell survival."[2] The decreased blood flow decreases oxygenation and the cell increases its anaerobic metabolism to survive. Scarce adenosine triphosphate (ATP)[3] (energy) is recruited to maintain vital functions and not contractility. ATP use in the myocyte is divided into 60% for systolic function, 15% for diastolic function, 5% for electrical activity, and 20% for cell membrane integrity.[3]

The so-called hibernating myocardium ceases contractility but maintains cellular metabolism.[4] The muscle reduces its contraction as a protective factor to consume minimal energy and prevent cell death. A histological analysis of hibernating myocardium demonstrated non-contractile myocytes with intact membranes and little or no evidence of metabolic apoptosis.[4] The stunned myocardium is also a mechanism of programmed cell survival, being characterized by contractile dysfunction that follows brief episodes of myocardial ischemia after blood flow has been restored.[5] Briefly, hibernation is a protective phenomenon that reduces contractility in the setting of a persistently decreased blood flow. On the other hand, stunned myocardium is a consequence of injury in cases in which contractility remains temporarily reduced despite the return of coronary flow.

It is not always simple to differentiate hibernated from fibrotic myocardium through tests. Each method assesses it according to the following principles of viability[4]:

Presence of myocardial blood flow

Myocardial blood flow can be assessed by capturing ^{99m}technitium-2-methoxyisobutyl-isonitrile (^{99m}Tc-MIBI).[6] MIBI (sestamibi) is a monovalent cation that along with ^{99m}Tc, forms a radiopharmaceutical that lodges in the mitochondria of myocardial cells. The retention of this tracer in intact mitochondria reflects viable myocytes. In cases of decreased cardiac uptake with ^{99m}Tc-MIBI, imaging can be acquired after the administration of nitrate to improve perfusion with vasodilator stimulation.[7] ^{99m}Tc-MIBI is not the best method for assessing viability, as viable regions with low blood flow can be misclassified as scars (Figure 1).

Cell membrane integrity

Cell membrane integrity can be assessed using thallium (on single photon emission computed tomography) and rubidium (on positron emission tomography [PET]) scans, which have a physiology similar to potassium ion. Thallium is not a radiopharmaceutical like ^{99m}Tc-MIBI but rather a radioisotope produced in cyclotron. The physical half-life of thallium-201 is 73 hours. The sodium-potassium pump acts on the cell membrane, enabling the assessment of its integrity through these substances, which are analogous to potassium.[8] Potassium, the main intracellular cation, is absent in scar tissue. As thallium does not bind to organelles within myocytes, it is pushed out of the cell by the same entry mechanism. Thallium excretion from the cell is called redistribution. In this process, normal tissues redistribute thallium faster than ischemic tissues. Therefore, most thallium protocols include only one tracer injection with two image acquisitions, which can consist of rest and redistribution or stress and redistribution.

The following scenarios are possible:

- Changed rest with improved redistribution, leading to necrosis with viability.
- Changed rest without improved redistribution, leading to necrosis without viability.
- Changed stress with improved redistribution, leading to ischemia with viability.
- Changed stress without improved redistribution, leading to necrosis without viability.
- Normal stress, leading to normal test findings (no redistribution image required).

In some cases, an additional 24-hour late imaging test may be performed after a low-dose reinjection. However, this does not happen with ^{99m}Tc-MIBI, which does not redistribute; therefore, separate injections are required for stress and rest studies at intervals of up to several days between steps.

Figure 2 shows the test performed on a patient admitted to the hospital with a history of infarction and catheterization with an occluded left anterior descending coronary artery but the presence of collaterals. The initial image taken after stress shows significant apical anterior hypoperfusion, while redistribution images show mild reversibility. As the reversibility area was small in the first acquisitions and the patient experienced symptoms and electrocardiographic changes during stress, late redistribution was performed. Normal tissues redistribute thallium faster than ischemic tissues, so perfusion improvement (viability sign) can be seen on images only after 24 hours.

Figure 3 shows a test performed with thallium-201. The top line shows rest images with hypoperfusion at the apex and distal portions of the anterior, septal, and inferior walls. The bottom line shows redistribution images (3 hours post-injection) with improved perfusion - a sign of viability.

Preserved metabolic activity

Metabolic myocyte activity can be measured by PET.[9] In the viability protocol, the patient is injected with ^{18}F-fluorodeoxyglucose (^{18}F-FDG), a glucose analog labeled with fluorine-18 when associated with a carbohydrate-free diet. In the situation of chronic ischemia of the hibernated myocardium, the oxygen supply is low and the myocardium partly uses the glycolytic (anaerobic) pathway for energy production, which may be inadequate to maintain contractility but sufficient to maintain cellular metabolism. If the patient is taking a ketotic diet (low in sugars), cellular uptake of this tracer will be low. The hibernated myocardium, unlike normal muscle, involves a chronically activated glycolytic pathway and will be able to capture ^{18}F-FDG through its residual glucose metabolism, showing viable areas.

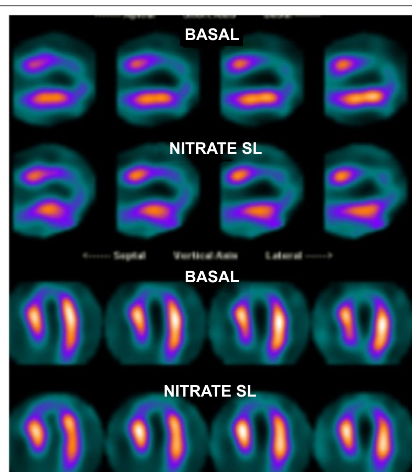

Image courtesy of Cardionuclear.

Figure 1 – *Test showing significant necrosis in the territory of the anterior descending coronary artery using 99mtechnitium-2-methoxyisobutyl-isonitrile, with no significant improvement in perfusion noted after nitrate administration.*

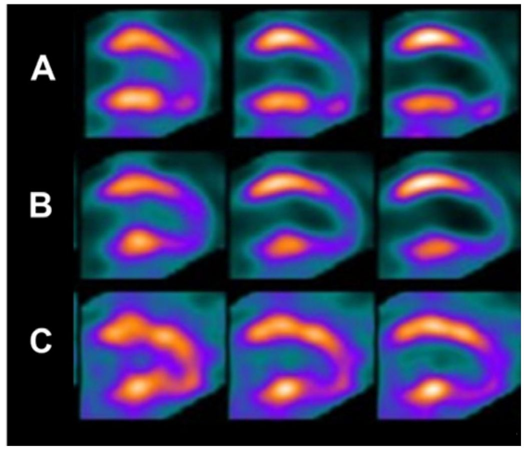

Image courtesy of Cardionuclear.

Figure 2 – *Test of an inpatient with a history of infarction and catheterization with an occluded left anterior descending coronary artery and the presence of collaterals. A) Image taken immediately after stress. B) Image taken after 3 hours of redistribution. C) Image taken after 24 hours of redistribution using thallium-201.*

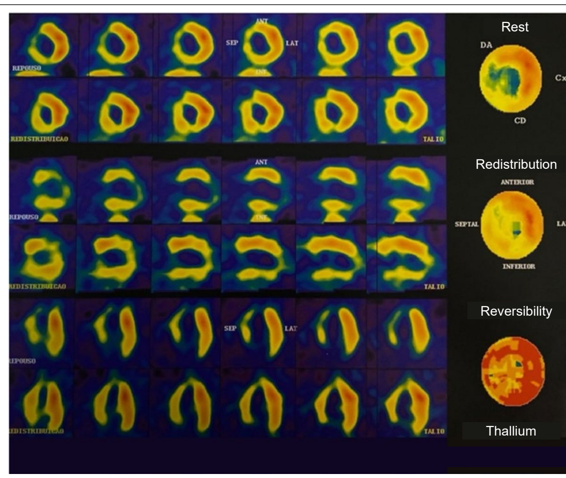

Image courtesy of Cardionuclear.

Figure 3 – *Test using thallium-201.*

The top line in Figure 4 shows a test with thallium-201 evidencing an area of perfusion defect[4] in the territory of the anterior descending coronary artery. The bottom line shows a test with ^{18}F-FDG evidencing increased capture[5] and, therefore, preserved metabolism precisely in areas deficient in thallium-201. These test results are compatible with myocardial viability. Mismatch (viable myocardium) occurs when the perfusion image is changed and metabolism is improved. Match (absent viability) occurs when cases are changed in both studies and, therefore, demonstrate defect pattern agreement (Figure 5).

^{18}F-FDG PET associated with cardiac magnetic resonance imaging (MRI) is considered the best method for detecting myocardial viability since MRI assesses the absence of myocytes using late gadolinium enhancement.[10] Interpretation of the results is based on analysis of the transmural extension of the enhancement in relation to the healthy region. When the length of the same segment is less than 50%, the myocardium is viable. When the extension of the same segment is greater than 50%, the myocardium is not viable.

Finally, viability can also be analyzed through the "contractile reserve" by dobutamine echocardiography.[11] Viable myocardium in this situation will have the following characteristics:

- Abnormal contractility at rest
- Improved contractility at a low dose of dobutamine
- Unchanged contractility at a high dose of dobutamine

A myocardium with ischemia and viability benefits most from revascularization. In such cases, the stress echocardiogram will have the following findings:

- Abnormal contractility at rest
- Improved contractility at a low dose of dobutamine
- Worsened contractility at a high dose of dobutamine

A viability study is not indicated in cases of a myocardium with normal contractility at rest. If there is some degree of kinesis, necrosis does not predominate. Knowledge of the concept of hibernation is essential to prevent an erroneous request for viability test based only on a previous history of infarction or some electrocardiographic changes. Table 1 summarizes the main viability assessment methods.[12]

Considerations about myocardial perfusion

Myocardial perfusion changes are not always segmented and homogeneous. Reports would be less complex if the areas without viability were exactly in segments irrigated by a single coronary artery. However, areas of necrosis surrounded by areas of ischemia (or even normal myocardium) in the same topography are a common finding on scintigraphy. For example, a patient may have necrosis without viability in the medial and apical anterior segments that totals 12% of the extension. However, other viable areas are irrigated by the anterior descending coronary artery, such as the basal anterior segments and the entire septal wall. The attending physician may consider not revascularizing this artery since the report showed no viability. However, the territory of the anterior descending coronary artery extends beyond the 12% described; thus, this

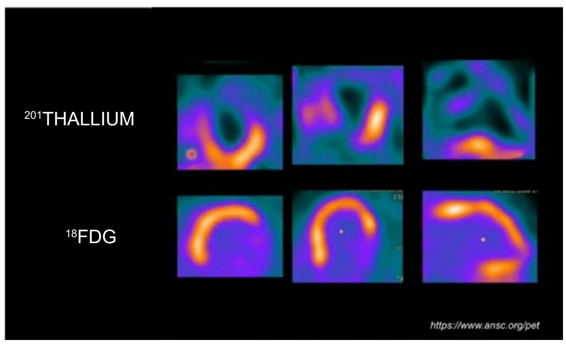

Figure 4 – *Image on the top line taken with thallium-201 showing an area of necrosis in the territory of the anterior descending coronary artery.*

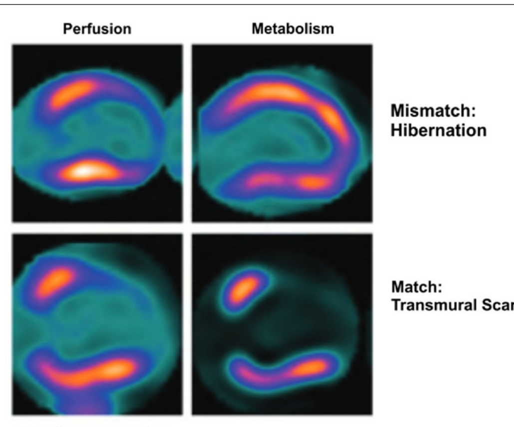

Figure 5 – *Image mismatch and match.*

Table 1 - Summary of the main viability assessment methods.

Methods	Radiation	Duration	Number of phases	Sensitivity	Specificity
Echocardiography with dobutamine	Absent	30 min	-----	77-89%	68-93%
^{99m}Tc-MIBI SPECT	Moderate	90-120 min	2 injections	81%	69%
Resonance	Absent	35 min	2 injections	92%	51-89%
Thallium-201	Discharge	3 h with additional 24-h IN image	1 injection	87%	54%
^{18}F-FDG PET	Moderate	1 h	1 injection	92%	63%

^{18}F-FDG PET, ^{18}F-fluorodeoxyglucose positron emission tomography; SPECT, single photon emission computed tomography; ^{99m}Tc-MIBI, ^{99m}technitium-2-methoxyisobutyl-isonitrile, IN, if necessary.

decision could compromise an important part of the muscle. If we consider three territories in the left ventricular myocardium, the percentage of each main coronary artery will be about 33% of the total. Therefore, the 12% proportion without viability in this area does not represent the physiological importance of the left anterior descending coronary artery. If a patient has lesions in the three main coronary arteries, coronary artery bypass graft surgery cannot be avoided due to a non-viable area of 10–15% and viable area of more than 80%. In addition, the Stich study already showed that a lack of viability was associated with no differences between drug therapy and revascularization.[13] The presence of viability proved to be a good prognostic factor regardless of the approach used.[14]

Most methods divide the myocardium into 17 segments, but there are only three main coronary arteries. Therefore, it is necessary to analyze exactly which segments are being irrigated by each of the coronary arteries in each case. Apical necrosis is a very common scintigraphic finding because tissue suffering almost always occurs firstly at the tip of the heart. When a vascular occlusion occurs in the leg, for example, fibrosis starts at the tip of the toes and may extend throughout the foot. The same occurs with the heart, justifying a high prevalence of tissue suffering in the apical region of the left ventricle.

The apical region comprises the apex (segment 17) and the distal portion of all walls (anterior, septal, inferior, and lateral).[15]

For example, necrosis may develop if the patient has an infarction involving medial occlusion of the anterior descending coronary artery. If short time is available to open the coronary artery, the fibrotic area is likely to be only at the apex. If the delta T is greater, this fibrosis will extend from the apex to the medial portion of the anterior wall and affect the septum.

A very relevant analysis involves determining whether the coronary lesion(s) is proximal or distal. If the patient has distal lesions and necrosis is present in the periapical segments, the absence of viability is less important even by a method that is not the gold standard, as a smaller tissue area is at risk.

However, if the patient has proximal or left main coronary lesions, necrosis in the distal portions of the left ventricle should not be decisive for ruling out revascularization. In these cases, a stress test or analysis of clinical and electrocardiographic changes is often more important in the choice of a particular therapy than a viability test alone.

Imaging tests were performed of a patient with a history of inferior wall infarction and three-vessel lesion. The tests were performed after coronary artery bypass graft surgery and showed necrosis sequelae in the apex and lower basal segment (Figure 6).

Figure 7 shows the case of a patient with a history of anterior wall infarction and lesions in the anterior and right descending coronary arteries. A viability test quantified necrosis in 15% of the apical anterior extension (bottom line). The use of a stress test was suggested (top row) as the lesions were proximal. Perfusion worsened in the middle and basal anterior segments beyond the bottom wall. The report indicated necrosis with ischemia and viability in the territory of the anterior descending coronary artery and ischemia in the territory of the right coronary artery.

Figure 8 shows the case of a patient with lesions in the three coronary arteries and an occluded anterior descending coronary artery. A viability test was requested, but a stress test (top row) was suggested to better guide treatment.

Despite the significant area of necrosis at rest, worsening that occurs after stress indicates the presence of viable myocardial peri-necrosis. Ischemia also occurs in the other periapical segments (septal, lateral, and inferior).

Another important change is right ventricular uptake only on post-stress images as a sign of severe ischemia. These findings indicate the need for myocardial revascularization surgery.

Final messages

No imaging method can assess viability with 100% sensitivity and specificity, so if it is clinically justified, the physician should consider revascularization.

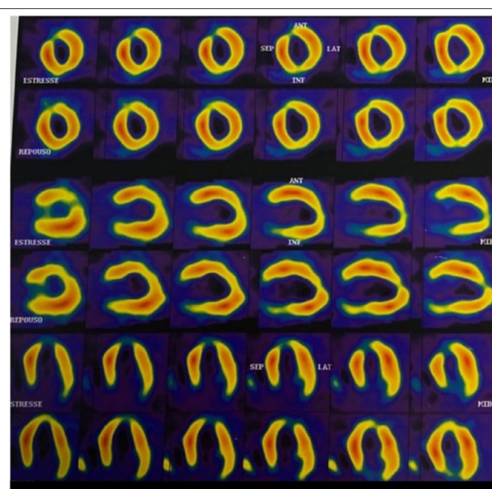

Image courtesy of Cardionuclear.

Figure 6 – *Imaging tests of a patient with a history of inferior wall infarction and a three-vessel lesion.*

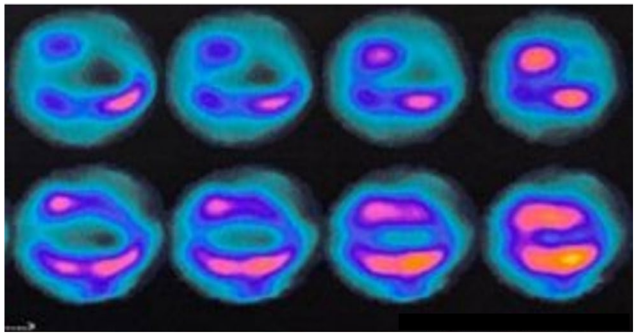

Image courtesy of Cardionuclear.

Figure 7 – *Image of a patient with a history of anterior wall infarction and lesions in the anterior and right descending coronary arteries.*

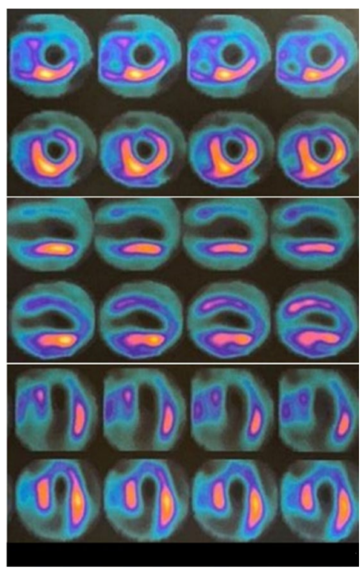

Image courtesy of Cardionuclear.

Figure 8 – *Test of a patient with lesions in the three coronary arteries and an occluded anterior descending coronary artery.*

The Stich study[13] showed that the absence of viability was associated with no differences between drug therapy and revascularization. However, an analysis performed 10 years after that study showed that the ejection fraction increase was greater in patients with viability (regardless of treatment approach).[16]

The Christmas study also reported that patients with heart failure using carvedilol experienced a greater increase in ejection fraction when viability was present.[17] Therefore, viability can be considered a useful indicator of good prognosis regardless of assessment method.

Areas with less than 30% viability should be analyzed very carefully, as each of the three main coronary territories corresponds to approximately 33% of the left ventricle. Not revascularizing a coronary artery due to a small percentage of fibrosis may compromise other segments also supplied by the same coronary artery.

When the fibrotic area is restricted to the apex and surrounding segments, it is important to analyze whether the coronary lesion(s) are proximal or distal. If they are distal, clinical treatment is indicated. If they are proximal, there is a greater tendency to perform invasive therapy due to the higher percentage of myocardium at risk, a stress test may aid in therapeutic decision.

Author's contributions

Data analysis and interpretation, statistical analysis, manuscript writing, and critical review of the manuscript for important intellectual content: GOMES MB.

Conflict of interest

the author has declared that she has no conflict of interest.

References

1. Rahimtoola SH. Coronary bypass surgery for chronic angina - 1981. Circulation. 1982;65;225-41. doi: https://doi.org/10.1161/01.CIR.65.2.225

2. Coronary artery surgery study (CASS): A randomized trial of coronary artery bypass surgery. Survival data. Circulation. 1983;68(5):939-50. doi: https://doi.org/10.1161/01.CIR.68.5.939

3. Braunwald E, Rutherford JD. Reversible ischemic left ventricular dysfunction: Evidence for the "hibernating myocardium". J Am Coll Cardiol. 1986;8(6):1467-70. doi: https://doi.org/10.1016/S0735-1097(86)80325-4

4. Rahimtoola SH. The hibernating myocardium. Am Heart J. 1989;117(1):211-21. doi: 10.1016/0002-8703(89)90685-6

5. Bolli R. Mechanism of myocardial "stunning". Circulation. 1990;82:723-38. doi: https://doi.org/10.1161/01.CIR.82.3.723

6. Li QS, Solot G, Frank TL, Wagner HN, Becker LC. Myocardial redistribution of technetium-99m-methoxyisobutyl isonitrile (SESTAMIBI). J Nucl Med. 1990;31(6):1069-76. PMID: 2140856.

7. Sciagra R, Bisi G, Santoro GM, Rossi V, Fazzini PF. Nitrate versus rest myocardial scintigraphy with technetium 99m-sestamibi: Relationship of tracer uptake to regional left ventricular function and its significance in the detection of viable hibernating myocardium. Am J Card Imaging 1995;9(3):157-66. PMID: 7549355.

8. Silva P, Galli M, Marcassa C. Deteccion de miocardiol viable con Talio-201. Arch Inst Cardiol Mex. 1992;62(6):565-72. PMID: 1285667.

9. Kobylecka M, Mączewska J, Fronczewska-Wieniawska K, Mazurek T, Płazińska MT, Królicki L. Myocardial viability assessment in 18FDG PET/CT study (18FDG PET myocardial viability assessment). Nucl Med Rev Cent East Eur. 2012;15(1):52-60. doi: https://doi.org/10.5603/nmr-18731

10. Souto AL, Souto RM, Teixeira IC, Nacif MS. Myocardial viability on cardiac magnetic resonance. Arq Bras Cardiol. 2017;108(5):458-69. doi: https://doi.org/10.5935/abc.20170056

11. Khemka A, Sawada SG. Dobutamine echocardiography for assessment of viability in the current era. Curr Opin Cardiol. 2019;34(5):484-9. doi: https://doi.org/10.1097/HCO.0000000000000658

12. Ker WD, Nunes TH, Nacif MS, Mesquita CT. Practical implications of myocardial viability studies. Arq Bras Cardiol. 2018;110(3):278-88. doi: https://doi.org/10.5935/abc.20180051

13. Bonow RO, Maurer G, Lee KL, Holly TA, Binkley PF, Desvigne-Nickens P, et al. Myocardial Viability and Survival in Ischemic Left Ventricular Dysfunction. N Engl J Med. 2011;364(17):1617-25. doi: https://doi.org/10.1056/nejmoa1100358

14. Bhat A, Gan GC, Tan TC, Hsu C, Denniss AR. Myocardial viability: from proof of concept to clinical practice. Cardiol Res Pract. 2016;2016:1020818. doi: https://doi.org/10.1155/2016/1020818

15. Mastrocola LE, Amorim BJ, Vitola JV, Brandão SC, Grossman GB, Lima RS et al. Update of the Brazilian Guideline on Nuclear Cardiology - 2020. Arq Bras Cardiol. 2020;114(2):325-429. doi: https://doi.org/10.36660/abc.20200087

16. Howlett JG, Stebbins A, Petrie MC, Jhund PS, Castelvecchio S, Cherniavsky A, et al.; STICH Trial Investigators. CABG Improves Outcomes in Patients With Ischemic Cardiomyopathy: 10-Year Follow-Up of the STICH Trial. JACC Heart Fail. 2019;7(10):878-87. doi: https://doi.org/10.1016/j.jchf.2019.04.018

17. Pennell DJ, Ray SG, Davies G, Burgess M, Webster J, Slomka P, et al. The Carvedilol Hibernation Reversible Ischaemia Trial, Marker of Success (CHRISTMAS) study: Methodology of a randomised, placebo controlled, multicentre study of carvedilol in hibernation and heart failure. Int J Cardiol. 2000;72(3):265-74. doi: https://doi.org/10.1016/S0167-5273(99)00198-9

Systematic Review Article

Role of Strain in the Early Diagnosis of Diabetic Cardiomyopathy

Papel do Strain no Diagnóstico Precoce da Cardiomiopatia Diabética

Thais Rossoni Weber da Silva[1], Roberto Léo da Silva[1], Adriana Ferraz Martins[1], Jefferson Luiz Brum Marques[2]

Department of Cardiology, Prof. Polydoro Ernani de São Thiago University Hospital, [1] Florianópolis, SC, Brazil. Institute of Biomedical Engineering, Federal University of Santa Catarina [2], Florianópolis, SC, Brazil.

Abstract

Background: Advanced echocardiography using two- and three-dimensional myocardial strain proposes to identify subclinical systolic dysfunction in different clinical conditions. Strain assessment plays an important role in the early diagnosis of diabetic cardiomyopathy in diabetes mellitus (DM). However, the findings of published articles are heterogeneous. Here we conducted a systematic review to analyze the current role of strain assessment in patients with DM. Methods: This systematic review of five databases identified 19 studies that used two-dimensional strain and 8 studies that used three-dimensional strain. Results: The studies of two-dimensional strain included 1,774 DM patients (mean age, 57.1 years; median age, 55 years; 47.5% women), while those of three-dimensional strain included 488 DM patients (mean age, 55.7 years; median age, 63 years; 51% women). Global longitudinal strain was the myocardial deformation marker that differed most frequently between the DM and control groups. Conclusion: Myocardial strain imaging by two- and three-dimensional speckle tracking echocardiography allows the identification of subclinical systolic dysfunction in DM patients, and differences become more marked when associated with risk factors and ventricular remodeling.

Introduction

Diabetes mellitus (DM), among the most prevalent diseases in the modern world, is a risk factor for heart failure that increases mortality, mainly from cardiovascular causes.[1] Cardiovascular complications are the leading cause of death in DM patients,[2,3] with diabetic cardiomyopathy being characterized by structural and functional cardiac changes without other known factors for the development of myocardial dysfunction, such as coronary heart disease, arterial hypertension, or significant valvular diseases.[4] Cardiac remodeling in diabetes results from cardiovascular autonomic neuropathy, renin-angiotensin-aldosterone system activation, interstitial myocardial fibrosis, microangiopathy, inflammatory cytokines, and metabolic changes such as hyperglycemia,[5,6] and its detection requires sensitive diagnostic methods.[7]

Keywords

Diabetes Mellitus, Echocardiography, Ventricular Function.

Mailing Address: Thaís Rossoni Weber da Silva •
Prof. Polydoro Ernani de São Thiago, Department of Cardiology, University Hospital R. Professora. Maria Flora Pausewang - Trinidad, Florianópolis, SC, Brazil 88036-800.
E-mail: thaisrossoni@yahoo.com
Manuscript received 2/28/2022; revised 3/10/2022; accepted 3/17/2022

DOI: 10.47593/2675-312X/20223502eabc293

The early diagnosis of diabetic cardiomyopathy is clinically relevant, as early lesions may be reversible[8,9] and therapy can be implemented to prevent cardiovascular disease progression. However, it remains little recognized by clinicians[1] due to the conflicting results of different populations[10] and the need for more sensitive and recently developed diagnostic tools. Left ventricular (LV) diastolic dysfunction was considered the initial sign on Doppler echocardiography.[11,12] Improved imaging methods such as speckle tracking echocardiography enabled the earlier detection of systolic myocardial dysfunction prior to diastolic dysfunction in asymptomatic subjects.[13,14]

The incorporation of new techniques such as myocardial strain on echocardiography increased the diagnostic sensitivity of speckle tracking, especially of subclinical myocardial dysfunction, and was validated by magnetic resonance imaging with myocardial tagging and sonomicrometry.[15] The most commonly used parameter is global longitudinal strain (GLS), the mean strain of myocardial segments in the longitudinal direction, a technique that is more reproducible and can identify subclinical LV dysfunction, a better risk predictor than LV ejection fraction (LVEF).[16] Another recent concept is multilayer analysis, which introduced an anatomical aspect into myocardial deformation assessment in which the three LV myocardial layers (endocardium, mesocardium, and epicardium) contribute to more effective contractions in different directions.[17] In contrast, three-dimensional myocardial strain enables a more objective assessment of LV systolic dysfunction without requiring calculations to predict ventricular geometric shape, with the additional benefit of being more reproducible than two-dimensional strain for avoiding marker loss outside the analyzed plane despite requiring high-quality images.[18]

Several studies aiming to assess cardiac function in DM patients using two- and three-dimensional strain reported worse myocardial deformation rates compared to controls. However, some such studies were small, heterogeneous, and presented several confounding factors. Thus, a review of the current evidence is necessary to understand knowledge gaps and revisit important issues. The present study aimed to identify whether advanced two- or three-dimensional speckle tracking echocardiography could demonstrate early cardiac lesions secondary to DM and define its current role for assessing DM patients. Thus, here we conducted a systematic review of the use of ventricular strain echocardiography in DM.

Methods

This systematic review was conducted according to the Preferred Reporting Items for Systematic Reviews and Meta-Analyses (PRISMA) guidelines. We searched the MEDLINE, EMBASE, SCOPUS, and WEB OF SCIENCE databases using the descriptors *"diabetic cardiomyopathy"* or *"speckle tracking"* or *"myocardial strain/dysfunction"* or *"ventricular function/dysfunction," "deformation imaging/analysis,"* or *"cardiac mechanics/function"* and *"diabetes"* or *"diabetic."* The search was limited to articles in humans; published in English, French, Spanish, or Portuguese; and published through January 31, 2022. The selection criteria for the articles were age older than 15 years, inclusion of control group without DM, no established heart disease, and speckle tracking description of the GLS value. Database references were gathered in the Mendeley® application and duplicates were removed. Two researchers (TRWS and RLS) searched the articles separately and agreed on the eligibility of the final selections. First, a broad search identified articles related to the topic by title and abstract screening. The exclusion criteria were a different target population or no control group; the presence of coronary artery disease or other structural disease; use of another imaging method for measuring myocardial deformation such as magnetic resonance imaging or tissue Doppler; no description of the GLS value; and case report, conference presentation, review, and editorial articles.

The articles were subsequently subjected to full-text review to identify those that presented the necessary data and fit the previous requirements. In studies with multiple subgroups of patients or controls, the lowest-risk subgroup was selected (Table 1). The studies were allocated to two- or three-dimensional speckle tracking groups for evaluation. The information extracted from the articles included author, year of publication, brand of equipment, study design, number of cases in the sample, age, sex, body mass index (BMI), blood pressure levels or diagnosis of hypertension, glycated hemoglobin (HbA1c) value, LVEF, GLS, global radial strain (GRS), and global circumferential strain (GCS) (Table 2). Studies of three-dimensional strain also included global strain area (GSA) (Tables 3 and 4).

Results

We identified 819 references in the electronic databases in the previous five years, excluding 123 duplicates. Of the remaining 696 studies, we obtained 75 full articles for analysis after title and abstract screenings. Another 49 studies were excluded (Figure 1). The review included 26 articles for qualitative analysis, which were classified into two main categories: two-dimensional strain (n = 19; Table 1) and three-dimensional strain (n = 8; Table 2). Only studies with a control group were included. The articles were mostly published in English, followed by French and Portuguese. Three[18–20] were prospective studies and the others were case-control studies.

The studies using two-dimensional strain resulted in a sample of 1,774 DM patients (mean age, 57.1 years; median age, 55 years; 47.5% women). A GE Vivid E9 ultrasound machine was most often used in these studies. The studies using three-dimensional strain resulted in a sample of 488 DM patients (mean age, 55.7 years; median age, 63 years; 51% women). All studies used the GE Vivid E9 device except for two that used an Philips iE33 ultrasound system.

Of the 19 analyzed studies, less than half excluded hypertensive patients from the DM group,[10,18,21–24] most involved type 2 DM (DM2) patients, and only three

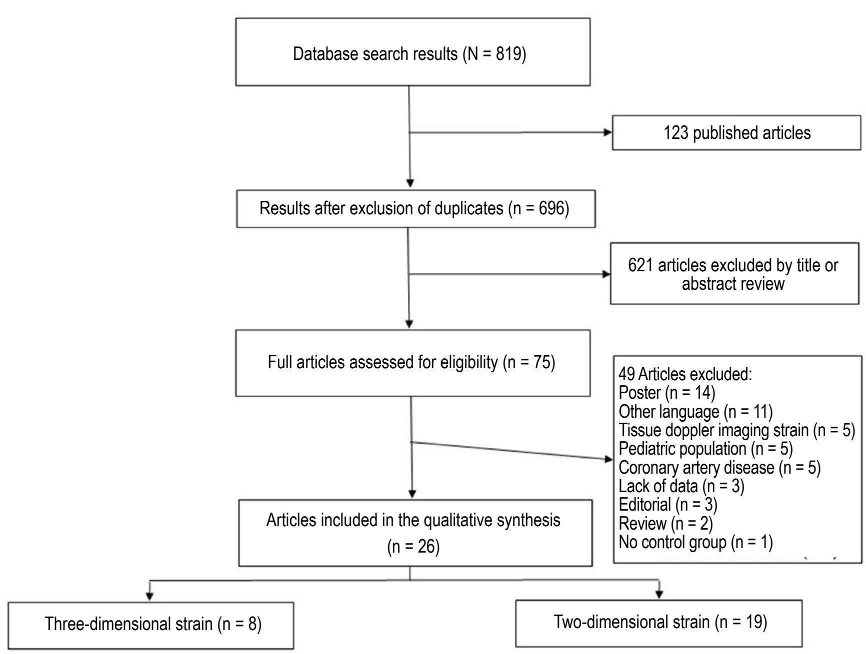

TDI: Tissue Doppler Imaging; CAD: Coronary Artery Disease; 3D: three-dimensional; 2D: two-dimensional. In the qualitative synthesis, one study was included in 2D and 3D strain.

Figure 1 – *Flowchart of search and selection of studies evaluating diabetic cardiomyopathy through bidimensional and three-dimensional strain.*

Table 1 – Clinical and demographic data of studies that evaluated diabetic cardiomyopathy using two-dimensional speckle tracking strain.

Author	N	Control	DM type	HbA1c	Control	Age, years (DM)	Age, years (Control)	Women, % (DM)	Women, % (Control)	BMI (DM)	BMI (Control)	SBP (DM)	SBP (Control)
Yamauchi et al.[7]	192	81	DM2	8.5	Healthy	61	57	48	54	25	22	131	123
Weber et al.[10]	40	40	DM1	8.0	Healthy	33	33	55	55	25	25	110	102
Tadic et al.[17]	48	44	DM2	7.3	Healthy	55	52	48	50	27	26	131	127
Ringle et al.[18]	66	26	DM1	7.7	Healthy	38	35	71	69	24	23	122	121
Ng et al.[20]	397	104	DM2	7.3	Healthy	58	50	46	43.3	29	-	141	123
Yang et al.[21]	47	27	DM2	6.1	Healthy	51	50	32	33	23	23	-	-
Wang et al.[22]	48	50	DM2	10.1	Healthy	54	50	52	50	23	23	127	122
Vukomanovic et al.[23]	50	40	DM2	7.3	Healthy	55	50	48	45	29	24	131	129
Vukomanovic et al.[24]	70	80	DM2	7.5	Healthy	52	49	44	43	28	26	126	124
Soufi Taleb Bendiab et al.[25]	93	107	DM2 + SAH	-	SAH	61	62	63	53	30	29	158	142
Tadic et al.[26]	50	55	DM2 + SAH	7.0	Healthy	56	51	48	47	27	26	145	128
Todo et al.[29]	177	79	DM2	8.8	Healthy	61	58	47	57	25	22	131	125
Van Ryckeghem et al.[30]	36	23	DM2	6.9	Healthy	62	57	14	48	28	26	149	140
Roberts et al.[31]	34	17	DM1/DM2	7.8	Healthy	42	41	29	35	27	25	125	121
Li et al.[32]	101	60	DM2	7.6	Healthy	52	54	53	53.3	24	23	123	123
Philouze et al.[33]	44	35	DM2	7.2	Healthy	56	52	41	51	27	24	126	123
Mochizuki et al.[34]	103	82	DM	8.6	Healthy	56	55	63	60	23	22	121	117
Jørgensen et al.[36]	57	80	DM2	6.1	Healthy	65	65	44	35	26	24	126	123
Stevanovic et al.[39]	121	40	DM2	8.2	Healthy	55	53	19	29	28	27	125	122

BMI, body mass index; DM, diabetes mellitus; DM1, type 1 DM; DM2, type 2 DM; HbA1c, glycated hemoglobin; N, number of patients with diabetes; SAH, systemic arterial hypertension; SBP, systolic blood pressure.

Table 2 – Clinical and demographic data from studies that evaluated diabetic cardiomyopathy by three-dimensional speckle tracking strain.

Author	N	Control	DM	HbA1c (%)	Control	Age, years (DM)	Age, years (Control)	Women, % (DM)	Women, % (Control)	BMI (DM)	BMI (Control)	SBP (DM)	SBP (Control)
Wang et al.[41]	40	40	DM2	-	Healthy	66±7	68±8	50	50	24.6±2	23.5±3	128±7	123±9
Wang et al.[44]	40	40	DM2	6.6±0.6	Healthy	68±8	68±7	50	55	24.9±3	24.4±3	128±9	126±10
Wang et al.[42]	38	45	DM2	7.0±0.6	Healthy	61±8	62±7	45	50	24.5±3	24.7±2	127±10	126±7
Luo et al.[43]	38	35	DM2	10.4±2.6	Healthy	59±7	58±76	32	32	24.9±2	24.3±2	128±9	107±6
Wang et al.[47]	40	40	DM2	-	Healthy	66±8	67±8	50	50	24.7±2	25.0±3	128±6	126±7
Wang et al.[45]	34	40	DM2	-	Healthy	65±7	64±8	50	50	24.0±2	24.5±3	125±8	125±7
Chen et al.[46]	192	81	DM2	6.1±0.4	Healthy	52 ± 8	50±6	50	49	25.1 ± 2	24.3 ± 2	122 ± 11	119 ± 10
Ringle et al.,[18]	66	26	DM1	7.7±1.3	Healthy	37±9	35±7	71	69	24.0±3	23.0±3	121±12	122±9

BMI, body mass index; DM, diabetes mellitus; DM1, type 1 diabetes mellitus; DM2, type 2 diabetes mellitus; HbA1c, glycated hemoglobin; N, number of patients with diabetes; SAH, systemic arterial hypertension; SBP, systolic blood pressure.

analyzed type 1 DM (DM1) cases. In one study,[25] the control group consisted of hypertensive patients without diabetes. Some studies evaluated DM patients with versus without hypertension, with versus without associated microvascular complications, or even subgroups in which uncontrolled risk factors were quantified. Another study presented a DM population prior to hospitalization with changed glycemic levels (HbA1c > 10%).[22]

Different assessments were studied in this population, such as myocardial work index,[26,27] myocardial torsion by speckle tracking,[28] right ventricular systolic dysfunction by speckle tracking,[29] cardiac function during physical activity and exercise capacity,[24,30,31] dispersion value between systolic strain peaks,[32] heart rate effect,[7] cardiac function during dobutamine stress echocardiography,[33] heart rate variability,[23] diastolic dysfunction progression,[34] and multilayer speckle tracking analysis.[17,23]

The echocardiographic characteristics of interest here are shown in Tables 3 and 4.

Discussion

The use of new imaging techniques for diagnosing diabetic cardiomyopathy has increased our knowledge through the identification of earlier lesions. Although LV diastolic

Table 3 – Systolic cardiac function evaluated by two-dimensional speckle tracking strain.

Author	Equipment	LVEF % (DM)	LVEF % (Control)	GLS (DM)	GLS (Control)	p (DM × Control)	GCS (DM)	GCS (Control)	p	GRS (DM)	GRS (Control)	p
Yamauchi et al.[7]	GE Vivid E9	66±5	66±5	-17.6±3	-20.3±2	<0.0001	-	-	-	-	-	-
Weber et al.[10]	GE S6	72±5	71±5	-21.7±2	-21.0±2	0.21	-	-	-	-	-	-
Tadic et al.[17]	GE Vivid 7	64±4	65±4	-18.8±2	-20.8±2	<0.001	-19.2±2	-21.4±3	<0.001	41.6±8	43.2±8.3	0.001
Ringle et al.[18]	Philips - IE33	60±8	61±3	-18.9±2	-20.5±2	0.0002	-25.4±3	-26.1±3	0.39	36.3±9	37.6±7	0.054
Ng et al.[20]	GE Vivid 7/E9	60±5	58±4	-17.3±2	-20.5±2	-	-	-	-	-	-	-
Yang et al.[21]	GE Vivid E9	58±3	59±2	-17.2±2	-20.2±3	0.04	-20.9±4	-22.1±3	0.06	37.4±12.6	40.3±11.8	0.45
Wang et al.[22]	GE Vivid E9	66±4	62±5	-19.6±2	-22.5±3	<0.0001	-	-	-	-	-	-
Vukomanovic et al.[23]	GE Vivid 7	64±5	63±4	-18.5±2	-21.1±3	<0.001	-18.9±2	-21.9±3	<0.001	37.2±8.1	42.1±8.6	0.007
Vukomanovic et al.[24]	GE Vivid 7	64±4	64±3	-18.4±2	-21.6±3	<0.001	-19.5±2.6	-22.0±3	<0.001	37.9±9.4	40.6±10.1	0.094
Soufi Taleb Bendiab et al.[25]	GE S6	61±6	62±6	-16.4±3	-17.8±3	<0.0001	-	-	-	-	-	-
Todo et al.[29]	GE Vivid E9	66±5	66±5	-17.6±3	-20.5±2	<0.0001	-	-	-	-	-	-
Van Ryckeghem et al.[30]	GE Vivid E9	66±8	66±9	-17.0±3	-19.8±2	<0.001	-	-	-	-	-	-
Tadic et al.[26]	GE Vivid 7	62±3	63±3	-17.7±2	-21.3±3	<0.001	-18.3±2.3	-22.1±3	<0.001	38.5±9.3	41.8±10.1	0.247
Roberts et al.[31]	GE Vivid E9	60±4	60±5	–18.6±2	–19.7±2	0.09	-	-	-	-	-	-
Li et al.[32]	GE Vivid E9	64±4	65±4	- 19.4±3	- 21.22±3	<0.001	-	-	-	-	-	-
Philouze et al.[33]	GE Vivid E95	64±8	64±7	-20.8±2	-20.2±3	NS	-	-	-	-	-	-
Mochizuki et al.[34]	GE Vivid E9	67±4	66±5	-20.5±2	-20.5±2	<0.05	-	-	-	-	-	-
Jørgensen et al.[36]	GE Vivid E9	65	63	-15.3±2	-15.9±2	0.13	-18.7±5	-18.1±4	0.49	-	-	-
Stevanovic et al.[39]	GE Vivid 7	62±4	62±5	-17.5±2	-24.4±2	<0.001	-	-	-	-	-	-

DM, diabetes mellitus; GCS, global circumferential strain; GLS, global longitudinal strain; GRS, global radial strain; LVEF, left ventricular ejection fraction.

Table 4 – Systolic cardiac function evaluated by three-dimensional speckle tracking strain.

Author	Equipment	LVEF % (DM)	LVEF % (Control)	GLS (DM)	GLS (Control)	p (DM × Control)	GCS (DM)	GCS (Control)	p	GRS (DM)	GRS (Control)	p	GSA (DM)	GSA (Control)	p
Wang et al.[41]	GE Vivid E9	61±6	61±5	-17.1±2.6	-18.4±3.0	<0.05	-17.8±2.7	-18.8±3.0	>0.05	49.0±8.9	51.0±9.0	>0.05	-29.1±4.0	-30.2±3.6	>0.05
Wang et al.[44]	GE Vivid E9	60±7	61±7	-17.0±2.6	-18.9±2.5	<0.01	-17.4±2.5	-18.7±2.9	<0.05	47.7±8.5	51.5±8.9	>0.05	-30.1±3.6	-30.6±4.0	>0.05
Wang et al.[42]	GE Vivid E9	58±6	58±6	-17.3±2.4	-19.9±2.6	<0.001	-17.2±2.7	-18.9±0.31	<0.05	47.7±7.9	53.2±10.0	<0.01	-30.2±3.4	-31.0±4.7	>0.05
Luo et al.[43]	IE33	68±2	66±3	–17.2±3.0	–20.8±2.8	<0.01	-22.9±3.0	-25.9±3.4	<0.05	-	-	-	-	-	-
Wang et al.,[47]	GE Vivid E9	60±7	60±6	-16.9±2.9	- 18.2±2.3	<0.05	-17.6±3.5	-18.1±2.2	>0.05	46.9±9.8	48.5±6.5	>0.05	-29.6±5.5	-30.0±3.2	>0.05
Wang et al.[45]	GE Vivid E9	60±7	60±7	- 17.6±2.1	-18.8±2.7	<0.05	-17.9±2.7	-18.1±3.0	>0.05	49.1±7.9	50.2±9.3	>0.05	-30.7±3.2	-31.2±4.3	>0.05
Chen et al.[46]	GE Vivid E9	65±8	67±4	-19.3±3.9	-20.1±3.2	>0.05	-19.7±4.9	-19.3±6.3	>0.05	45.4±7.0	45.7±7.5	>0.05	-30.3±5.5	-33.0±6.6	>0.05
Ringle et al.,[18]	IE33	60±8	61±3	-17.5±2.0	-19.0±2.0	>0.05	-	-	-	-	-	-	-	-	-

DM, diabetes mellitus; GSA, global strain area; GCS, global circumferential strain; GLS, global longitudinal strain; GRS, global radial strain; LVEF, left ventricular ejection fraction.

dysfunction has traditionally been believed to precede systolic dysfunction, subclinical systolic dysfunction detected by GLS may be the first sign of diabetic cardiomyopathy.[14]

GLS is the myocardial deformation marker that most frequently differs between DM and control groups. Some studies established a specific GLS value for the diagnosis of subclinical ventricular dysfunction based on the statistical analysis of the values obtained in the sample. In these studies, the incidence of subclinical ventricular dysfunction was 40–45% in the diabetic population.[20,35] The fewer studies that used other parameters, such as GCS[17,23,24,26] or GRS[23], identified myocardial function differences using two-dimensional strain. These differences were not detected using LVEF. Tadic et al.[17] showed a GRS difference only in a DM and hypertension group. Likewise, Jørgensen et al. reported a GCS difference among subgroups of DM patients with more risk factors.[36]

Multilayer speckle tracking analysis can show differences between DM and control groups.[17,23,24,37] Despite being a new technology that requires further validation, this tool locates myocardial lesions and detects possible changes early.[38] Tadic et al. studied healthy controls, DM2 patients, and/or patients with systemic arterial hypertension (SAH) and reported multidirectional strain change; hypertension as a factor for LV mechanical deterioration; involvement of all myocardial layers due to DM and SAH; and a correlation between glycemic control (fasting glucose and HbA1c), GLS, and LV layer–specific strain.

In the previous five years, only three studies followed the participants. Studies including DM2 patients had larger sample sizes. Stevanovic et al. and Ng et al. followed up more than 100 subjects and demonstrated that GLS was a strong predictor of cardiovascular events in multivariate analysis.[20,39] Ringle et al. evaluated a group of DM1 patients a mean 37 years of age without cardiovascular risk factors who presented an absolute strain value lower than the control population and a significantly decreased absolute strain value during follow-up; however, no events were observed in the follow-up period. This study showed no correlation between GLS and metabolic status in terms of glycemic control, diabetes duration, or coexisting microvascular complications.[18]

Of the 19 articles analyzed, only four[10,31,33,36] identified no GLS differences and demonstrated subclinical myocardial function reduction attributable to diabetes. These studies analyzed DM1 and/or DM2 patients but with clearly fewer risk factors, such as SAH, overweight and obesity, dyslipidemia, renal function measured by creatinine clearance, lower glycemic levels (HbA1c < 8%), which, when present, were controlled in addition to showing no or smaller differences in LV structural parameters such as ventricular mass index and relative wall thickness. This information is useful for predicting a better prognosis for these patients and encouraging good control of comorbidities.

Several authors studied possible contributors to worsen systolic function in patients with diabetes. Yang et al. studied the relationship between microvascular complications and LV systolic function and reported decreased GLS in the group without complications that was even greater in the group with microvascular complications.[21] Soufi et al. studied hypertensive patients with and without diabetes and showed that the association of SAH and DM further decreases ventricular systolic function when evaluated by strain and that the two independent variables for this decreased absolute GLS value were DM2 and relative posterior wall thickness.[25] Jørgensen et al. designed a study to assess the influence of risk factors in DM patients and reported an association between systolic blood pressure, BMI, HbA1c, and LV structure and function. Thus, risk factors should be weighed when analyzing studies that assess diabetic cardiomyopathy to avoid confounding factors. Regardless, this population has a high prevalence of comorbidities, and poor metabolic control can interfere with cardiac function.

As for glycemic control, Lind et al. analyzed 20,985 DM1 patients and concluded that even after adjusting for other cardiovascular risk factors, the risk of heart failure was still four-fold higher in patients with poor glycemic control than in those with excellent glycemic control and that each 1% increase in HbA1c corresponded to a 30% increase in the risk of developing heart failure.[40] Li et al. explored the relationship between glycemic control and LV dysfunction in DM2 patients through HbA1c[32] and found that LVEF showed no difference; however, ventricular mass index and mitral E-wave velocity differed between the DM and control groups, with a greater difference in the group with worse glycemic control. In addition, there was no GLS difference between the group with good glycemic control and the control group. This study showed a correlation between HbA1c, ventricular mass index, and E/e' ratio, and GLS. Wang et al.[22] showed an intergroup difference in GLS; however, there was already an LVEF difference. This study highlights the poor glycemic control in the DM2 group prior to hospitalization, with an HbA1c value around 10%.

Contrary evidence was reported by studies that showed no difference between DM and control groups with populations with better-controlled risk factors.[10,18,31,36] Three-dimensional speckle tracking analysis identified a lower absolute GLS value in subjects with diabetes versus controls.[18,41–46] Depending on the associated risk factor, other parameters also showed differences, such as GCS[42–46] and GRS.[42,47] Chen et al. concluded that three-dimensional speckle tracking strain detects LV dysfunction in DM patients with poor glycemic control and that myocardial dysfunction is associated with DM duration and HbA1c.[46] Wang et al. demonstrated that fasting glucose, dyslipidemia, and BMI were significant risk factors for LV remodeling in DM2 patients. Those with normal ventricular geometry showed differences in only GLS compared to controls, while DM patients with LV remodeling showed lower absolute GLS, GCS, GSA, and GRS values.[44] Hepatic steatosis is another condition highly prevalent in DM2, being associated with LV remodeling and subclinical ventricular dysfunction; of the three-dimensional strain parameters, GLS presented the most evident change.[42] Finally, intensive treatment with an insulin pump improved LV systolic function, proving a sensitive and accurate diagnostic technique that could even provide data on the therapeutic effect.[43]

As previously reported,[18,48] image acquisition and the analysis of myocardial deformation by three-dimensional speckle tracking was faster than that by two-dimensional speckle tracking; however, high-quality images are required to ensure an accurate strain analysis.

Conclusion

Myocardial strain imaging by two- and three-dimensional speckle tracking echocardiography enables the identification of subclinical systolic dysfunction in DM patients that becomes more marked when associated with risk factors and ventricular remodeling. The introduction of tools like the layer-specific method allows for a broader understanding of myocardial involvement in DM. Despite few prospective studies assessing clinical outcomes, there is evidence of an association between GLS and cardiovascular events in DM patients.

Authors' contributions

Research creation and design:: Silva TRW, Silva RL; Data acquisition: Silva TRW, Silva RL; Data analysis and interpretation: Silva TRW, Martins AF; Statistical analysis: Silva RL; Manuscript writing: Silva TRW, Silva RL, Martins AF; Critical revision of the manuscript for important intellectual content: Silva TRW, Silva RL, Martins A, Marques JLB.

Conflict of interest

The authors have declared that they have no conflict of interest.

References

1. Stanton AM, Vaduganathan M, Chang LS, Turchin A, Januzzi JL, Aroda VR. Asymptomatic diabetic cardiomyopathy: an underrecognized entity in type 2 diabetes. Curr Diab Rep. 2021;21(10). doi: https://doi.org/10.1007/s11892-021-01407-2

2. Miller RG, Costacou T, Orchard TJ. Risk factor modeling for cardiovascular disease in type 1 diabetes in the pittsburgh epidemiology of diabetes complications (EDC) study: A comparison with the diabetes control and complications trial/epidemiology of diabetes interventions and complication. Diabetes. 2019;68(2):409-19. doi: https://doi.org/10.2337/db18-0515

3. Pedreanez A, Mosquera J, Munoz N, Robalino J, Tene D. Diabetes, heart damage, and angiotensin II. What is the relationship link between them? A minireview. Endocr Regul. 2022;56(1):55-65. doi: https://doi.org/10.2478/enr-2022-0007

4. Rubler S, Dlugash J, Yuceoglu YZ, Kumral T, Branwood AW, Grishman A. New type of cardiomyopathy associated with diabetic glomerulosclerosis. Am J Cardiol. 1972;30(6):595-602. doi: https://doi.org/10.1016/0002-9149(72)90595-4

5. Jia G, Hill MA, Sowers JR. Diabetic cardiomyopathy. Circ Res. 2018;122(4):624-38. doi: https://doi.org/10.1161/CIRCRESAHA.117.311586

6. Chong CR, Clarke K, Levelt E. Metabolic remodelling in diabetic cardiomyopathy. Cardiovasc Res. 2017;113(4):422-30. doi: https://doi.org/10.1093/cvr/cvx018

7. Yamauchi Y, Tanaka H, Yokota S, Mochizuki Y, Yoshigai Y, Shiraki H, et al. Effect of heart rate on left ventricular longitudinal myocardial function in type 2 diabetes mellitus. Cardiovasc Diabetol. 2021;20(1). doi: https://doi.org/10.1186/s12933-021-01278-7

8. Aepfelbacher FC, Yeon SB, Weinrauch LA, D'Elia J, Burger AJ. Improved glycemic control induces regression of left ventricular mass in patients with type 1 diabetes mellitus. Int J Cardiol. 2004;94(1):47-51. doi: https://doi.org/10.1016/j.ijcard.2003.04.012

9. Grandi AM, Piantanida E, Franzetti I, Bernasconi M, Maresca A, Marnini P, Guasti L, Venco A. Effect of glycemic control on left ventricular diastolic function in type 1 diabetes mellitus. Am J Cardiol. 2006 Jan 1;97(1):71-6. doi: https://doi.org/ 10.1016/j.amjcard.2005.07.110.

10. Weber TR, Silva RL, Cossul S, Alves MS, Lee SV der S, Brum Marques JL. The use of echocardiography in type 1 diabetes. Rev Port Cardiol. 2021;40(10):757-65. doi: https://doi.org/10.1016/j.repc.2020.11.012

11. Di Bonito P, Moio N, Cavuto L, Covino G, Murena E, Scilla C, et al. Early detection of diabetic cardiomyopathy: Usefulness of tissue Doppler imaging. Diabet Med. 2005;22(12):1720-5. doi: https://doi.org/10.1111/j.1464-5491.2005.01685.x

12. From AM, Scott CG, Chen HH. The development of heart failure in patients with diabetes mellitus and pre-clinical diastolic dysfunction. A population-based study. J Am Coll Cardiol. 2010;55(4):300-5. doi: https://doi.org/10.1016/j.jacc.2009.12.003

13. Strom JA. Diabetic heart disease: Insights from cardiac mechanics. J Am Soc Echocardiogr. 2014;27(5):489-92. doi: https://doi.org/10.1016/j.echo.2014.03.008

14. Ernande L, Bergerot C, Rietzschel ER, De Buyzere ML, Thibault H, et al. Diastolic dysfunction in patients with type 2 diabetes mellitus: Is it really the first marker of diabetic cardiomyopathy? J Am Soc Echocardiogr. 2011;24(11):1268-1275.e1. doi: https://doi.org/10.1016/j.echo.2011.07.017

15. Amundsen BH, Helle-Valle T, Edvardsen T, Torp H, Crosby J, Lyseggen E, et al. Noninvasive myocardial strain measurement by speckle tracking echocardiography: Validation against sonomicrometry and tagged magnetic resonance imaging. J Am Coll Cardiol. 2006;47(4):789-93. doi: https://doi.org/10.1016/j.jacc.2005.10.040

16. Kalam K, Otahal P, Marwick TH. Prognostic implications of global LV dysfunction: A systematic review and meta-analysis of global longitudinal strain and ejection fraction. Heart. 2014;100(21):1673-80. doi: https://doi.org/:10.1136/heartjnl-2014-305538

17. Tadic M, Cuspidi C, Vukomanovic V, Ilic S, Obert P, Kocijancic V, et al. Layer-specific deformation of the left ventricle in uncomplicated patients with type 2 diabetes and arterial hypertension. Arch Cardiovasc Dis. 2018;111(1):17-24. doi: https://doi.org/10.1016/j.acvd.2017.01.014

18. Ringle A, Dornhorst A, Rehman MB, Ruisanchez C, Nihoyannopoulos P. Evolution of subclinical myocardial dysfunction detected by two-dimensional and three-dimensional speckle tracking in asymptomatic type 1 diabetic patients: a long-term follow-up study. ECHO Res Pract. 2017;4(4):73-81. doi: https://doi.org/10.1530/ERP-17-0052

19. Stevanovic A, Dekleva M. The importance of subclinical left ventricular dysfunction and blood pressure pattern in asymptomatic type-2 diabetic patients: the diagnostic and prognostic significance of tissue Doppler parameters, left ventricular global longitudinal strain, and night. J Diabetes Complications. 2018;32(1):41-7. doi: https://doi.org/10.1016/j.jdiacomp.2017.07.022

20. Ng ACT, Bertini M, Ewe SH, an der Velde ET, Leung DY, Delgado V, et al. Defining subclinical myocardial dysfunction and implications for patients with diabetes mellitus and preserved ejection fraction. Am J Cardiol. 2019;124(6):892-8. doi: https://doi.org/10.1016/j.amjcard.2019.06.011

21. Yang QM, Fang JX, Chen XY, Lv H, Kang CS. The systolic and diastolic cardiac function of patients with type 2 diabetes mellitus: an evaluation of left ventricular strain and torsion using conventional and speckle tracking echocardiography. Front Physiol. 2022;12:726719. doi:10.3389/fphys.2021.726719

22. Wang T, Li L, Huang J, Fan L. Assessment of subclinical left ventricle myocardial dysfunction using global myocardial work in type 2 diabetes mellitus patients with preserved left ventricle ejection fraction. Diabetol Metab Syndr. 2022;14(1):17. doi: https://doi.org/10.1186/s13098-021-00781-x

23. Vukomanovic V, Tadic M, Suzic-Lazic J, Kocijancic V, Celic V. The relationship between heart rate variability and left ventricular layer-specific deformation in uncomplicated diabetic patients. Int J Cardiovasc Imaging. 2017;33(4):481-90. doi: https://doi.org/10.1007/s10554-016-1023-9

24. Vukomanovic V, Suzic-Lazic J, Celic V, Cuspidi C, Petrovic T, Grassi G, et al. The relationship between functional capacity and left ventricular strain in patients with uncomplicated type 2 diabetes. J Hypertens. 2019;37(9):1871-6. doi: https://doi.org/10.1097/HJH.0000000000002125

25. Soufi Taleb Bendiab N, Ouabdesselam S, Henaoui L, Lopez-Sublet M, Monsuez JJ, Benkhedda S. Impact of diabetes on cardiac function in patients with high blood pressure. Int J Environ Res Public Health. 2021;18(12). doi: https://doi.org/10.3390/ijerph18126553

26. Tadic M, Cuspidi C, Pencic B, Grassi G, Celic V. Myocardial work in hypertensive patients with and without diabetes: An echocardiographic study. J Clin Hypertens. 2020;22(11):2121-7. doi: https://doi.org/10.1111/jch.14053

27. Wang T, Li L, Huang J, Fan L. Assessment of subclinical left ventricle myocardial dysfunction using global myocardial work in type 2 diabetes mellitus patients with preserved left ventricle ejection fraction. Diabetol Metab Syndr. 2022;14(1):17. doi: https://doi.org/10.1186/s13098-021-00781-x

28. Yang QM, Fang JX, Chen XY, Lv H, Kang CS. The systolic and diastolic cardiac function of patients with type 2 diabetes mellitus: an evaluation of left ventricular strain and torsion using conventional and speckle tracking echocardiography. Front Physiol. 2022;12. doi: https://doi.org/10.3389/fphys.2021.726719

29. Todo S, Tanaka H, Yamauchi Y, Yokota S, Mochizuki Y, Shiraki H, et al. Association of left ventricular longitudinal myocardial function with subclinical right ventricular dysfunction in type 2 Diabetes mellitus. Cardiovasc Diabetol. 2021;20(1):212. doi: https://doi.org/10.1186/s12933-021-01404-5

30. Van Ryckeghem L, Keytsman C, Verbaanderd E, Frederix I, Bakelants E, Petit T, et al. Asymptomatic type 2 diabetes mellitus display a reduced myocardial deformation but adequate response during exercise. Eur J Appl Physiol. 2021;121(3):929-40. doi: https://doi.org/10.1007/s00421-020-04557-5

31. Roberts TJ, Barros-Murphy JF, Burns AT, MacIsaac RJ, MacIsaac AI, Prior DL, et al. Reduced exercise capacity in diabetes mellitus is not associated with impaired deformation or twist. J Am Soc Echocardiogr. 2020;33(4):481-9. doi: https://doi.org/10.1016/j.echo.2019.11.012

32. Li C, Yuan M, Li K, Bai W, Rao L. Value of peak strain dispersion in discovering left ventricular dysfunction in diabetes mellitus. Sci Rep. 2020;10(1). doi: https://doi.org/10.1038/s41598-020-78621-7

33. Philouze C, Obert P, Nottin S, Benamor A, Barthez O, Aboukhoudir F. Dobutamine stress echocardiography unmasks early left ventricular dysfunction in asymptomatic patients with uncomplicated type 2 diabetes:

a comprehensive two-dimensional speckle-tracking imaging study. J Am Soc Echocardiogr. 2018;31(5):587-97. doi: https://doi.org/10.1016/j.echo.2017.12.006

34. Mochizuki Y, Tanaka H, Matsumoto K, Sano H, Shimoura H, Ooka J, et al. Impact of left ventricular longitudinal functional mechanics on the progression of diastolic function in diabetes mellitus. Int J Cardiovasc Imaging. 2017;33(12):1905-14. doi: https://doi.org/10.1007/s10554-017-1198-8

35. Stevanovic A, Dekleva M. The importance of subclinical left ventricular dysfunction and blood pressure pattern in asymptomatic type-2 diabetic patients: the diagnostic and prognostic significance of Tissue Doppler parameters, left ventricular global longitudinal strain, and night. J Diabetes Complications. 2018;32(1):41-7. doi: https://doi.org/10.1016/j.jdiacomp.2017.07.022

36. Jørgensen PG, Jensen MT, Biering-Sørensen T, Mogelvang R, Fritz-Hansen T, Vilsbøll T, et al. Burden of uncontrolled metabolic risk factors and left ventricular structure and function in patients with type 2 diabetes mellitus. J Am Heart Assoc. 2018;7(19):e008856. doi: https://doi.org/10.1161/JAHA.118.008856

37. Berceanu M, Mirea O, Donoiu I, Militaru C, Saftoiu A, Istratoaie O. Myocardial function assessed by multi-layered two-dimensional speckle tracking analysis in asymptomatic young subjects with diabetes mellitus type 1. Cardiology. 2020;145(2):80-7. doi: https://doi.org/10.1159/000504532

38. Ananthapadmanabhan S, Vo G, Nguyen T, Dimitri H, Otton J. Direct comparison of multilayer left ventricular global longitudinal strain using CMR feature tracking and speckle tracking echocardiography. BMC Cardiovasc Disord. 2021;21(1):1-10. doi: https://doi.org/10.1186/s12872-021-01916-8

39. Stevanovic A, Dekleva M. The importance of subclinical left ventricular dysfunction and blood pressure pattern in asymptomatic type-2 diabetic patients: the diagnostic and prognostic significance of Tissue Doppler parameters, left ventricular global longitudinal strain, and night. J Diabetes Complications. 2018;32(1):41-7. doi: https://doi.org/10.1016/j.jdiacomp.2017.07.022

40. Lind M, Bounias I, Olsson M, Gudbjörnsdottir S, Svensson AM, Rosengren A. Glycaemic control and incidence of heart failure in 20 985 patients with type 1 diabetes: An observational study. Lancet. 2011;378(9786):140-6. doi:10.1016/S0140-6736(11)60471-6

41. Wang Q, Tan K, Xia H, Gao Y. Association of pulse pressure with left ventricular geometry and function in elderly nonhypertensive patients with diabetes: A 3D speckle tracking echocardiography study. J Clin Ultrasound. 2017;45(7):416-25. doi: https://doi.org/10.1002/jcu.22484

42. Wang Q, Ma W, Xia J. Nonalcoholic fatty liver is associated with further left ventricular abnormalities in patients with type 2 diabetes mellitus: a 3-dimensional speckle-tracking study. J ULTRASOUND Med. 2018;37(8):1899-911. doi: https://doi.org/10.1002/jum.14536

43. Luo HX, Zhou XL, Kou HJ, XW, Wu Q, Zou CP, et al. Improvement of continuous subcutaneous insulin infusion on patients with type 2 diabetes mellitus by 3-dimensional speckle tracking echocardiography. Int J Cardiovasc Imaging. 2018;34(3):379-84. doi: https://doi.org/10.1007/s10554-017-1245-5

44. Wang Q, Tan K, Xia H, Gao Y. Left ventricular structural alterations are accompanied by subclinical systolic dysfunction in type 2 diabetes mellitus patients with concomitant hyperlipidemia: An analysis based on 3D speckle tracking echocardiography. Echocardiography. 2018;35(7):965-74. doi: https://doi.org/10.1111/echo.13858

45. Wang Q, Tan K, Xia H, Gao Y. Left ventricular metabolic remodeling and accompanied dysfunction in type 2 diabetic patients: A 3D speckle tracking analysis. Echocardiography. 2019;36(3):486-94. doi: https://doi.org/10.1111/echo.14248

46. Chen X, Guo H, Yang Q, Fang J, Kang X. Quantitative evaluation of subclinical left ventricular dysfunction in patients with type 2 diabetes mellitus by three-dimensional echocardiography. Int J Cardiovasc Imaging. 2020;36(7):1311-9. doi: https://doi.org/10.1007/s10554-020-01833-5

47. Wang Q, Tan K, Xia H, Gao Y. The further negative effect of hyperuricemia on left ventricular structure and function in patients with type 2 diabetes mellitus: a transthoracic 3d speckle tracking imaging study. Metab Syndr Relat Disord. 2019;17(9):436-43. doi: https://doi.org/10.1089/met.2019.0048

48. Reant P, Barbot L, Touche C, Dijos M, Arsac F, Pillois X, et al. Evaluation of global left ventricular systolic function using three-dimensional echocardiography speckle-tracking strain parameters. J Am Soc Echocardiogr. 2012;25(1):68-79. doi: https://doi.org/10.1016/j.echo.2011.10.009

Case Report

Late Presentation of COVID-19-Associated Transmural Myocardial Infarction with Non-Obstructive Coronary Atherosclerosis

Apresentação Tardia de Infarto Agudo do Miocárdio Transmural Sem Obstrução Coronariana Aterosclerótica Associado à COVID-19

Jaime Paula Pessoa Linhares Filho[1], Matheus Cardoso de Aragão[2], João Bosco Breckenfeld Bastos Filho[1], Ricardo Paulo de Souza Rocha[1], Fábio Holanda Lacerda[1], Francisco de Assis Carvalho de Santana[1]

[1]Hospital OTOclínica,Fortaleza, [2]School of Medicine, Federal University of Ceará, Fortaleza, CE, Brazil.

Introduction

There has been an increased incidence of coronavirus-associated thromboembolic events during the coronavirus disease 2019 (COVID-19) pandemic.[1] However, most cases presented with venous thrombotic events, mainly deep vein thrombosis and pulmonary thromboembolism,[2] whereas arterial and coronary phenomena are rare.[3]

Several pathophysiological factors can explain the relationship between COVID-19 infection and increased embolic phenomena. The main factors are increased inflammatory mediators, the release of prothrombotic factors, and endothelial dysfunction.[4,5]

Cardiovascular presentations are also common in patients with COVID-19, such as atypical chest pain, dyspnea, arrhythmias, and myocardial injury with increased troponin levels.[6] However, chest pain and increased troponin levels in the absence of coronary obstruction are rare and restricted to a few case reports.[7,8] In addition, cardiovascular signs and symptoms associated with coronavirus infection occur in the acute stage of the disease with a symptomatic condition. Late presentation after complete symptom resolution is rarely reported.

Objective

Here we describe the case of a patient with the late presentation of chest pain associated with increased myocardial injury biomarkers after hospital discharge from a COVID-19 admission. The patient underwent coronary cineangiography and cardiac magnetic resonance imaging (MRI), and the syndromic diagnosis was myocardial infarction with non-obstructive coronary atherosclerosis (MINOCA). These results highlight the possibility of cardiovascular presentations in a subacute COVID-19 infection context.

Keywords

Myocardial Infarction; Myocarditis; Coronavirus; COVID-19; Biomarkers.

Mailing Address: Jaime Paula Pessoa Linhares Filho •
Avenida Antônio Sales, 990, 3º andar, Joaquim Távora. CEP 60135-100 – Fortaleza, CE, Brazil.
E-mail: jaimepaulapessoa@hotmail.com
Manuscript received 2/8/2022; revised 3/10/2022; accepted 5/2/2022

DOI: 10.47593/2675-312X/20223502eabc290

Clinical case description

A 55-year-old man was admitted to the Emergency Department of our hospital with complaints of sudden-onset severe chest pain unrelated to exertion and was not treated with irradiation. The patient denied other associated symptoms.

Before this clinical condition, the patient had been admitted to an inpatient bed in our hospital for 13 days with the diagnosis of COVID-19 and had used a nasal oxygen cannula and the following medications: dexamethasone, codeine, colchicine, and prophylactic enoxaparin. One day after hospital discharge, he started complaining of chest pain.

A physical examination revealed a heart rate of 92 bpm, blood pressure of 122/80 mmHg, no significant changes on cardiac and pulmonary auscultation, good peripheral perfusion, and symmetrical pulses. His chest pain did not worsen with deep inspiration or palpation.

Personal history

The patient had a normal weight and no known risk factors or other diseases, nor was he regularly taking any medication. At the time of admission, he was no longer in pain.

Differential diagnosis

The following diagnostic hypotheses were proposed due to the recent COVID-19 infection and his clinical presentation: myocarditis, pericarditis, acute coronary syndrome, pulmonary thromboembolism, and Takotsubo syndrome.

Diagnostic investigation

After being admitted to the Emergency Department, the patient underwent a 12-lead electrocardiography (ECG) and troponin collection. The ECG showed sinus rhythm and an anterosuperior divisional block without changes suggestive of ischemia (Figure 1). The high-sensitivity troponin levels were: 555.7 ng/L, 1,038 ng/L, 1,029 ng/L, and 853.5 ng/L. The other biochemical tests showed no significant changes.

Transthoracic echocardiography (TTE) showed no segmental contractility or valve changes.

Next, as he reported feeling chest pain and his biomarker levels were increased, he underwent coronary angiography, which showed no significant coronary obstructions (Figure 2).

Based on the diagnostic hypothesis of myocarditis, a cardiac MRI was performed and showed an area of late transmural enhancement located in the apical region of the left ventricle compatible with acute myocardial infarction (Figure 3, Videos 1 and 2). The test was

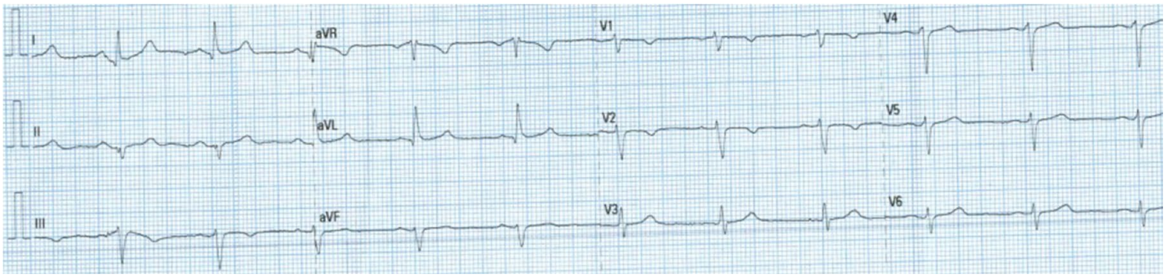

Figure 1 – *Electrocardiogram taken on admission.*

Figure 2 – *Absence of significant coronary obstructions on coronary angiogram.*

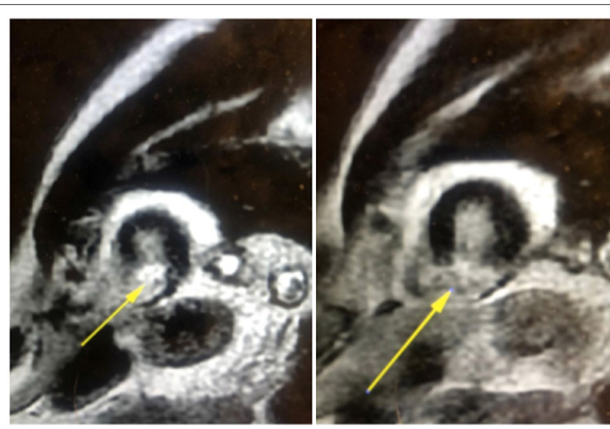

Figure 3 – *Cardiac magnetic resonance images showing late transmural enhancement in the apical region of the left ventricle (yellow arrow).*

performed 6 days after the event with no signs of high signal intensity on T2-weighted sequences suggestive of myocardial edema.

The coronary angiogram was reviewed by two interventional cardiologists. However, no coronary obstruction that could have gone unnoticed was identified.

Thus, the diagnostic hypotheses were ruled out due to absence of enhancement suggestive of myocarditis on cardiac MRI; the absence of electrocardiographic and echocardiographic signs suggestive of pericarditis (as well as significant biomarker increase with chest pain not characteristic of pericarditis); the absence of electrocardiographic (sinus tachycardia and/or S1Q3T3 pattern) and echocardiographic signs (no right ventricular dysfunction and/or signs of pulmonary hypertension) suggestive of pulmonary thromboembolism; and the absence of echocardiographic segmental contractility changes suggestive of Takotsubo syndrome.

Accordingly, we started the patient on dual antiplatelet therapy and a statin. He developed no new symptoms and was discharged from the hospital.

Discussion

In this case, in the absence of coronary obstructions, ventricular dysfunction, and/or segmental contractility changes, the main diagnostic hypotheses were myocarditis and MINOCA. In this scenario, MRI was an essential differential diagnosis tool.[9]

After the complementary MRI findings, we believe that COVID-19-related factors may have influenced the formation of coronary thrombosis or distal emboli and resulted in the transmural pattern of late enhancement in the left ventricle.

In this sense, we observed a rare cardiovascular complication potentially associated with COVID-19 infection that has a temporally atypical clinical presentation. Thus, we must pay attention to the possibility of late coronary events in COVID-19 patients and consider the possible persistence of inflammatory injury secondary to COVID-19 in the medium term. New studies may be necessary to identify the real incidence and clinical impact of these changes.

Authors' contributions

study conception: Linhares Filho JPP, Lacerda FH; study design: Linhares Filho JPP; data analysis and interpretation: Linhares Filho JPP, Aragão MC; manuscript writing: Linhares Filho JPP, Aragão MC; data/image analysis and manuscript review: Bastos Filho JBB, Rocha RPS; final approval of the submitted manuscript: Lacerda FH, Santana FAC.

Conflict of interest

The authors have declared that they have no conflict of interest.

References

1. Costa IB, Bittar CS, Rizk SI, Araújo Filho AE, Santos KA, Machado TI, et al. O coração e a COVID-19: o que o cardiologista precisa saber. Arq Bras Cardiol. 2020;114(5):805-16.

2. Klok FA, Kruip MJ, van der Meer NJ, Arbous MS, Gommers DA, Kant KM, et al. Incidence of thrombotic complications in critically ill ICU patients with COVID-19. Thromb Res. 2020;191:145-7. doi: https://doi.org/10.1016/j.thromres.2020.04.013

3. Cheruiyot I, Kipkorir V, Ngure B, Misiani M, Munguti J, Ogeng'o J. Arterial Thrombosis in Coronavirus Disease 2019 Patients: A Rapid Systematic Review. Ann Vasc Surg. 2021;70:273-81. doi: https://doi.org/10.1016/j.avsg.2020.08.087.

4. Giustino G, Pinney SP, Lala A, Reddy VY, Johnston-Cox HA, Mechanick JI, et al. Coronavirus and Cardiovascular Disease, Myocardial Injury, and Arrhythmia: JACC Focus Seminar. J Am Coll Cardiol. 2020;76(17):2011-23. doi: https://doi.org/10.1016/j.jacc.2020.08.059.

5. Imazio M, Klingel K, Kindermann I, Brucato A, De Rosa FG, Adler Y, et al. COVID-19 pandemic and troponin: indirect myocardial injury, myocardial inflammation or myocarditis? Heart. 2020;106(15):1127-1131. doi: https://doi.org/10.1136/heartjnl-2020-317186.

6. Lala A, Johnson KW, Januzzi JL, Russak AJ, Paranjpe I, Richter F, et al.; Mount Sinai COVID Informatics Center. Prevalence and Impact of Myocardial Injury in Patients Hospitalized With COVID-19 Infection. J Am Coll Cardiol. 2020;76(5):533-46. doi: https://doi.org/10.1016/j.jacc.2020.06.007.

7. Meizinger C, Klugherz B. Focal ST-segment elevation without coronary occlusion: myocardial infarction with no obstructive coronary atherosclerosis associated with COVID-19-a case report. Eur Heart J Case Rep. 2021 Jan 12;5(2):ytaa532. doi: https://doi.org/10.1093/ehjcr/ytaa532.

8. Burkert FR, Niederreiter L, Dichtl W, Mayr A, Virgolini I, Klauser A, et al. Case report of a COVID-19-associated myocardial infarction with no obstructive coronary arteries: the mystery of the phantom embolus or local endothelitis. Eur Heart J Case Rep. 2021;5(2):ytaa521. doi: https://doi.org/10.1093/ehjcr/ytaa521

9. Aragão RC, Alves MC, Passos HD, Gonçalves LF, Baumworcel L, et al. Myocardial Injury in COVID-19: a Challenge for Clinical Cardiologists. Arq Bras Cardiol. 2020;115(1):139-41. doi: https://doi.org/10.36660/abc.20200434.

Dilated Cardimiopathy as Initial Presentation of Mucopolysacaridosis in Infant

Cardimiopatia Dilatada em Lactente como Apresentação Inicial de Mucopolissacaridose

Ludimila dos Anjos Teixeira Romão[1], Fátima Derlene da Rocha Araújo[1], Camila Magalhães Silva[1], Rodrigo Rezende Arantes[1], Zilda Maria Alves Meira[1]

Hospital das Clínicas, Departments of Pediatric Cardiology and Medical Genetics, Federal University of Minas Gerais[1], Belo Horizonte, MG, Brazil.

Introduction

Mucopolysaccharidoses are rare genetic diseases caused by decreased lysosomal enzymes that act in the catabolism of glycosaminoglycans, connective tissue extracellular matrix polymers. Glycosaminoglycans progressively accumulate in the airways, mucous membranes, lungs, bones, joints, heart, liver, eyes, ears, and central and peripheral nervous systems. The multiple affected organs characterize its multisystemic presentation with a wide spectrum of severity and clinical presentations. The most severe phenotype is Hurler syndrome (type I mucopolysaccharidosis), with an incidence of 0.61–1.30 per 100,000 live births.[1]

The heart is affected in more than 50% of mucopolysaccharidosis cases,[2] with both valvular and myocardial involvement in addition to a possible association with systemic arterial hypertension (SAH).[3]

Specific treatment consists of enzyme replacement therapy (ERT), which, along with hematopoietic stem cell transplantation (HSCT), prolong the child's life and improves their symptoms, especially if started early.[4–6]

Case report

Our patient was a male infant with a birthweight of 3,360 g and no perinatal complications. At eight months of age, he developed sweating during feedings, vomiting, and irritability. He was evaluated in the emergency room, where a chest X-ray showed remarkable cardiomegaly (Figure 1B). The patient had a previous history of a neuro-psychomotor developmental delay, recurrent respiratory infections, upper respiratory obstruction, hydrocephalus requiring ventriculoperitoneal shunt implantation, and recurrent bilateral inguinal hernia. The parents were young and non-consanguineous, and the couple's first child was stillborn without an identified cause.

At nine months of age, the patient was evaluated in a tertiary pediatric cardiology service and was already using captopril. He had persistent heart failure (HF) signs and symptoms in addition to a weight-height deficit, weighing 8,880 g (Z-score: -2.44). A general examination showed several dysmorphisms such as infiltrated facies (Figure 1A), a high and narrow palate, gingival hypertrophy, a saddle nose, pectus carinatum, inguinal hernias, an umbilical hernia, an extensive Mongolian spot, a lumbar hump, bilateral diffuse corneal opacification, and a claw hand. A cardiovascular examination showed a regular heart rhythm without murmurs, a heart rate of 130 bpm, O_2 saturation of 98%, a systolic blood pressure of 120 mmHg (p: 99.93), a diastolic blood pressure of 60 mmHg (p: 99.74), a palpable liver at 5 cm from the right costal margin, and a non-palpable spleen.

Echocardiography (Figure 1C) showed a significantly increased left ventricle (LV) with a diastolic diameter of 42 mm (Z-score: 4.4) and a systolic diameter of 34 mm (Z-score: 5.6) in addition to diffuse hypocontractility with an LV ejection fraction (LVEF) of 39% and 42% by the Teichholz and Simpson's methods, respectively, and global longitudinal strain (GLS) of 13.7%. His right ventricular systolic function was slightly compromised, with a tricuspid annular plane systolic excursion of 10 mm (Z-score: -2.84) and lateral tricuspid annulus S' of 6.0 cm/s (Z-score: -3.60). The mitral and aortic valves had mild leaflet thickening without associated dysfunction.

The patient underwent pharmacological treatment for the HF and was referred for a genetic evaluation, which confirmed the diagnosis of type I mucopolysaccharidosis. His urine glycosaminoglycan level was 880 mcg/mg (reference range [RR], 133–274 mcg/mg). Glycosaminoglycan electrophoresis showed the presence of dermatan and heparan sulfate. Alpha-iduronidase (IDUA) levels of the plasma and leukocytes were reduced at 0.10 nmoL/h/mg protein (RR, 6.6–34 nmol/h/mg protein) and 0.11 nmol/h/mg protein (RR, 27–71 nmoL/h/mg protein), respectively. A molecular genetic analysis detected the W402X/W402X variant in both alleles of the *IDUA* gene. A radiographic evaluation showed dysostosis multiplex, ovoid vertebrae, paddle-shaped ribs, convergence of the proximal region of the metacarpals, a shallow acetabulum, and small ilia — signs compatible with the diagnosis of mucopolysaccharidosis.

Electrocardiography revealed sinus rhythm, a heart rate of 136 bpm, QRS complex axis at +60º, a PR interval of 80 ms, a corrected QT interval of 366 ms, T-wave inversions in D2 and D3, a deep Q wave at V6, and signs of LV overload.

ERT was instituted at 11 months of age with reduced liver volume, weight gain, improved general condition, reduced upper respiratory obstruction, and greater diet acceptance. At 12 months, HSCT was indicated, but the family refused to

Keywords

Mucopolysaccharidosis I; Child; Cardiomyopathy, Dilated.

Mailing Address: Ludimila dos Anjos Teixeira Romão •
ludimilanjos@gmail.com
Manuscript received 9/22/2021; revised 3/25/2022; accepted 4/13/2022

DOI: 10.47593/2675-312X/20223502eabc255

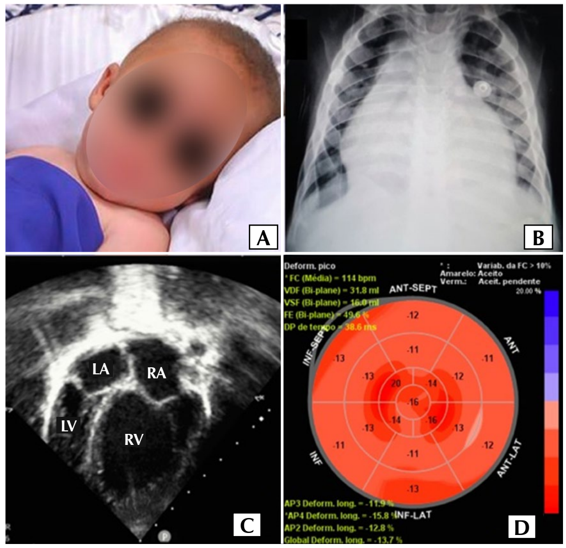

LA, left atrium; LV, left ventricle; RA, right atrium; RV, right ventricle.

Figure 1 – *Infant with type 1 mucopolysaccharidosis and dilated cardiomyopathy. Infiltrated facies (A). Chest X-ray showing cardiomegaly and pulmonary congestion (B). Echocardiographic images showing enlarged left chambers (C) and global longitudinal strain (D).*

provide consent. At 16 months of age, the infant presented with an infectious respiratory intercurrence that resulted in acute decompensation of the treatment-refractory HF and culminated in death.

Discussion

Mucopolysaccharidosis is rare but associated with characteristic phenotypic findings that should arouse syndromic suspicion. A careful and detailed evaluation associated with knowledge of the disease presentation can lead to a suspected diagnosis that, once confirmed, is amenable to treatment that changes the natural course of the disease.[5,7]

The reported patient had phenotypic characteristics of mucopolysaccharidosis such as infiltrated facies, palate changes, gingival hypertrophy, saddle nose, pectus carinatum, Mongolian spots, a lumbar hump, restricted knee and elbow mobility, claw hands, corneal opacity, inguinal hernias, and an umbilical hernia.

The cardiovascular system involves glycosaminoglycan deposits in structures such as the valvular endocardium, subvalvular apparatus, myocardium, conduction system, and vessels, especially the coronary arteries.[3] This condition can cause conduction disorders, myocardial hypertrophy, valvular dysfunction, coronary heart disease, and sometimes SAH (Table 1).

The most common echocardiographic findings are mitral and aortic valve changes.[2] The leaflets are generally thickened, the mitral subvalvular apparatus involves shortened chordae tendineae, and the papillary muscles are thickened, possibly associated with valvular regurgitation or stenosis. Theodore *et al*. reported a case series that reiterated the findings of valvular changes in mucopolysaccharidosis.[9] Myocardial dysfunction, in turn, is uncommon, but types I, II, and VI are correlated with more severe cardiovascular involvement[3] and a worse prognosis. In the case reported here, the valvular changes were mild and lacked repercussion, but there was a significantly reduced LVEF and GLS.

The conduction system may present a broad spectrum abnormality ranging from frequent sinus tachycardia to severe arrhythmias with a risk of sudden death. In the case studied here, the electrocardiographic changes were attributed to chamber dilation.

Even with pronounced glycosaminoglycan deposits in the myocardium, ventricular function is impaired in only a minority of patients. Davison *et al*. evaluated 29 children with type I mucopolysaccharidosis, reporting that five of them had dilated cardiomyopathy at the initial presentation. Similarly, Wiseman *et al*.[4] studied a group of 44 children with type I mucopolysaccharidosis diagnosed in the first four months of life; of them, only six presented with severe dilated cardiomyopathy, with an LVEF of 15–40%. Hirth *et al*.[5] also corroborated the rare onset of HF as the main mucopolysaccharidosis presentation and detected several mutations in their patients, including *W402X/W402X*, which was identified in the reported case. The ventricular function of all patients recovered after ERT or HSCT. However, the present case was diagnosed late and the patient's ventricular function was unable to recover prior to death due to infectious complications.

The presence of myocardial dysfunction of undefined etiology associated with phenotypic characteristics of mucopolysaccharidosis in infants should raise early diagnostic suspicion of the disease. The introduction of specific treatments and the management of several associated morbidities greatly impacts patient quality of life.

Authors' contributions

Research creation and design: Romão LAT; Data acquisition: Romão LAT, Arantes RR; Manuscript writing:

Table 1 - Clinical, echocardiographic, and electrocardiographic findings in infants diagnosed with mucopolysaccharidosis.

	More frequent	Less frequent
personal history	- Recurrent respiratory infections - Weight-height deficit - Delayed neuro-psychomotor development	- Syncope and pre-syncope - Tiredness during feedings - Intolerance to physical exercise
Clinical characteristics	- Coarse facies - Macroglossia - Bone anomalies - thoracolumbar kyphosis, joint restriction, camptodactyly (claw hands), carpal tunnel syndrome - Inguinal and/or umbilical hernias - Corneal opacities	- Retinitis - Blindness - Extensive Mongolian spots
Cardiovascular physical examination	- Normal or functional heart murmurs	- Arterial hypertension - Heart failure signs (tachypnea, tachycardia, hepatomegaly, edema) - Heart murmurs related to mitral and/or aortic valve regurgitation and/or stenosis
Electrocardiography	- Atrioventricular blocks - Sinus tachycardia	- Signs of myocardial ischemia (inverted T-wave, ST segment change) - Extrasystoles - Ventricular tachycardia
Echocardiography	- Thickened, dysmorphic, and/or poorly mobile valve leaflets - Valve regurgitation (mitral and aortic) - Infiltrated myocardium aspect - Fibrotic and dense endocardium	- Valve stenosis (mitral and aortic) - Calcification of the subvalvular apparatus - Shortened chordae - Thick papillary muscles - Ventricular dysfunctions - Cardiac chamber dilation - Left ventricular apical aneurysm - Ventricular wall dyskinesia - Endocardial fibroelastosis - Ascending aorta dilation - Increased aorta thickness - Coronary dilation and thickening - Coarctation of the aorta

Romão LAT, Silva CM; Data analysis and interpretation: Araújo FDR; Critical revision of the manuscript for important intellectual content: Araújo FDR, Meira ZMA.

Conflict of interest

The authors have declared that they have no conflict of interest.

Referências

1. Valayannopoulos V, Nicely H, Harmatz P, Turbeville S. Mucopolysaccharidosis VI. Orphanet J Rare Dis. 2010;5:5. doi: https://doi.org/10.1186/1750-1172-5-5
2. Park MK. Park Cardiologia Pediátrica. 6a ed. Rio de Janeiro: Elsevier, 2015.
3. Boffi L, Russo P, Limongelli G. Early diagnosis and management of cardiac manifestations in mucopolysaccharidoses: a practical guide for paediatric and adult cardiologists. Ital J Pediatr. 2018 Nov 16;44(Suppl 2):122. doi: https://doi.org/10.1186/s13052-018-0560-3
4. Wiseman DH, Mercer J, Tylee K, Malaiya N, Bonney DK, Jones SA, et al. Management of mucopolysaccharidosis type IH (Hurler's syndrome) presenting in infancy with severe dilated cardiomyopathy: a single institution's experience. J Inherit Metab Dis. 2013;36(2):263-70. doi: https://doi.org/10.1007/s10545-012-9500-3
5. Hirth A, Berg A, Greve G. Successful treatment of severe heart failure in an infant with Hurler syndrome. J Inherit Metab Dis. 2007;30(5):820. doi: https://doi.org/10.1007/s10545-007-0613-z
6. Wraith JE, Beck M, Lane R, van der Ploeg A, Shapiro E, Xue Y, et al. Enzyme replacement therapy in patients who have mucopolysaccharidosis I and are younger than 5 years: results of a multinational study of recombinant human alpha-L-iduronidase (laronidase). Pediatrics. 2007;120(1):e37-46. doi: https://doi.org/10.1542/peds.2006-2156
7. Braunlin EA, Harmatz PR, Scarpa M, Furlanetto B, Kampmann C, Loehr JP, Ponder KP, Roberts WC, Rosenfeld HM, Giugliani R. Cardiac disease in patients with mucopolysaccharidosis: presentation, diagnosis and management. J Inherit Metab Dis. 2011;34(6):1183-97. doi: https://doi.org/10.1007/s10545-011-9359-8
8. Galimberti C, Madeo A, Di Rocco M, Fiumara A. Mucopolysaccharidoses: early diagnostic signs in infants and children. Ital J Pediatr. 2018;44(Suppl 2):133. doi: https://doi.org/10.1186/s13052-018-0550-5
9. Teodoro JVT, Ribeiro LA, Ferreira Neto JM, Ferreira VM, Grangeiro CH, Oliveira AN. Mucopolissacaridoses IV e VI: Aspectos ao Ecocardiograma Bidimensional com Strain pelo Speckle Tracking em uma Série de Casos. Arq Bras Cardiol: Imagem cardiovasc. 2021;34(2):eabc159
10. Davison JE, Toledano M, Simmonds J, Cleary MA. Dilated cardiomyopathy at presentation of mucopolysaccharidosis type IH (Hurler syndrome): Clinical characteristics and management outcome. Molecular Genetics and Metabolism. 2018;123(2):S37A.

Diagnosis of Coronary Anomaly of the Circumflex Artery With Retroaortic Course by Transthoracic Echocardiography (Rac Sign) Confirmed by Computed Tomography Coronary Angiography: A Case Series

Diagnóstico de Anomalia Coronariana da Artéria Circunflexa com Trajeto Retroaórtico por meio do Ecocardiograma Transtorácico (RAC Sign) e Confirmação pela Angiotomografia de Artérias Coronárias: Série de Casos

Raul Serra Valério[1], Alfredo A. Eyer Rodrigues[1,2], Carlos Eduardo Suaide Silva[1], Marly Uellendahl MD, PhD[1,2], Luciano de Figueiredo Aguiar Filho[1,3]

[1]Diagnóstico da América S/A (DASA); [2]Federal University of São Paulo (UNIFESP); [3]Dante Pazzanese Cardiology Institute (IDPC).

Introduction

Congenital coronary artery anomaly (CCAA) is a relatively rare condition with an estimated population prevalence of 0.21–5.79%.[1] CCAA presents a wide spectrum of variations and can be classified into origin and course, intrinsic, and termination anomalies.[1,2] The CCAA with the highest prevalence is the anomalous origin of the circumflex artery (CxA) from the right coronary sinus (RCS) with an estimated prevalence of 0.3–0.8%.

CCAA usually travels along a retroaortic course and may present different originations, such as from a common ostium with the right coronary artery (RCA), from separate ostia in the RCS, or from the proximal segment of the RCA.[2–4]

Although this anomaly is usually benign, i.e., with the characteristic of not causing symptoms, ischemia, or cardiovascular outcomes, numerous cases in the specialized literature associate this anomaly with episodes of angina, ischemia, and acute myocardial infarction. This infrequent progression is mainly associated with factors related to the coronary artery origin angulation to extrinsic compression caused by aortic root dilation and the presence of an intramural course in the aortic wall.[5–10]

Transthoracic echocardiography (TTE) is a noninvasive and easily accessible tool that allows a limited assessment of some findings suggestive of CCAA. [10] One of these findings is the retroaortic anomalous coronary sign (RAC sign), a signal proposed by Witt et al. in 2017.[10–12]

The RAC sign is characterized by a hyperechoic tubular image located on the atrial face of the atrioventricular groove perpendicular to the aorta. This finding showed high sensitivity for the diagnosis; therefore, it has a high relationship with the presence of anomalous origin of the CxA from the RCS with a retroaortic course.[10–12]

Keywords

Cardiovascular Abnormalities; Echocardiography; Computed Tomography Angiography.

Mailing Address: Raul Serra Valério •
Endereço: Rua Jorge Americano, 497, Ap 141 São Paulo, SP, Brazil. CEP: 05083-130.
E-mail: raulsvalerio@gmail.com
Manuscript received 11/11/2021; revised 11/25/2021; accepted 3/2/2022

DOI: 10.47593/2675-312X/20223502eabc271

On the other hand, coronary computed tomography angiography (CCTA is a robust diagnostic tool in the anatomical assessment of the coronary tree and, therefore, the diagnosis of CCAA. As it is a noninvasive method with high temporal and spatial resolution, CCTA is currently considered the first-choice method for suspected CCAA as described in the 2010 appropriate use criteria for CCTA of the American Heart Association (AHA).[4,13]

Compared to invasive coronary angiography (ICA), CCTA is superior for CCAA assessments, especially in cases of course anomalies involving the ostium and proximal third of the coronary arteries, intrinsic anomalies (myocardial bridging), and termination anomalies (fistulas). CCTA also stands out compared to ICA due to the possibility of a three-dimensional evaluation that allows the analysis of the close relationship between the coronary and other cardiac and non-cardiac structures, mainly the aortic root and pulmonary artery, extremely important data in the prognostic assessment of CCAA.

This case series aimed to demonstrate the agreement between the echocardiographic finding (RAC sign) and the noninvasive anatomical assessment by CCTA, its high sensitivity, and the assessment of the presence or absence of myocardial ischemia in the absence of obstructive atherosclerotic lesions.

Case Reports

Case 1

A 52-year-old man had a body mass index (BMI) of 27.3 kg/m^2, had dyslipidemia, was using a high-potency statin, and had a history of stable atypical angina and intermediate cardiovascular risk by the Diamond-Forrester classification. A stress test (ST) and three-dimensional transthoracic echocardiography (3D-TTE) were requested to complement the diagnosis.

The 3D-TTE showed preserved global and segmental systolic function (end-diastolic volume [EDV], 122 mL; end-systolic volume [ESV], 44 mL; left ventricular ejection fraction [LVEF], 64%) and global longitudinal strain (GLS; 18.6%) were within the normal range (Figure 1). The diastolic function parameters were preserved and the heart valves showed no significant anatomical or functional changes.

However, a hyperechoic tubular image characteristic of the RAC sign was observed in the apical windows suggestive of a CxA anomalous retroaortic coronary course (Figure 2, Video 1).

The Bruce protocol was included in the ST and was effective and reached 99% of the age-predicted maximal heart rate. The patient presented no clinical symptoms on physical exertion and demonstrated excellent functional capacity, adequate blood pressure behavior, and the absence of arrhythmias or electrocardiographic criteria for myocardial ischemia (Figure 3).

The CCTA findings complemented the diagnosis (Figures 4 and 5), corroborating the echocardiographic findings and showing an anomalous origin of the CxA from the RCS in a single ostium and at an acute angle (30°) traveling the

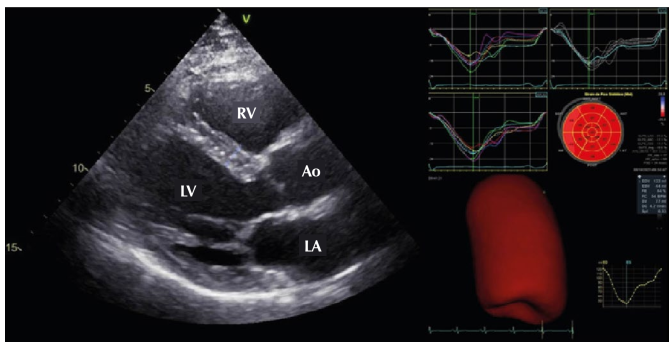

Ao, aorta; LA, left atrium; LV, left ventricle; RV, right ventricle. Source: Images obtained in the cardiovascular imaging sector of DASA S/A.

Figure 1 – *Echocardiographic window in parasternal long-axis view showing the cardiac chambers with preserved dimensions (left). Graphs and bullseyes of preserved left ventricular global longitudinal strain (top right) and left ventricular systolic function by three-dimensional echocardiography showing a preserved LV ejection fraction (bottom right).*

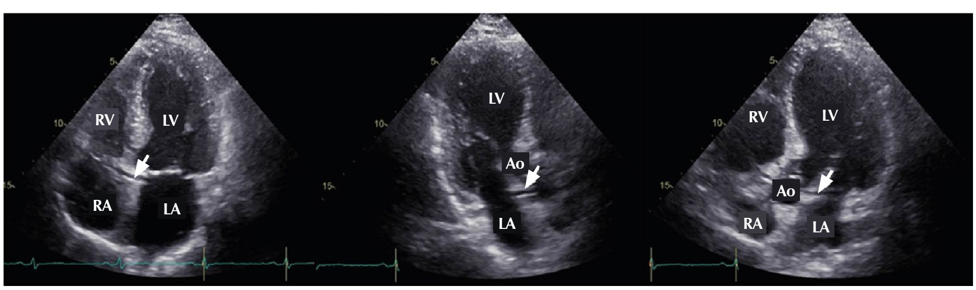

Ao, aorta; LA, left atrium; LV, left ventricle; RA, right atrium; RAC, retroaortic anomalous coronary; RV, right ventricle. Source: Images obtained in the cardiovascular imaging sector of DASA S/A.

Figure 2 – *Echocardiographic four-, three-, and five-chamber sections showing the RAC sign (white arrow), which suggests an anomalous origin of the CxA with a retroaortic course.*

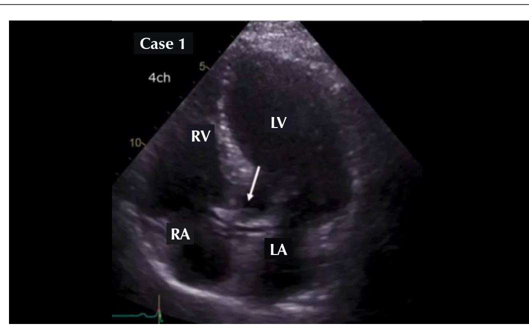

LA, left atrium; LV, left ventricle; RA, right atrium; RV, right ventricle. Source: Images obtained in the cardiovascular imaging sector of DASA S/A.

Video 1 – *Four-chamber apical echocardiogram showing the retroaortic anomalous coronary sign (white arrow).*

retroaortic course without signs of intramural course or extrinsic compression by the aortic root (aortic root with a maximum diameter of 32 mm). As for atherosclerosis, CCTA showed a 29 Agatston calcium score with atherosclerotic plaques in two segments of the coronary tree and no significant luminal reduction.

Case 2

A 53-year-old man who was asymptomatic had a BMI 28 kg/m^2, had dyslipidemia, and was using a high-potency statin came to our service for routine tests.

He underwent successful myocardial perfusion scintigraphy (MPS) with ST on a treadmill (Ellestad protocol), reaching the age-predicted maximal heart rate (Figure 6). The patient presented no clinical symptoms, arrhythmias, or electrocardiographic changes suggestive of ischemia during the ST. MPS showed a preserved LVEF at rest (58%) and under stress (65%) and no perfusion defects.

The 3D-TTE presented cardiac chambers with preserved dimensions and normal global and segmental ventricular systolic function (EDV, 123 mL; ESV, 46 mL; and LVEF, 63%). GLS demonstrated preserved values (20.9%), while the diastolic function analysis findings were normal. No anatomical or functional valve changes were identified (Figure 7). The apical section showed a hyperechoic tubular image compatible with the RAC sign (Figure 8).

CCTA performed as a diagnostic complement identified an anomalous CxA origin from the RCS with a common ostium

Source: Images obtained in the cardiovascular imaging sector of DASA S/A.

Figure 3 – *Electrocardiographic tracing of the stress test (at rest on the left and peak exertion on the right) without electrocardiographic signs of myocardial ischemia on exertion.*

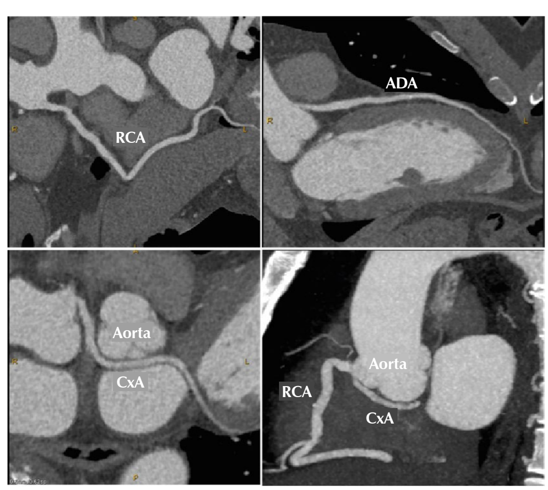

ADA, anterior descending artery; CxA, circumflex artery; RCA, right coronary artery. Source: Images obtained in the cardiovascular imaging sector of DASA S/A.

Figure 4 – *Computed tomography coronary angiography showing the absence of significant luminal reduction and the presence of anomalous origin of the CxA from a single ostium and its retroaortic course.*

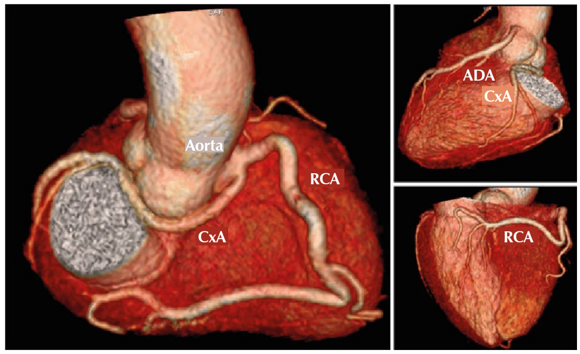

ADA, anterior descending artery; CxA, circumflex artery; RCA, right coronary artery. Source: Images obtained in the cardiovascular imaging sector of DASA S/A.

Figure 5 – *3D reconstruction of CT coronary angiography showing the coronary anatomy with an anomalous course and absence of atherosclerotic plaques.*

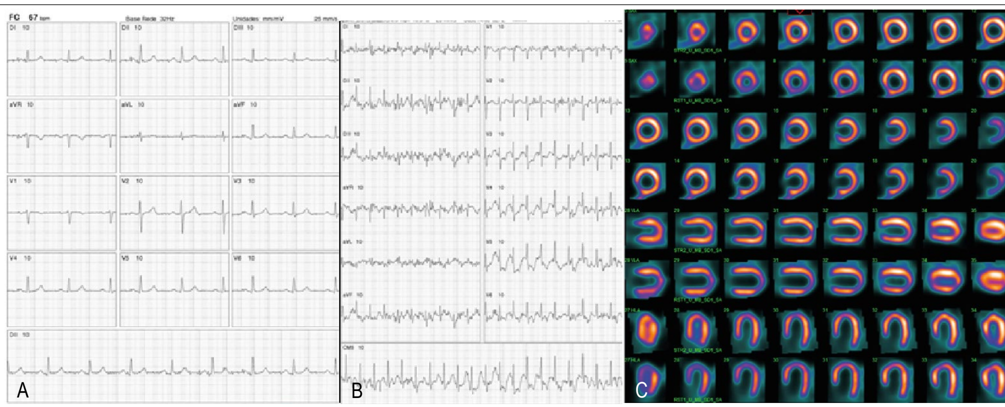

Source: Images obtained in the cardiovascular imaging sector of DASA S/A.

Figure 6 – *Electrocardiographic tracing (A, at rest; B, at peak exertion) without criteria for ischemia and myocardial perfusion scintigraphy with no perfusion changes (C).*

with the RCA at an acute angle (35°) and with a retroaortic course. The course showed no luminal reduction and no signs of intramural course or extrinsic compression by the aortic root (maximum aortic root diameter, 33 mm) (Figures 9 and 10).

Case 3

A 31-year-old woman who had a BMI 20 kg/m^2, was asymptomatic, and had no known comorbidities was referred for routine TTE. The TTE showed preserved global and segmental biventricular systolic function. Her GLS (22.8%) and diastolic function were within the normal range. No significant anatomical and functional valve changes were identified. However, a hyperechoic tubular image was also visualized in apical sections perpendicular to the aorta, consistent with the RAC sign and suggestive of coronary anomaly (Figure 11, Video 2).

As a diagnostic complement, CCTA showed an anomalous origin of the CxA from the RCS in a separate ostium in an acute angle (26°), at a retroaortic course, and with no intramural course (Figures 12 and 13). No extrinsic compression by the aortic root was observed (largest aortic root diameter, 26 mm). An atherosclerosis assessment presented a coronary calcium score of zero and absence of atherosclerotic plaques in the coronary segments.

In this case, no myocardial ischemia investigation was performed.

Discussion

Here we reported a series of three cases of a suspected CxA anomalous retroaortic course due to a TTE characteristic finding known as the RAC sign. Corroborating the data in the literature, this finding presented high diagnostic sensitivity since the coronary anomaly was confirmed in all cases on a noninvasive anatomical CCTA evaluation.

We also highlighted that CCTA is the gold standard method for CCAA evaluations since it is an easy and noninvasive way to analyze the characteristics of the coronary anomaly and provides important complementary information that can suggest a worse prognosis, such as the coronary ostium outflow angulation, the presence of an intramural course, and the relationship between the coronary artery and adjacent cardiac or non-cardiac structures.

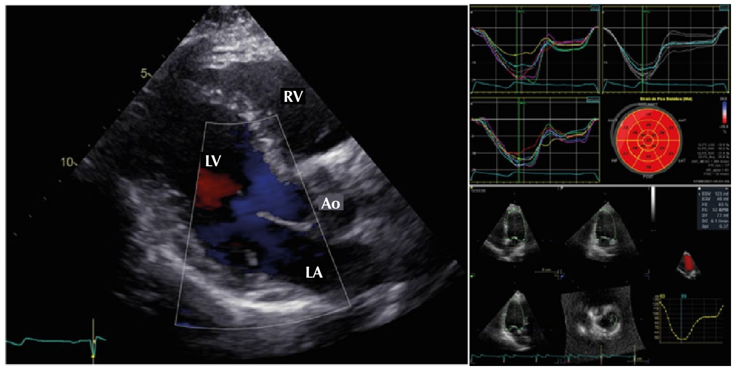

Ao, aorta; LA, left atrium; LV, left ventricle; RV, right ventricle. Source: Images obtained in the cardiovascular imaging sector of DASA S/A.

Figure 7 – *Parasternal long-axis echocardiographic window (left), global longitudinal strain (top right), and preserved global systolic function by three-dimensional echocardiography (bottom right).*

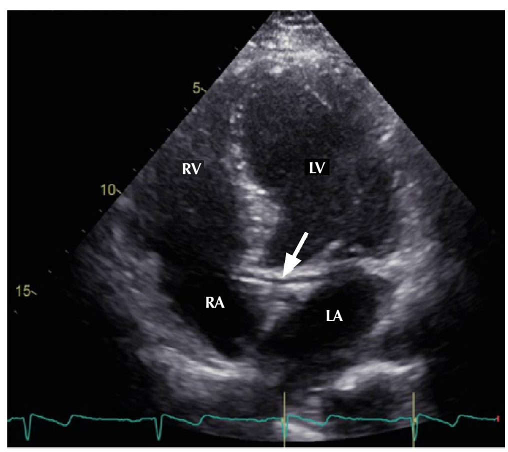

LA, left atrium; LV, left ventricle; RA, right atrium; RAC, retroaortic anomalous coronary; RV, right ventricle. Source: Images obtained in the cardiovascular imaging sector of DASA S/A.

Figure 8 – *Echocardiographic five-chamber section demonstrating the RAC sign (white arrow), characteristic of anomalous CxA with a retroaortic course.*

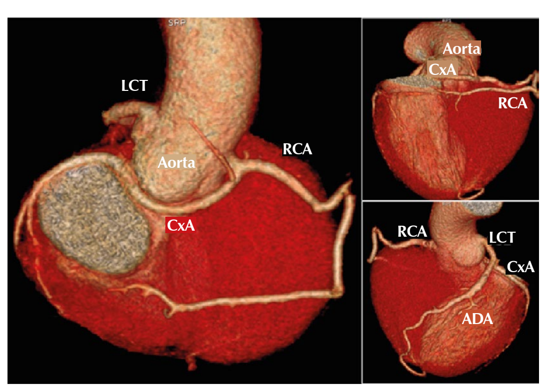

ADA, anterior descending artery; CxA, circumflex artery; LCT, trunk of the left coronary artery; RCA, right coronary artery. Source: Images obtained in the cardiovascular imaging sector of DASA S/A.

Figure 9 – *Three-dimensional reconstruction of computed tomography coronary angiography showing the coronary anatomy with an anomalous course and absence of atherosclerotic plaques.*

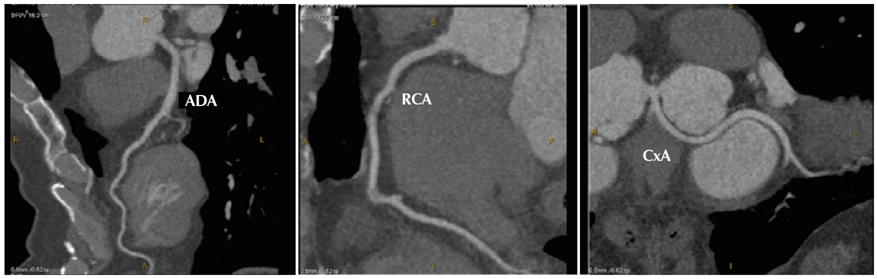

ADA, anterior descending artery; CxA, circumflex artery; RCA, right coronary artery. Source: Images obtained in the cardiovascular imaging sector of DASA S/A.

Figure 10 – *Computed tomography coronary angiography showing the absence of significant luminal reduction and the presence of an anomalous CxA origin from a single ostium and retroaortic course.*

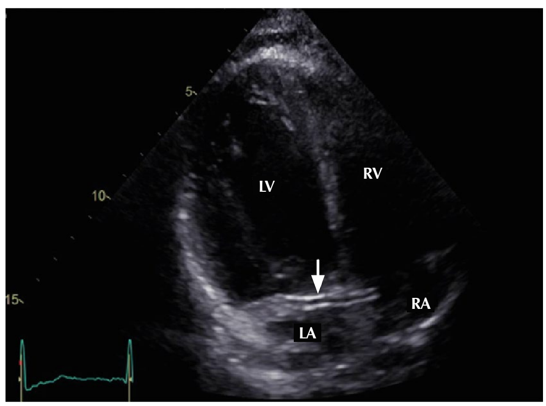

VE: ventrículo esquerdo; VD: ventrículo direito; AD: átrio direito; AE: átrio esquerdo. Source: Images obtained in the cardiovascular imaging sector of DASA S/A.

Figure 11 – *Apical four-chamber echocardiographic view showing tubular hyperechoic image – RAC sign (white arrow), suggestive of anomalous CxA origin with retroaortic course.*

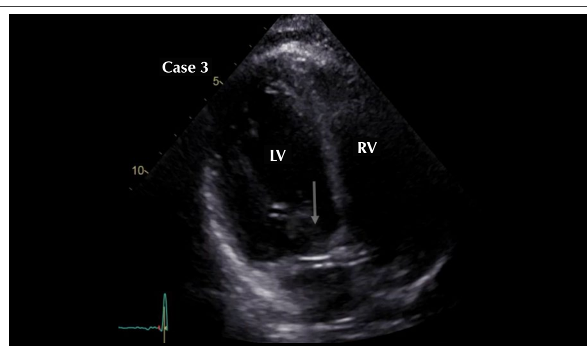

LV, left ventricle; RV, right ventricle. Source: Images obtained in the cardiovascular imaging sector of DASA S/A.

Video 2 – *Four- and three-chamber apical view echocardiogram showing the retroaortic anomalous coronary sign (white arrow).*

It is important to emphasize that an ST was performed in two of the cases described here to investigate myocardial ischemia. The results of both were negative, once again corroborating the findings in the literature, which mostly state that this anomalous course has a benign progression. However, as already mentioned, there are several reports of major and minor cardiovascular events related to this anomaly, a fact that supports the indication of ischemia research in cases of this diagnosed anomaly.

Conclusion

This case series highlights the fundamental role of TTE in the diagnostic confirmation of CCAA by the presence of the RAC sign, especially in cases with a retroaortic origin of the CxA. Despite the limitations inherent to the method, TTE has robust ability to identify this anomaly; thus, its use should always be considered so that a diagnostic opportunity is not missed.

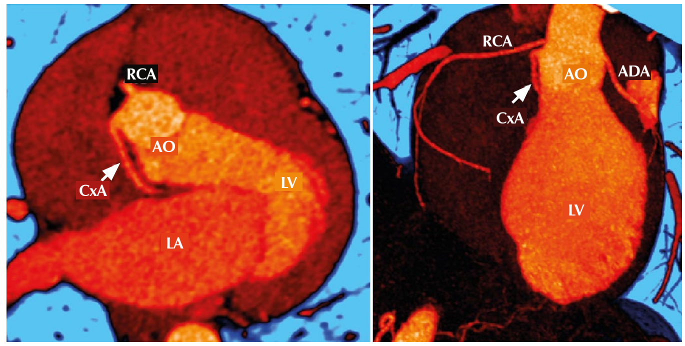

Ao, aorta; ADA, anterior descending artery; CxA, circumflex artery; LA, left atrium; LV, left ventricle; RCA, right coronary artery. Source: Images obtained in the cardiovascular imaging sector of DASA S/A.

Figure 12 – *Tomographic section reconstruction showing the anomalous origin of the CxA from the RCS in a separate ostium and with a retroaortic course (white arrow).*

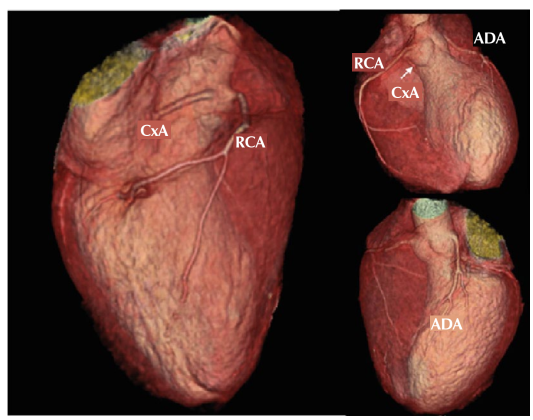

ADA, anterior descending artery; CxA, circumflex artery; RCA, right coronary artery. Source: Images obtained in the cardiovascular imaging sector of DASA S/A.

Figure 13 – *Three-dimensional reconstruction of computed tomography angiography of the coronary arteries showing the coronary anatomy with an anomalous course and absence of atherosclerotic plaques.*

Authors' contributions

Valério RS, Aguiar Filho LF: research conception and design; Silva CES, Aguiar Filho LF: data collection; Valério RS: manuscript writing; Uellendahl M, Rodrigues AAE, Silva CES, Aguiar Filho LF: critical review of the manuscript for important intellectual content.

Conflict of interest

The authors have declared that they have no conflict of interest.

References

1. Pérez-Pomares JM, de la Pompa JL, Franco D, Henderson D, Ho SY, Houyel L, et al. Congenital coronary artery anomalies: a bridge from embryology to anatomy and pathophysiology--a position statement of the development, anatomy, and pathology ESC Working Group. Cardiovasc Res. 2016;109(2):204-16. doi: https://doi.org/10.1093/cvr/cvv251

2. Cheezum MK, Liberthson RR, Shah NR, Villines TC, O'Gara PT, Landzberg MJ, et al. Anomalous Aortic Origin of a Coronary Artery From the Inappropriate Sinus of Valsalva. J Am Coll Cardiol. 2017;69(12):1592-608. doi: https://doi.org/10.1016/j.jacc.2017.01.031

3. Opolski MP, Pregowski J, Kruk M, Witkowski A, Kwiecinska S, Lubienska E, et al. Prevalence and characteristics of coronary anomalies originating from the opposite sinus of Valsalva in 8,522 patients referred for coronary computed tomography angiography. Am J Cardiol. 2013;111(9):1361-7. doi: https://doi.org/10.1016/j.amjcard.2013.01.280

4. Pursnani A, Jacobs JE, Saremi F, Levisman J, Makaryus AN, Capuñay C, et al. Coronary CTA assessment of coronary anomalies. J Cardiovasc Comput Tomogr. 2012;6(1):48-59. doi: https://doi.org/10.1016/j.jcct.2011.06.009

5. Del Torto A, Baggiano A, Guglielmo M, Muscogiuri G, Pontone G. Anomalous origin of the left circumflex artery from the right coronary sinus with retro-aortic course: A potential malign variant. J Cardiovasc Comput Tomogr. 2020;14(5):e54-5. doi: https://doi.org/10.1016/j.jcct.2019.01.021

6. Barriales Villa R, Díaz Molina B, Arias Castaño JC, Medina Alba R, Casariego

Rosón R, Penas Lado M. Isquemia miocárdica causada por una arteria circunfleja anómala [Myocardial ischemia caused by an anomalous circumflex coronary artery]. Rev Esp Cardiol. 2002;55(2):200-2. Spanish. doi: https://doi.org/10.1016/s0300-8932(02)76581-0

7. Kejriwal NK, Tan J, Gordon SP, Newman MA. Retroaortic course of the anomalous left main coronary artery: is it a benign anomaly? A case report and review of literature. Heart Lung Circ. 2004;13(1):97-100. doi: https://doi.org/10.1016/j.hlc.2004.01.013

8. Aydin M, Ozeren A, Peksoy I, Cabuk M, Bilge M, Dursun A, et al. Myocardial Ischemia caused by a coronary anomaly: left circumflex coronary artery arising from right sinus of valsalva. Tex Heart Inst J. 2004;31(3):273-5. PMID: 15562848.

9. Samarendra P, Kumari S, Hafeez M, Vasavada BC, Sacchi TJ. Anomalous circumflex coronary artery: benign or predisposed to selective atherosclerosis. Angiology. 2001;52(8):521-6. doi: https://doi.org/10.1177/000331970105200803

10. Mancinelli A, Golino M, Miglierina E, My I, Crippa M, De Ponti R. Three Echocardiographic Signs to Identify Anomalous Origin of the Circumflex Coronary Artery from the Right Sinus of Valsalva: A Case Report. CASE (Phila). 2020;4(5):324-7. doi: https://doi.org/10.1016/j.case.2020.07.008

11. Witt CM, Elvert L, Konik E, Ammash N, Foley D, Foley T. The Rac Sign: Retroaortic Anomalous Coronary Artery Visualization By Transthoracic Echocardiography. J Am Coll Cardiol. 2017;69(11):649. doi: http://dx.doi.org/10.1016/S0735-1097(17)34038-X

12. Witt CM, Elvert LA, Konik EA, Ammash NM, Foley DA, Foley TA. The RAC Sign: Retroaortic Anomalous Coronary Artery Visualization by Transthoracic Echocardiography. JACC Cardiovasc Imaging. 2018;11(4):648-9. doi: https://doi.org/10.1016/j.jcmg.2017.06.011

13. Taylor AJ, Cerqueira M, Hodgson JM, Mark D, Min J, O'Gara P, et al.; American College of Cardiology Foundation Appropriate Use Criteria Task Force; Society of Cardiovascular Computed Tomography; American College of Radiology; American Heart Association; American Society of Echocardiography; American Society of Nuclear Cardiology; North American Society for Cardiovascular Imaging; Society for Cardiovascular Angiography and Interventions; Society for Cardiovascular Magnetic Resonance, Kramer CM, Berman D, Brown A, Chaudhry FA, Cury RC, Desai MY, Einstein AJ, Gomes AS, Harrington R, Hoffmann U, Khare R, Lesser J, McGann C, Rosenberg A, Schwartz R, Shelton M, Smetana GW, Smith SC Jr. ACCF/SCCT/ACR/AHA/ASE/ASNC/NASCI/SCAI/SCMR 2010 appropriate use criteria for cardiac computed tomography. A report of the American College of Cardiology Foundation Appropriate Use Criteria Task Force, the Society of Cardiovascular Computed Tomography, the American College of Radiology, the American Heart Association, the American Society of Echocardiography, the American Society of Nuclear Cardiology, the North American Society for Cardiovascular Imaging, the Society for Cardiovascular Angiography and Interventions, and the Society for Cardiovascular Magnetic Resonance. J Am Coll Cardiol. 2010;56(22):1864-94. doi: https://doi.org/10.1016/j.jacc.2010.07.005

Primary Cardiac Lymphoma: Role of Imaging Multimodality in Diagnosis

Linfoma Cardíaco Primário: o Papel da Multimodalidade de Imagem na Abordagem Diagnóstica

Julia Werneck Paulino Soares de Souza[1], Luiza Telles de Andrade Alvares[1], Maria Paula Righeti Gonçalves[1], Ana Beatriz Aisemann Goulart Paiva[2], Ricardo Lopes Ferreira[3], Marcelo Goulart Paiva[3]

[1]Estácio de Sá University – Presidente Vargas Campus, Rio de Janeiro, RJ, Brazil; [2]School of Medical Sciences of Santos, Santos, SP, Brazil; [3]DASA Hospital 9 de Julho, São Paulo, SP, Brazil.

Abstract

Intracardiac masses are a diagnostic challenge since their symptoms can be common to cardiovascular pathologies. Some methods, whether invasive or not, enable differential diagnosis, histological confirmation, and adequate treatment. To better understand the importance of imaging multimodality and the approach to managing cardiac tumors, we investigated a case of a primary cardiac lymphoma in which the multidisciplinary approach allowed rapid diagnosis and treatment, including of intercurrences, with a promising initial response despite fatal progression due to severe acute respiratory syndrome coronavirus 2 infection.

Introduction

Intracardiac masses are a diagnostic challenge as their symptoms can be common to cardiovascular pathologies. Diagnostic methods, whether invasive or not, enable differential diagnosis, histological confirmation, and adequate treatment. To better understand the importance of imaging multimodality and the approach to managing cardiac tumors (CTs), here we report the clinical case of a patient with a mass in the right atrium (RA).

Case report

An 82-year-old woman with nonspecific symptoms was admitted for investigation on March 10, 2020. She denied any oncological history. The patient was emaciated, pale, eupneic, and hemodynamically stable. Laboratory tests showed mildly increased lactic dehydrogenase (LDH) and C-reactive protein (CRP) levels. It also demonstrated negative HIV and negative tumor marker serology. An electrocardiogram (ECG) revealed sinus rhythm with ventricular extrasystole. Computed tomography of the chest showed a dilated suprahepatic vena cava/right atrium (RA). The assessment was limited by the absence of contrast, with an axial diameter of 5.9 cm and no lymphadenopathy identified. Cardiac magnetic resonance imaging (MRI) revealed RA enlargement and the presence of a mass measuring 3.7 × 1.5 cm in the proximal region of the superior vena cava (SVC). Heterogeneous perfusion and delayed enhancement were noted in addition to tissue characterization suggestive of a neoplastic origin (Figure 1A). Fluorodeoxyglucose (^{18}FDG) positron emission tomography CT (PET/CT) showed increased uptake in the para-caval and lateral RA region (maximum standardized uptake value, 18.8) (Figure 1B). Transesophageal echocardiography (TEE) showed a sessile echo-dense image with no cleavage plane on the RA wall close to the SVC outflow measuring 4.1 × 1.7 cm with subsequent endocardial biopsy (Figures 1C–E). A pathological examination identified high-grade B-cell non-Hodgkin's lymphoma and positive immunohistochemistry for BCL-2, Bcl-6, CD10, CD20 (Pan B), LCA (CD45), and Ki 67 (MIBI-1, positive in 95% of neoplastic cells) (Figure 2). The proposed treatment was cytoreduction with dexamethasone 20 mg for 4 days, followed by six cycles of R-mini-CHOP (rituximab 375 mg/m^2, doxorubicin 25 mg/m^2, vincristine 1 mg, cyclophosphamide 400 mg/m^2, and prednisone 60 mg from D1 to D5) with a 21-day interval and the first cycle divided into two stages. The patient presented with complete atrioventricular block (CAVB) on D4 for which a definitive pacemaker was indicated. She was discharged from the hospital after completing the first treatment cycle. Control TEE performed after two cycles of chemotherapy showed mass reduction (1.4 × 0.7 cm) with increased echo density (Figure 1F). She was readmitted on June 16, 2020 with respiratory failure due to severe acute respiratory syndrome coronavirus 2 (SARS-CoV-2) infection. Transthoracic echocardiography (TTE) showed no evidence of the mass in the RA, and she died on June 27, 2020.

Discussion

CTs are infrequent, while primary CTs (PCTs) are even rarer, with an incidence of 0.05% on autopsies, while metastatic tumors are 20–40 times more frequent. About 90% of PCTs are benign (myxomas, lipomas, fibroelastomas, etc.), while the other 10% are malignant, of which 95% are sarcomas and 5% are lymphomas and mesotheliomas. Primary cardiac lymphoma (PCL) represents 1.3% of PCTs, while a CT secondary to disseminated lymphoma occurs in 9–24% of cases.[1-3] PCL is more frequent in women, especially in those after the fifth decade of life and those with immunocompromised status (acquired immunodeficiency syndrome or post-transplant immunosuppression).[4]

Clinical presentations are nonspecific, including chest pain, arrhythmia, congestion, pericardial effusion, SVC syndrome,

Keywords

Cardiovascular Diseases, Echocardiography, Lymphoma.

Mailing Address: Marcelo Goulart Paiva •
Rua Periquito, 210/92B. CEP: 04514-050 – São Paulo, SP, Brazil.
E-mail: mgpaiva123@gmail.com

Manuscript received 2/8/2022; revised 2/16/2022; accepted 3/28/2022

DOI: 10.47593/2675-312X/20223502eabc286

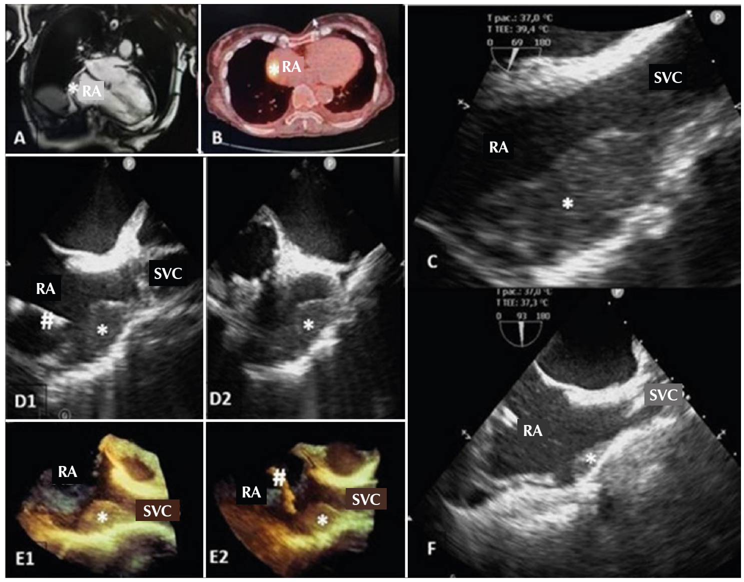

* mass; # biotome; RA right atrium, SVC superior vena cava.

Figure 1 – *A- Cardiac MRI 4 Chambers. B- PET/CT with 18FDG. C e D - TEE 2D bicaval. E- TEE 3D bicaval. F- TEE 2D bicaval.*

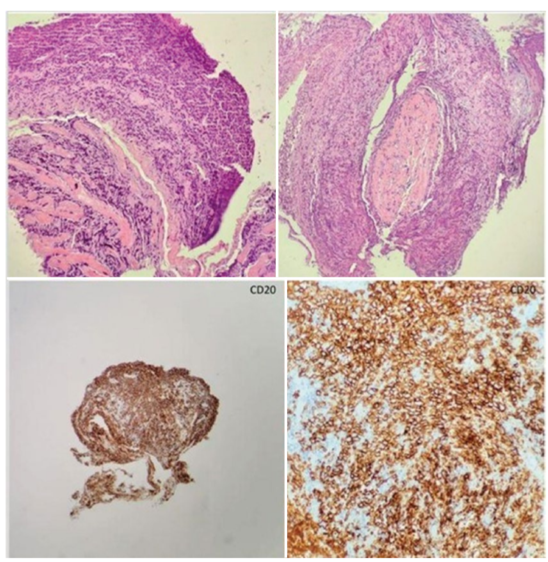

Figure 2 – *Upper images Hematoxylin and eosin stain: Large lymphocytes with prominent cytoplasm and nucleoli. Lower images High-grade non-Hodgkin's B-cell lymphoma, immunohistochemistry CD20 (+) which may indicate suitability for treatment with rituximab.*

and sudden death.[2] Laboratory findings include leukocytosis, neutrophilia, increased erythrocyte sedimentation rate, CRP, LDH, ß2-microglobulin, and carcinoembryonic antigen. No single ECG finding is considered diagnostic, with ventricular or supraventricular arrhythmias and atrioventricular block being the most common. Chest radiography may show an increased cardiac area (mainly in the RA), pleural effusion, and pulmonary congestion.[3]

Echocardiography allows the rapid noninvasive assessment of the PCL and is usually the initial approach. TTE has a sensitivity of 55–60%, while TEE reaches 97–100%. The PCL presents as a homogeneous infiltrative mass with a broad base located in the right cavities, predominantly in the RA, and can invade nearby structures. It usually presents with pericardial effusion. The use of ultrasound contrast allows a differential diagnosis with non-vascularized masses (thrombi), as the presence of perfusion suggests malignant tumors (hypervascularity).[5] CT assesses the extent of the mass and its relationship with cardiac and extracardiac structures, such as a low- or normal-density epicardial or myocardial infiltrative mass.[3, 5, 6] On cardiac MRI, the lesions are poorly defined with delayed enhancement (unlike sarcomas that present with necrosis). Tissue characterization, a vascularization study, and the definition of myocardial and pericardial infiltration show the possibility of a cardiac tumor. PCL presents iso- or high-intensity signals on T2 and iso- or low-intensity signals on T1 images. Pericardial inversion-recovery images may show a high-intensity signal in the pericardial fluid suggestive of malignancy. Being located in the RA, having a diameter greater than 5 cm, the presence of a hemorrhagic pericardial effusion, and late enhancement are also suggestive of malignancy. Comparatively, MRI has higher sensitivity than CT (90–92% vs. 71–73%, respectively).[3] Hypermetabolism on ^{18}FDG PET/CT is suggestive of a malignant tumor.[3,7]

A definitive diagnosis comes from the histological study of the mass or a cytological analysis of the pericardial fluid (positive in 2/3 of cases); a biopsy of the mass can be collected and analyzed by interventional (endovascular) or surgical cardiology.[2,3] Diffuse B-cell lymphoma is the most common histological type (80% of cases), followed by follicular, Burkitt, and T-cell lymphoma.[2,3] Surgical biopsy is chosen in cases of hemodynamic instability (cardiac tamponade, superior or inferior vena cava syndrome, and blood flow obstruction) and left-chamber tumors (to minimize embolic risk). In other situations, the endovascular biopsy can be guided by intracardiac or transesophageal echocardiography as in the case presented here.[6,8]

Complete surgical resection is usually very difficult, being restricted to cases with great hemodynamic repercussions.[9] The R-CHOP regimen, the most commonly used clinical treatment protocol, significantly impacts survival. Increased complications such as arrhythmias, atrioventricular block, myocardial wall rupture, and death soon after the start of chemotherapy have been described. Of the proposed approaches to minimizing such risks, pre-treatment with corticosteroids and vincristine, a 50% reduction in the initial dose of cyclophosphamide and doxorubicin, and, more commonly, fractionation of the first cycle into two steps with a 15-day interval similar to we what we did here, is required.[4,10] The response is favorable in 79% of cases, with complete remission achieved in 59%.[9,10] Treatment responses can be assessed as reduced tumor burden on echocardiography or MRI and by reduced metabolic activity on PET/CT.[3,5,10]

PCL behaves aggressively, resulting in death in a few months when not properly treated. On the other hand, compared to other malignant tumors, it responds favorably to treatment with improved long-term survival.[4] Immunodeficiency, extracardiac involvement, left ventricular involvement, and presence of arrhythmia are markers of a worse prognosis.[4] Disease-free survival increased from 12 to 24 months after rituximab was included in the chemotherapy treatment.[4,10]

Conclusion

Here we reported a case of PCL in which the multidisciplinary approach allowed rapid diagnosis and treatment, including intercurrence, with a promising initial response despite fatal progression due to SARS-CoV-2 infection.

Authors' contribution

Manuscript design, data collection, writing, and critical review: Souza JWPS, Alvares LTA, Gonçalves MPR, Paiva ABAG, Ferreira RL, Paiva MG

Conflict of interest

The authors have declared that they have no conflict of interest.

References

1. Habertheuer A, Ehrlich M, Wiedemann D, Mora B, Rath C, Kocher A. A rare case of primary cardiac B cell lymphoma. Journal of Cardiothoracic Surgery. 2014 [cited 2022 Apr 8];9(1). Available from: https://cardiothoracicsurgery.biomedcentral.com/articles/10.1186/1749-8090-9-14

2. Tyebally S, Chen D, Bhattacharyya S, Mughrabi A, Hussain Z, Manisty C, et al. Cardiac Tumors: JACC CardioOncology State-of-the-Art Review. JACC CardioOncol. 2020;2(2):293-311. doi: https://doi.org/10.1016/j.jaccao.2020.05.009.

3. Miguel CE, Bestetti RB. Primary cardiac lymphoma. Int J Cardiol. 2011 Jun 16;149(3):358-63. doi: https://doi.org/10.1016/j.ijcard.2010.02.016.

4. Singh B, Ip R, Ibrahim Al-Rajjal A, Kafri Z, Al-Katib A, Hadid T. Primary Cardiac Lymphoma: Lessons Learned from a Long Survivor. Case Rep Cardiol. 2016;2016:7164829. doi: https://doi.org/10.1155/2016/7164829.

5. Wang S, Li M, Zhang L, Xie M. Multimodal imaging evaluation of a primary cardiac lymphoma in an immunocompetent patient. Echocardiography. 2018;35(12):2121-2123. doi: https://doi.org/10.1111/echo.14150.

6. Mankad R, Herrmann J. Cardiac tumors: echo assessment. Echo Res Pract. 2016;3(4):R65-R77. doi: https://doi.org/10.1530/ERP-16-0035

7. Nijjar PS, Masri SC, Tamene A, Kassahun H, Liao K, Valeti U. Benefits and limitations of multimodality imaging in the diagnosis of a primary cardiac lymphoma. Tex Heart Inst J. 2014;41(6):657-9. doi: https://doi.org/10.14503/THIJ-13-3595

8. Schneider CM, Buiatti A, Schwamborn K, Dirschinger RJ. Diagnosis of a rare cardiac human herpesvirus-8 positive B-cell lymphoma manifestation: a case report of a transoesophageal echocardiography-guided trans-septal catheter biopsy. Eur Heart J Case Rep. 2018;2(2):yty037.

9. Grantomo J, Pratita J, Rachmat J, Saraswati M. A rare case of primary cardiac lymphoma and the role of early surgical debulking: a case report. Eur Heart J Case Rep. 2018;2(4):yty116. doi: https://doi.org/10.1093/ehjcr/yty116

10. Shah K, Shemisa K. A "low and slow" approach to successful medical treatment of primary cardiac lymphoma. Cardiovasc Diagn Ther. 2014;4(3):270-3. doi: https://doi.org/10.3978/j.issn.2223-3652.2014.04.01